Analysis of Ribosome Biogenesis from Three Standpoints: Investigating the Roles of Ribosomal RNA, Ribosomal Proteins and Assembly Factors

MADHUMITHA RAMESH

Bachelor of Technology (Industrial Biotechnology)

Anna University, Chennai, India

Submitted in partial fulfillment of the requirements for the degree of

Doctor of Philosophy (Biological Sciences)

Carnegie Mellon University, Pittsburgh, USA

February 11, 2016

Thesis Advisor: **Dr. John L. Woolford**

Committee members: Dr. Marcel P. Bruchez, Dr. C. Joel McManus, Dr. Andrea J. Berman

Table of Contents

Table of Figures

Abstract

Ribosomes are ubiquitous and abundant molecular machines composed of ribosomal RNA (rRNA) and ribosomal proteins (r-proteins). They play a central role in the cell by translating the genetic code in mRNA to form polypeptides. Because of their large size and the complexity of molecular interactions within ribosomes, we do not still fully understand how they are synthesized in the cell. Yet, a thorough knowledge of ribosome biogenesis is crucial to understand cellular homeostasis and various disease states including ribosomopathies and cancer. In addition, ribosomes serve as an interesting paradigm to understand the principles that dictate the formation and function of the many different ribonucleoprotein particles that play vital roles in the cell. In addition to the rRNA and r-protein components, *trans*-acting assembly factors play indispensable roles in synthesizing functional ribosomes. Fundamentally, ribosome biogenesis is driven by a network of molecular interactions that evolve in time and space, as assembly progresses from the nucleolus to the cytoplasm.

We sought to gain a deeper understanding of ribosome biogenesis in *Saccharomyces cerevisiae* by investigating the molecular interactions that drive ribosome assembly. Recent structural studies have revealed a number of such molecular interactions at high resolution. Based on these, our investigation was carried out from the perspectives of all three players that are involved in constructing ribosomes, with a specific emphasis on eukaryote-specific elements of rRNAs and r-proteins.

From the standpoint of rRNA, we performed the first systematic study to investigate the potential functions of nearly all of the eukaryotic rRNA expansion segments in the yeast large ribosomal subunit. We showed that most of them are indispensable and play vital roles in ribosome biogenesis. Based on the steps of ribosome biogenesis in which each of them participates, we showed that there is neighborhood-specific functional clustering of rRNA and r-protein interactions that drive ribosome

assembly. Further, we found evidence for possible functional co-evolution of eukaryotic rRNA and eukaryote-specific elements of r-protein.

From the standpoint of r-protein, we used rpL5 as a paradigm for constantly evolving molecular interactions as assembly progresses. Apart from recapitulating Diamond-Blackfan anemia missense mutations in yeast, we characterized interactions formed by specific regions of rpL5 and propose that these interactions potentially govern the loading of 5S RNP *en bloc* to the nascent large ribosomal subunit, to ensure proper rotation of the 5S RNP during biogenesis, and to further recruit proteins necessary for the test drive of subunits in the cytoplasm.

From the standpoint of assembly factors, we analyzed a so-called group of ITS2 cluster proteins, Nop15, Cic1 and Rlp7 and identified the extensive protein-protein interactions and analyzed protein-RNA interactions that they make. Using our data, we were able to localize Rlp7 to the ITS2 spacer in the pre-rRNA and to identify potential mechanisms for their function. Having identified a network of molecular interactions, we suggest that these proteins orchestrate proper folding of rRNA through this network, and stabilize and facilitate the early steps of assembly. Further, based on their location in the preribosome, these factors might serve to ensure proper progression of early steps of assembly to enable subsequent processing of the ITS2 spacer in the middle steps, possibly by recruiting the ATPase Has1.

Thus, we have investigated early nucleolar and late nuclear steps of ribosome assembly in the light of molecular interactions formed by rRNA, r-protein and assembly factors that participate in eukaryotic ribosome assembly. Lessons that emerged from this study and tools developed in the process provide a starting point for further investigations pertaining to the roles of eukaryote-specific segments of molecules that participate in ribosome biogenesis, and serve as a paradigm for how a dynamic network of molecular interactions can drive the assembly of complex macromolecular structures.

Abbreviations

- aa.   – amino acid

- AF   – Assembly Factor

- CP   – Central Protuberance

- CRAC   – Crosslinking and Analysis of cDNAs

- Cryo-EM   – Cryo Electron Microscopy

- DBA   – Diamond Blackfan Anemia

- EMSA   – Electromobility shift assay

- ES   – Expansion Segment/Expansion Segments

- ETS   – External Transcribed spacer

- Fig.   – Figure

- ITS   – Internal Transcribed Spacer

- LSU   – Large ribosomal subunit

- ORF   – Open reading frames

- pre-rRNA   – Pre-ribosomal RNA

- RNA   – Ribonucleic Acid

- RNP   – Ribonucleoprotein

- r-protein   – Ribosomal protein

- rp   – Ribosomal protein

- rRNA   – Ribosomal RNA

- WT   – Wild-Type

- SGD   – Saccharomyces Genome Database

- SHAPE   – Selective 2'-hydroxyl acylation assayed by primer extension

Notes and Nomenclature

- As per convention, yeast gene names (DNA) are capitalized and italicized and proteins are not.

- Ribosomal proteins/r-proteins are referred either as rpL__ or L__ (for example, rpL17 or L17). Synonyms and counterparts in other ribosomal protein nomenclature systems are indicated as and when needed.

- A3-factors: Those assembly factor proteins, when depleted, affect processing of $27SA_3$ pre-rRNA, causing it to accumulate.

- B-factors: Those assembly factor proteins, when depleted, affect processing of 27SB pre-rRNA, causing it to accumulate.

- "Early"-acting r-proteins/rRNA: Those, when mutated, result in an accumulation of $27SA_2$ or $27SA_3$ pre-rRNA.

- "Middle"-acting r-proteins/rRNA: Those, when mutated, result in an accumulation of 27SB pre-rRNA unaccompanied by an increase in 7S pre-rRNA levels.

- "Late"-acting r-proteins/rRNA: Those, when mutated, result in an accumulation of 7S pre-rRNA.

- A3 phenotype: Accumulation of $27SA_3$ pre-rRNA, often accompanied by a decrease in $27SB_S$ pre-rRNA. We also typically observe relatively rapid turnover of preribosomes in mutants with an A3 phenotype. This step in pre-rRNA processing is referred to as the "A3 step" or "A3 processing step"

- 27SB has both a short and a long form, indicated by $27SB_S$ and $27SB_L$ respectively.

- ITS2 spacer – Internal transcribed spacer 2, part of pre-rRNA between 5.8S and 25S mature rRNA that is processed during ribosome assembly.

- Proximal stem – Helix formed by interaction of the 3' end of 5.8S rRNA and the 5' end of 25S rRNA.

Acknowledgements

They say it takes a village to raise a child. The same can be said for a PhD. I would like to thank a few people who made this journey possible, fruitful and memorable.

First and foremost, I am sincerely grateful for **Dr. John Woolford**, for the immense personal and professional development opportunities I had under his mentorship. Having really enjoyed his class back in 2010, I sent him an email asking about doing a rotation in his lab, while being a complete stranger to yeast molecular biology. I am very glad he replied saying "terrific" in capital letters followed by a few too many exclamation points! That was an indication of what lay ahead - he has always been readily available to help and brings his effervescent, contagious enthusiasm to work every day. I hope to emulate him in many respects, starting off with being an inspiring scientist and a wonderful teacher. Borrowing from an essay[*] I love, "he observes, he judges and he guides". He never tells me what to do; instead, he tells me what I want to do myself. As I have learnt recently, all of these are hallmarks of a great 'colleague-coach', someone who breaks down performance into its component parts and makes 'achieving one's potential' seem more methodical. Paraphrasing from the article, the coach is someone who is on your side of the fence to help you achieve your maximum potential, and help you figure out how to get there along the way. John's style of pedagogy fits that description perfectly. Thanks to him being the excellent coach that he is, the journey in his lab has been a superlative learning experience for me and I will remain very grateful for that.

Next, I would like to thank my committee members **Dr. Marcel Bruchez, Dr. Joel McManus and Dr. Andrea Berman**. I admire their outstanding research and I have enjoyed how their brilliant and interesting perspectives turn every committee meeting into an engaging brainstorming session. I would like to thank them for helping me with their feedback and supporting me through a challenging project.

On that note, I would also like to thank all the professors and staff in our department for making this such a wonderful place to learn and grow. Special thanks to **Ena Miceli** and **Dr. Shoba Subramanian** for guiding me through various steps in grad school.

No words are enough to accurately describe how big a role **my lab mates** have played in shaping my experience and growth here. I owe them big time. I have been very fortunate to experience how diverse backgrounds, thoughts and personalities can come together to form a breeding ground for fun and productivity. I doubt I will ever get to work with such an amazing team in the future, but I hope I do. Our lab meetings have helped me define the course of my projects; and my lab mates have invested an incredible amount of effort in proofreading and perfecting every piece I have written or presented. **Jelena Jakovljevic** has nearly been my life coach during my time here, and I have learnt so much from her. A lion's share of my health consciousness inspiration comes from her. **Jill Dembowski**'s impeccable work ethic inspired me and I am glad we developed a wonderful scientific collaboration that resulted in my first publication. My experience with **Jason Talkish** and **Michael Gamalinda** has been remarkable; they have influenced my first few formative years in lab in numerous ways. I cannot do enough justice to describing how important my 'squad' **(Salini Konikkat, Karen Kormuth, Beril Tutuncuoglu**; 'Squad' H/T: Taylor Swift) has been to my PhD years. I deeply admire Beril's wisdom, charisma and perseverance in research. Our funny, yet profound conversations have shaped the way I think about quite a few things in science and life. (aka, thanks for all your profound one-liners and for telling me French don't do take-out coffee!). Karen is my awesome buddy in most everyday things and definitely my go-to person for pretty much everything "American". I have learnt from her about how to rise up to occasions and turnaround tough situations with incredible poise and pragmatism (aka, thanks for dragging me along to Mike's workout class every single time!). I have had the pleasure of sharing my grad school journey with Salini since the first day I landed in the US. She inspires me with her resilience, while her sense and depth of purpose amaze me! (aka, thanks for singing and making those evenings so much better!). **Stephanie**

Biedka, the newest member of our lab, is such an integral part of what makes our lab so awesome and I am glad our times in the lab overlapped, if only for a few months. I also have had the pleasure of working with undergrads, experiencing mentoring from the other end. I particularly enjoyed working with Luke who contributed to one of the techniques I developed.

They say days are long and years are short in a PhD. So true! For someone who moved half way across the globe, there have been numerous friends who have made Pittsburgh feel like home for me on a day-to-day basis. Thanks to all of my classmates for the help and support in our thesis writing meetings and through the years, especially to **Shanna, Olivia** (yay, MellonFIT), **John and Zhongling**. I owe special thanks to my buddies and partners in crime - **Jigar and Sahil,** for their unwavering support in grad school life and for all the fun. I look forward to taking these cherished memories with me as I go forward. Many other people have made my grad school experience richer with their presence and redefined my view of the world – including several friends from CMU, friends from music practice/SPICMACAY and MellonFIT. **Suchi, Swati, Vinitha, Lavanya, Sachi** (for a #205D full of chocolates, laughter, conversations and fun), **Swetha** (the best last-minute proofreading savior), **Venkat, Sreekanth, Shivram, Charan, Ganga, Divya, Tanvi, Preethi, Rathika** and many more people including the CMU shuttle driver **Ronda**, (who baked me a wonderful cheesecake) - I owe you all big time!

Words fail to express how important **Apoorva** (we even went to the RNA meeting together!), **Priyamvada** and **Ram**, my friends-philosophers-guides-soulmates-sounding boards-cheerleaders have been to this PhD journey. They have been my *humsafars*, inspiring me to be my best self every day, helping me navigate every single turn along the way and making my life better with their *je ne sais quoi*. It is not an exaggeration to say that any of this simply would not have been possible without them.

Having been born and raised in a modest family in semi-urban India, doing a PhD at Carnegie Mellon is as close as it gets to living a dream. I am fortunate to have my entire extended **family** (especially my

incredibly inspiring and affectionate grandparents, Alama-Sathyanarayana and Padma-Subramanian) offering me a bottomless bowl of motivation, day after day. Not a day passes without me feeling an overwhelming sense of unalloyed love and gratitude towards **Amma (Lalitha), Appa (Ramesh) and my brother Chuchan (Sudharsan)**. They pray for me and sacrifice their own pursuits for me. Day after day, they choose and dare to believe in me, even though the path ahead seems nothing like anything we have ever known. They happily put their sweat, soul and resources in making me part of their dreams and my education and growth part of their desires**. I shall remain grateful forever – to them, and for them.

* http://www.newyorker.com/magazine/2011/10/03/personal-best

**https://www.linkedin.com/pulse/google-gets-its-new-ceo-thanks-entire-generations-sacrifice-baruah

1. Introduction

Ribosomes are ribonucleoprotein particles that synthesize proteins by translation of messenger RNA. Eukaryotic ribosomes are composed of a large (60S) and a small (40S) subunit, which together constitute the 80S ribosome. These subunits perform distinct functions (Green and Noller, 1997) – the small subunit is involved in mRNA decoding, matching the codon with the cognate amino acyl tRNA, while the large subunit hosts the peptidyl transferase center that catalyzes peptide bond formation followed by polypeptide release (Steitz, 2008). Considerable strides have been made in understanding the process of translation and how the ribosome functions (Schmeing and Ramakrishnan, 2009). On the other hand, understanding how ribosomes assemble has remained a complicated and challenging problem (de la Cruz et al., 2015; Woolford, 2015).

Owing to the wealth of genomic and proteomic information along with the robust genetic and biochemical tools developed for it, *Saccharomyces cerevisiae* has emerged as an ideal model organism to study the evolutionarily conserved process of ribosome biogenesis. Similar to those in other organisms, ribosomes in *S. cerevisiae* are incredibly complex, consisting of four ribosomal RNAs (rRNA) – 5S, 5.8S, 25S (in the large subunit) and 18S (in the small subunit) and 79 r-proteins (r-proteins).

A giant leap in our understanding of ribosomes came from the elucidation of the crystal structure of the eukaryotic ribosome, (Fig. 1-1), (Ben-Shem et al., 2011; Ben-Shem et al., 2010; Klinge et al., 2011; Klinge et al., 2012). It provides a snapshot of the locations of r-proteins and the mature rRNA in its folded state. These and other recent groundbreaking cryo-EM data of unprecedented resolution, (Fig. 1-2) (Anger et al., 2013; Armache et al., 2010a; Bradatsch et al., 2012; Leidig et al., 2014), (Wu et al., manuscript in review) have facilitated audacious attempts to use structural information to answer deeper mechanistic questions about biogenesis. Various high-throughput studies on the yeast

interactome (Goll and Uetz, 2006; McCann et al., 2015; Tarassov et al., 2008; Yu et al., 2008) have

supplemented these structural advances to provide valuable clues to understand biogenesis.

Figure 1-1: Crystal structural model of the S. cerevisiae large ribosomal subunit (PDB ID: 4V88)
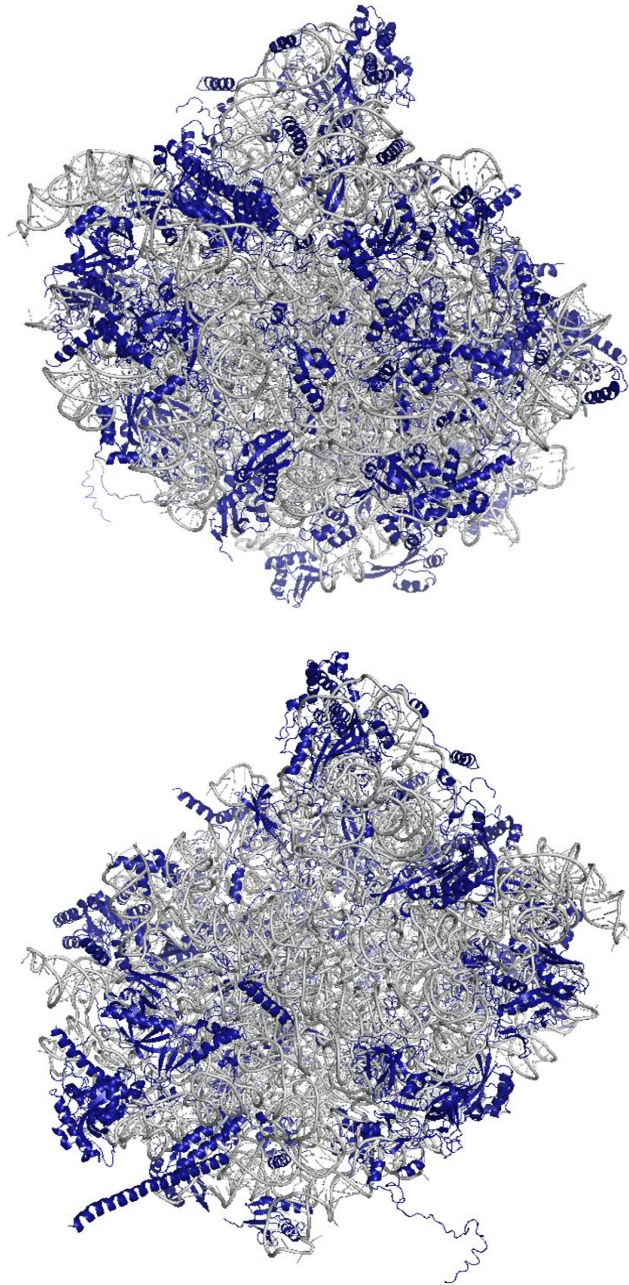
Fig. 1-1: Crystal structural model of the *S. cerevisiae* large ribosomal subunit (Protein Data Bank ID: 4V88). R-proteins are shown in blue and rRNA is shown in gray. Both solvent interface (top) and subunit interface (bottom) are shown.

Figure 1-2: Structural model of the S. cerevisiae nascent late nuclear stage large ribosomal subunit

based on cryo-EM studies
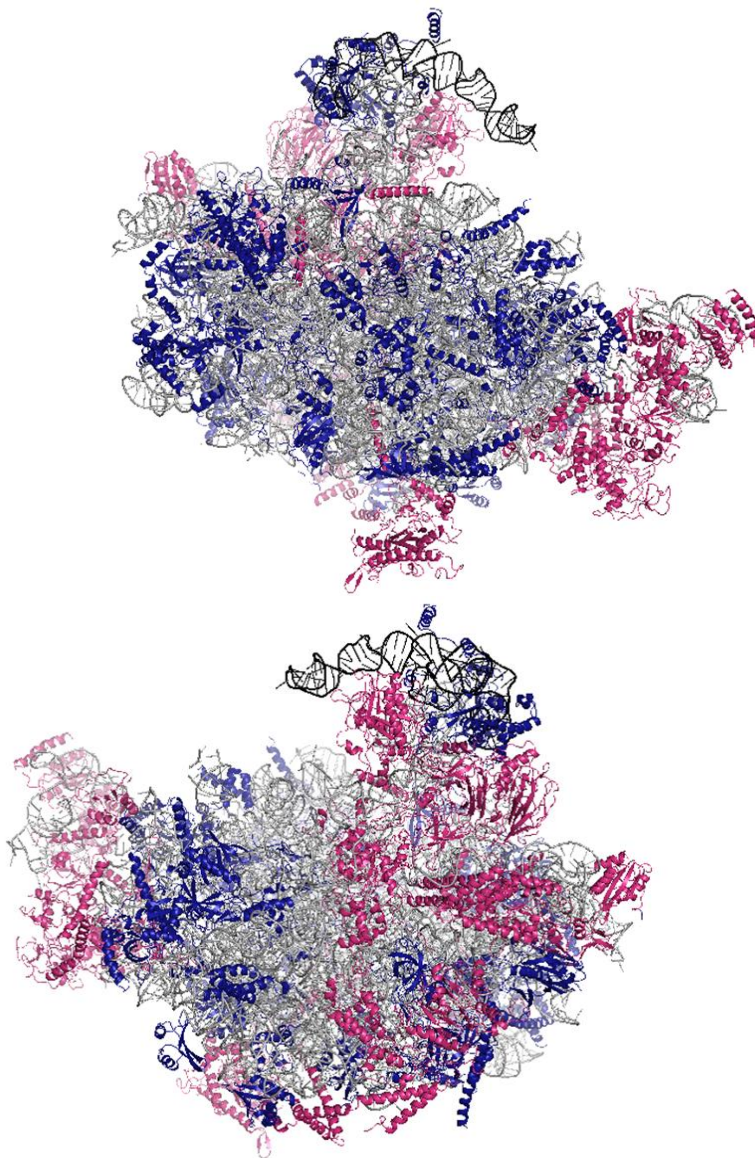
Fig. 1-2: Structural model of the S. cerevisiae nascent late nuclear stage large ribosomal subunit based on cryo-EM studies (Wu et al., manuscript in review).

R-proteins are shown in blue, rRNA is shown in gray and assembly factors are shown in pink. Both solvent interface (top) and subunit interface (bottom) are shown.

1.1 Ribosome biogenesis

Our knowledge of the principles governing ribosome assembly has been gleaned from extensive research on the mechanistic underpinnings of bacterial ribosome assembly, and their counterparts and exceptions that have been discovered in eukaryotes concurrently (Mizushima and Nomura, 1970; Nomura, 1973; Shajani et al., 2011). In addition to the rRNA core and the r-proteins that are associated with it, eukaryotic ribosome biogenesis *in vivo* requires a large number of conserved *trans*-acting assembly factors (Henras et al., 2008; Thomson et al., 2013; Woolford and Baserga, 2013) – proteins and snoRNAs that facilitate assembly progressively in the nucleolus, nucleoplasm and cytoplasm. Overall, eukaryotic ribosome biogenesis is composed of multiple coordinated processes including:

- Transcription, processing and modification of rRNA

- Translation, folding and modification of r-proteins

- Nuclear import of r-proteins and assembly factors

- Proper folding of rRNA

- Binding and tightening of r-proteins

- Binding, function and release of assembly factors

- Nuclear export of the preribosome

Thus, the mechanistic picture of biogenesis that has emerged from an increasing body of research is that of spatio-temporally regulated interplay between RNA folding and r-protein binding, concomitant with pre-rRNA processing. (Fig. 1-3)

Figure 1-3: Key processes and players in ribosome biogenesis *in vivo*
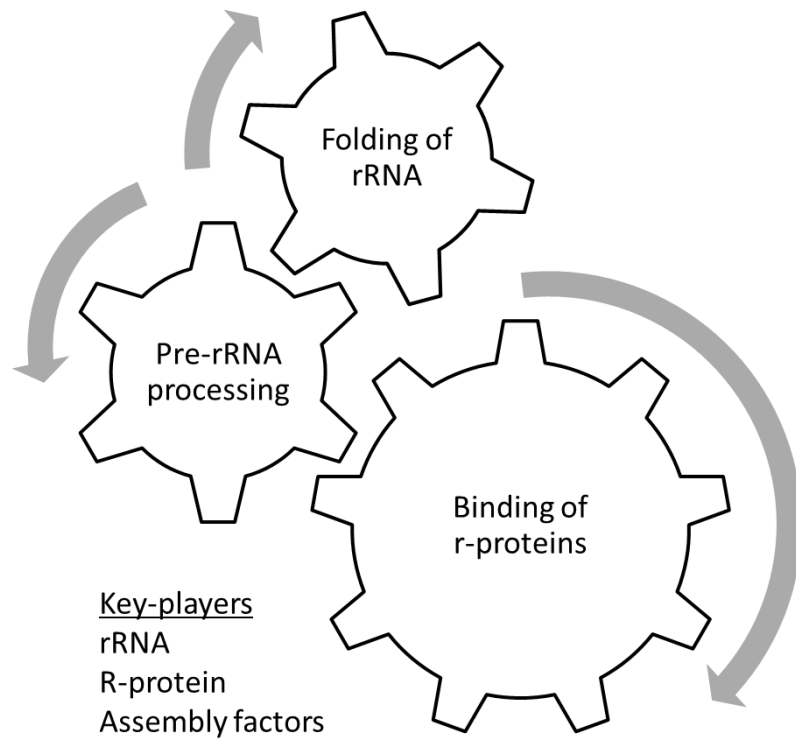
Fig. 1-3: Key processes and players in ribosome biogenesis *in vivo*.

Folding of rRNA, pre-rRNA processing and association of r-proteins occur concurrently. They drive each other and are driven by each other. The key players in this process are rRNA and r-proteins that become part of the mature ribosome, along with numerous *trans*-acting assembly factors that facilitate and drive the key processes.

1.2.1. Pre-rRNA Processing

Pre-rRNA in yeast is transcribed from a fraction of the 200 tandemly repeated rDNA genes. In the nucleolus, three of the four rRNAs (5.8S, 25S and 18S) are transcribed by Pol I as a single precursor called the 35S pre-rRNA (Fig. 1-4A). In the 35S pre-rRNA, the mature rRNAs are separated by two **I**nternal **T**ranscribed **S**pacers (ITS1 and ITS2) and are flanked by two **E**xternal **T**ranscribed **S**pacers (ETS1 and ETS2). 5S rRNA is transcribed separately by Pol III.

Once transcribed, the pre-rRNAs are modified by pseudouridylation and methylation, mediated by a number of snoRNPs (Fromont-Racine et al., 2003; Henras et al., 2008; Woolford and Baserga, 2013). Our understanding of these modifications is still incomplete; they are thought to fine-tune rRNA structure and folding. The 35S pre-rRNA undergoes a number of endonucleolytic cleavages and exonucleolytic processing events that result in the removal of the spacers in a complex pathway, illustrated in Fig. 1-4B and explained below.

The earliest steps of processing of the 35S pre-rRNA contained in the 90S particle are successive endonucleolytic cleavages at A_0 and A_1 sites that form the 32S pre-rRNA. The A_1 cleavage step generates the 5' end of the mature 18S rRNA. This is followed by cleavage at the A_2 site in ITS1 that separates the 20S pre-rRNA contained in the pre-40S particle and the $27SA_2$ pre-rRNA contained in the pre-60S particle. Thus, the A_2 cleavage step is a point of bifurcation in the pathway that enables independent maturation of the 40S and the 60S subunits. Following this, the 20S pre-rRNA is exported to the cytoplasm along with the assembly factors and r-proteins with which it is associated. In the cytoplasm, the final cleavage at site D generates the 3' end of the mature 18S rRNA.

Maturation of the pre-60S particle is more complex and has two alternative pathways that differ by 6-7 nucleotides in the 5' ends of mature 5.8S rRNA that they generate. While both forms of 5.8S rRNA are functional, ribosomes containing these different forms may translate different sets of mRNAs

(Schmitt and Clayton, 1993). The first pathway that occurs 85% of the time involves cleavage at the A_3 site in ITS1 resulting in the 27SA$_3$ pre-rRNA. This is followed by exonucleolytic processing of the 27SA$_3$ pre-rRNA until the B_S site, removing ITS1 and making the 27SB$_S$ pre-rRNA. This step, known as the 'A3 step', is one of the focus areas of Chapter 4. The other pathway involves cleavage at the B_L site to form the 27SB$_L$ pre-rRNA. These steps generate the 5' end of the mature 5.8S rRNA. Concurrently, the independently processed 5S rRNA is loaded onto the preribosome along with its protein partner (Zhang et al., 2007). Following this, both the 27SB pre-rRNA forms are cleaved at the C_2 site in ITS2. This is followed by exonucleolytic trimming of the 3' end of 5.8S rRNA and the 5' end of 25S rRNA to generate the mature rRNAs of the large subunit, which is exported to the cytoplasm.

Figure 1-4: Schematic representation of an rDNA repeat and steps in pre-rRNA processing
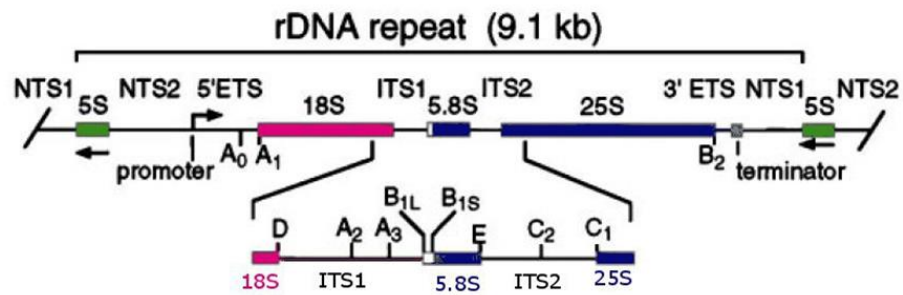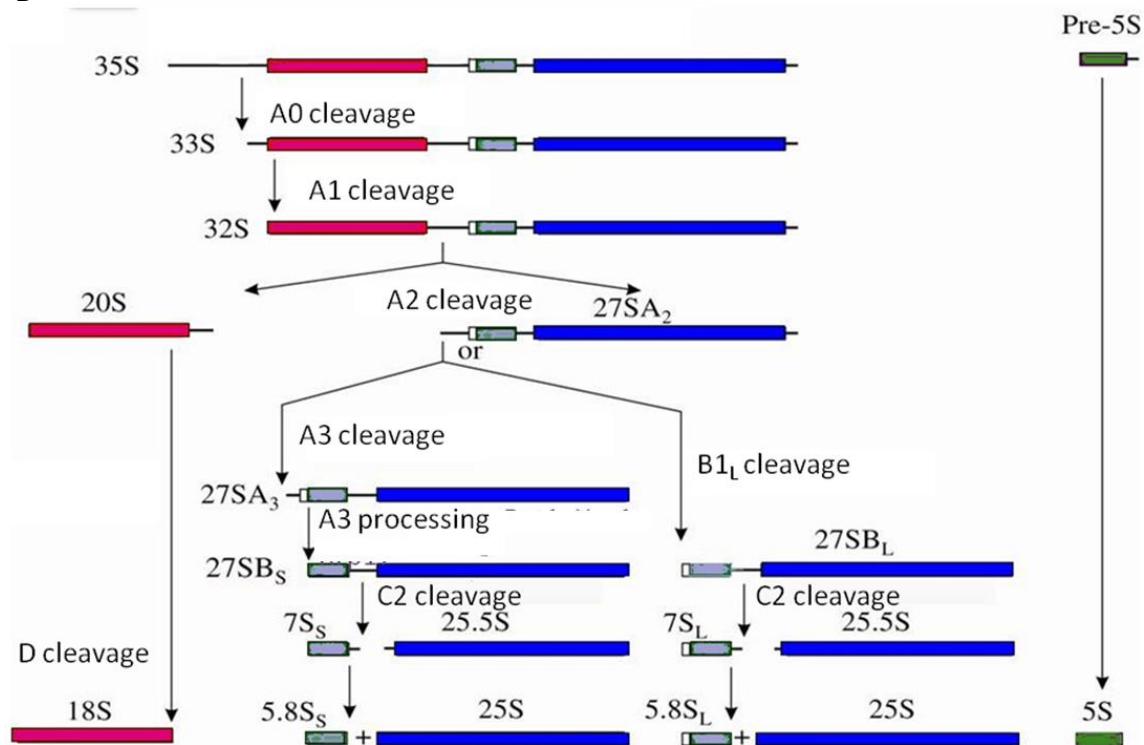
Fig. 1-4: Schematic representation of an rDNA repeat and steps in pre-rRNA processing.

A. rDNA repeat. The mature rRNA interrupted by the spacers are shown, along with the sites of cleavage and processing.

B. Pre-rRNA processing pathway. The small subunit-bound rRNA is shown in pink; the other rRNAs are destined to be part of the large subunit. The names of each pre-rRNA species are shown, and the steps used to process them are indicated.

1.2.2. rRNA folding

Considering the fact that RNA forms the catalytic core of the ribosome, understanding how rRNA folds into its precise functional structure is an important aspect of our understanding of ribosome biogenesis. Ribosomal RNA has served as an example for understanding the principles that dictate folding of long RNAs and how RNA folding drives the assembly of large RNPs.

As rRNA is transcribed from genomic repeats of rDNA, it begins to form local secondary structures (Fig. 1-5). Binding of proteins to these local structures and many other factors alter the schemes of RNA folding pathways. Long-range tertiary interactions are then established, leading to interdomain contacts and compaction of the large RNA structure. The internal loops and helix junctions thus formed can serve as hinges to aid in the movement of helices, to enable rearrangements. As a general theme, long RNAs seem to assemble from the periphery to the core, with important functional centers being assembled towards the end of the folding pathway. As is the case with other long RNAs, there is heterogeneity in the rRNA folding pathways and kinetics: some fraction of the RNA population acquires its final structures while the remaining fraction mis-folds into kinetically trapped intermediates (Woodson, 2008, 2015).

Many factors aid in the folding of rRNA into its final, functional structure. Among the most important of these factors are metal ions, cations, molecular crowding effects and various proteins that bind and dictate further folding events.

Emerging structural techniques have revolutionized our understanding of RNA folding. While single molecule techniques are useful in understanding the heterogeneous pathways of RNA folding, development in techniques like X-ray crystallography, small-angle X-ray scattering, nuclear magnetic resonance and cryo-electron microscopy have been utilized to study the folding of various RNAs. In my work, development of a new method to assay RNA structures is discussed in Chapter 5.

Figure 1-5: Secondary structure of large subunit ribosomal RNA in yeast *S. cerevisiae*

Saccharomyces cerevisiae
large subunit ribosomal RNA

A 3D-based secondary structure, generated by RiboVision.
Saved on 11/11/2015, 12:40:55

Fig. 1-5: Secondary structure of large subunit ribosomal RNA from yeast *S. cerevisiae*.

Different domains of 25S rRNA are colored in different colors and numbered. 5.8S rRNA is shown in brown and 5S rRNA is shown in a lighter shade of green and labeled. Image adapted from RiboVision website (http://apollo.chemistry.gatech.edu/RiboVision/)

1.2.3. Binding and tightening of proteins

Ribosomal proteins (r-proteins) and ribosome assembly factors bind to the newly transcribed rRNA, concomitant with nascent rRNA folding (Fig. 1-6). The binding of proteins in turn affects both rRNA folding and pre-rRNA processing as shown in Fig. 1-3. The roles of both r-proteins and assembly factors are discussed separately in the following sections.

Because assembly factors are only associated with the assembling ribosome and not with the mature ribosome, they have been used to affinity purify specific pre-ribosomal intermediates in the maturation pathway, as shown in Fig. 1-7. Despite the fact that it is challenging to identify assembly factors that exclusively associate with a particular intermediate in ribosome assembly, this method has been used to analyze the composition of preribosomal intermediates extensively.

Figure 1-6: Schematic representation of proteins binding to newly transcribed pre-rRNA
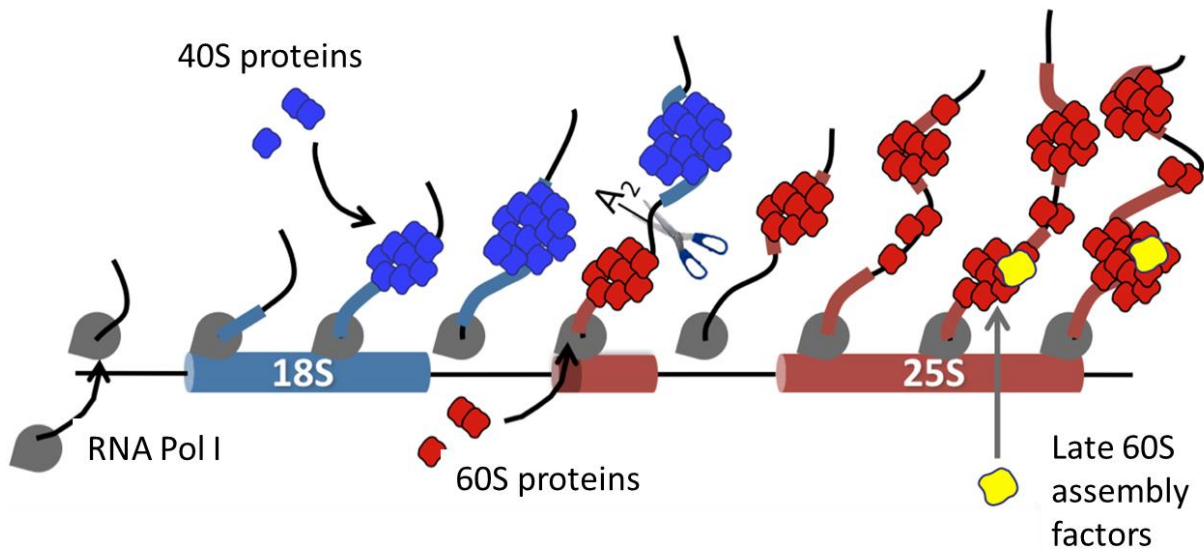
Fig. 1-6: Schematic representation of proteins binding to newly transcribed pre-rRNA.

The basic rDNA transcription unit is shown as cylinders and sticks. Pre-rRNA is produced by RNA Pol I in the nucleolus. 40S subunit r-proteins and assembly factors (blue) and 60S subunit r-proteins and assembly factors (red) start binding the newly synthesized pre-rRNA. Endonucleolytic cleavage at the A2 site then separates the assembly of the large subunit from that of the small subunit. More assembly factors (yellow) associate with the nascent ribosome later during maturation, enabling further rearrangements.

Figure 1-7: Various preribosomal intermediates in the maturation of the ribosome
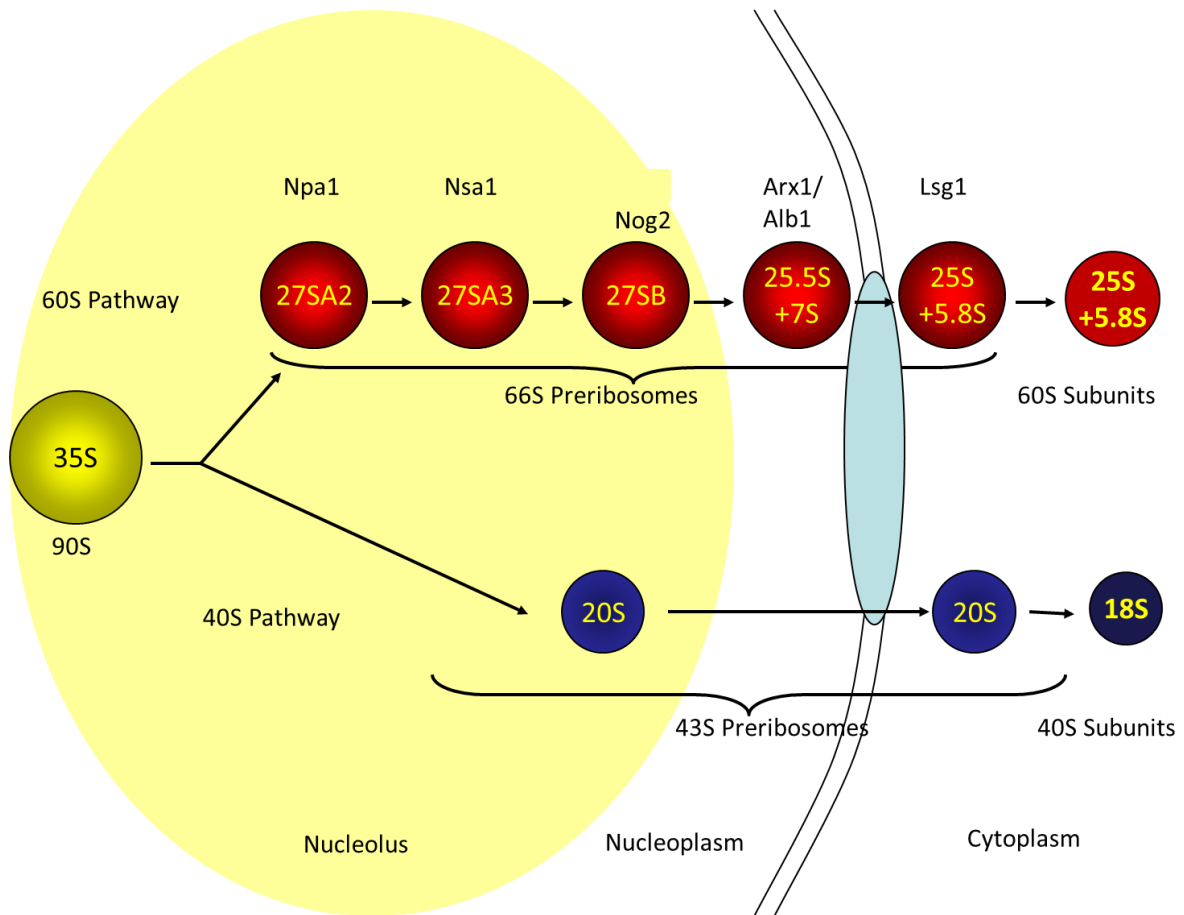
Fig. 1-7: Various preribosomal intermediates in the maturation of the ribosome.

Shown here is schematic representation of the various cellular compartments and intermediates in the maturation of the ribosome. The divergence of the 60S and the 40S subunit maturation pathways is represented. Assembly factors that are typically used as baits for affinity purification of each particle are shown above the 60S preribosomal intermediates. Note that this representation does not necessarily indicate that the assembly factors shown are unique to that particular preribosomal intermediate.

1.3.1. Roles of ribosomal RNA in ribosome biogenesis

Various pre-rRNA processing steps have been canonically used as landmarks for ribosome biogenesis. It is a well-established notion that accurate rRNA folding is a consequence of proper progression of consecutive steps in assembly. But studies of direct roles played by rRNA itself in the biogenesis of the subunits are less common. Since ribosomal DNA is present in multiple copies in the genome, paucity of our knowledge about the functions of rRNA may be attributed to the lack of robust tools to make and assay mutations in ribosomal DNA. On one hand, it is not surprising that mutations in ribosomal DNA would cause deficient assembly of ribosomes, since ribosomal RNA forms the structural core to which r-proteins are bound, in addition to forming the catalytic core of the ribosome. On the other hand, eukaryotic ribosomal RNA has spacers and expansion segments in addition to the universally conserved rRNA core. A question that has always intrigued researchers is, whether these eukaryote-specific insertions are indeed necessary for ribosome biogenesis. Pioneering studies by the Gerbi and Peculis labs, and others, have addressed this and shown that some of these eukaryotic regions are necessary for proper ribosome biogenesis (Cote and Peculis, 2001; Gerbi, 1996; Peculis and Greer, 1998). This thesis aims to expand on the notion that sections of ribosomal RNA play specific roles in the biogenesis of the ribosome. Expansion segments are the primary subject of analysis in Chapter 2 and the neighborhood around internal transcribed spacer 2 (ITS2) is dealt with in Chapter 4.

1.3.2. Roles of r-proteins in ribosome biogenesis

Eukaryotic ribosomes contain 79-80 r-proteins. Our lab has performed a comprehensive analysis of ribosome assembly defects observed when a wide range of r-proteins are depleted individually (Gamalinda et al., 2014; Gamalinda and Woolford, 2015). Similar to their prokaryotic counterparts, r-proteins associate with the nascent eukaryotic ribosome in a hierarchical manner, even though there are multiple, parallel pathways of assembly. The association of r-proteins with the preribosome gets tighter as assembly progresses, perhaps concomitant with the nascent ribosome itself becoming more stable. In addition, studies from our lab have established that assembly of the large ribosomal subunit begins at the convex solvent side, followed by the polypeptide exit tunnel and then finally the central protuberance. The final steps of ribosome assembly seem to occur around regions that are important for ribosome function. This is consistent with the fact that many mutations that are prevalent in ribosomopathies occur in these proteins that assemble later in the pathway. Before the newly-made large subunits enter the translating pool of ribosomes, they pass through checkpoints to ensure that they can function accurately (de la Cruz et al., 2015; Woolford, 2015).

While we have a catalog of phenotypes corresponding to the absence of each LSU r-protein, researchers are particularly becoming more interested in illuminating the significance of specific molecular interactions formed by parts of ribosomal proteins with other proteins and rRNA. Of late, research in the field is becoming specifically inclined towards understanding the functions of eukaryote-specific, often disordered, tails or extensions of r-proteins and how they may serve to recruit the corresponding r-protein to the assembling ribosome, or form functionally important interactions with other components of the preribosome (Gamalinda and Woolford, 2014; Stelter et al., 2015) (Tutuncuoglu et al., manuscript in review). This thesis includes a detailed analysis on molecular interactions of one such exemplary r-protein, rpL5. (Chapter 3)

1.3.3. Roles of assembly factors in ribosome biogenesis

As mentioned before, ribosome biogenesis *in vivo* requires around 200 assembly factors that are not part of mature ribosomes (Henras et al., 2008; Woolford and Baserga, 2013). The assembly factors perform a plethora of functions and are of various types including but not limited to chaperones and scaffolding proteins, GTPases, RNA helicases, endo- and exo-nucleases, proteins involved in recycling and snoRNPs involved in base modifications (pseudouridylation and methylation). These assembly factors were initially identified using genetic screens and tools (Ripmaster et al., 1992). Further identification and characterization of assembly factors has been driven by modern advances such as high throughput mass spectrometry combined with the capability to purify specific assembly intermediates by affinity purification (Harnpicharnchai et al., 2001; Rappsilber, 2011; Trakselis et al., 2005; Warner, 2001). Thus, we are now capable of classifying assembly factors based on the specific steps of pre-rRNA processing in which they participate, and a table corresponding to such phenotypes of assembly factor depletions can be found in (Woolford and Baserga, 2013). This permits a comprehensive examination of all the factors involved in a particular step, yielding detailed mechanistic insights into a step (Panse and Johnson, 2010).

1.4. Why is it important to study ribosome biogenesis?

- In a rapidly growing yeast cell, 60% of total transcription is devoted to ribosomal RNA, 50% of RNA polymerase II transcription and 90% of mRNA splicing are devoted to r-proteins (Noller, 2012; Warner, 1999).   Mechanistic insights into such an energy-consuming process are still lacking.

- Owing to their role in translation, ribosomes are important in regulating gene expression, which makes understanding their biogenesis imperative. (Green and Noller, 1997)

- Ribosomes themselves and the process of their biogenesis show a high degree of evolutionary conservation, both structurally and functionally. Also, the ribosome is a ribozyme, as the peptidyl transferase activity, which is the crux of ribosome function, is performed by rRNA (Moore and Steitz, 2011; Steitz and Moore, 2003). Hence, many pioneers of the field surmise that ribosomes and their biogenesis are our clues to the RNA world and the mechanisms thereof (Noller, 2012).

- Ribosomes exemplify a ribonucleoprotein machine and many parallels can be drawn based on the principles underlying biogenesis for other such RNP machines such as the spliceosome.

- These studies are crucial in medicine as they relate to antibiotic resistance (Tenson and Mankin, 2006) and a variety of ribosomopathies (Danilova and Gazda, 2015; Freed et al., 2010; Scheper et al., 2007). Ribosome biogenesis has been shown to be upregulated in malignant conditions; hence ribosomes are the target of a large body of anti-cancer drug related research (Chan et al., 2011; Danilova and Gazda, 2015; Hannan et al., 2011; Montanaro et al., 2008; Ruggero and Pandolfi, 2003). On the other hand, defects in a crucial process such as ribosome biogenesis, when not monitored, can themselves trigger cancer. A mechanistic understanding of ribosome biogenesis is crucial in order to use these observations in therapy.

2. Eukaryote-specific rRNA expansion segments play vital roles in ribosome biogenesis

2.1. Background

A universal core secondary structure for ribosomal RNA (rRNA) has been identified across all kingdoms of life (Clark et al., 1984; Gutell et al., 1993; Veldman et al., 1981). However, eukaryotic rRNA has extra blocks of sequences relative to that of prokaryotic rRNA, which have been designated as "expansion segments" (ES). These expansion segments are interspersed throughout the various domains of the rRNA secondary structure core at specific, conserved sites (Fig. 2-1). They exhibit a striking degree of variability in multiple respects: (1) not all expansion segments are found in all species, and (2) they vary in their length and sequence both within and among different species; they even vary between different rRNA repeats of the same organism (Gonzalez et al., 1985). ES also have been referred to as variable regions and divergent domains as discussed in (Gerbi, 1996). In eukaryotes, there are 12 expansion segments in the small subunit rRNA (ES_S) and 41 in the large subunit rRNA (ES_L) compared to *E.coli* rRNA, which is often used as the paradigm for prokaryotic rRNA, although only a subset of these are present in any given eukaryote species. Though expansion segments have been a continued focus of research interest, their inherent variability and the limited availability of robust systems to study ribosomal RNA mutations have impeded our understanding of the functions of expansion segments.

In addition to high sequence variability, expansion segments exhibit internal sequence repetition and cryptic sequence simplicity, with a bias for certain tri- and tetra- nucleotides (Hancock and Dover, 1988). The GC base composition bias of expansion segments also contributes significantly to base composition differences observed in rRNAs of different species (Ware et al., 1983). While methyl groups are present in the universal core, they do not appear to be present in expansion segments (Wakeman and Maden, 1989). The secondary structure of ES exhibits less variability compared to the sequence variability and may reflect evolutionary constraints (Ruiz Linares et al., 1991). Thus, although they are similar in their overall topology, owing to their variability in sequences, expansion segments cannot be readily superimposed from one organism to the next.

Figure 2-1: Ribosomal RNA expansion segments of the large ribosomal subunit
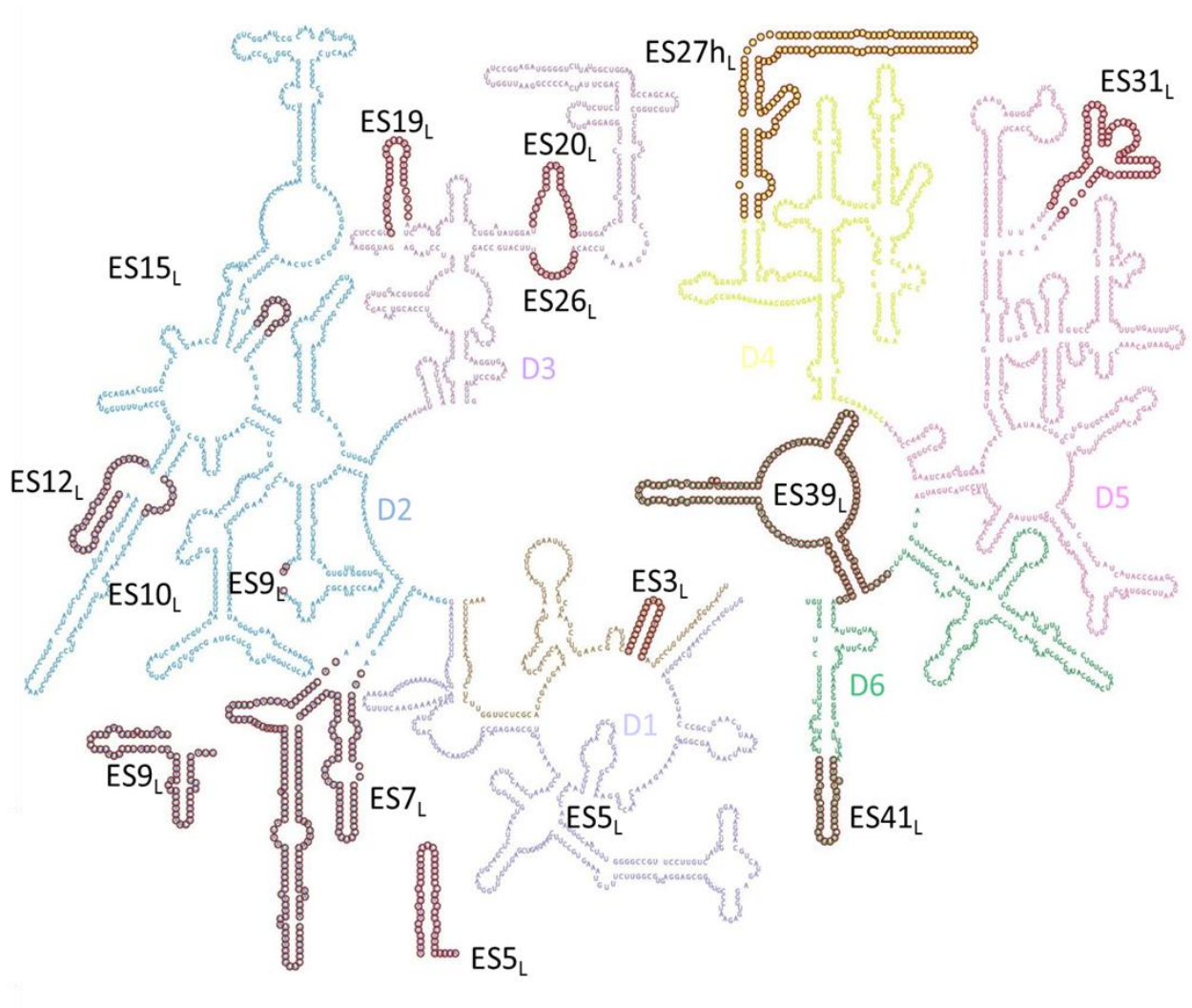
Fig. 2-1: Ribosomal RNA expansion segments of the large ribosomal subunit.

Secondary structure of *Saccharomyces cerevisiae* large subunit ribosomal RNA (rRNA) is shown. Different domains are distinguished by different colors. The expansion segment deletions studied are highlighted by maroon circles and labeled.

The recent surge in the availability of high resolution cryo-EM and crystal structures of eukaryotic ribosomes (Anger et al., 2013; Armache et al., 2010a; Ben-Shem et al., 2011; Jenner et al., 2012; Spahn et al., 2001; Taylor et al., 2009) has considerably improved our understanding of expansion segments, yielding some interesting insights. Expansion segments are responsible for a majority of the 40% increase in the size of ribosomes from prokaryotes to eukaryotes. (Gerbi, 1996; Jenner et al., 2012). In addition, a small subset of expansion segments can explain most of the size difference between yeast and metazoan rRNA. Indeed, their size and the branching pattern of their helical stems seem to increase progressively in higher eukaryotes (Fig. 2-3). In general, eukaryotic rRNA expansion segments of the large ribosomal subunit are located predominantly in two clusters on the solvent side, although they are distributed across the different domains of secondary structure (Fig. 2-2 and 2-3). Importantly, they do not directly interrupt the functional centers, including the subunit interface (Anger et al., 2013; Armache et al., 2010a; Ben-Shem et al., 2011; Gerbi, 1996). Thus, ribosomes of higher eukaryotes have been described as having a conserved core, with a shell consisting of a flexible outer layer formed by the helical insertions and extensions of the expansion segments (Melnikov et al., 2012). Their clustering on the solvent-exposed surface of the ribosome potentially enables a multitude of molecular interactions by these ES to modulate ribosome assembly and function.

Since ribosomal RNA has often been used as a paradigm for evolutionary studies, the origins of expansion segments have always intrigued researchers. It has been suggested that that ES evolved from insertions and selection of prokaryotic rRNA sequences, since *E.coli* rRNA permitted insertions at 35 sites, most of which coincided with known sites of expansion segments in eukaryotes. (Yokoyama and Suzuki, 2008).

Figure 2-2: Pymol representation of the large subunit rRNA showing expansion segments
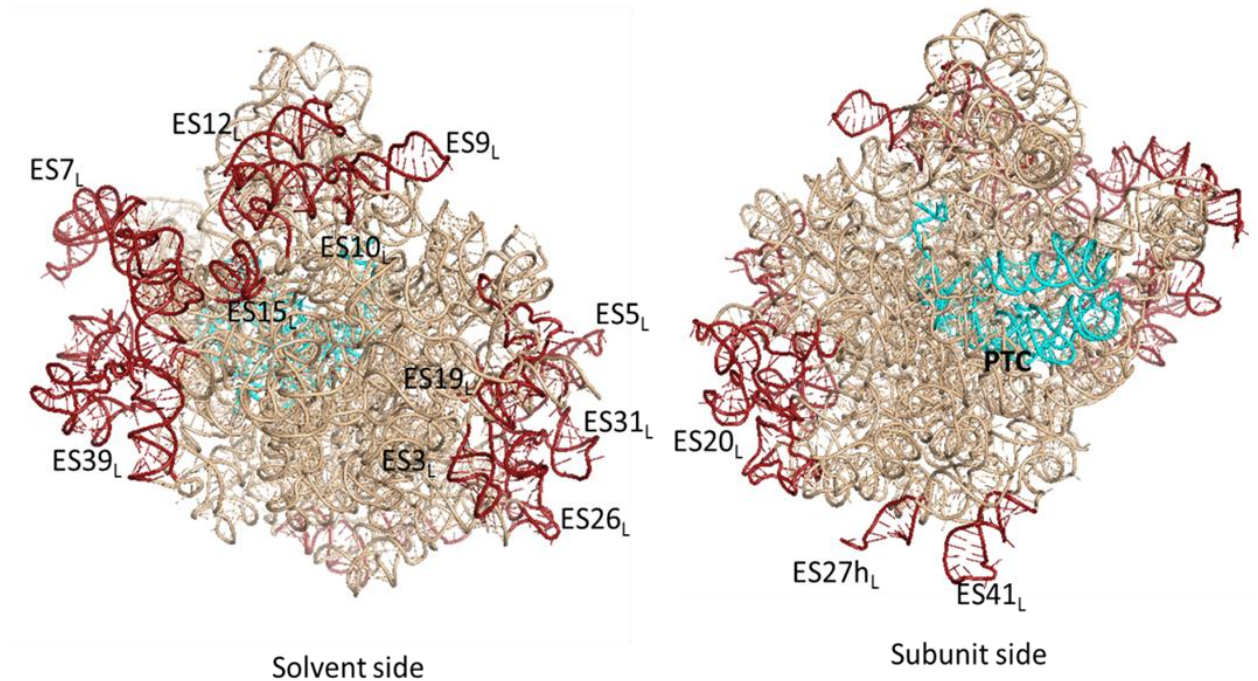
Fig. 2-2: Pymol representation of the large subunit rRNA showing expansion segments.

Expansion segment deletions studied are highlighted in maroon and labeled. The peptidyl transferase center (PTC) is shown in cyan. Both the solvent side and subunit side (obtained after an 180° rotation of the solvent side) are shown.

Figure 2-3: Expansion segments progressively increase in size and complexity in eukaryotes
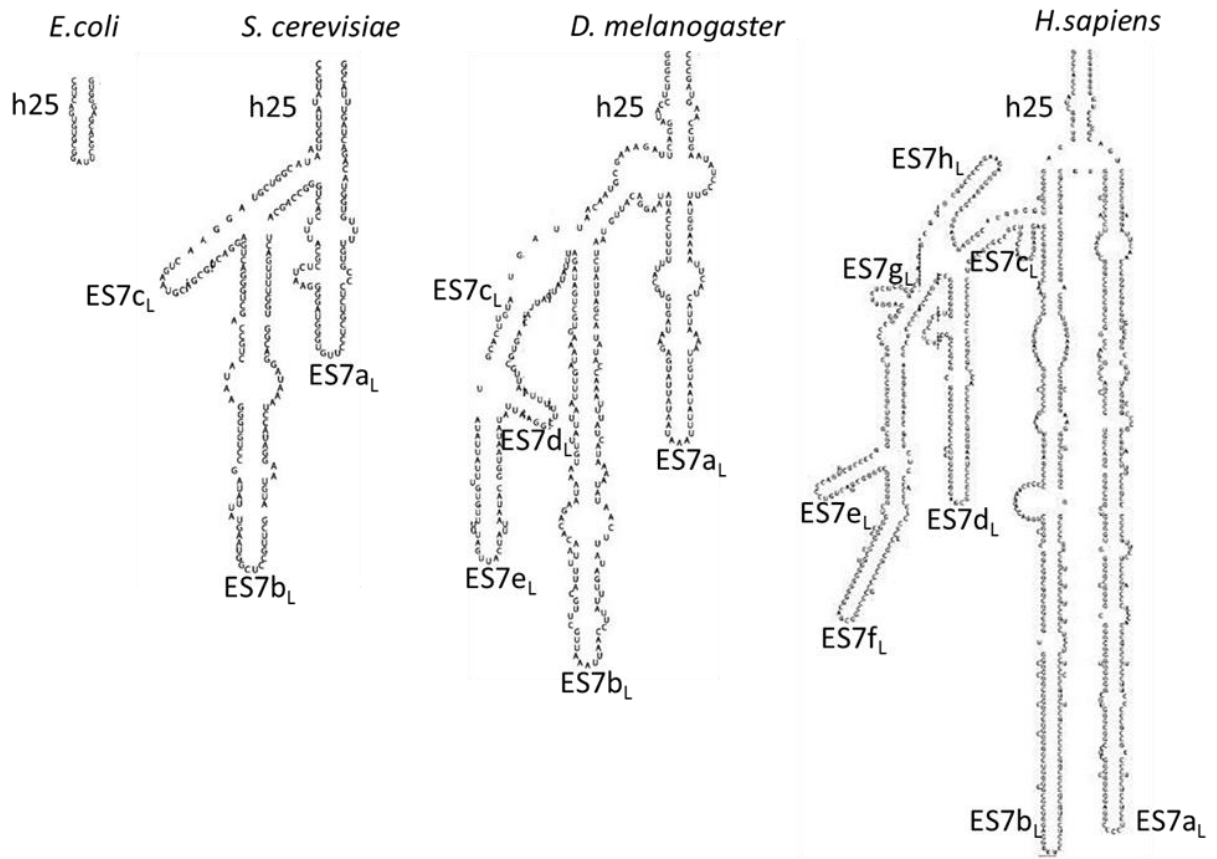
Fig. 2-3: Expansion segments progressively increase in size and complexity in eukaryotes.

Helix 25 (h25) is shown as an example to demonstrate increase in sequence length (not to scale) and the number of helical branches of ES7$_L$, from *E.coli* through *H.sapiens*.

2.1.1. Do expansion segments have essential functions?

Perhaps the most interesting question about expansion segments pertains to their function. It has not been determined fully if ES are innocuous, dispensable insertions that arose during the course of evolution, or instead, whether they have specific functions in the cell. The high degree of variability observed in expansion segment sequences and their observed location away from the functional centers of ribosomes suggests that they may not directly participate in conserved aspects of translation.

Various studies have been carried out to investigate if expansion segments might have roles in processes such as ribosome biogenesis or function. On one hand, replacing the $ES19_L$ region of yeast large subunit rRNA with *E.coli* or mouse ES sequences was tolerated without apparent loss of function (Musters et al., 1991). Also, insertions in the $ES5_L$ and $ES9_S$ regions of yeast and insertions near the 3' end of the large subunit rRNA in *Tetrahymena* were judged as functional (Musters et al., 1990; Musters et al., 1989). In contrast, an insertion upstream of the intron in the large subunit rRNA of *Tetrahymena* was not tolerated, and a deletion of *Tetrahymena* $ES27_L$ prevented growth (Sweeney et al., 1994). Interestingly, the $ES27_L$ deletion could be rescued by replacement with $ES27_L$ sequences from another organism, but not with random sequences, leading the authors to hypothesize that these regions share an essential function that is not reflected in their primary sequences. Further evidence that expansion segments might carry out specific functions was revealed by deletion mutagenesis of yeast $ES7_L$ and $ES27_L$. The larger deletion mutations of these expansion segments were lethal due to defects in ribosome biogenesis (Jeeninga et al., 1997). For those expansion segments that are essential, several studies have supported the notion that their secondary structure is more important for their function than their sequence (Jeeninga et al., 1997; Sweeney et al., 1994).

An interesting function for expansion segments arises from their complementarity with some mRNAs, raising the possibility that expansion segments might affect the translation of those

27

complementary mRNAs. Furthermore, it has been suggested that expansion segments could contribute to the functional heterogeneity of *Plasmodium* ribosomes (Waters et al., 1995). More recent structural studies have identified other potential roles for expansion segments: 1) two expansion segments form additional intersubunit bridges in yeast, and 2) expansion segments have been suggested to facilitate access of translation factors – $ES6_S$ near both the mRNA entry and exit sites, and $ES27_L$ near the polypeptide exit tunnel (Spahn et al., 2001). Further, $ES24_L$ was proposed to play a role in co-translational protein localization (Halic et al., 2004). Despite the growing body of evidence indicating the importance of expansion segments in ribosome biogenesis and function, a thorough deletion mutagenesis survey that could yield valuable insights into the functions of expansion segments, has yet to be done.

Here, we systematically investigated the functions of 14 expansion segments of the large subunit of *S.cerevisiae* ribosome, by deletion mutagenesis. We found that twelve expansion segments studied are necessary for optimal growth, suggesting that the majority of expansion segments play indispensable functions. The steady-state levels of mature 25S rRNA are severely diminished in all of the mutants that exhibit a growth deficiency, indicative of improper ribosome biogenesis of mature 25S rRNA. We further categorize expansion segments into early nucleolar, middle and late nuclear phenotypic groups, based on their pre-rRNA processing phenotype, and point out the possibility of distinct neighborhoods in the assembling ribosome being involved in distinct steps of ribosome biogenesis. We also discuss potential models by which eukaryote-specific elements on the ribosome might have co-evolved to perform functions in ribosome biogenesis. Taken together, our data indicate that many expansion segments are indispensable, demonstrate potential functions for expansion segments in ribosome biogenesis, and explain some of their distinct roles in ribosome biogenesis.

2.2. Results

2.2.1. Description of ES mutants and the system to assay their phenotype

The presence of around 200 copies of rDNA repeats in the yeast genome has made analysis of rDNA mutants challenging. In order to assay the *in* vivo phenotype of ES deletions, we used a strain carrying a temperature sensitive mutation in a subunit of Pol I (NOY504) (Nogi et al., 1993) We transformed this strain with a plasmid (pWL160) (Cole and LaRiviere, 2008; Liang and Fournier, 1997) containing an rDNA unit driven by Pol II from a *GAL* promoter. At the permissive temperature, endogenous chromosomally-derived WT rRNA is made. But at the restrictive temperature, the transcription of chromosomal rDNA is shut off and the only source of rRNA to the cell is the rRNA derived from the plasmid (pWL160) (Fig. 2-4). This plasmid contains an oligonucleotide tag within ES5$_L$ of 25S rRNA and another tag within 18S rRNA, in order to differentiate plasmid-derived rRNA from the residual endogenous rRNA.

We introduced 14 ES deletion mutations into the plasmid-borne 25S rDNA and assayed for each of their effects on ribosome biogenesis. Although reported nucleotide definitions of ES can vary (Anger et al., 2013; Armache et al., 2010a; Gerbi, 1996; Taylor et al., 2009), the exact ES deletions examined in this study are indicated in Fig. 2-18 and highlighted in Fig. 2-1. In some cases where an ES deletion involved truncating a helix in the middle, we introduced tetraloops to maintain the stability of the helix and minimize secondary effects. With the exception of ES24$_L$ and ES4$_L$ (which is formed by the proximal stem comprised of both 5.8S and 25S rRNA), we have examined nearly all of the ES of the large subunit rRNA in yeast (Cote and Peculis, 2001; Halic et al., 2004; Peculis and Greer, 1998). Technical limitations also prevented us from studying ES27$_L$ in its entirety; hence we studied a partial deletion of ES27$_L$ as marked in Fig. 2-1, denoted henceforth as ES27h$_L$.

Figure 2-4: System used for rDNA mutagenesis
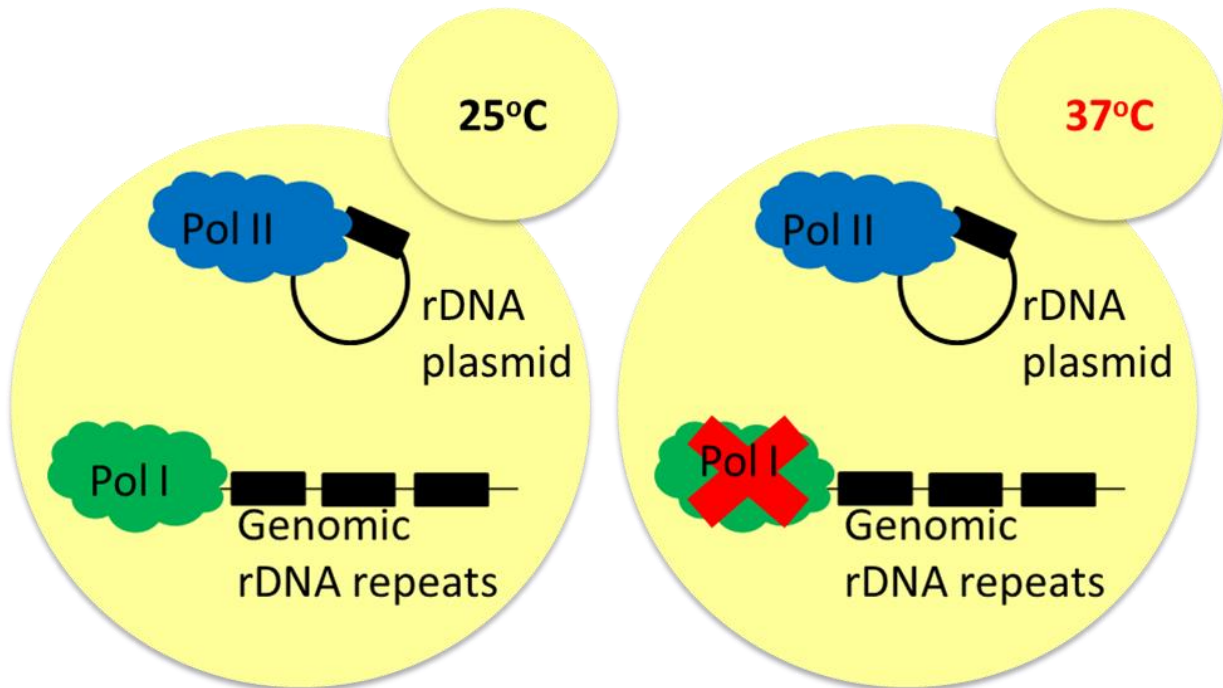
Fig. 2-4: System used for rDNA mutagenesis.

Illustration of the yeast strains and the mechanism of endogenous rDNA transcription shut off showing both the permissive temperature (left) and the restrictive temperature conditions (right). rDNA transcriptional unit is shown as black boxes.

To specifically assay the efficacy of turning off chromosomal rDNA transcription and investigate the levels of plasmid-derived pre-rRNA, we used the no rDNA (empty vector) control and the ES3Δ_L mutant that contained a deletion in the region assayed by primer extension, such that we could differentiate mutant from endogenous pre-rRNA by size (and hence, electrophoretic mobility). We assayed 27S pre-rRNA levels by primer extension at different time points after shifting to the restrictive temperature (Fig. 2-5). We found that the levels of genome-derived rRNA progressively diminished while the mutant plasmid-derived pre-rRNA was stably expressed over a 24 hour period. Following this, we decided to use a 6 hour shift to the restrictive temperature in order to assay phenotypic effects of all further ES deletions. While there is residual pre-rRNA from the endogenous WT rDNA transcription even after the 6 hour shift, we also wanted to minimize secondary effects arising from prolonged shift to the restrictive temperature.

Figure 2-5: Levels of pre-rRNAs after shifting to the restrictive temperature
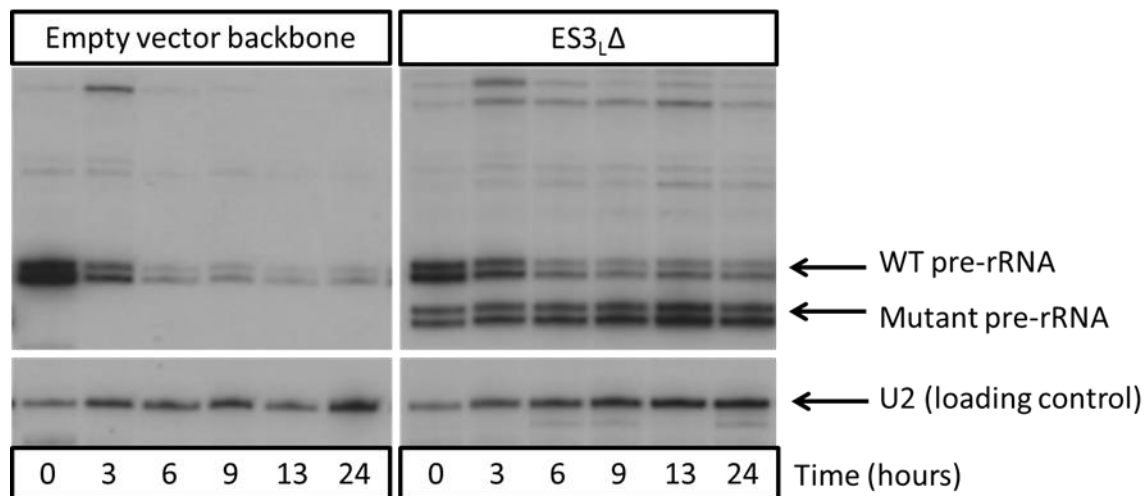
Fig. 2-5: Levels of pre-rRNAs after shifting to the restrictive temperature.

We used the ES3$_L$Δ mutant that has a deletion in the region being reverse-transcribed using the ITS2B oligonucleotide primer, resulting in a shorter cDNA product. Levels of endogenous WT pre-rRNA and plasmid derived mutant pre-rRNA that is shorter in size (right panel, shorter) were measured by primer extension assay, using total RNA extracted after multiple time points after shifting to the restrictive temperature. U2 snRNA is the loading control.

2.2.2. Most ES_L are necessary for optimal growth

In order to address whether ES are innocuous, dispensable eukaryotic insertions in rRNA, or if they are essential, we first assayed for the viability of the 14 ES$_L$ deletion mutants by spotting serial dilutions of log phase cultures onto solid growth media (Fig. 2-6 and see also, Fig. 2-7). At the permissive temperature (left panels) when the chromosome-derived WT rRNA is expressed, all the mutant strains grow optimally as expected. When grown at the restrictive temperature (right panels), 12 of the 14 ES deletion mutants exhibited a growth defect compared to the WT control (second row of spots in each panel). The growth phenotype of these 12 ES$_L$ deletion mutants more closely resembled the no rDNA control (first row of spots in each panel), presumably resulting from the pre-existing pool of ribosomes and incomplete shut off of Pol I. Hence, we refer to them as 'lethal' ES mutants or 'essential' ES henceforth. Thus, all the ES$_L$ tested, except ES19$_L$ and ES27h$_L$ are necessary for viability, suggesting that most ES$_L$ play indispensable functions in the cell.

Figure 2-6: Spotting assay to demonstrate growth defects in ES mutants
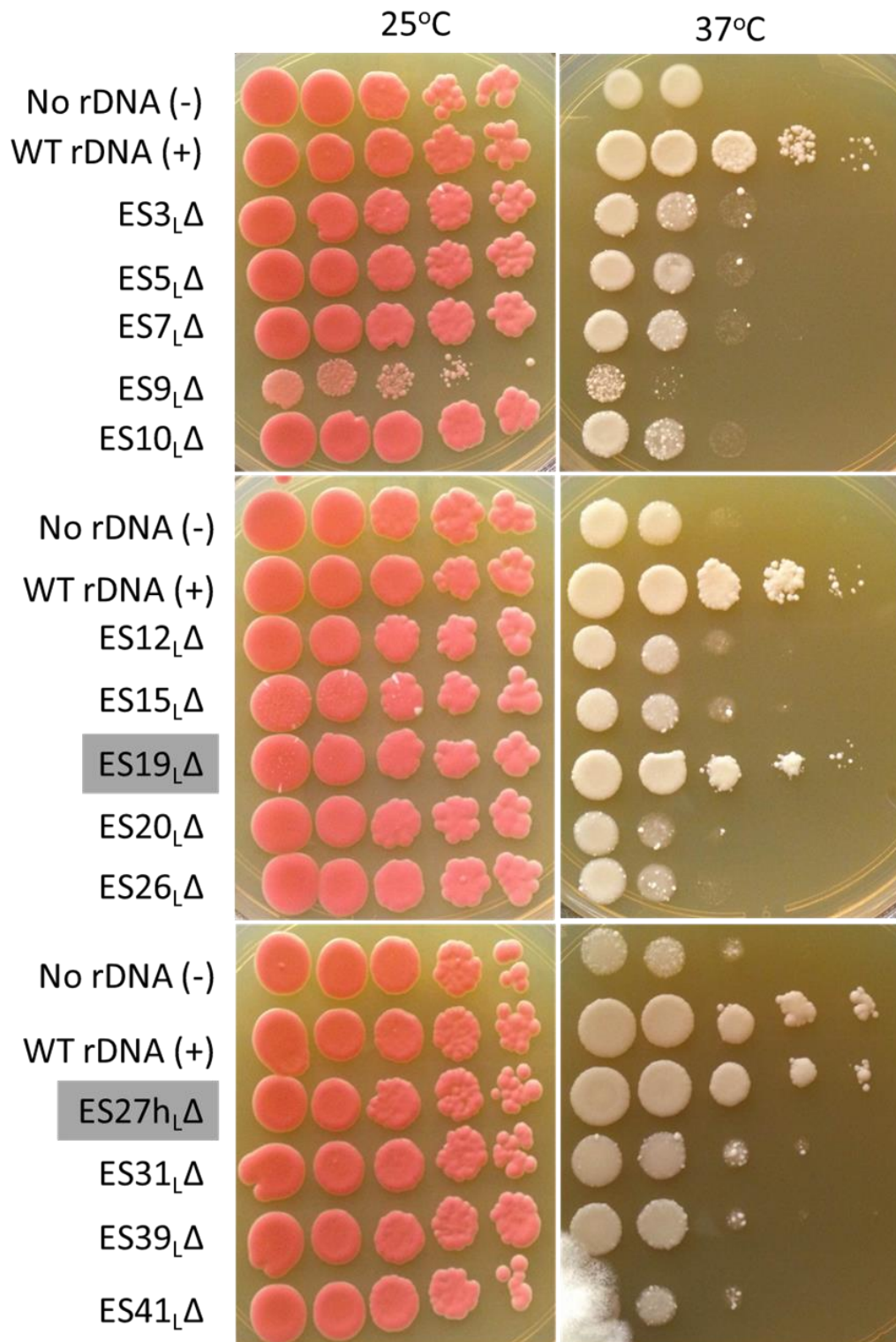
Fig. 2-6: Spotting assay to demonstrate growth defects in ES mutants.

Serial dilutions of log phase yeast cultures were spotted onto solid medium and grown either at the permissive temperature (25°C, left panels) or at the restrictive temperature (37°C, right panels). Empty vector ("No rDNA") and WT controls ("WT rDNA") are indicated. The non-essential ES are highlighted with gray labels. Note that a slightly less dense culture of $ES9_L$ was used. Similar results were observed across at least three independent biological replicates.

Figure 2-7: Streaking assay to demonstrate growth defects in ES mutants
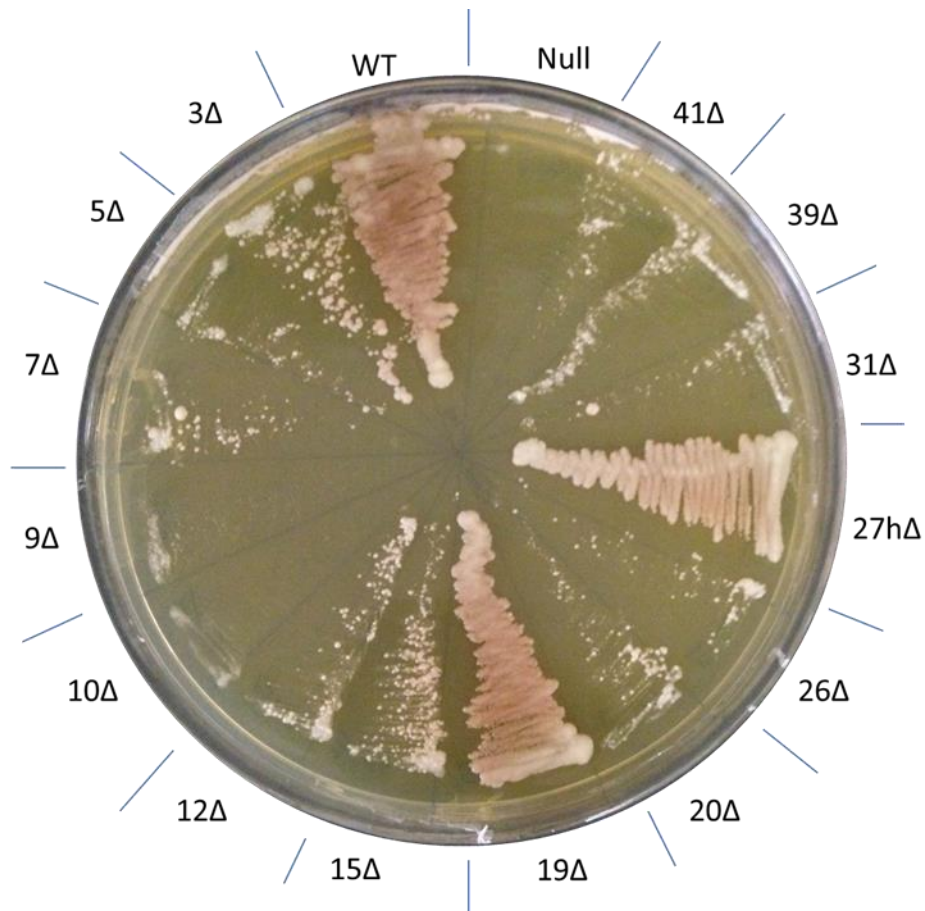
Fig. 2-7: Streaking assay to demonstrate growth defects in ES mutants.

Consistent with the results from the spotting assay (Fig. 2.6), investigating viability by streaking out on solid media shows that all ES deletion mutations, except those of ES19$_L$ and ES27h$_L$, are lethal.

2.2.3. Essential ES$_L$ and ES27h$_L$ function in 60S biogenesis

Since ES are eukaryote-specific, we hypothesized that these extra rRNA elements may have evolved to perform eukaryote-specific functions related to the ribosome, including eukaryotic ribosome biogenesis, nuclear export of nascent ribosomal subunits and/or eukaryote-specific functions in translation. Since defects in ribosome biogenesis will mask any further defects in translation in these mutants, we decided to begin assaying for ribosome biogenesis-related functions. These are described in detail below. In order to potentially reveal translation defects in the non-essential mutants, we also assayed the effects of translation-inhibiting drugs on the growth of the non-essential ES19Δ_L and ES27hΔ_L mutants. However, even the WT strain failed to grow in the presence of these drugs at the restrictive temperature (Fig. 2-8). Thus, technical limitations of this assay precluded us from assaying for translation defects in the non-essential ES$_L$ mutants.

Figure 2-8: Attempts to assay defects in translation in non-lethal ES$_L$ mutants

A

25°C

YEPGal

+ Erythromycin   + Cycloheximide   + Paromomycin

+ Anisomycin   + Neomycin   + Hygromycin

B

37^oC

YEPGal

+ Erythromycin

+ Cycloheximide

+ Paromomycin

+ Anisomycin

+ Neomycin

+ Hygromycin
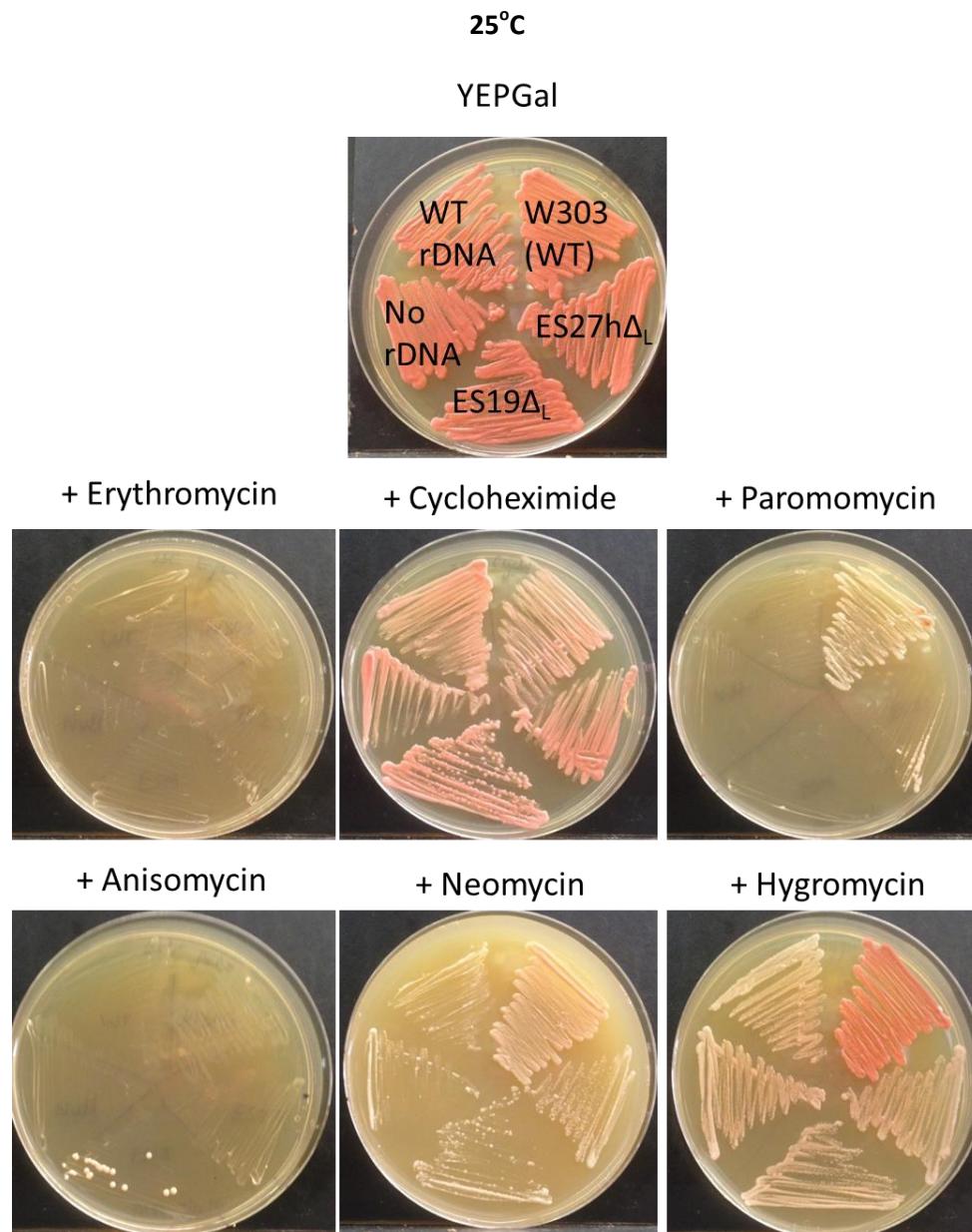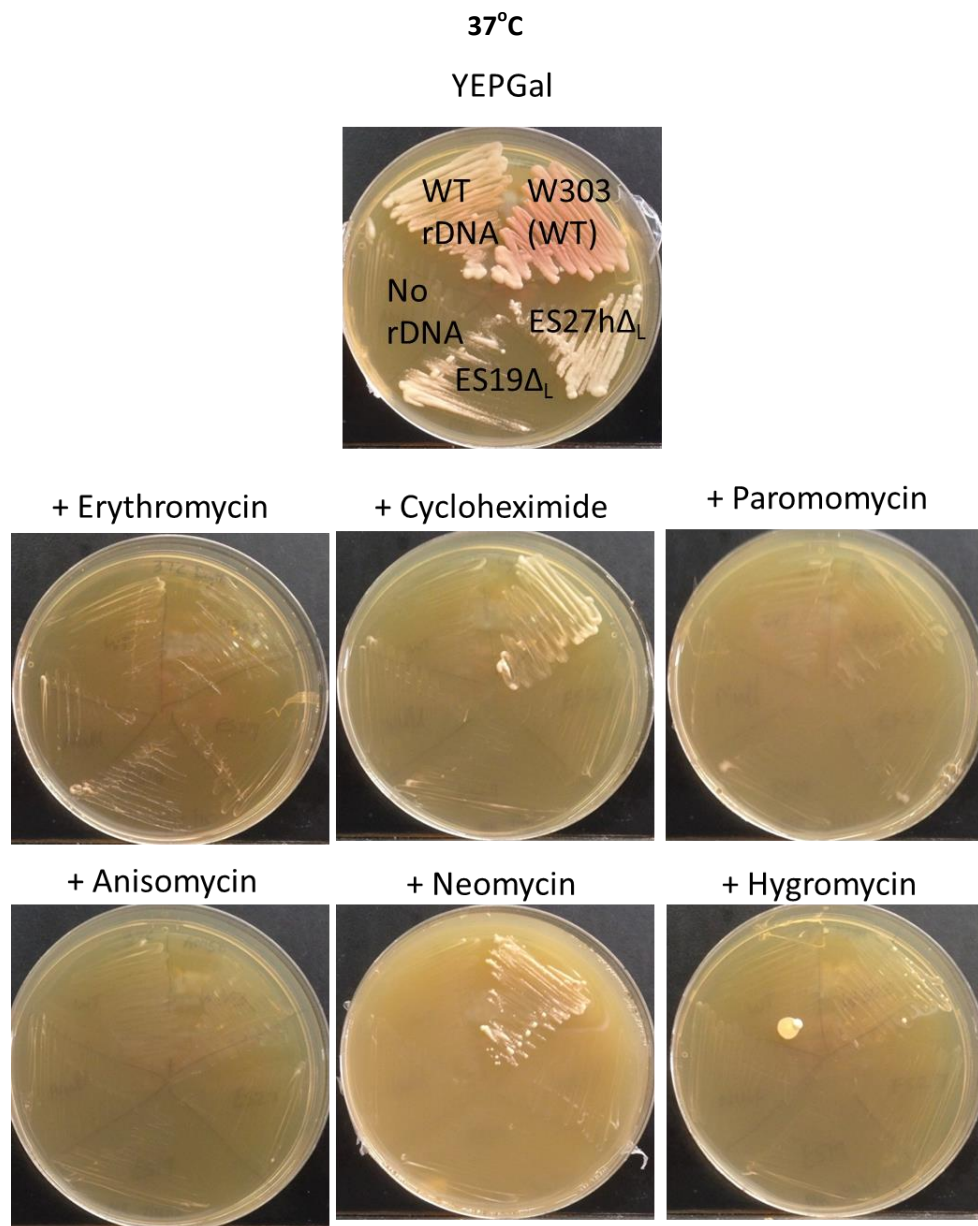
Fig. 2-8: Attempts to assay defects in translation in non-lethal ES$_L$ mutants.

Wild type strain (W303), Nomura strain with the PolI temperature sensitive mutation carrying either WT rDNA plasmid (WT rDNA), rDNA plasmid with ES19Δ_L mutation, rDNA plasmid with ES27hΔ_L mutation, or no rDNA (no rDNA) were streaked out on YEPGal solid media and grown at either 25°C (A) or at 37°C (B) in the presence of various translation inhibitor drugs. Plates were photographed after 5 days. The following concentrations of drugs were used:

- Erythromycin: 3mg/ml
- Cycloheximide: 0.1 µg/ml
- Paromomycin: 2mg/ml
- Anisomycin: 15 µg/ml
- Neomycin: 5mg/ml
- Hygromycin: 20 µg/ml

We sought to identify defects in ribosome biogenesis in representative mutants using sucrose gradient centrifugation to display polysomes and free ribosomal subunits. ES5Δ_L (Fig. 2-9D) and ES12Δ_L (Fig. 2-9E) were chosen as representatives for essential ES, and ES19Δ_L (Fig. 2-9B) and ES27hΔ_L (Fig. 2-9C) were chosen as representatives for non-essential ES. These strains, along with a WT control (Fig. 2-9A), were grown at the permissive temperature, then shifted to the restrictive temperature for 6 hours prior to preparing extracts for gradient analysis. It should be noted under these conditions, synthesis of new WT rRNA from the chromosome is largely blocked. But a pre-existing pool of WT rRNA remains unperturbed in the cells. Thus, if any of these mutants caused defects in 60S subunit biogenesis, we expect that the 60S peak would be lower, compared to that of 40S subunits (reflected as a decrease in 60S/40S subunit ratio, in comparison with the WT strain). However, we do not expect to observe other characteristic indicators of a 60S subunit biogenesis defect such as a diminished 80S peak or halfmer polysomes.

Figure 2-9: Sucrose gradient centrifugation to identify defects in 60S subunit biogenesis
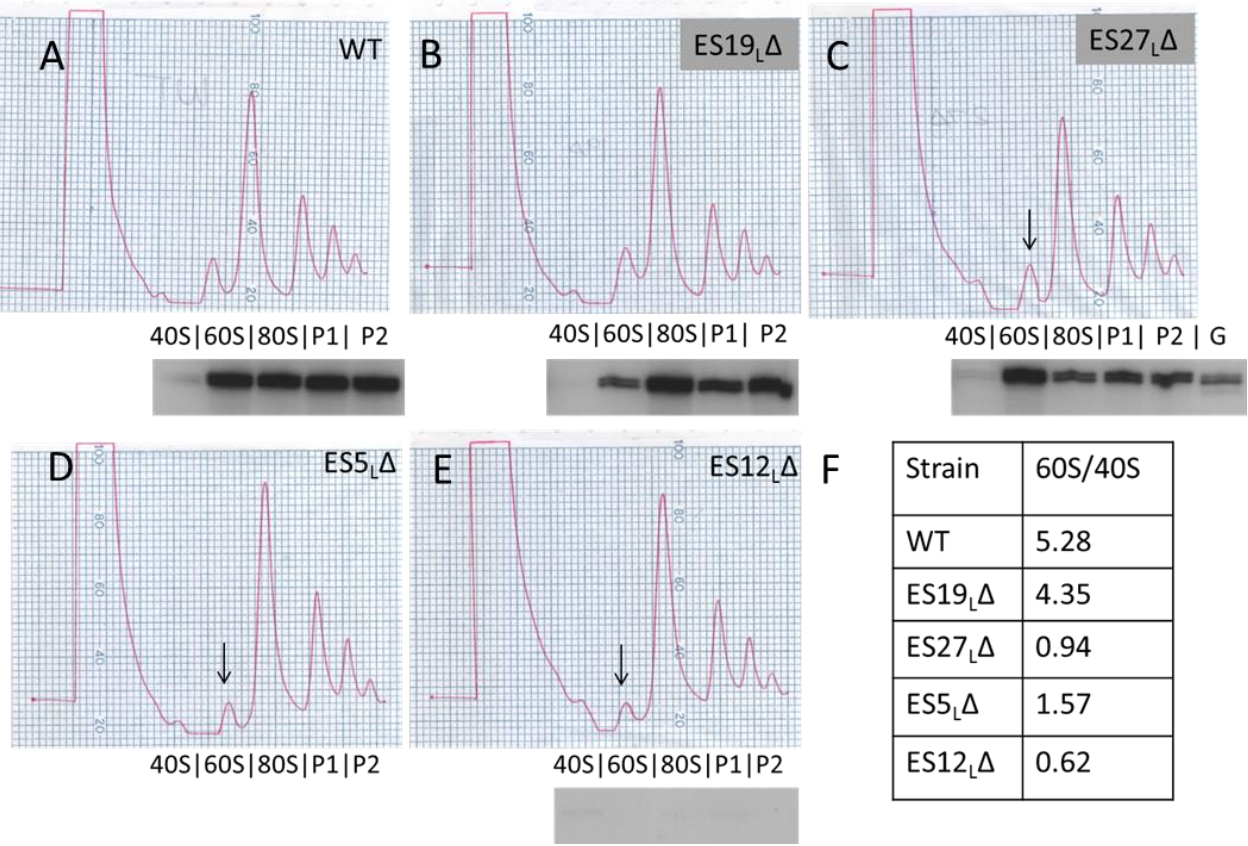
Fig. 2-9: Sucrose gradient centrifugation to identify defects in 60S subunit biogenesis.

(A-E): Sucrose gradient centrifugation to assay for defects in 60S subunit biogenesis - in WT (A), non-essential ES mutants (B, C) and representative essential ES mutants (D,E). Arrows shown in (D), (E) and (C) indicate the decreased 60S peak in the essential ES mutants and in the non-essential ES27hLΔ mutant respectively, compared to WT (A). In this assay, defects in 60S subunit biogenesis are discerned exclusively by a decreased 60S peak and a decreased 60S/40S ratio compared to WT. We do not expect a characteristic decrease in the 80S peak or halfmer polysomes as in other ribosome biogenesis mutants, since we are not perturbing the existing pool of ribosomes in our ES mutants. Primer extension assay using a tag specific to plasmid-derived 25S rRNA is shown underneath the polysome curves to indicate those fractions that contain plasmid-derived mature 25S rRNA. As shown in (C), a sequencing lane with G was used to map the 5' end of 25S rRNA. The primer extension assay could not be performed on ES5$_L$Δ in (D), since the deletion encompasses the plasmid-specific tag, thereby eliminating the binding site of the reverse transcription primer.

(F): Ratios of area under the curve of 60S/40S subunits in mutant compared to WT, quantified from (B-F). All the ES mutants shown, except ES19$_L$Δ, have multifold decrease in 60S/40S ratio compared to WT, indicative of defects in 60S biogenesis.

Consistent with potential functions in 60S subunit biogenesis, the lethal mutants ES5Δ_L (Fig. 2-9D) and ES12Δ_L (Fig. 2-9E) showed a decreased 60S peak and exhibited a multifold decrease in the 60S/40S ratio in comparison with the WT control (Fig. 2-9F). We surmise that other essential ES$_L$ deletion mutants will exhibit a similar effect in this assay, and we used other assays described below in order to confirm that. Among the non-essential ES mutants, while ES19Δ_L resembled the WT control, ES27hΔ_L surprisingly exhibited a decreased 60S peak and multifold decrease in the 60S/40S ratio, indicating that ES27hΔ_L may play a dispensable role in 60S biogenesis (Fig. 2-9, A-C)

In order to further confirm that the observed effects were indeed arising from the plasmid-derived rDNA, we performed a primer extension assay using the plasmid-specific 25S rRNA tag. We detected the 5' end of 25S rRNA in the 60S, 80S, and polysome fractions P1 and P2 (but not in the 40S fraction, as expected) of the WT, ES19Δ_L and ES27hΔ_L samples. This is consistent with our observation that the non-essential mutants can synthesize plasmid-derived mature 25S rRNA at near WT levels. On the other hand, in the lethal mutant ES12Δ_L, we were not able to detect plasmid-derived 25S rRNA in any fraction, indicating severe defects in large subunit biogenesis.

In order to more definitively assay whether deletions of ES affected synthesis of mature 25S rRNA, we performed a northern blot of total cellular RNA extracted after shifting to the restrictive temperature (Fig. 2-10), and probed for plasmid-derived 25S (first panel) and 18S rRNA (second panel) using oligonucleotides complementary to the plasmid-specific tag. Strikingly, all the lethal ES deletions resulted in severely diminished, sometimes undetectable levels of mature 25S rRNA, while levels of small subunit 18S rRNA remained relatively stable. This confirms that all the essential ES play a role in the biogenesis of the large subunit. Those mutants that can produce WT levels of 25S rRNA also exhibit WT-like growth, suggesting that the observed growth deficiencies primarily result from defective synthesis of stable 25S rRNA.

Figure 2-10: Representative northern blot of total cellular RNA extracted from ES mutants
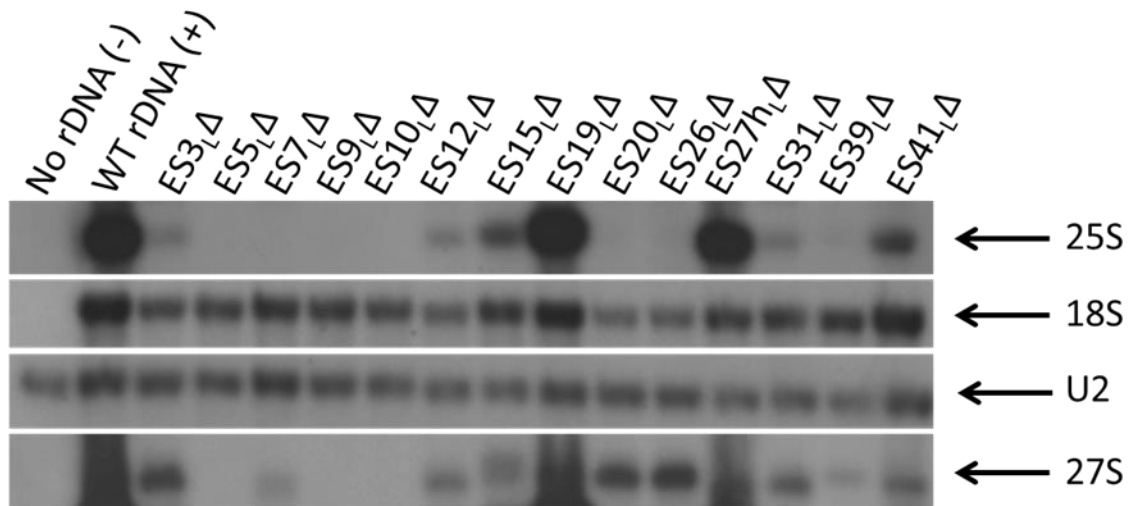
Fig. 2-10: Representative northern blot of total cellular RNA extracted from ES mutants.

Each blot was probed with various oligonucleotides in order to detect rRNAs and pre-rRNAs. Similar effects were observed in three different biological replicates. U2 snRNA is the loading control. Only the plasmid-derived 25S, 18S and 27S rRNAs are detected, since plasmid-specific oligonucleotide tags were used to probe for these RNA species.

2.2.4. Various ES_L function in different steps of ribosome assembly

Ribosome biogenesis proceeds in a series of pre-rRNA processing steps (Fig. 2-11) which have been used to demarcate the progress of assembly in biogenesis mutants. Thus, we examined which pre-rRNA processing steps are affected in each of the ES mutants by northern blotting and primer extension. We defined 'early'-acting ES as those when deleted result in an increase in levels of $27SA_2$ and $27SA_3$ pre-rRNA accompanied by a relative decrease in 27SB pre-rRNA. This step occurs in the nucleolus. We defined 'late'-acting ES as those when deleted result in an increase of 7S pre-rRNA, processing of which begins in the nucleoplasm. ES mutants that result in an increase of 27S pre-rRNA that cannot be explained by an increase in 27SA pre-rRNA (while not resulting in an increase in 7S pre-rRNA) were categorized as 'middle' acting.

Figure 2-11: An illustration of sections of the pre-rRNA processing pathway in yeast
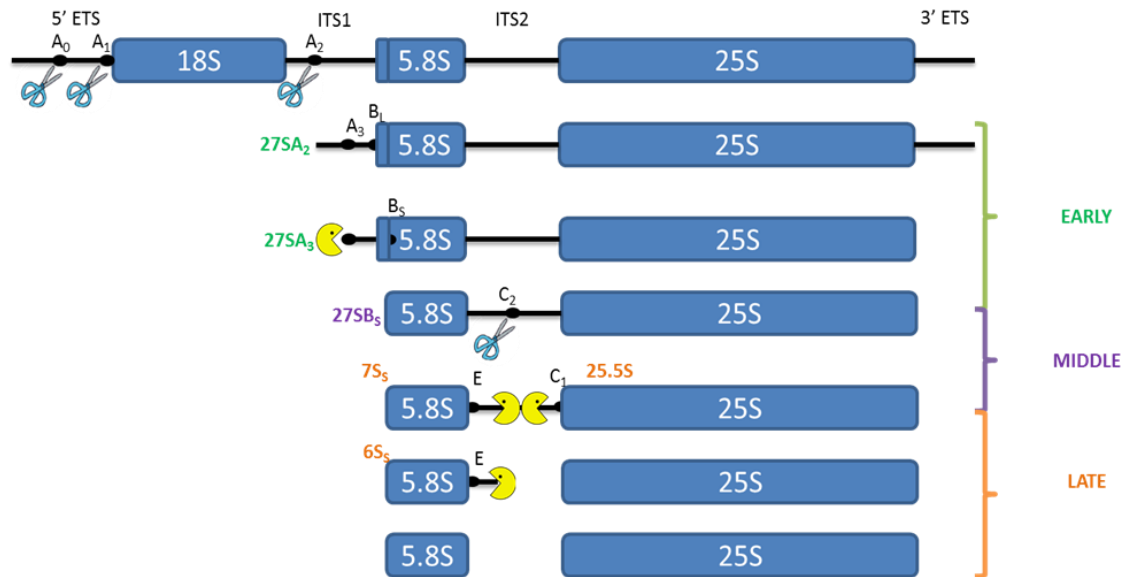
Fig. 2-11: An illustration of sections of the pre-rRNA processing pathway in yeast.

Early, middle and late processing steps and intermediates are color coded in green, purple and orange respectively and various pre-rRNA species are indicated

Compared to the WT rDNA control, we observed that ES39Δ_L showed increased levels of 27SA$_2$ pre-rRNA relative to later 27S pre-rRNA processing intermediates (Fig. 2-12). In addition, ES5Δ_L, ES7Δ_L and ES15Δ_L showed a relative increase of the 27SA$_3$ pre-rRNA species accompanied by a concomitant decrease in 27SB$_S$ pre-rRNA. Hence, we categorize ES39Δ_L, ES5Δ_L, ES7Δ_L and ES15ΔL (indicated by text underlined in green in Fig. 2-12) as early-acting ES, with ES39Δ_L affecting 27SA$_2$ processing and the remainder affecting 27SA$_3$ pre-rRNA processing.

Since 27SB pre-rRNA intermediate is long-lived (Kos and Tollervey, 2010), and since the primer extension assay described above measures the combined levels of endogenous genomic rRNA and rRNA from the plasmid, we were not able to unequivocally determine increases in 27SB levels, characteristic of the 'middle' steps. However, we were able to infer plasmid-derived 27S (A+B) pre-rRNA accumulation (Fig. 2-10) using the plasmid-specific oligonucleotide complementary to 25S rRNA in several ES mutants, most noticeably in ES3Δ_L, ES20Δ_L and ES26Δ_L. There are two observations worth noting here. First, relative life times of various pre-rRNA intermediates are different (Kos and Tollervey, 2010), hence the effects on the long-lived 27SB pre-rRNA may be overrepresented in the steady-state northern blot assay shown in Fig. 2-10. Second, it has been shown that the particle becomes increasingly stable as assembly proceeds (Gamalinda et al., 2014). Since this steady-state measurement is indicative of a combination of accumulation and turnover, there may be a bias towards later, more stable 27SB particles. Based on these, we conclude that ES3$_L$, ES20$_L$ and ES26$_L$ fall into the 'middle' acting category which includes mutants that fail to process 27SB.

Figure 2-12: Relative steady-state levels of various 27S pre-rRNAs (27SA2, 27SA3, 27SBL, 27SBS) in

ES mutants, assayed by primer extension
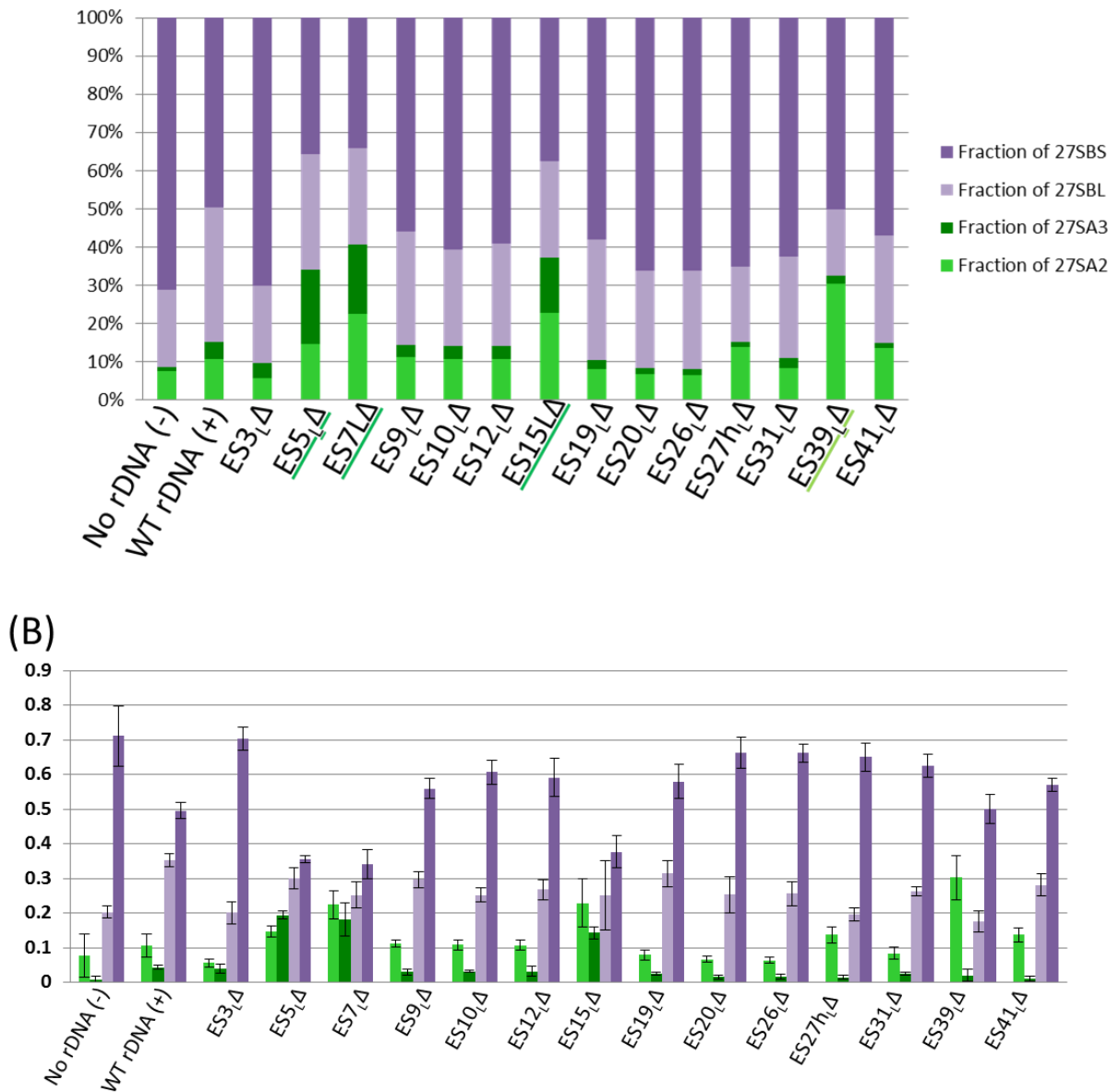
Fig. 2-12: Relative steady-state levels of various 27S pre-rRNAs (27SA$_2$, 27SA$_3$, 27SB$_L$, and 27SB$_S$) in ES mutants, assayed by primer extension.

(A) After normalizing each lane with respect to the U2 loading control, the fraction of each species of pre-rRNA (27SA$_2$, 27SA$_3$, 27SB$_L$ or 27SB$_S$) was calculated as a percentage of total 27S pre-rRNA in that lane (27SA$_2$ + 27SA$_3$ + 27SB$_L$+27SB$_S$). 27SA processing intermediates are shown in shades of green (27SA$_2$ is light green and 27SA$_3$ is dark green). 27SB processing intermediates are shown in shades of purple (27SB$_L$ is light purple and 27SB$_S$ is dark purple). We expect to see an increase in green 27SA pre-rRNA and a concomitant decrease in purple 27SB pre-rRNA in the "early" ES mutants. Note that the levels of pre-rRNA species observed here in this primer extension assay are a combination of both residual endogenous WT and plasmid-derived mutant pre-rRNA. Shown here are the mean values from three biological replicates.

(B) A different representation of (A), error bars represent standard deviation.

To identify 'late' acting ES mutants, we assayed for effects on 7S pre-rRNA processing by northern blotting of RNAs separated on acrylamide gels, using U3 snoRNA as a loading control (Fig. 2-13). After normalizing for loading, we calculated the ratio of levels of 7S pre-rRNA in the mutants to 7S pre-rRNA in the WT control in the same blot with the same exposure. Using this assay, we identified $ES9_L$, $ES10_L$, $ES12_L$, $ES31_L$ and $ES41_L$ among the essential ES as possessing a late-acting function characterized by 7S pre-rRNA accumulation. Of these, $ES31\Delta_L$ seemed to possess the highest accumulation of 7S pre-rRNA. Strikingly, the non-essential mutant $ES27h\Delta_L$ also showed a slight increase in 7S pre-rRNA which could partially explain the deficit (Fig. 2-9C) in producing 60S subunits observed in the sucrose gradient assay. Those ES mutants that result in an accumulation of 7S pre-rRNA are underlined in orange in Fig. 2-13. In addition, we observed that 7S pre-rRNA levels decreased in the early- and middle-acting ES, consistent with inefficient processing of upstream pre-rRNAs.

Figure 2-13: Northern blot of total cellular RNA extracted from ES mutants probed with oligonucleotides in order to detect 7S pre-rRNA
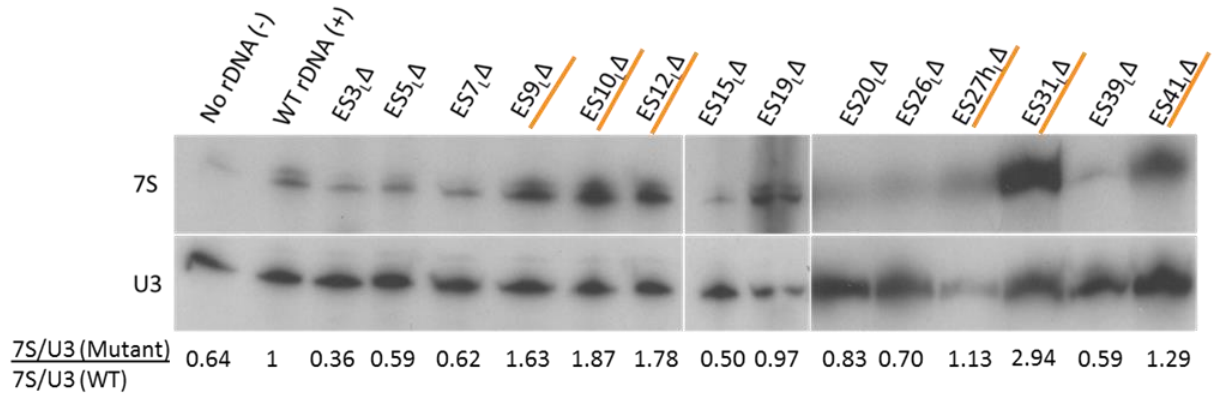
Fig. 2-13: Northern blot of total cellular RNA extracted from ES mutants probed with oligonucleotides in order to detect 7S pre-rRNA.

U3 snoRNA is the loading control. Shown below the blot, are numbers corresponding to fold increase of 7S in each mutant compared to WT, after normalizing for loading. Thus, a mutant that has a ratio of >1 has an accumulation of 7S pre-rRNA (a characteristic of late-acting ES) and a mutant that has a ratio of <1 has a decrease in 7S pre-rRNA this (may result from early- or middle-acting phenotypes). ES mutants that result in an accumulation of 7S pre-rRNA over and above that of WT (ratio >1) are highlighted in orange.

2.3. Discussion

In this study, we have demonstrated that most eukaryote-specific ES within large subunit rRNA are necessary for optimal growth. We further show that the inviability of ES deletion mutants is accompanied by an inability to synthesize stable mature 25S rRNA, which indicates that they are defective in large ribosomal subunit biogenesis. To begin to probe for molecular mechanisms by which these ES may affect large subunit biogenesis, we categorized the essential ES into early (ES39$_L$, ES5$_L$, ES7$_L$ and ES15L), middle (ES3$_L$, ES20$_L$ and ES26$_L$) and late (ES9$_L$, ES10$_L$, ES12$_L$, ES31$_L$ and ES41$_L$) functional classes. Taken together, this systematic study of ES deletions settles a long-standing debate about the dispensability of ES (Gerbi, 1996), demonstrates that they are necessary for the synthesis of stable mature rRNA, and identifies roles for these large subunit ES in specific steps of 60S ribosomal subunit biogenesis.

Below, we have highlighted any relevant previous information available on that particular ES$_L$ and interpreted the results of ES deletions in the light of contacts they make with ribosomal proteins. ES19$_L$: This is the only dispensable ES among the ones we studied under these conditions. We observed near WT levels of 25S rRNA being made in the ES19Δ_L, in agreement with its healthy growth phenotype. (Musters et al., 1991) showed that this region (referred to as V9 in their study) can be replaced by corresponding *E.coli* or mouse sequences without any discernable effect on ribosome assembly and function. Even though (van Beekvelt et al., 2000) have indicated that deletion of V9 may have slight effects on biogenesis of 25S rRNA, our deletion more closely resembles the one used by Musters et al 1991 and is consistent with their finding that this region is dispensable. ES19$_L$ makes minimal contacts with the ribosomal proteins L25, L8 and L2 in the mature 60S subunit (Ben-Shem et al., 2011). As pointed out previously, (van Beekvelt et al., 2000) it is clear that binding of those ribosomal proteins to this ES is not necessary for their recruitment, since the ribosomal proteins themselves are essential.

ES27h$_L$: This is the largest ES present in *Saccharomyces cerevisiae.* We assayed only a partial deletion in this study, due to technical limitations we faced in mutagenesis. We found that although this deletion did not strongly inhibit growth, it resulted in a slight accumulation of 7S pre-rRNA. This could partially explain the decrease in levels of 60S ribosomal subunits observed in this mutant by the more sensitive sucrose gradient assay, even though we observed near-WT levels of mature 25S rRNA being made. Processing of 7S pre-rRNA has been shown to be dispensable for the normal function of the ribosome (Rodriguez-Galan et al., 2015), hence it is not surprising that this mutant yields a slight 7S pre-rRNA processing defect while it exhibits no growth defect. This has been a very intriguing expansion segment previously for various reasons. Apart from serving as a major binding site of the export factor Arx1, which is also non-essential (Bradatsch et al., 2012), this ES has been shown to adopt two conformations, with the helix stem either toward the L1 stalk or toward the polypeptide exit tunnel (Leidig et al., 2013; Zhang et al., 2014). While several groups have studied the effects of insertions in this ES, a previous deletion analysis concurred with our results on the dispensability of this part of ES27$_L$ (Jeeninga et al., 1997). The same study had pointed out the larger deletions of ES27$_L$ were lethal and resulted in defective ribosome biogenesis. This ES is also known to have a putative quadruplex-forming sequence, the functions of which are yet unknown (Karen Kormuth, personal communication).

ES39$_L$: This is evidently the earliest acting ES; its deletion causes accumulation of the early 27SA$_2$ pre-rRNA processing intermediate. This is a large ES, occupying a major segment of rRNA Domain 6. Ribosomal proteins that bind to Domain 6, including L33, L16 and L20 and L3, have been previously shown to function in early steps of ribosome assembly. Hence, this deletion phenotype agrees with the function of ribosomal proteins that bind this ES.

ES5$_L$: This early-acting ES is located in rRNA Domain 1. In accordance with the depletion phenotype of the ribosomal proteins that bind this ES and other regions of domain 1, such as L8 and L36, deletion of ES5$_L$ results in an early-acting ribosome assembly phenotype.

ES7$_L$: This is the second largest ES in yeast and its deletion causes an early phenotype. It forms major contacts with early acting ribosomal proteins including L4, L6, L7, L33 and L20. Consistent with our results, (Jeeninga et al., 1997) showed that this ES is necessary for growth and for processing of 27SA pre-rRNA.

ES15$_L$: This ES, present in rRNA domain 2, is surrounded by L4, L18 and L6, all of which have an early phenotype when depleted.

ES3$_L$: This ES is the only ES in 5.8S rRNA. ES3Δ_L results in an accumulation of 27S pre-rRNA that is not accompanied by an evident increase in 27SA. Consistent with this observation, it establishes multiple contacts with L25, a protein that has been implicated in the middle processing steps as well.

ES20$_L$, ES26$_L$: These ES are located in rRNA domain 3. They form loops on opposite sides of a stem and are involved in several stacking and other non-canonical interactions (Ben-Shem et al., 2011). We classify them as 'middle' acting since they have a strong accumulation of 27S pre-rRNA that is not accounted for by an increase in 27SA. In the mature ribosome, they make contacts with L27 and L34, depletions of which have been shown to have a middle processing defect. In addition, an assembly factor Nop7 has been shown to UV crosslink to these sites (Granneman et al., 2011). Although the depletion of Nop7 has been shown to have an early phenotype, we believe that Nop7 may have other functions in the middle steps that may be uncovered by mutating its binding site with these ES.

ES9$_L$, ES10$_L$, ES12$_L$: These ES are all located in domain 2 in the secondary structure, near H38 and are located underneath the central protuberance of the ribosome. Proteins that localize near the central

protuberance have been implicated in the late nuclear processing steps; this trend is consistent with the phenotypes exhibited by these ES deletions. ES12Δ_L also results in a slight increase in 27S pre-rRNA, similar to a few other ribosomal assembly mutants deficient in 7S processing. Also, a recent study showed that the central protuberance undergoes a major structural change prior to export of the assembling ribosome (Leidig et al., 2014), coincident with the late pre-rRNA processing steps, which further adds credence to the hypothesis that these ES enable proper construction of the central protuberance and other related events that eventually lead to nucleocytoplasmic export of the assembling ribosome.

ES41$_L$: Deletion of ES41$_L$ located near the 3' end of 25S rRNA, leads to a mild accumulation of 7S pre-rRNA, while also leading to a slight increase in the levels of 27S pre-rRNA. The effect of deletion of this ES on production of mature 25S seems modest.

2.3.1. Location of ES in specific neighborhoods correlates with their ribosome assembly phenotype

Having developed a catalog of ES phenotypes, we sought to understand if the reported phenomenon of clustering of ribosomal proteins according to their function in successive steps of ribosome biogenesis (Gamalinda et al., 2014) extends to ES. In order to do this, we color coded early-middle-late acting ES and ribosomal proteins in shades of green-purple-orange in Fig. 2-14A and Fig. 2-14B respectively. Recognizing that ES are localized only to the periphery of the solvent interface of the large subunit, as opposed to ribosomal proteins that are distributed more evenly, we observed that the early acting ES localize to the equatorial belt, the middle-acting ES localize near the bottom third and the late acting ES localize near the central protuberance (Fig. 2-14). This pattern of ES clustering according to their function in successive steps of ribosome biogenesis is reminiscent of the functional clustering of ribosomal proteins reported by our lab previously (Fig. 2-14).

Figure 2-14: A model for ES functions and neighborhood-specific effects in ribosome biogenesis
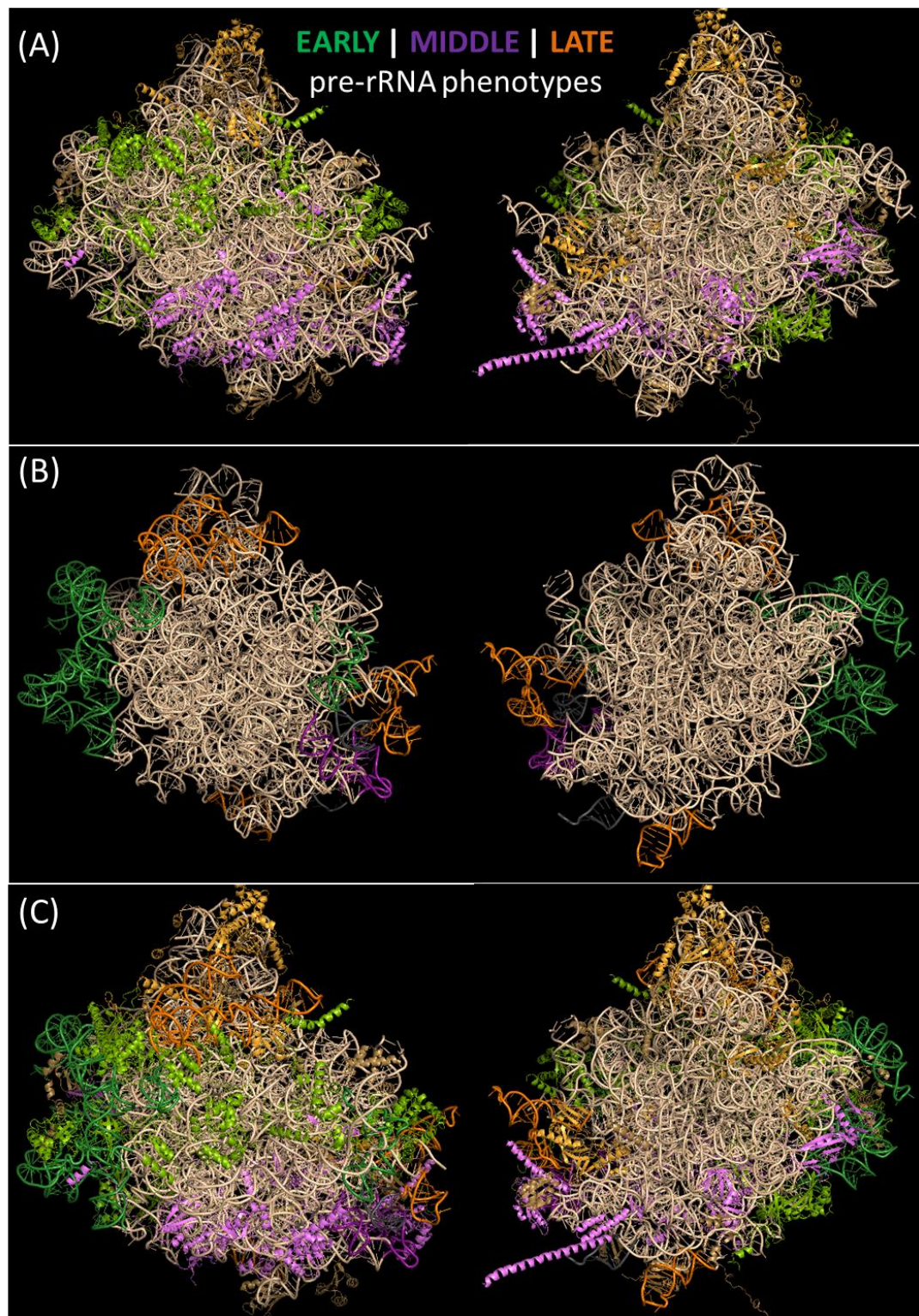
Fig 2.14 (A-C): A model for ES functions and neighborhood-specific effects in ribosome biogenesis.

(A) Previously known (Gamalinda et al., 2014) ribosomal protein depletion phenotypes using the (early-green, middle-purple, late-orange) color scheme .

(B) Structural model of the large ribosomal subunit showing ES color-coded according to the pre-rRNA processing steps in which they function. Both solvent interface (left) and subunit interface (right) are shown. Green-colored ES participate in 27SA processing (early steps) and localize to the equatorial belt. Purple-colored ES participate in 27S processing, but not specifically 27SA processing (middle steps). They localize near the bottom third of the solvent side of the ribosome, near the PTC. Orange-colored ES participate in 7S pre-rRNA processing (late steps) and localize near the central protuberance.

(C) Superimposition of (A) on (B). See Results and Discussion for details of the model.

In order to explore this idea further, we have represented each of the ES studied along with the ribosomal proteins that make contact with that particular ES in the crystal structure of the yeast ribosome, (Fig. 2-15, 2-18), (Ben-Shem et al., 2011). It is apparent that in a majority of the cases, the phenotype caused by deletion of a particular ES corresponds to the phenotype caused by depletion of the ribosomal proteins that it contacts.

This functional clustering of both rRNA and ribosomal proteins on the solvent interface has interesting implications. First, it adds credence to the possibility that as the ribosome is constructed, there may be neighborhood-specific effects on pre-rRNA processing and stability. This study extends the observed hierarchy of ribosomal protein assembly and our results suggest that the hierarchy might extend to RNA-protein neighborhoods, not just ribosomal proteins, on the assembling ribosome.

Figure 2-15: ES deletion phenotypes resemble phenotypes of depletion of nearby ribosomal proteins
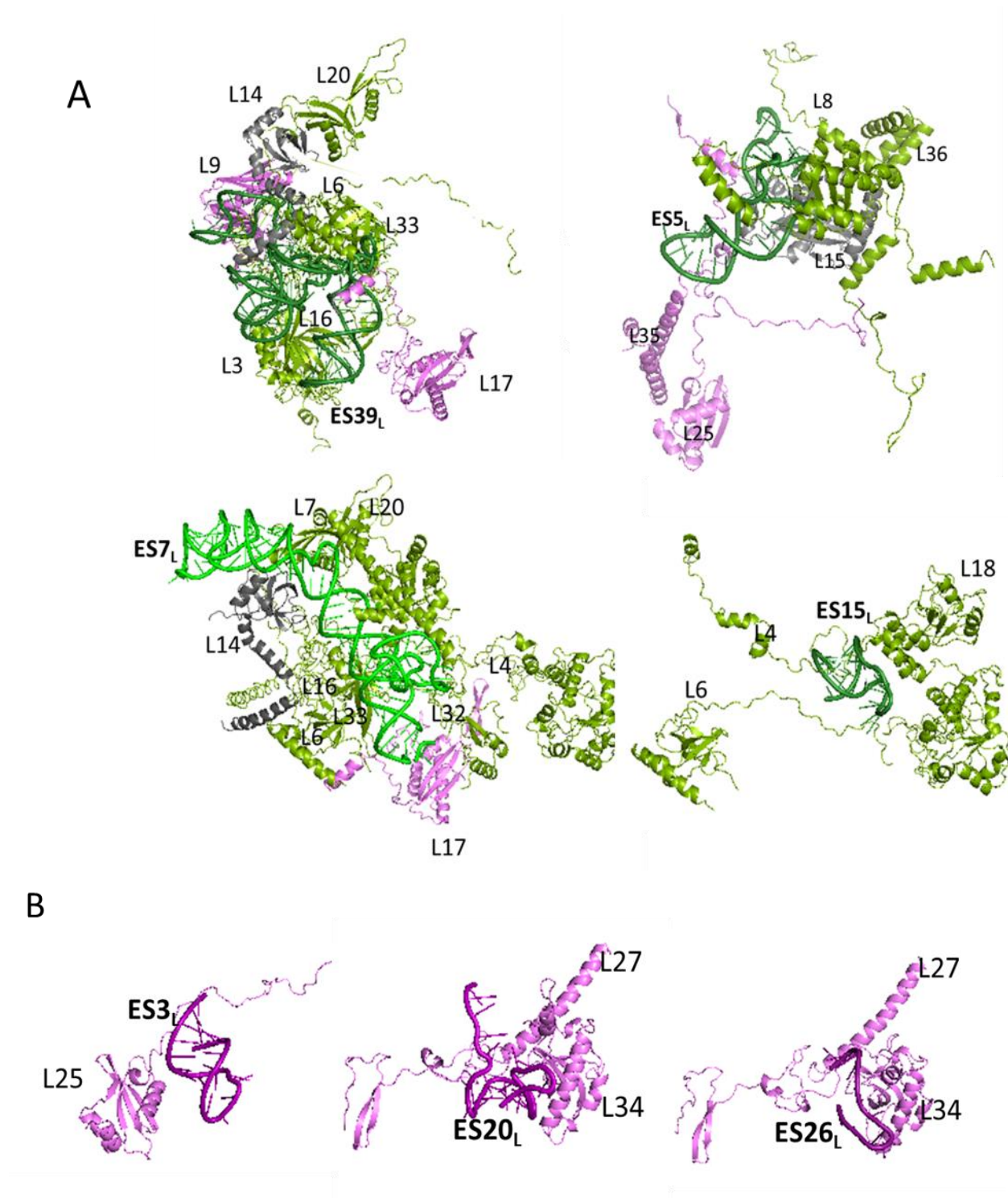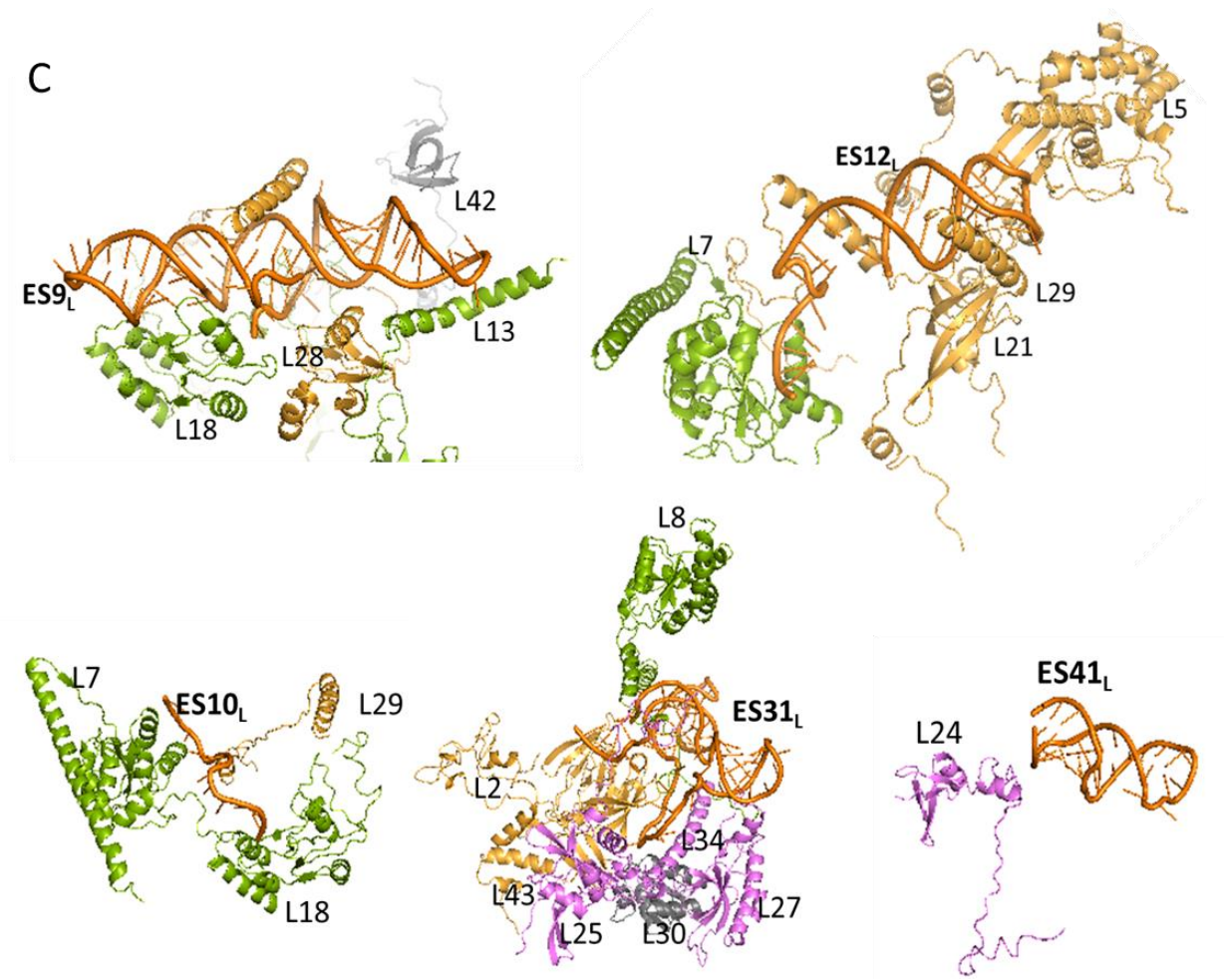
Fig. 2.15 (A-C): ES deletion phenotypes resemble phenotypes of depletion of nearby ribosomal proteins.

Each of the essential ES tested in this study shown individually along with the ribosomal proteins that form crystal structure contacts with that particular ES, (also see Fig. 2-17) color-coded as before according to function.

(A) Early-acting ES and ribosomal proteins

(B) Middle –acting ES and ribosomal proteins

(C) Late-acting ES and ribosomal proteins

2.3.2. A case study on ES31Δ_L

Perhaps the only glaring exception to the neighborhood-specific separation of ribosome assembly functions of ES arises from the deletion phenotype of ES31Δ_L. While its location in the equatorial belt predicts that it might have an early-acting phenotype, in reality, we observe a predominantly late phenotype in the ES31Δ_L mutant. We zoomed in on this neighborhood to understand its contacts and built a model for its function based on its contact with ribosomal protein L8 (rpL8) (Fig. 2-16). The depletion of rpL8 was shown to cause an early-acting phenotype, consistent with its presence in the equatorial belt. On the other hand, deletion of the eukaryote-specific tail of rpL8 that intimately contacts ES31Δ_L, has been shown to cause a later 7S pre-rRNA accumulation phenotype (Beril Tutuncuoglu, personal communication), which is similar to the phenotype that ES31Δ_L exhibits. Thus, what initially appeared to be an exception to the neighborhood-specific phenotype rule, turned out to be an informative sign about how eukaryote-specific RNA-protein elements that contact each other exhibit similar functions in ribosome assembly. Strikingly, as shown in Fig. 2-16, the 3' end of 5.8S, which is the site of processing by the exosome during the 7S pre-rRNA processing and other late steps, is encompassed by ES31_L, which might also begin to suggest potential proximity effects at play, resulting in a late phenotype in this mutant.

Figure 2-16: A case study of eukaryote-specific ribosomal protein-rRNA elements
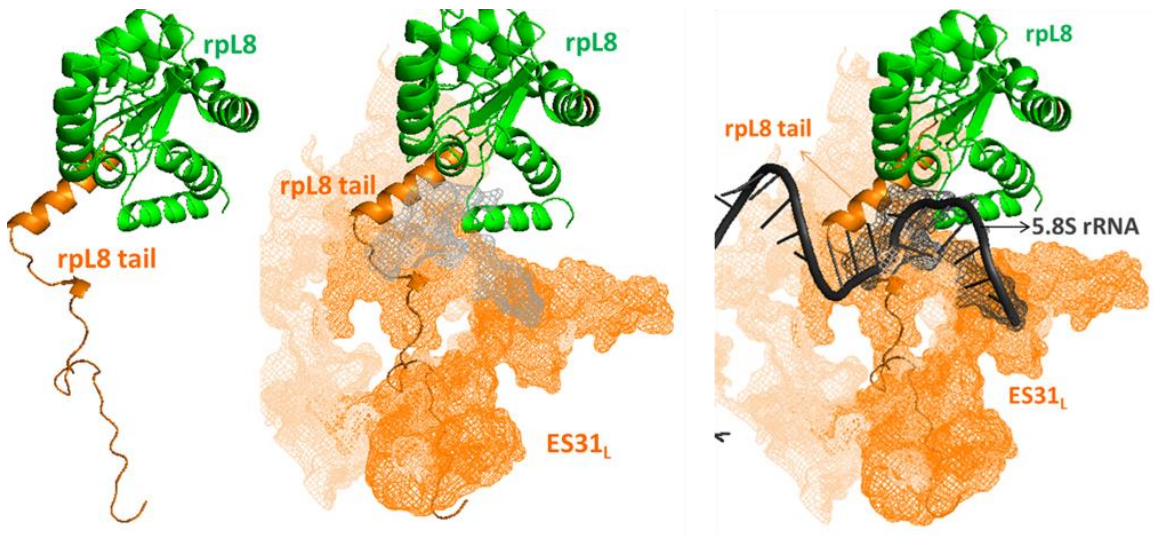
Fig. 2-16: A case study of eukaryote-specific ribosomal protein-rRNA elements.

The left panel shows the body of rpL8 (in green, consistent with its 'early' role in ribosome assembly) and its eukaryote-specific tail (in orange, consistent with its 'late' role in ribosome assembly). The center panel shows the contact established between the 'late' acting $ES31_L$ (shown as an orange colored mesh) and the tail of rpL8. The right panel shows the 3' end of 5.8S rRNA (dark gray) to denote the terminal site of pre-rRNA processing by the exosome. $ES31_L$ is in close contact with the 3' end of 5.8S rRNA.

2.3.3. ES may have co-evolved as a scaffold for eukaryote-specific protein elements on the assembling ribosome

Several eukaryote-specific assembly factors such as Rlp7, Arx1, Rrp5 and Nop7 have been crosslinked to ES (Bradatsch et al., 2012; Dembowski et al., 2013c; Granneman et al., 2011; Lebaron et al., 2013). In this study, we observed that there is functional similarity in ribosome biogenesis between ES rRNA and neighboring ribosomal proteins. Furthermore, eukaryotic RNA elements and eukaryotic protein elements localize together on the solvent-exposed side of the ribosome and make numerous contacts (Fig. 2-17), (Ben-Shem et al., 2011). Combined with our observation about similar functions of eukaryote-specific ES31Δ_L and the eukaryote-specific extension of L8 in ribosome assembly, these lines of evidence raise the possibility that eukaryote-specific protein-RNA elements may have co-evolved and perform similar functions in the cell. Speculating on why ES have evolved in eukaryotes in the first place, it is tempting to suggest that they may have co-evolved with the ribosomal proteins in order to provide the scaffold for binding the plethora of eukaryote-specific protein elements, including assembly factors, ribosomal proteins and their tails. Once extant technical challenges are overcome, mutations in eukaryote-specific regions of proteins in tandem with eukaryote-specific RNA elements may lead to interesting insights about the function of these eukaryotic elements.

Using this study as a starting point and adopting an evolutionary standpoint, it would be interesting to replace expansion segments with those of other eukaryotes and assay for rescue of phenotypes with corresponding eukaryotic proteins, to understand how these expansion segments have continued to evolve.

Furthermore, rRNA plays active roles in various steps of translation, over and above that of merely serving as a scaffold for binding ribosomal proteins, across various kingdoms (Dahlberg, 1989). Extending this to eukaryote-specific rRNA ES, it is tempting to ask if such active eukaryote-specific roles exist for these ES in ribosome assembly as well (Fig. 2-18)

Fig. 2-17: Eukaryote-specific rRNA ES and r-proteins are located in close proximity on the surface of the ribosome.

Only the large subunit is shown. Figure adapted from Beril Tutuncuoglu's work. The legend indicates various colors used.

Figure 2-18: Table showing ES mutations, their phenotypes and their ribosomal protein contacts

ES	Mutation								
ES3	116G-137C	L25 (7)							
ES5	115A-157A	L15(11)	L8 (9)	L35 (4)	L36 (3)	L25 (1)			
ES7	439C-620U	L4 (18)	L7 (14)	L6(14)	L33 (9)	L20 (9)	L14 (7)	L32 (2)	L17 (2)	L16 (1)
ES9	717C-784A	L18 (14)	L29 (7)	L13 (4)	L28 (3)	L42 (1)			
ES10	977C-986U	L7 (3)	L18 (1)	L29 (1)					
ES12	1066G-1102A	L29 (9)	L21 (5)	L5 (4)	L7 (4)				
ES15	1345G-1359C	L4 (6)	L18 (2)	L6 (2)					
ES19	1554U-1582C	L25 (2)	L8 (2)	L2 (1)					
ES20	1626U-1648A	L27 (11)	L34 (5)						
ES26	1807G-1818U	L27 (4)	L34 (1)						
ES27	1949G-2097U	L19 (2)							
ES31	2519A-2588U	L8 (15)	L2 (11)	L27 (6)	L34 (4)	L25 (3)	L30 (2)	L43 (1)	
ES39	3155U-3293U	L14 (20)	L33 (16)	L16 (15)	L6 (11)	L17 (6)	L20 (6)	L3 (5)	L9 (5)
ES41	3337G-3367C	L24 (2)							

Fig. 2-18: Table showing ES mutations, their phenotypes and their ribosomal protein contacts.

Both ES and ribosomal proteins (Gamalinda et al., 2014) are color coded according to their deletion/depletion phenotype (Early: Green; Middle: Purple; Late: Orange). The number in brackets denotes the number of atomic contacts made (Ben-Shem et al., 2011). Lighter shades represent fewer than 5 atomic contacts. Non-essential ES and ribosomal proteins with undetermined function are shown in gray.

2.4. Summary

In summary, we have shown that most eukaryote-specific rRNA expansion segments of the large ribosomal subunit are indispensable and participate in various steps of ribosome biogenesis. While complementing a vast body of literature about the functions of ribosomal proteins, this study settles the debate about the dispensability of expansion segments and identifies a catalog of specific functions of these eukaryote-specific insertions in ribosome biogenesis. These results provide a framework for further investigation of eukaryote-specific features of ribosome assembly and function and pave the way for many further studies from evolutionary, RNA structure, ribosome assembly and translation standpoints.

2.5.   Materials and Methods

Construction and growth of yeast strains

As the parent strain, we used NOY504 (JWY10423, MATa rrn4::LEU2 ade2-101 ura3-1 trpl-lleu2-3,112 his3-11 canl-100), a strain lacking the Rpa12 subunit of Pol1 that renders it temperature-sensitive (a gift from the Nomura lab) (Nogi et al., 1993). This strain was transformed with the pWL160 plasmid (a gift from the Fournier lab) encoding WT RNA as the positive control or pRS314 Trp vector backbone as the 'no rDNA' negative control.

Handling of the NOY504 based strains was done similar to the method described previously (Henry et al., 1994). Briefly, small cultures of the controls and the mutant yeast strains were grown to log phase at 25°C in minimal galactose medium. Cultures were then diluted and endogenous ribosomal RNA was depleted by shifting cultures to 37°C for 6 hours. The mid log-phase cells were then harvested by centrifugation at 5000 rpm for 5 minutes at 4°C for further experiments.

Mutagenesis

Size and location of ES deletions were devised from definitions of ES insertion regions from (Gerbi, 1996) and secondary structures derived from comparative analysis (Gutell et al., 1993). Mutagenesis of the ES regions (Fig. 2-17) was carried out in the pWL160 plasmid (a generous gift from the Fournier lab) using the Quikchange Lightning kit from Agilent Technologies and the mutagenesis was verified by sequencing. All oligonucleotide sequences used in this study are available upon request.

Growth assays of ES mutants

Small 5 ml cultures of the control and mutant strains were grown in C-Trp+Gal media overnight. Ten-fold serial dilutions of the yeast strains bearing either the controls (positive control: NOY504 with pWL160, JWY10430 and negative control: NOY504 with pRS314, JWY10429) or one of the 14 mutant

plasmids (JWY10431-JWY10444) were spotted on to YEPD plates starting with an OD of 1 and grown either at 25°C and photographed after 3 days or at 37°C and photographed after 5 days.

Sucrose gradient analysis

Fractionation of preribosomes, ribosomes and polyribosomes and subsequent analysis was carried out as described (Talkish et al., 2014b). The image was digitized using the PlotDigitizer software. Area under the curve for each peak was calculated using the trapezoidal rule and subsequently, 60S/40S ratios were determined using Excel.

RNA analysis

RNA extraction and subsequent northern blotting assays were performed as described previously. (Horsey et al., 2004). Assaying steady state pre-rRNA processing by primer extension was carried out using the Transcriptor reverse transcriptase (Roche) as described. (Talkish et al., 2014b)

Illustrations

PDB file of the crystal structure of the ribosome (PDB ID: 4V88) (Ben-Shem et al., 2011) was manipulated using the PyMol software (Schrodinger, 2015) to produce the structural images and RiboVision software (Bernier et al., 2014) was used for generation of some of the secondary structures shown here.

3. Investigation of the molecular interactions of r-protein L5

3.1. Introduction

3.1.1. Ribosomal proteins play vital roles in ribosome assembly

Although the peptidyl transferase functional core of the ribosome is exclusively made up of ribosomal RNA (Dahlberg, 1989), ribosomal proteins play indispensable roles in synthesizing functional ribosomes, both in prokaryotes and eukaryotes. Landmark studies by Nomura and Nierhaus to carry out *in vitro* reconstitution of prokaryotic ribosomal subunits (Mizushima and Nomura, 1970; Nierhaus and Dohme, 1974; Nomura, 1973; Röhl and Nierhaus, 1982) led to further research on the various roles of ribosomal proteins in the assembly of ribosomal subunits. While investigations of the functions of assembly factors had preceded investigations of the roles of ribosomal proteins in eukaryotic ribosome assembly, research in the past decade has seen exceptional strides in our understanding of the roles of ribosomal proteins in ribosome biogenesis; see (de la Cruz et al., 2015; Gamalinda and Woolford, 2015) for reviews. In particular, the availability of high-resolution X-ray crystallographic and cryo-EM structures has amplified the scope of these lines of investigation (Ben-Shem et al., 2011; Leidig et al., 2014), (Wu et al., manuscript in review). In the light of these recent advances, we are now able to ask deeper questions and better interpret previous results about the mechanistic roles of these ribosomal proteins and their protein domains, and the significance of the multitude of molecular contacts that they make in the context of an RNP.

3.1.2. Common themes emergent from the functions of ribosomal proteins in yeast LSU biogenesis

The large ribosomal subunit (LSU) in *Saccharomyces cerevisiae* contains 46 ribosomal proteins (r-proteins or rps). While there are a handful of eukaryote-specific ribosomal proteins, many conserved ribosomal proteins also possess eukaryote-specific, often disordered, extensions or tails (Armache et al., 2010b). Ribosomal proteins (specifically, often the eukaryotic counterparts of the primary binder r-proteins described in prokaryotes), bind the pre-rRNA as it is transcribed, guide the folding of pre-rRNA and stabilize long-range interdomain RNA contacts. As assembly progresses in a 5'-3' fashion with respect to the pre-rRNA, r-proteins that form these initial encounter complexes become more tightly associated with preribosomes. Consequently, the assembling ribosome tends to get more stable, as evident by less sensitivity to high salt treatments (Gamalinda et al., 2014). In order to more definitively investigate the roles of these r-proteins, many researchers have used strains that conditionally express r-proteins, since many of the ribosomal proteins are essential for cell viability (Ohmayer et al., 2013; Poll et al., 2009). These studies established that binding of r-proteins to the assembling ribosome is co-operative and hierarchical, although generally speaking, ribosome assembly proceeds via multiple, parallel pathways.

3.1.3. Ribosomal protein L5, the 5S RNP and LSU assembly

Of the 46 ribosomal proteins of the yeast LSU, ribosomal protein L5 (rpL5) is the focus of this project. rpL5 has continued to be a subject of research interest and has been referred to both as L1 (Deshmukh et al., 1995; Yeh et al., 1996) and as L18 (Leidig et al., 2014) in literature (Fig. 3-1). rpL5 is conserved (Fig. 3-2) across kingdoms. Most importantly, it binds 5S rRNA (Fig. 3-1), which is one of the three rRNAs of the eukaryotic LSU. Interestingly, early in the pathway of LSU assembly, rpL5 and another ribosomal protein, rpL11, associate with 5S rRNA and are loaded onto the assembling ribosome *en bloc,* to form what is called the central protuberance (CP). Two assembly factors Rpf2, Rrs1 (Zhang et al.,

2007) have been shown to be necessary for this loading process. These assembly factors Rpf2 and Rrs1, along with ribosomal proteins rpL5 and rpL11, and 5S rRNA constitute the 5S RNP. Thus, assembly of the 5S RNP and its association with the LSU itself is itself an example of how RNPs assemble, since it involves rRNA, ribosomal proteins and assembly factors.

Depletion of any of the protein components of the 5S RNP has been shown to cause an accumulation of 27SB pre-rRNA (Talkish et al., 2012; Zhang et al., 2007). However, these mutants seem to be capable of producing (and sometimes even accumulating) 7S pre-rRNA, which is the immediate product of 27SB processing. With respect to the depletion of rpL5, we observe both an increase in the steady-state levels of 27SB pre-rRNA accompanied by an accumulation of 7S pre-rRNA. Thus, even though the CP is loaded onto preribosomes early in the pathway, it is the late nuclear steps of ribosome assembly (27SB pre-rRNA processing), that seem to be defective in the absence of rpL5, or any other component of the CP.

Figure 3-1: Pymol illustration of the position of L5 on the ribosome and the preribosome
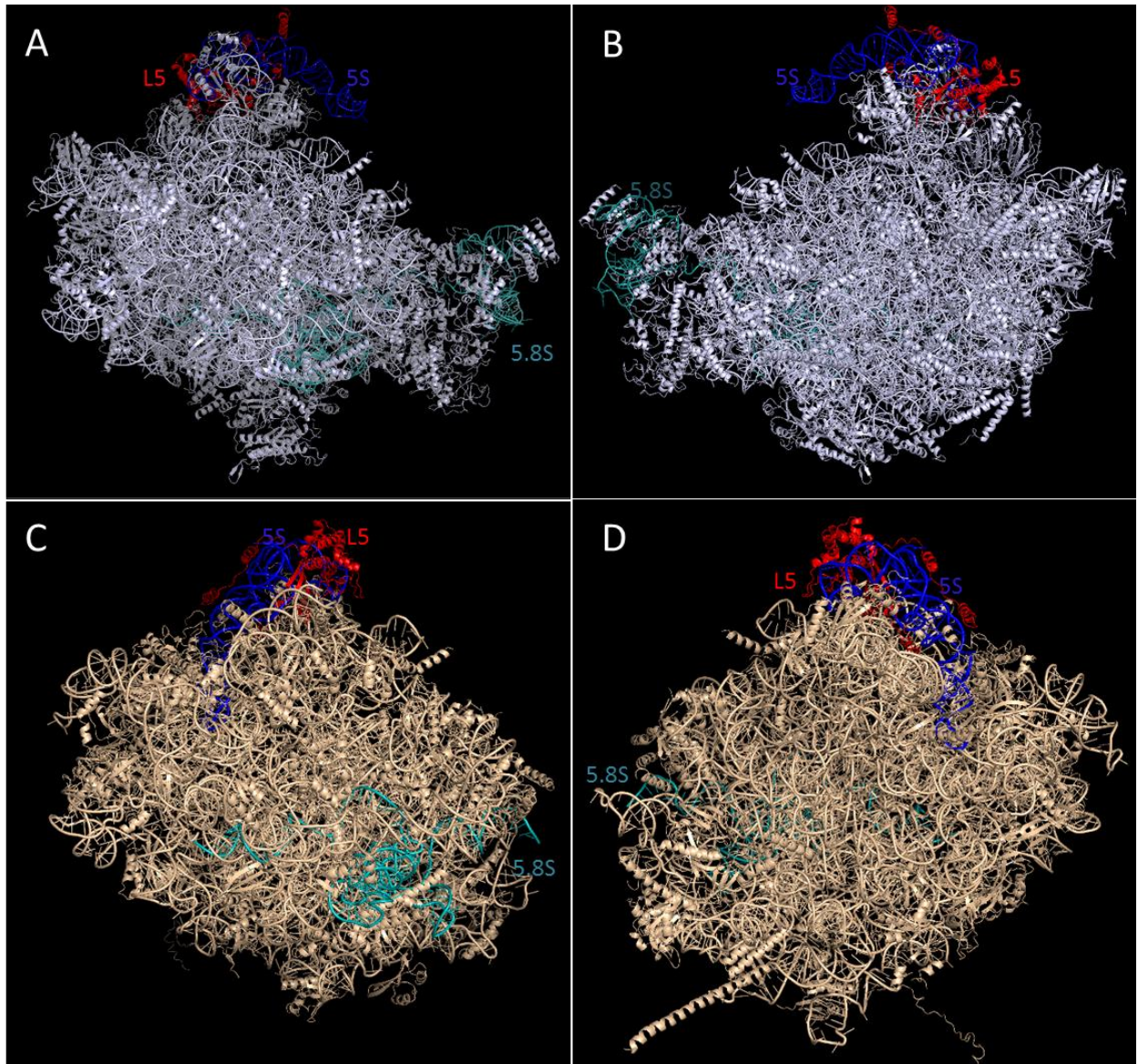
Fig. 3-1: Pymol illustration of the position of L5 on the ribosome and the preribosome.

(A) Solvent interface of the pre-ribosome. 25S rRNA is shown in light blue, L5 is shown in red and 5S pre-rRNA is shown in blue. 5.8S pre-rRNA is shown in teal for orientation.

(B) Subunit interface, same as (A).

(C) Solvent interface of the mature ribosome. Colors are the same as in (A), except for mature 25S rRNA which is shown in beige.

(D) Subunit interface of the mature ribosome. Colors are the same as in (C).

Figure 3-2: Multiple sequence alignment of L5 from various eukaryotes shows a high degree of conservation

```
S.cerevisiae              MAFQKDAKSSAYSSRFQTPFRRRREGKTDYYQRKRLVTQHKAKYNTPKYRLVVRFTNKDI    60
Schizosaccharomyces_pombe MPFIKAVKSSPYFSRYQTKYRRRREGKTDYYARKRLIAQAKNKYNAPKYRLVVRFSNRFV    60
Arabidopsis_thaliana      MVFVKSTKSNAYFKRYQVKFRRRRDGKTDYRARIRLINQDKNKYNTPKYRFVVRFTNKDI    60
Caenorhabditis_elegans    MGLVKVIKNKAYFKRYQVKLRRRREGKTDYYARKRLTVQDKNKYNTPKYRLIVRITNKDV    60
Drosophila_melanogaster   MGFVKVVKNKQYFKRYQVKFRRRREGKTDYYARKRLTFQDKNKYNTPKYRLIVRLSNKDI    60
Xenopus_laevis            MGFVKVVKNKAYFKRYQVKFRRRREGKTDYYARKRLVIQDKNKYNTPKYRMIVRVTNRDI    60
Mus_musculus              MGFVKVVKNKAYFKRYQVRFRRRREGKTDYYARKRLVIQDKNKYNTPKYRMIVRVTNRDI    60
Homo_sapiens              MGFVKVVKNKAYFKRYQVKFRRRREGKTDYYARKRLVIQDKNKYNTPKYRMIVRVTNRDI    60
                          * : *   *.. * .*:*.   ****:*****  * **  * * ***:****::**.:*: :

S.cerevisiae              ICQIISSTITGDVVLAAAYSHELPRYGITHGLTNWAAAYATGLLIARRTLQKLGLDETYK   120
Schizosaccharomyces_pombe TCQIVSSRVNGDYVLAHAHSSELPRYGIKWGLANWTAAYATGLLVARRALAKVGLADKYE   120
Arabidopsis_thaliana      VAQIVSASIAGDIVKASAYAHELPQYGLTVGLTNYAAAYCTGLLLARRVLKMLEMDDEYE   120
Caenorhabditis_elegans    VAQLAYSKIEGDVVVASAYSHELPRYGLKVGLTNYAAAYATGLLLARRHLKTIGLDSTYK   120
Drosophila_melanogaster   TVQIAYARIEGDRVVCAAYSHELPKYGIQVGLTNYAAAYCTGLLVARRVLNKLGLDSLYA   120
Xenopus_laevis            ICQIAYARIEGDMIVCAAYSHELPKYGIKVGLTNYASAYCTGLLLARRLLNKFGLDKVYE   120
Mus_musculus              ICQIAYARIEGDMIVCAAYAHELPKYGVKVGLTNYAAAYCTGLLLARRLLNRFGMDKIYE   120
Homo_sapiens              ICQIAYARIEGDMIVCAAYAHELPKYGVKVGLTNYAAAYCTGLLLARRLLNRFGMDKIYE   120
                           *:  : : **  : . *:: ***:**:   **:*:::**.****:*** *   . : . *

S.cerevisiae              GVEEVEGEYELTEAVEDGPRPFKVFLDIGLQRTTTGARVFGALKGASDGGLYVPHSENRF   180
Schizosaccharomyces_pombe GVTEPEGEFELTEAIEDGPRPFKVFLDVGLKRTSTGSRVFGAMKGASDGGLFIPHSPNRF   180
Arabidopsis_thaliana      GNVEATGEDFSVEPT-DSRRPFRALLDVGLIRTTTGNRVFGALKGALDGGLDIPHSDKRF   179
Caenorhabditis_elegans    GHEELTGEDYNVEEE-GDRAPFKAVLDIGLARTTTGSKIFAVMKGVADGGINVPHSESRF   179
Drosophila_melanogaster   GCTEVTGEEFNVEPVDDGPGAFRCFLDVGLARTTTGARVFGAMKGAVDGGLNIPHSVKRF   180
Xenopus_laevis            GQVEVTGDEYNVESIDGEPGAFTCYLDAGLTRTTTGNKVFGALKGAVDGGLSIPHSTKRF   180
Mus_musculus              GQVEVNGGEYNVESIDGQPGAFTCYLDAGLARTTTGNKVFGALKGAVDGGLSIPHSTKRF   180
Homo_sapiens              GQVEVTGDEYNVESIDGQPGAFTCYLDAGLARTTTGNKVFGALKGAVDGGLSIPHSTKRF   180
                          * * *     .*        *    ** ** **:** ::*...:**. ***: :*** .**

S.cerevisiae              PGWDFETEEIDPELLRSYIFGGHVSQYMEELADDDEERFSELFKGYLADDIDADSLEDIY   240
Schizosaccharomyces_pombe PGFDIETEELDDETLRKYIYGGHVAEYMEMLIDDDEERYQKQFSGLIADGIESDQLEDIY   240
Arabidopsis_thaliana      AGFHKENKQLDAEIHRNYIYGGHVSNYMKLLGEDEPEKLQTHFSAYIKKGVEAESIEELY   239
Caenorhabditis_elegans    FGFDQESKEYNAEAHRDRILGKHVADYMTYLKEEDEDRYKRQFSKFLAAGLNADNLVATY   239
Drosophila_melanogaster   PGYSAETKSFNADVHRAHIFGQHVADYMRSLEEEDEESFKRQFSRYIKLGIRADDLEDIY   240
Xenopus_laevis            PGYDSESKEFNAEVHRKHIFAQNVAEYMRLLMEEDEDAYKKQFSQYIKNGVTADQVEDLY   240
Mus_musculus              PGYDSESKEFNAEVHRKHIMGQNVADYMRYLMEEDEDAYKKQFSQYIKNNVTPDMMEEMY   240
Homo_sapiens              PGYDSESKEFNAEVHRKHIMGQNVADYMRYLMEEDEDAYKKQFSQYIKNSVTPDMMEEMY   240
                          *:  *.:. : :  *   *  .*::** * ::: :  . *. :   : : :      *

S.cerevisiae              TSAHEAIRADPAFKPTEKKFTKEQYAAESKKYRQTKLSKEERAARVAAKIAALAGQQ---   297
Schizosaccharomyces_pombe AEAYAKIREDPSFQKSGKDA--AAFKAESLKYTQRKLTAEERKERFNAKVIEAGRA----   294
Arabidopsis_thaliana      KKVHAAIRADPNPKKTVK-P----APKQHKRYNLKKLTYEERKNKLIERVKALNGAGGDD   294
Caenorhabditis_elegans    QKVHSAIRADASPAAKK-------AAKPSKRHTAKRLTYDERKQRVADKKALLLQLKEQQ   292
Drosophila_melanogaster   KKAHQAIRNDPTHKVTAKKS----SAVTKKRWNAKKLTNEQRKTKIAAHKAAYVAKLQSE   296
Xenopus_laevis            KKAHAGIRENPVHEKKPK------KEVKKKRWNRAKLSLEQKKDRVAQKKASFLRAQEKA   294
Mus_musculus              KKAHAAIRENPVYEKKPK------REVKKKRWNRPKMSLAQKKDRVAQKKASFLRAQERA   294
Homo_sapiens              KKAHAAIRENPVYEKKPK------KEVKKKRWNRPKMSLAQKKDRVAQKKASFLRAQERA   294
                          ..:  **  :        .              :    :::  ::  :. :

S.cerevisiae              -------   297
Schizosaccharomyces_pombe -------   294
Arabidopsis_thaliana      DDEDDEE   301
Caenorhabditis_elegans    E------   293
Drosophila_melanogaster   TEA----   299
Xenopus_laevis            DS-----   296
Mus_musculus              AES----   297
Homo_sapiens              AES----   297
```

Fig. 3-2: Multiple sequence alignment of L5 from various eukaryotes shows a high degree of conservation.

This output was generated using the Clustal Omega software. The residues are color coded according to their chemical nature, and the degree of conservation is marked with either "*" (identical) or ":" (similar).

3.1.4. 5S RNP rotation prior to nuclear export

A groundbreaking discovery that emerged from recent structural studies (Leidig et al., 2014), (Wu et al., manuscript under review) has rekindled research interest in the 5S RNP. It was found that preribosomes affinity-purified with a late nuclear assembly factor tag (Alb1, and more recently, Nog2) revealed a remarkably different conformation of the 5S RNP (pre-rotated state), one in which it is turned nearly 180° away from its position in mature ribosomes. In order to attain nuclear export competency, the 5S RNP undergoes a dramatic rotation to form its mature-like conformation (post-rotated state). The working model is that this is a late nuclear quality control step, which then triggers the binding of nuclear export factors. Although the exact mechanistic details of the power stroke that causes this rearrangement are still rudimentary, high-resolution structures have identified potential key players in this rotation step. As rpL5 remains associated with 5S rRNA throughout this process, rpL5 also undergoes a dynamic shift in its atomic contacts as the 5S RNP rotation happens.

3.1.5. Studying ribosomal protein L5 by investigating its molecular interactions

In order to explore the various roles played by ribosomal protein L5 in assembling the 5S RNP, its association with the LSU, rotation of the 5S RNP, and generally, proper biogenesis of functional large ribosomal subunits, we first evaluated the significance of the plethora of contacts formed by rpL5 during the course of LSU assembly. As mentioned before, the recent surge in availability of high resolution structural models permits us to adopt this strategy that has the power to shed light on the molecular mechanisms that enable the proper construction of the LSU. Hence, the relevant molecular contacts of rpL5 are discussed in the section below, and detailed explanations of strategies we adopted to disrupt these molecular interactions are described in the Results section.

Loading the 5S RNP onto the preribosome

The process of assembling the 5S RNP itself begins in the cytoplasm, where the nuclear transport adaptor protein Syo1 binds rpL5 via its HEAT repeats (Calvino et al., 2015; Kressler et al., 2012). The N-terminal 41 amino acids of rpL5 are necessary and sufficient for its interaction with Syo1. It has also been proposed that Syo1 binding shields at least a part of the 5S rRNA binding surface of rpL5. Syo1 also binds rpL11, which is topologically and functionally associated with ribosomal protein L5. Then, the heterotrimeric L5-Syo1-L11 complex is imported into the nucleus in a synchronous, stoichiometric fashion using Kap104 as the nuclear import receptor. Once the heterotrimer is imported into the nucleus, it is released from Kap104 in a Ran-GTP-dependent manner and can now bind 5S rRNA, which is transcribed in the nucleus by PolIII. The interaction of ribosomal protein L5 with 5S rRNA has been recapitulated *in vitro* and studied extensively (Nazar et al., 1979; Yaguchi et al., 1984). Syo1 is subsequently released after this step, perhaps concomitant with the association of this L5-L11-5S rRNA complex with the LSU, aided by the assembly factors Rpf2 and Rrs1. A recently solved crystal structure of Rpf2 and Rrs1 has reinforced the notion that these assembly factors are important for the loading of the 5S RNP on to the assembling LSU (Asano et al., 2015; Kharde et al., 2015). Jelena Jakovljevic from our lab and others are currently examining the roles of Rpf2 and Rrs1 in greater detail, and their results will complement the findings of this study.

Components of 5S RNP affect late nuclear steps of pre-rRNA processing

As mentioned before, depletion of most proteins (Gamalinda et al., 2014) and rRNA expansion segments of the central protuberance (as shown in Chapter 2) cause defects in late nuclear steps of assembly, specifically in 7S pre-rRNA processing, and often accompanied by a delay in the previous 27SB processing step. One of the other key events happening around the same time during assembly is the major structural rearrangement involving an 180° rotation of the 5S RNP, described above. It is unclear what exact roles various molecules of the central protuberance play in this rotation step. However,

recent data from our work (in collaboration with the Gao lab) has found that depletion of ribosomal protein L21 largely blocks rotation of the 5S RNP. Whether this is direct or indirect, or the exact mechanistic underpinnings of this phenotype, is not known. Interestingly, L5 interacts with L21 in the mature ribosome (post-rotated state), but not in the pre-rotated state (Fig. 3-3). The possible ramifications of this interaction for the proper rotation of 5S RNP are discussed in the Results section.

Nuclear export and subsequent cytoplasmic steps

Once the 5S RNP attains its post-rotated conformation, it acquires nuclear export competence. Final stages of ribosome biogenesis occur in the cytoplasm where the last ribosomal proteins, such as rpL10 bind the preribosome (Lo et al., 2010). Ribosomal protein L10 plays a major role in the intersubunit rotation that occurs in each cycle of protein synthesis, and hence its recruitment and stable association is an important step in the final cytoplasmic stages of ribosome biogenesis (Hofer et al., 2007; Sulima et al., 2014a). In addition, the almost-mature ribosome now undergoes a test drive for its functional competence, including verifying the capability of the CP to carry out intersubunit rotation, as it does during the elongation phase of translation (Sulima et al., 2014b). rpL5 and rpL10 interact through their C-terminal tails in the cytoplasm, as evident in the crystal structure of mature ribosomes (Fig. 3-4). Remarkably, the C-terminal tails of both rpL5 and rpL10 are eukaryote-specific. The potential implications of this interaction are addressed in this chapter.

Figure 3-3: Pymol representation of the atomic contacts between L21 and L5
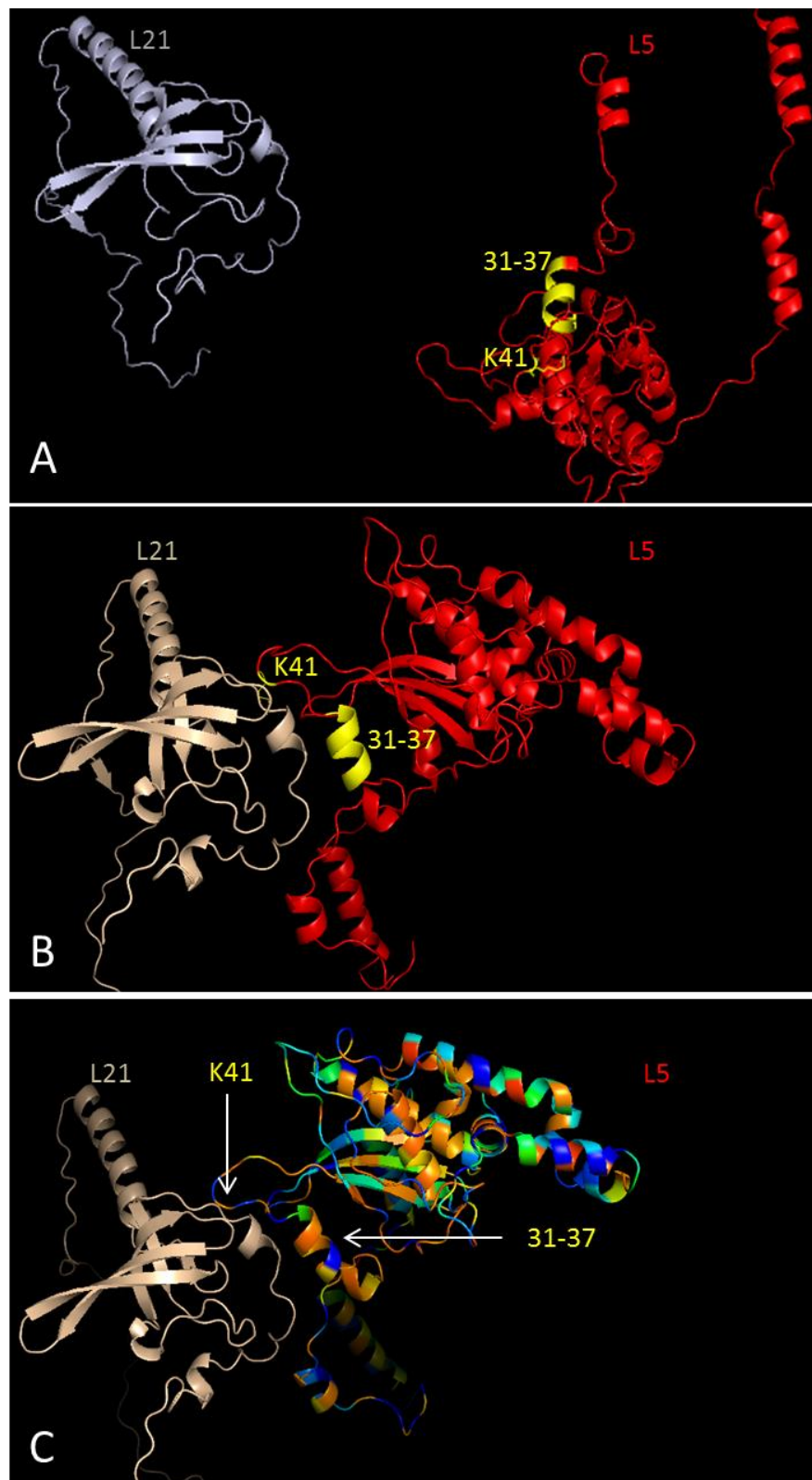
Fig. 3-3: Pymol representation of the atomic contacts between L21 and L5.

(A) In the context of the preribosome. L21 is shown in bluish white, L5 is shown in red and the mutated helix (aa. 31-37) and residue (K41) are shown in yellow.

(B) In the context of the mature ribosome, L21 is shown in beige, L5 is shown in red and the mutated helix (aa. 31-37) and residue (K41) are shown in yellow.

(C) Atomic contacts between L21 and L5, with L5 represented as a heatmap. Warmer colors are more conserved. The residues mutated are indicated by arrows.

Figure 3-4: Pymol representation of the atomic contacts formed between L5 and L10
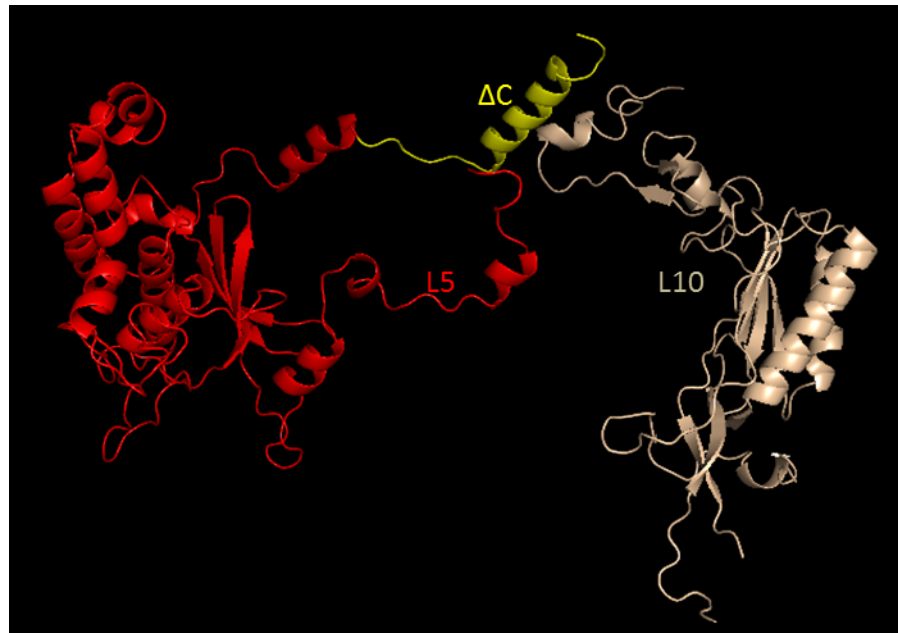
Fig. 3-4: Pymol representation of the atomic contacts formed between L5 and L10.

 Pymol cartoons of L5 (red) showing the C-terminal tail (yellow) contacting L10 (beige) in the mature ribosome. Unlike other *rpl5-* mutations, the preribosome structure is not shown, since L10 associates with the ribosome only in the cytoplasm.

3.1.6. rpL5 and disease

Since ribosome biogenesis and function are fundamental to the homeostasis of the cell, they are linked to nearly every cellular process. Regulating ribosome biogenesis and function becomes especially important when considering how expensive it is for the cell to synthesize ribosomes (Warner, 1999). Mutations that prevent assembly of functional ribosomes result in a class of diseases that have been referred to as ribosomopathies (Danilova and Gazda, 2015; Freed et al., 2010; Hannan et al., 2011; Montanaro et al., 2008; Scheper et al., 2007; Sulima et al., 2014b). Homozygous mutations in ribosomal proteins are embryonic lethal, since most ribosomal proteins are essential. However, at one end of the spectrum, heterozygous mutations lead to various cancers (hyperproliferation), but also to hypoproliferative diseases like anemia, at the other end of the spectrum. This conundrum of mutations in r-proteins causing hypoproliferation (e.g., anemia) that eventually leads to oncogenesis and the question of why these mutations lead to tissue-specific phenotypes have puzzled researchers.

Specifically looking at potential roles of *rpl5* mutations in diseases, it is known that ribosomal protein L5 inhibits Mdm2-mediated p53 ubiquitination and subsequent degradation. When rpL5 does not efficiently assemble into ribosomes, it can bind to Mdm2, a negative regulator of p53, and thus activate p53. Thus, rpL5 provides one of the links between the p53 pathway and ribosomes (Nishimura et al., 2015; Teng et al., 2013; Zhou et al., 2015). In the light of this result, perhaps it is unsurprising that mutations in L5 were identified in T-cell acute lymphoblastic leukemia patients (De Keersmaecker et al., 2013).

On the other hand, mutations in rpL5 have also been identified in a number of patients with Diamond-Blackfan Anemia (DBA) (Cmejla et al., 2009). These mutations are associated with cleft palate and abnormal thumbs in these patients (Gazda et al., 2008). An explanation for the (hypoproliferative/hyperproliferative) duality of these disease phenotypes was proposed with respect to

rpl10 mutations (Sulima et al., 2014b). It was suggested that the *rpl10* mutation that halts ribosome assembly and cell proliferation (hypoproliferation) leads to acquisition of suppressor mutations, which in turn enable the cells to overcome the hypoproliferation and ribosome assembly arrest. However, the suppressor mutations do not rescue the various other defects in the *rpl10* mutant, including defects in intersubunit rotation and translation fidelity, and these defects ultimately lead to oncogeneis (hyperproliferative). Thus, bypass of quality control was suggested as a potential pathway to oncogenesis. It remains to be seen if these sorts of suppressor mutations exist for other *rpl* mutants, especially *rpl5* mutants*.*

In addition, considering the plethora of contexts in which rpL5 functions during ribosome biogenesis, it is tempting to speculate that the disease-causing nature of these mutations may be primarily driven by their defective ribosome biogenesis phenotypes at the molecular level.

3.2. Results

3.2.1. Rationale behind mutations

In order to tease apart the potential mechanistic roles of ribosomal protein L5 in various ribosome assembly processes, including pre-rRNA processing, loading of 5S RNP onto the preribosomes, rotation of 5S RNP and nuclear export of assembling ribosomes, we assayed the *in vivo* effects of various mutations in *RPL5*. The rationale behind each mutation is explained below.

Mutations that affect the interaction between ribosomal proteins L5 and L21

As mentioned before, it was recently discovered that the 5S RNP undergoes nearly an 180° rotation during ribosome biogenesis (Leidig et al., 2014) (Wu et al., manuscript under review). Moreover, cryo-EM data show that depletion of L21 largely blocks rotation of the 5S RNP (unpublished data, Beril Tutuncuoglu and Gao Lab). As shown in Fig. 3-3A, we find that, in the pre-rotated preribosome purified using the TAP tagged AF Nog2, L5 and L21 do not make atomic contacts. On the other hand, in the mature ribosome (Fig. 3-3B), L5 and L21 contact each other through a helix-helix interaction (aa. 31-37 of L5), and through a conserved loop residue on L5, K41 (Fig. 3-2). This led to the hypothesis that the L5-L21 interaction may be necessary for locking the 5S RNP into its post-rotated state.

In order to test this hypothesis, we replaced each of the amino acids (aa.31-37) that form this α-helix of rpL5, with alanine. We chose to perform a series of alanine substitutions because we wanted to minimize disruptions to the α-helical structure, while potentially abolishing this interaction with L21. We refer to this mutation as *rpl5-(31-37Ala).*

With respect to loop residue K41, it was evident from the multiple sequence alignment (Fig. 3-2) and the L5 conservation heatmap (Fig. 3-3C), that K41 is conserved. K41 was replaced with both alanine (K41A) and glutamic acid (K41E). While glutamic acid reverses the charge on the lysine residue, the van der Waal's volume of glutamate (109 Å^3) is comparable to that of lysine (135 Å^3).

Mutations that correspond to human DBA missense mutations

A number of mutations in humans that cause DBA occur in *RPL5*, as noted in the Introduction. We asked if we could recapitulate these human DBA mutations in yeast rpL5 to study their molecular phenotype in more detail. In order to do this, we obtained an updated list of human DBA mutations (http://www.dbagenes.unito.it/home.php?select_db=RPL5; Dr.Irma Dianzani, personal communication) and used sequence comparison software (Fig 3-5) to identify homologous residues in yeast. Consistent with the previous multiple sequence alignment results, (Fig. 3-2), we observed that yeast and human rpL5 proteins showed a striking degree of conservation. Among the list of human DBA mutations, many mutations were nonsense or frameshift mutations often rendering the putative protein extremely truncated. Recapitulating these mutations in yeast will result in polypeptides that are only a few amino acids long. Thus, we surmise that these nonsense and missense mutations might closely resemble the haploinsufficiency phenotype of rpL5 in diploids. In haploid yeast, this may be analogous to the null phenotype that occurs in strains where rpL5 is depleted. Hence, investigating the effects of missense DBA mutations offered a pragmatic first step, as opposed to recapitulating the nonsense and the frameshift mutations.

Once we identified the homologous residues in yeast ribosomal protein L5 as described above, we mutated them (Fig. 3-5) and assayed their effects on ribosome biogenesis. In some cases, the homologous residues did not perfectly line up, but were one or two amino acids upstream or downstream. In such cases, we mutated the nearest identical residue, as shown in the boxed regions of Fig. 3-5. Thus, we made the following three mutations in *RPL5*: A291V, G138S and Y129G (Fig. 3-6).

Figure 3-5: Sequence alignment between yeast and human L5

Results of SIM with:

Sequence 1: Yeast (297 residues)
Sequence 2: A2RUM7|A2RUM7_HUMAN (297 residues)

using the parameters:

Comparison matrix: BLOSUM62
Number of alignments computed: 20
Gap open penalty: 12
Gap extension penalty: 4

49.5% identity in 297 residues overlap; Score: 744.0; Gap frequency: 2.0%

```
Yeast         1 MAFQKDAKSSAYSSRFQTPFRRRREGKTDYYQRKRLVTQHKAKYNTPKYRLVVRFTNKDI
A2RUM7|A2R    1 MGFVKVVKNKAYFKRYQVKFRRRREGKTDYYARKRLVIQDKNKYNTPKYRMIVRVTNRDI
                * * *   *   ** * *   ************* ***** * * ********  ** ** **

Yeast        61 ICQIISSTITGDVVLAAAYSHELPRYGITHGLTNWAAAYATGLLIARRTLQKLGLDETYK
A2RUM7|A2R   61 ICQIAYARIEGDMIVCAAYAHELPKYGVKVGLTNYAAAYCTGLLLARRLLNRFGMDKIYE
                ****    * **   *** **** **   **** **** **** *** *   * *   *

Yeast       121 GVEEVEGEYELTEAVEDGPRPFKVFLDIGLQRTTTGARVFGALKGASDGGLYVPHSENRF
A2RUM7|A2R  121 GQVEVTGDEYNVESIDGQPGAFTCYLDAGLARTTTGNKVFGALKGAVDGGLSIPHSTKRF
                *  ** *     *       * *  ** ** ***** ******** ****  *** **

Yeast       181 PGWDFETEEIDPELLRSYIFGGHVSQYMEELADDDEERFSELFKGYLADDIDADSLEDIY
A2RUM7|A2R  181 PGYDSESKEFNAEVHRKHIMGQNVADYMRYLMEEDEDAYKKQFSQYIKNSVTPDMMEEMY
                ** * *   *     *   *   * **  * **   **         * *       * * *

Yeast       241 TSAHEAIRADPAFKPTEKKFTKEQYAAESKKYRQTKLSKEERAARVAAKIAALAGQQ
A2RUM7|A2R  241 KKAHAAIRENPVYEKKPKKEVKK------KRWNRPKMSLAQKKDRVAQKKASFLRAQ
                ** ***  *          ** *         *       * *   *** * *      *
```

Fig. 3-5: Sequence alignment between yeast and human L5.

Shown here is the output from the SIM server (http://web.expasy.org/sim/). A2RUM7 denotes human L5. The regions corresponding to the human DBA mutations are boxed.

Figure 3-6: Yeast L5 amino acid residues corresponding to the human DBA mutations
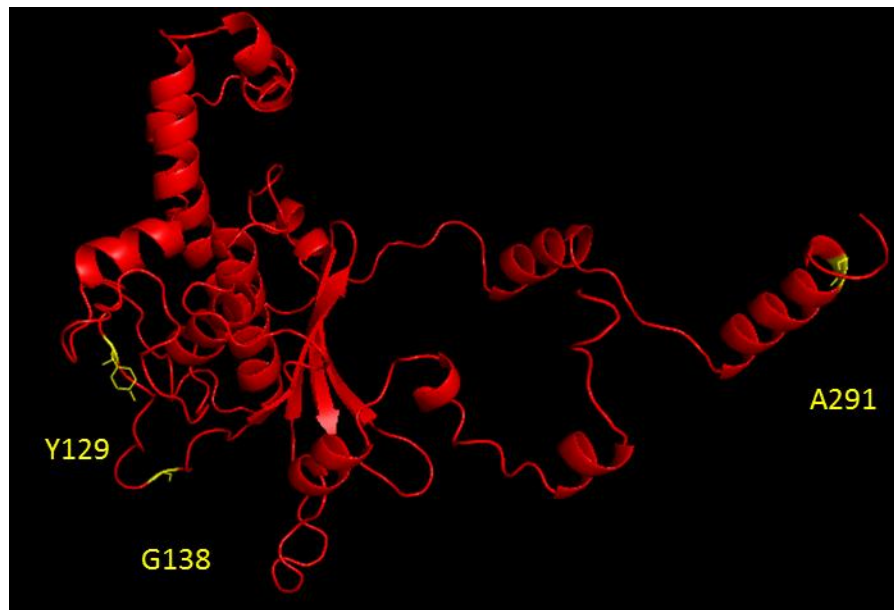
Fig. 3-6: Yeast L5 amino acid residues corresponding to the human DBA mutations.

Pymol representation of homologous yeast residues corresponding to human DBA mutations are shown in yellow with their side chains. The rest of L5 is shown in red as a cartoon.

Mutation that affects L5-L10 interaction

Since we are particularly interested in understanding how the rotated state of the 5S RNP is stabilized, we carefully studied the contacts that L5 form with preribosomes, post-rotation. In addition, an emergent area of interest in ribosome assembly research corresponds to studying the various roles played by N- and C-terminal extensions of ribosome proteins, many of which extend long distances across the surface of ribosomes (Gamalinda and Woolford, 2014; Stelter et al., 2015), (Tutuncuoglu et al., manuscript under review). Strikingly, post rotation, the C-terminal tail of L5 forms an interaction with the eukaryote-specific C-terminal extension of ribosomal protein L10, which assembles into the ribosome only in the cytoplasm (Fig. 3-4), (Lo et al., 2010). Moreover, the tails of both L5 and L10 that form this interaction are eukaryote-specific (Klinge et al., 2011). We postulate that this interaction and more generally, the C-terminal tail of L5 itself, may have specific roles in ribosome biogenesis.

In order to test this idea, we truncated the rpL5 protein at aa. 273, around 25 amino acids upstream of the C-terminus. Henceforth, we refer to this mutant as *rpl5-ΔC*.

Mutation that affects L5-25S rRNA contact

Continuing on the theme of understanding how the 5S RNP is assembled and rotated during ribosome biogenesis, we wanted to disrupt the interaction between rpL5 and large subunit rRNA (Fig. 3-7). We do not observe a major difference in the way amino acids 173-179 of rpL5 interact with the large subunit rRNA in the preribosome and the mature ribosome. Interestingly, an assembly factor that is close to rpL5 and is part of the 5S RNP during assembly, Rpf2, has been shown to crosslink to the same nucleotides in large subunit rRNA that interact with rpL5. This opens up the possibility that this rpL5-rRNA interaction may be dynamic and could play a vital role in cementing rpL5 (and hence, the 5S RNP) to the rest of the large subunit during early stages of CP assembly. In order to study this interaction, we mutated the loop formed by aa. 173-179 of rpL5, by substituting all of these residues with alanine. Henceforth, we refer to this mutation as *rpl5-(173-179Ala)*.

Figure 3-7: Pymol representation of the contacts between L5 and the large subunit pre-rRNA and rRNA
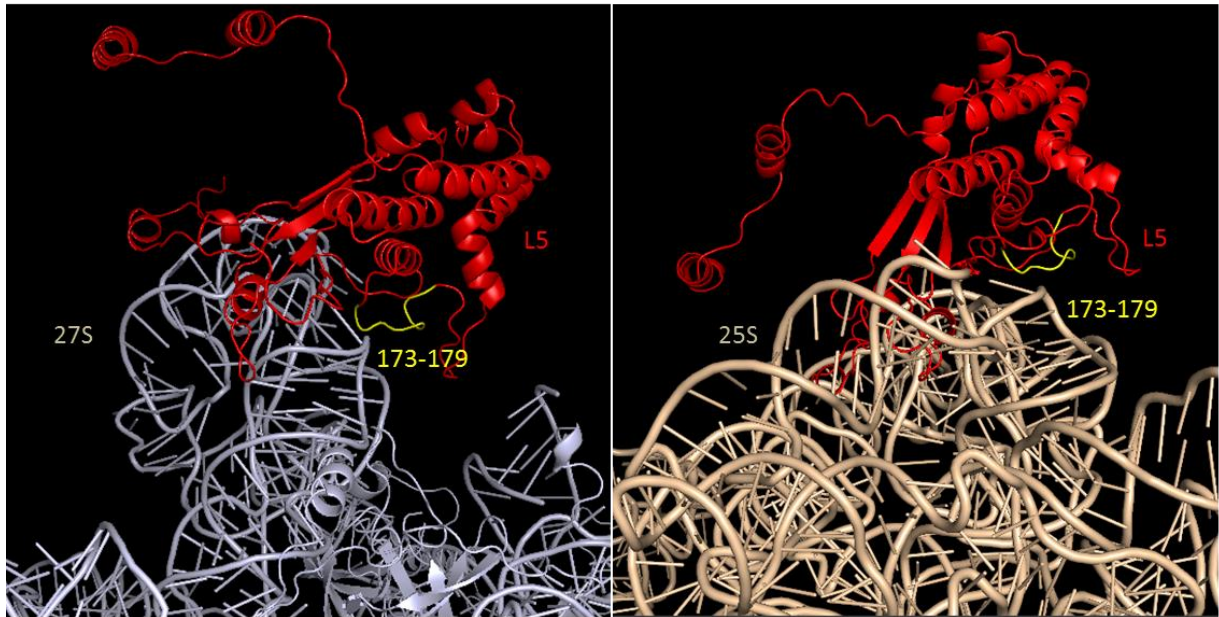
Fig. 3-7: Pymol representation of the contacts between L5 and the large subunit pre-rRNA and rRNA.

(A) L5 is shown in red and the L5 loop that contacts 25S in the mature rRNA is shown in yellow. Large subunit rRNA of the assembling ribosome is shown in bluish white.

(B) L5 shown as in (A). Mature large subunit rRNA is shown in beige.

3.2.2. Construction of rpL5 depletion strain for mutagenesis

Since there is only one copy of the *RPL5* gene in the yeast genome and because L5 is essential, we attempted to place it under the control of a *GAL* promoter. In this manner, we developed a strain conditionally expressing *RPL5* to assay the effects of the absence of rpL5 in the cell. After regular protocols failed to generate this strain, we resorted to using long ultramer oligonucleotides for generating the *GAL-HA-RPL5* (JWY10446) strain. Depletion of L5 in this strain was confirmed by the inability of various clones of this strain to grow on glucose-containing media (Fig. 3-8) and by western blotting (Fig. 3-10B).

In parallel, the *RPL5* ORF with along with upstream and downstream sequences was cloned into the pRS315 vector (Fig. 3-9) and verified by sequencing. All of the mutations described above were made in this construct using the QuikChange Lightning mutagenesis kit and were verified by sequencing.

Figure 3-8: Confirmation of glucose repression of *GAL-HA-RPL5*
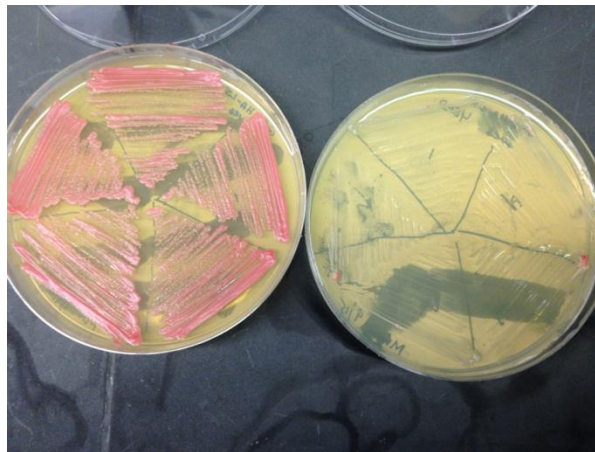
Fig. 3-8: Confirmation of glucose repression of GAL-HA-RPL5.

Five clones of the newly constructed*GAL-HA-RPL5* strain grown on YEPGal (Left) and YEPGlu (Right)

solid media, incubated at 30$^{\text{o}}$C for three days.

Figure 3-9: Cloning the *RPL5* ORF into the pRS315 vector
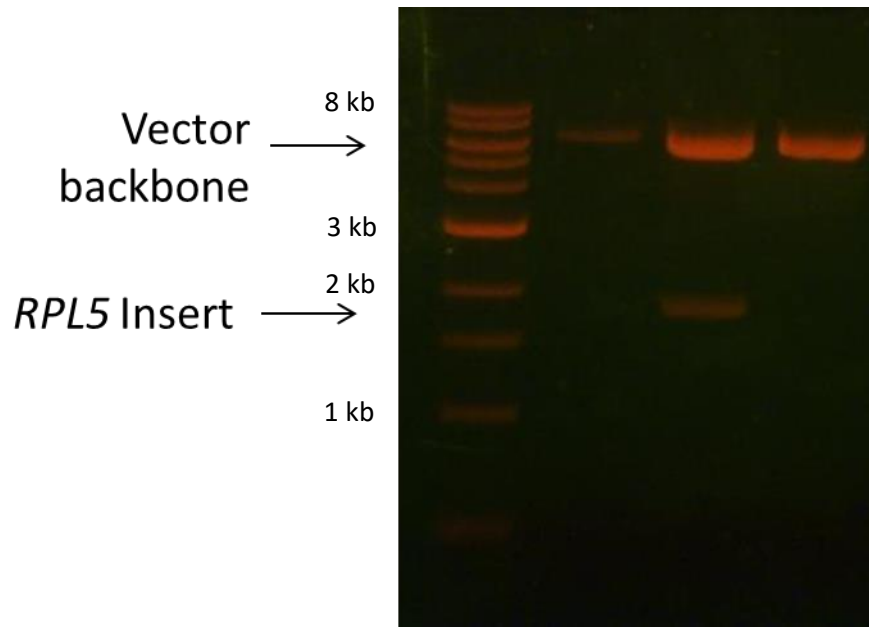
Fig. 3-9: Cloning the *RPL5* ORF into the pRS315 vector.

Restriction digested fragments visualized by EtBr staining on a 1% agarose gel. The expected size of the vector backbone and the insert (L5 ORF) are indicated. Lane 1: Vector with no insert. Lane 2: Positive candidate, verified subsequently by sequencing. Lane 3: Negative candidate.

3.2.3. Depletion of rpL5 parallels a severe defect in growth

Although it was known that the *RPL5* gene is essential, we wanted to verify the growth phenotype of the *GAL-HA-RPL5* strain, specifically to and examine whether the depletion of rpL5 paralleled the slowing of growth. To do so, we grew a starter culture of *GAL-HA-RPL5* in YEPGal to log phase and used this culture to inoculate into either YEPGal or YEPGlu liquid media. We followed the growth of these strains by measuring their OD610 at multiple time points over a period of 24 hours. The cultures were diluted as and when needed, to maintain the cells in log phase growth. As shown in Fig. 3-10A, the growth curves corresponding to the WT (Galactose) and rpL5-depleted (Glucose) diverged within the first few hours after shifting to YEPGlu medium.

Whole cell lysates were prepared from samples withdrawn at various time points after the shift to glucose-containing media. The proteins were separated by electrophoresis, blotted and probed with antibodies for L5. The results showed that the levels of rpL5 protein in the cells decreased over time (Fig. 3-10B) and paralleled the growth defect (Fig. 3-10A). This confirms that rpL5 is necessary for cell viability. Based on these observations, for all further experiments, we decided to use a 16-hour shift to glucose medium in order to completely deplete rpL5, while minimizing secondary effects that might arise due to a longer shift.

Figure 3-10: Shut-off of genomic L5 expression parallels growth defect in *GAL-HA-L5*
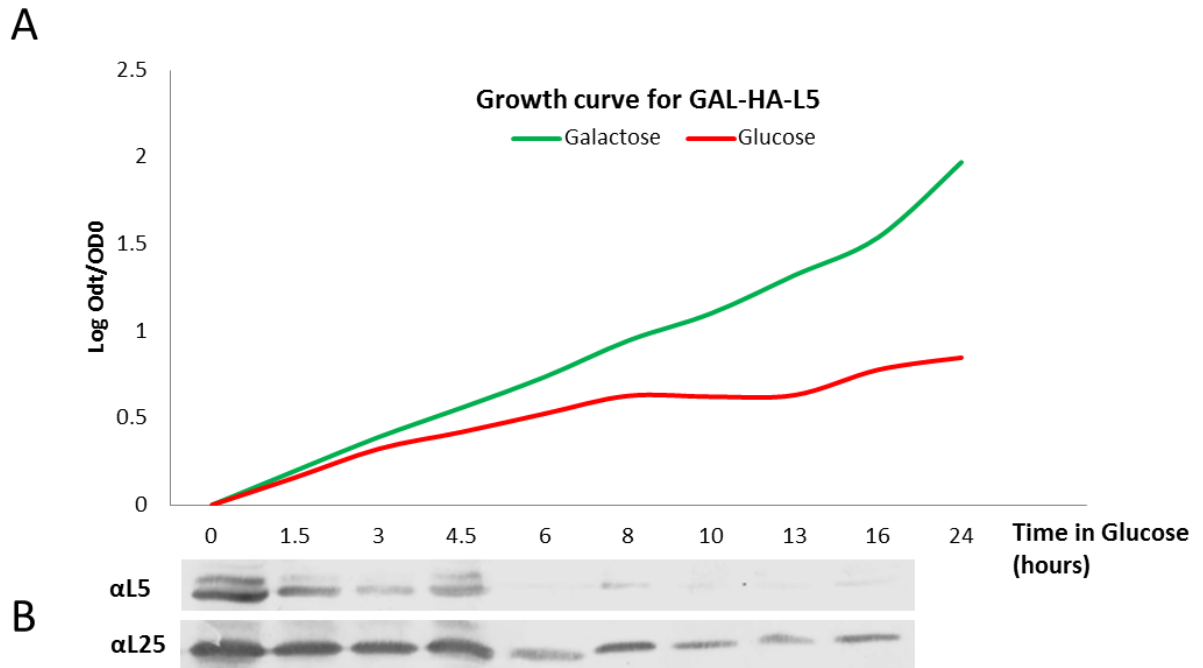
Fig. 3-10: Shut-off of genomic L5 expression parallels growth defect in *GAL-HA-L5.*

(A) Growth curves for the *GAL-HA-L5* culture grown either in YEPGal (green) or YEPD (red). OD was measured at the time points indicated on the X-axis over a 24 hour period and the cultures were diluted accordingly to maintain them at log phase at regular intervals.

(B) Western blot showing depletion of endogenous L5 protein (top panel) when *GAL-HA-L5* is grown in glucose, roughly coincident with the slowing of growth shown in (A). L25 (bottom panel) is used as a loading control for comparison.

3.2.4. Effect of rpL5 mutations on viability

We began to assay the *in vivo* phenotype of the *rpl5⁻* mutants by first assaying their growth. Serial dilutions of log phase cultures were spotted onto solid media containing either galactose or glucose (Fig. 3-11). We tested the growth phenotype at three different temperatures in order to reveal any temperature/cold sensitivity exhibited by the mutants.

At 30°C, (Fig. 3-11A) on galactose medium (left panels), most mutants grew normally as expected, since genomic WT *RPL5* is expressed under these conditions. The only exception seems to be the *rpl5-ΔC* mutant that exhibits slightly slower growth, even though equal ODs of cultures were spotted, raising the possibility that the mutant may exert partial dominance over wild-type RPL5. On glucose medium (right panels), when endogenous *RPL5* expression is turned off, we observe that the *rpl5-(31-37Ala)*, *rpl5-ΔC* and *rpl5-(173-179Ala)* mutants are unable to grow. Their growth closely resembles the empty vector negative control (top row), while the rest of the mutants exhibit growth comparable to that of WT (second row).

Interestingly, at 37°C, (Fig. 3-11B) on galactose medium (left panels), the dominant phenotype of the *rpl5-ΔC* mutant observed at 30°C was exacerbated. On glucose medium (right panels), when endogenous *RPL5* expression is turned off, we observe that *rpl5-(31-37Ala)*, *rpl5-ΔC* and *rpl5-(173-179Ala)* are unable to grow, as expected from their growth defect at 30°C. The DBA mutant *rpl5-A291V* seems to exhibit slight temperature sensitivity.

Similar results were observed at 16°C, (Fig. 3-11C). On galactose medium (left panels), most mutants grew normally as expected while the dominant phenotype of the *rpl5-ΔC* mutant observed at 30°C was exacerbated. On glucose medium (right panels), when endogenous *RPL5* expression is turned off, we observe that *rpl5-(31-37Ala), rpl5-ΔC* and *rpl5-(173-179Ala)* are unable to grow, as expected from their growth defect at 30°C.

Figure 3-11: Growth phenotype of *rpl5-* mutants

A

C-Leu + Galactose   C-Leu + Glucose

B

37ºC

Empty vector
WT L5
31-37Ala
K41A
K41E
A291V

Empty vector
WT L5
G138S
Y129G
ΔC
173-179Ala

C-Leu + Galactose   C-Leu + Glucose

C

18ºC

Empty vector
WT L5
31-37Ala
K41A
K41E
A291V

Empty vector
WT L5
G138S
Y129G
ΔC
173-179Ala
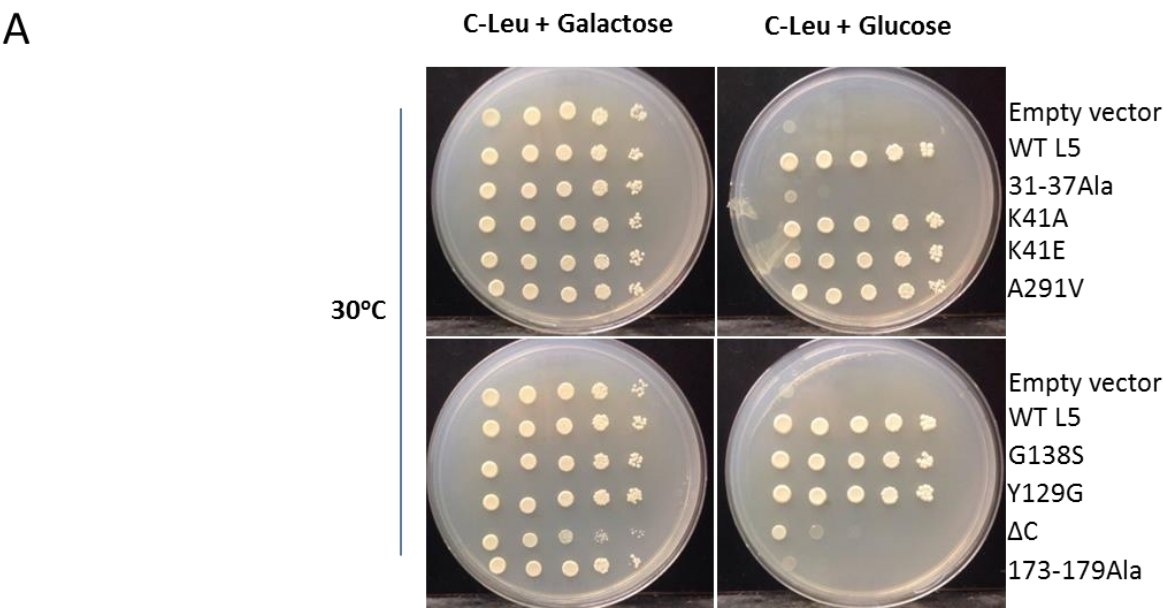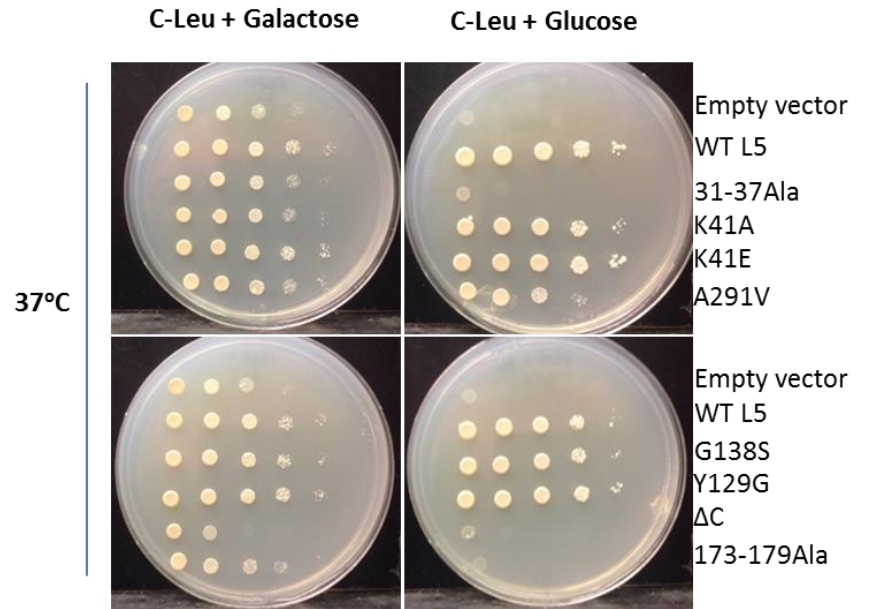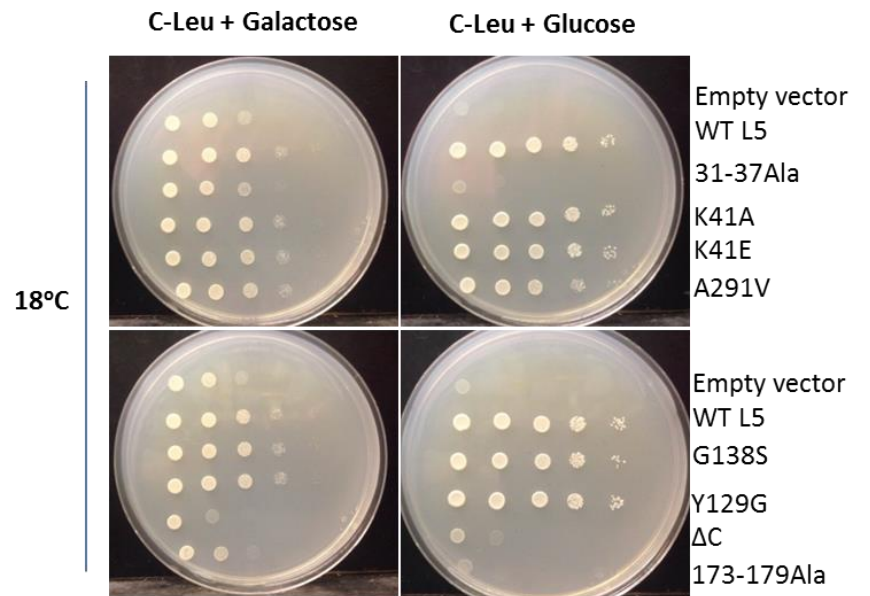
Fig. 3-11: Growth phenotype of *rpl5-* mutants.

(A)   Serial dilutions of log phase yeast cultures were spotted onto solid medium and assayed for

growth at 30°C, either on C-Leu + Gal solid media (left panels, genomic L5 is expressed) or on

C-Leu solid media (right panels, only plasmid-derived L5 is expressed). Empty vector and

WT controls ("WT L5") are indicated on each plate.

(B): Same as (A), except, growth was assayed at 37°C.

(C): Same as (A), except, growth was assayed at 18°C.

3.2.5. Lethal rpl5 mutants are defective in ribosome biogenesis

Having identified the lethal *rpl5*[-] mutations, we asked if the lethality is due to defects in synthesizing

stable ribosomes. We separated total RNA extracted from various control strains and mutants on an

agarose gel, blotted it and probed for mature 25S rRNA (Fig. 3-12). Consistent with their growth defect,

for each of the *rpl5* mutants that exhibited lethality, we observed that the levels of 25S rRNA were

severely diminished, comparable to the diminished levels in the rpL5 depleted samples (lanes 2 and 4).

This suggests that lethality exhibited by these mutants is due to an inability to generate stable 25S

rRNA.

We included the *GAL-HA-RPL5* strain grown under either YEPGal or YEPGlu (lanes 1 and 2) as a

control, since this is the first time this particular depletion strain was being used for these experiments,

and in order to identify any minimal media-specific effects on the phenotype. The phenotype of mutants

grown in rich media (lanes 1 and 2) and those grown in minimal media (lanes 3 and 4) are nearly

identical, although the effects seem stronger in the rich media depletion conditions. These more

pronounced effects could result from the faster doubling times of both WT and mutant strains when

grown in rich media.

Figure 3-12: Assaying defects in ribosome biogenesis by northern blotting
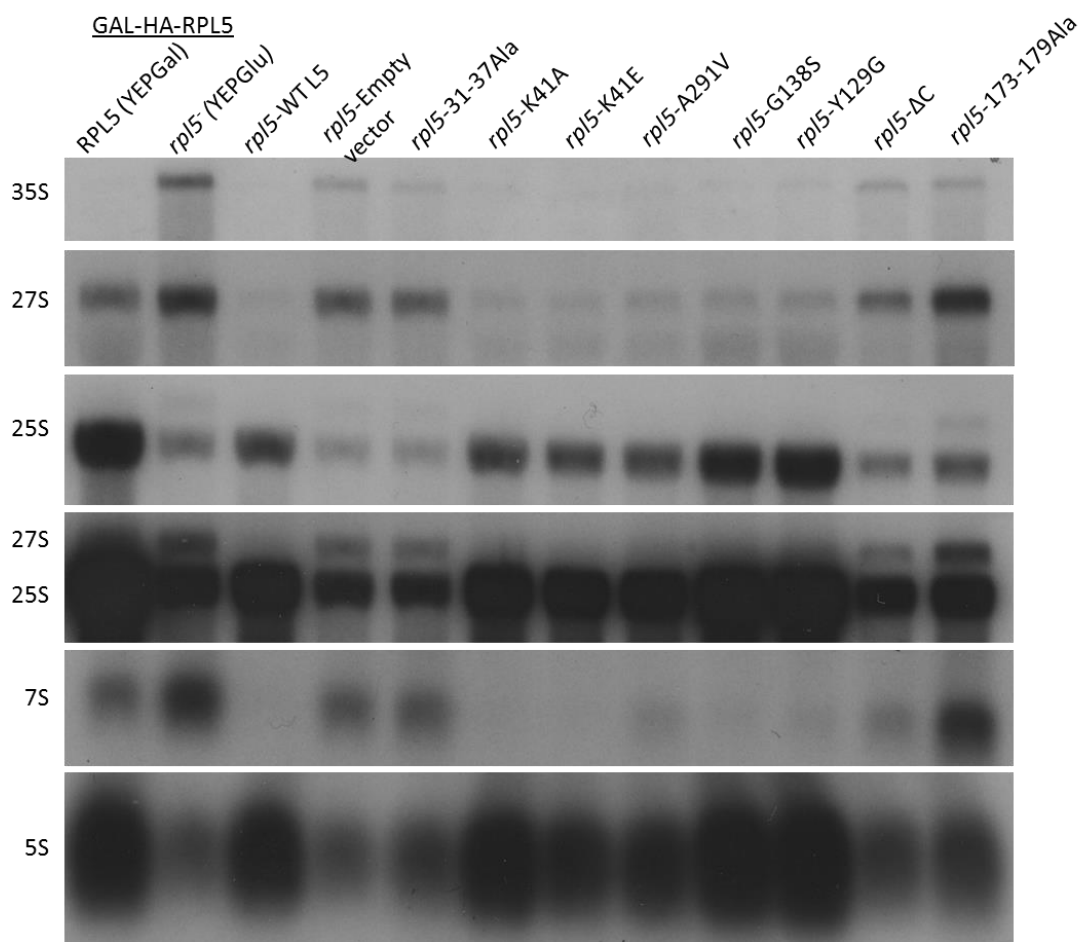
Fig. 3-12: Assaying defects in ribosome biogenesis by northern blotting.

Northern blot of total cellular RNA extracted from *rpl5-* mutants, probed with various oligonucleotides in order to detect rRNAs and pre-rRNAs, as indicated on the left. 27S, 7S and 35S pre-rRNAs were detected using the ^{32}P-labeled ITS2A oligonucleotide probe. The first two lanes correspond to *GAL-HA-RPL5* grown in galactose and glucose, respectively. The rest of the lanes correspond to plasmid-bearing *GAL-HA-RPL5* grown on C-Leu+Gal and then shifted to C-Leu for 16 hours. The control/mutant plasmid carried by each strain is indicated above the lane.

3.2.6. Pre-rRNA processing defects in rpl5- mutants

Ribosome assembly proceeds via a series of exonucleolytic and endonucleolytic processing steps that have conventionally been used as landmarks for various stages of ribosome assembly (Fig. 3-13). We used a northern blotting assay (Fig. 3-11) to probe for various pre-rRNAs, including an oligonucleotide primer that detects 35S, 27S and 7S pre-rRNAs. We observed the following:

(i)   For all of the viable *rpl5* mutants, the pre-rRNA processing pattern closely resembled that in WT cells. Hence, our further results focus only on the lethal mutants (lanes 5, 7 and 8) and the depletion phenotypes (lanes 2 and 4), and compare them to WT cells (lanes 1 and 3)

(ii)   The depletion of L5 (lanes 2 and 4) and other lethal *rpl5*$^-$ mutants (lanes 5, 7 and 8) tend to slow down pre-rRNA processing overall, since we observed an increase in the 35S pre-rRNA precursor (top panel). This effect was more pronounced when grown in rich media (lane 2).

(iii)   Concomitant with the dramatic decrease in the levels of 25S mature rRNA, we observed an increase of the 27S precursor RNAs in the lethal mutants and the lethal depletion mutants (2nd panel). This is also evident in an overexposed film after probing for the mature 25S rRNA, where we detect the 27S precursor that accumulates in these mutants in addition to mature 25S rRNA (4th panel).

(iv)   The increase in 27S precursor RNA was accompanied by an increase in the 7S pre-rRNA (precursor to the 5.8S rRNA) in both the depletion as well as the other lethal mutants (5th panel). The only exception to this pattern was the *rpl5-ΔC* mutant that seemed to accumulate less 7S pre-rRNA compared to the depletion. This suggests that these lethal mutants are blocked in late nuclear steps of assembly, similar to the rpL5 depletion phenotype.

(v)   Finally, the steady state levels of 5S rRNA seem to be severely diminished in the lethal and the depletion mutants. Whether this is due to an inability of the mutant L5 protein to

associate with 5S, or if it is an effect of inability to assemble 5S RNP into preribosomes or

faulty ribosome synthesis leading to turnover, is not clear at this point.

Figure 3-13: An illustration of portions of the pre-rRNA processing pathway in yeast
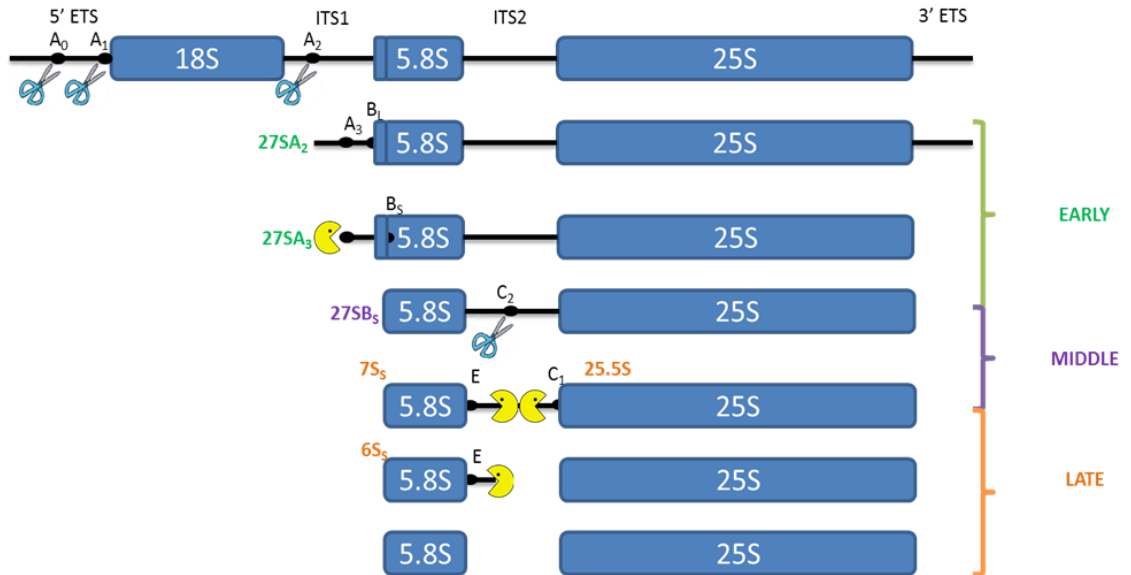
Fig. 3-13: An illustration of portions of the pre-rRNA processing pathway in yeast.

Early, middle and late processing steps as well as processing intermediates are color coded in green, purple and orange respectively. Various pre-rRNA species are indicated.

3.2.7. Assaying preribosome composition in rpl5 mutants

In order to analyze the effects of these mutations on the assembly of various ribosomal proteins and to gain a more mechanistic understanding of the phenotype of these mutants using changes in the association of assembly factors, we assayed preribosome composition in our *rpl5* mutants.

TAP tagging Nop7

In order to do this, we wanted to TAP-tag a suitable assembly factor that could be used to affinity purify preribosomes. We could then assay the protein composition of the purified preribosomes. Nop7 was chosen as a suitable assembly factor to TAP-tag for two reasons:

(i) Nop7 associates with the pre-ribosome early on in the ribosome biogenesis pathway and is not released until very late. Thus, examining Nop7 particles could enable us to inspect the effects of *rpL5* mutations during most stages of assembly when L5 is normally present.

(ii) Previous studies have shown that Nop7 is not affected by depletion of L5; hence we will still be able to purify ample quantities of preribosomes to assay their composition in a robust manner.

Fig. (3-14) shows a western blot that confirms that Nop7 is indeed TAP-tagged in the *GAL-HA-RPL5* strain, as seen by the band corresponding to the expected size of Nop7-TAP, detected by both Nop7 and TAP antibodies.

Figure 3-14: Western blotting of whole cell lysate to verify TAP-tagging of Nop7 in the
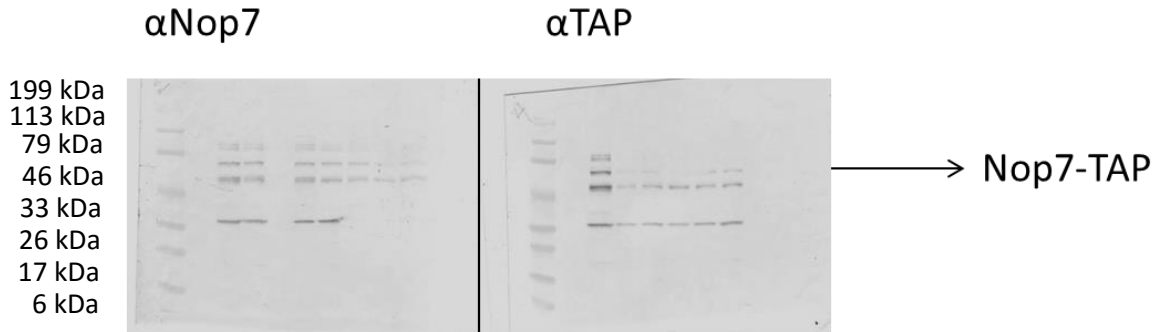
GAL-HA-RPL5 **strain**

Fig. 3-14: Western blotting of whole cell lysate to verify TAP-tagging of Nop7 in the GAL-HA-RPL5 strain.

The left panel shows the blot probed with anti-Nop7 antibody and the right panel shows the blot probed with anti-TAP antibody. The expected size of Nop7-TAP protein is marked. Lane 1 corresponds to the negative control (*GAL-HA-RPL5*). Subsequent lanes are candidates 1 through 8.

3.3. Discussion/Next steps

Here, we sought to investigate the effects of mutations that potentially abrogate various molecular contacts established by rpL5 and those that recapitulate the mutations found in human DBA patients. We found that our alanine substitution mutations *rpl5-(31-37Ala) and rpl5-(179-179Ala),* and the *rpl-ΔC* mutation resulted in lethality. We also showed that these lethal mutants are defective in late nuclear steps of LSU biogenesis. On the other hand, our yeast *rpL5⁻* missense mutations that were analogous to the human DBA mutations did not result in lethality or any obvious defects in biogenesis. While this is a work in progress, below we discuss the potential implications of these results in the light of the rationale behind the mutations and outline further experiments to ascertain our hypotheses (Fig. 3-15).

Figure 3-15: Table summarizing various mutants, their growth and pre-rRNA processing phenotypes, revealed by various assays

	L5 depletion	31-37Ala	K41A	K41E	A291V	G138S	Y129G	C-del	173-179Ala
Type	L5 nearly absent	L21 helical interaction	L21 loop interaction	L21 loop interaction	DBA	DBA	DBA	L10 interaction	25S interaction
Growth at 30°C	Lethal	Lethal	Normal	Normal	Normal	Normal	Normal	Lethal, slightly dominant	Lethal
Growth at 37°C	Lethal	Lethal	Normal	Normal	Slightly slower	Normal	Normal	Lethal, dominance exacerbated	Lethal
Growth at 18°C	Lethal	Lethal	Normal	Normal	Slightly slower	Normal	Normal	Lethal, dominance exacerbated	Lethal
25S / 18S	↓	↓	Normal	Normal	Normal	Normal	Normal	↓	↓
5S / 5.8S	↓	↓	Normal	Normal	Normal	Normal	Normal	↓	↓
35S	↑	↑	Normal	Normal	Normal	Normal	Normal	↑	↑
27S	↑	↑	Normal	Normal	Normal	Normal	Normal	↑	↑
7S / 6S	↑	↑	Normal	Normal	↑	Normal	Normal	↑	↑

Fig. 3-15: Table summarizing various mutants, their growth and pre-rRNA processing phenotypes, revealed by various assays.

3.3.1. Implications of potential disruption of the rpL5-rpL21interaction

The *rpl5-(31-37Ala)* mutant was designed to potentially disrupt the interaction between rpL5 and rpL21 that is established exclusively after rotation of 5S RNP (Fig. 3-3). We observed that mutation of this α-helical interaction was detrimental to growth and production of mature 25S rRNA. We also found that 27S and 7S pre-rRNA accumulate in this mutants, suggesting that late nuclear steps of ribosome assembly are affected (Fig. 3-11, Fig. 3-12). Interestingly, results obtained by Beril Tutuncuoglu in our lab have demonstrated the reciprocal relationship of the interaction between rpL5 and rpL21. She mutated the α-helix of rpL21 that forms this interaction and showed that the mutation results in a similar phenotype.

In addition to the α-helical interaction, rpL5 and rpL21 also form a loop interaction, as evident in the crystal structure of the mature ribosome. Missense mutations (*rpl5-K41A and rpl5-K41E*) of the rpL5 loop residue that contacts the loop of rpL21 resulted in no discernable phenotype in this study. However, preliminary results from Beril Tutuncuoglu show that the mutation of the corresponding loop in rpL21 can rescue the phenotype of the α-helical mutation in rpL21 described above. She proposes that together, *rpl21⁻* loop mutations loosen the interaction with the assembly factor Rrs1, such that the initial contact with Rrs1 can be more easily broken and rpL21 can now establish contact with rpL5. This result opens up a plethora of possibilities about how the dynamics of this switch in molecular interactions made by rpL21 might enable rotation and further lock down the rotated state by establishing the rpL5-rpL21 contact. The first step from the perspective of rpL5 would be to generate combination mutants where both the α-helix and the loop residue are mutated. If we do see a rescue of the phenotype of the *rpl5-(31-37Ala)* α-helical mutation, we would infer that the molecular contact of rpL5 and rpL21 is important in an Rrs1-independent fashion (Fig. 3-3).

3.3.2. DBA mutants – further analysis

In our analysis, none of the DBA missense mutants resulted in a strong, discernable phenotype in synthesis of mature 25S rRNA (Fig. 3-12). However, potential inefficiencies in the functioning of the ribosome can be revealed by assaying their translational fidelity. Hence, we plan to assay their growth on media containing various translation-inhibiting drugs. If we do not see any defects in assembly and function whatsoever in the existing set of mutants, we will resort to making other homologous disease mutations and combinations of those mutations, and further assaying for ribosome biogenesis and function in those mutants.

3.3.3. Does rpL10 fail to associate in the C-terminal truncation mutant?

Perhaps the most striking finding that emerged from this mutational analysis was the lethality, defects in late nuclear steps of ribosome assembly and a slight dominance over WT rpL5 exhibited by the C-terminal truncation mutant *rpl5-ΔC*. As mentioned before, the goal of this truncation was to potentially disrupt the interaction between rpL5 and rpL10 that occurs after nuclear export. Interestingly, a previous study from our lab analyzed the effect of this deletion (Deshmukh et al., 1995). Consistent with our results, they found that this truncation caused lethality. They also noted that while this mutant *rpl5* can bind 5S rRNA, it binds less well in comparison with the WT rpL5. Remarkably, the authors assayed the ability of this *rpl5* truncation mutant to assemble into polysomes. They found that, while this mutant co-sedimented with the 60S LSU fraction, it failed to sediment with the 80S ribosome and the polysome fractions. This result would be expected if binding of rpL10 and subsequent cytoplasmic test drive steps were disrupted in this mutant, in the light of the recent knowledge that has emerged about the late steps of ribosome assembly.

We will test this hypothesis by the following series of experiments. First, we will assay the changes in protein composition of the *rpl5-ΔC* mutant prior to nuclear export by affinity purifications followed by

mass spectrometry, using the *GAL-HA-RPL5 NOP7-TAP* strain that we recently built. Next, we will test for successful nuclear export of preribosomes in this mutant using a GFP-tagged rpL25 reporter. If we find that preribosomes are exported in this mutant, we would like to test the association of rpL10 by affinity purifying cytoplasmic preribosomes with an appropriate assembly factor tag (preferably Kre35). We speculate that this mutant may be deficient in the recruitment of rpL10. If we observe that rpL10 does not associate with the preribosome, we will test if the lethal phenotype of this mutant can be rescued by overexpression of rpL10. Further, we will assay for any translation defects when the mutant is expressed in the presence of WT rpL5, by assaying the ability of the strain to grow on media containing various translation inhibiting drugs.

Overall, we hypothesize that this *rpl5-ΔC* mutant may be deficient in recruiting rpL10 to the preribosome. The slight dominance that we observe in this mutant may result from indirect, as opposed to direct means of recruiting rpL10. For instance, the C-terminal tail of rpL5 may be necessary to remove an assembly factor that might be precluding the association of rpL10. Once the assembly factor is removed, rpL10 can associate and form the eukaryote-specific contact with the C-terminal tail of rpL5. (Fig. 3-4)

3.3.4. Does the rRNA interaction mutant affect loading of 5S RNP onto the LSU?

The mutation that putatively disrupts the interaction of the loop of rpL5 with 25S rRNA (Fig. 3-7) led to lethality and severely diminished levels of 25S rRNA (Fig. 3-11, Fig. 3-12). As pointed out before, this interaction of rpL5 with the LSU rRNA seems to exist both in the pre-rotated and post-rotated state, even though this overall central protuberance region undergoes a major structural change during the rotation. This suggests that rpL5 and helix 87 that it binds as it latches on initially to the assembling ribosome, may move *en bloc,* while keeping their initial contacts intact. This raises the possibility that this interaction is important for the loading of the 5S RNP initially during biogenesis. The fact that the

assembly factor Rpf2 that aids 5S RNP loading shares this binding site with rpL5 seems to reinforce this hypothesis. Hence, the reason why this mutation is lethal and has a severe ribosome biogenesis effect could be a partially explained by lack of efficient assembly of 5S RNP early in assembly (Fig. 3-1, Fig. 3-7)

To examine this idea, we will test for the association of other 5S RNP proteins in this mutant by analysis of the protein composition of the preribosome. If it does turn out that 5S RNP cannot assemble efficiently onto the preribosome, we will ask if overexpressing rpL11 can rescue this effect, since bolstering other nearby contacts between the 5S RNP and the preribosome could overcome the inability of rpL5 to latch on to the preribosome. In an alternative scenario where there may be a dynamic molecular switch mediated by a competition between rpL5 and Rpf2 for the same site on helix 87, either for the recruitment of rpL5 or for the release of Rpf2, we expect to see synthetic effects between *rpf2⁻* mutants and *rpl5⁻* mutants that disrupt its interaction with helix 87.

3.4.   Summary

Taken together, data emerging from our mutational analyses indicate that rpL5 can perform a plethora of functions in ribosome assembly, by way of its various molecular interactions (Fig. 3-15). We have begun to reveal and tease apart the significance of each of these interactions and functions in this study. While further experiments are necessary to establish precise molecular models for each of these functions, this study is exemplary for how a non-enzymatic protein that is part of an RNP can perform various functions in various contexts. These different functional contexts can be defined by the set of various proximal molecular interactions formed by rpL5 (these molecular interactions may differ in space and time), allosteric effects and dynamics of global changes that occur in the RNP particle (such as rotation of the 5S RNP).

3.5. Materials and methods

- Construction of yeast strains: Construction of the *GAL-HA-RPL5* in the W303 strain background was accomplished using ultramer oligonucleotides as described previously (Longtine et al., 1998). PCR product containing the *GAL1* promoter followed by an ATG codon and sequences encoding 3HA were generated. This PCR product that also contains *TRP1* selectable marker gene and sequences complimentary to *RPL5*, was transformed into haploid W303 strain such that the PCR cassette for the GAL promoter can recombine immediately upstream of the start codon. Candidates were first screened by ability grow on media lacking tryptophan and were then tested for inability to grow on glucose medium (since L5 is essential) and verified further by western blotting using an anti-HA antibody.

- Growth of yeast strains: Unless otherwise specified, yeast strains were grown either in YEPGlu (1% yeast extract, 2% peptone and 2% dextrose) or YEPGal (1% yeast extract, 2% peptone and 2% galactose) at 30°C. Phenotypic assays were conducted after 16 hours of growth in glucose medium, unless indicated otherwise.

- Growth Assays: Spotting assays were performed as described in the main text. For the growth curve, the OD 610nm was measured and further, 10ml samples of cultures were withdrawn at stated intervals from a 200 ml culture. The parent culture was diluted to maintain growth.

- Generation of *rpl5* mutant alleles: The *S. cerevisiae RPL5* ORF including around 800bp upstream of the start codon and 150bp downstream of the stop codon was cloned into pRS315 using *BamHI* and *HindIII*. Mutations were introduced using the Quickchange Lightning kit from Agilent Technologies. The mutations made are described in detail in the main text. Plasmids bearing mutant alleles were transformed into *GAL-HA-RPL5* strain that was generated, and maintained on media lacking leucine.

- RNA analysis: RNA from log-phase yeast cultures was extracted as described previously (Horsey et al., 2004). A Nano Drop spectrophotometer (Thermo Fisher) was used to quantify RNA. 5µg RNA was

used for northern blotting. For the agarose northerns, total cellular RNA was separated by electrophoresis on an 1.2% agarose gel for 6 hours at 150V and blotted, such that RNAs of all sizes can be assayed.

- Protein extraction, SDS-PAGE and Western blotting were performed as described in (Talkish et al., 2014b).

- Sequences of oligonucleotide probes are available upon request.

4. Analyzing protein and RNA interactions formed by the ITS2 cluster proteins (Nop15, Cic1 and Rlp7)

4.1. Introduction

Ribosome biogenesis in eukaryotes is spatio-temporally coordinated and facilitated by around 200 *trans*-acting factors consisting of assembly factor proteins and snoRNAs (Henras et al., 2008; Woolford and Baserga, 2013). These factors orchestrate various critical events of the assembly pathway including folding, processing, and modification of rRNA and concomitant binding of ribosomal proteins into the assembling ribosome. Thus, the assembly factors perform diverse, indispensable roles in ribosome biogenesis ranging from scaffolding functions to serving as enzymes.

4.1.1. Why do we need to study assembly factors in greater depth?

Even though bacterial ribosomes have been previously reconstituted *in vitro* in the absence of assembly factors, the involvement of such a large number of evolutionarily conserved assembly factors participating in ribosome biogenesis indicates that they might have distinct and as yet unexplored roles. The classic approach to study the function of these assembly factors (henceforth, the term 'assembly factors' is used to refer primarily to protein assembly factors), most of which are essential, has been to study how their depletion affects pre-rRNA processing. This has allowed characterization of the consequences of the overall absence of each of many assembly factors. There have also been many studies on the roles of enzymatic assembly factors (Kressler et al., 2010; Martin et al., 2013; Rawling and Baserga, 2012; Rodriguez-Galan et al., 2013). But the less obvious functions of assembly factors like scaffolding and facilitating the formation of proper rRNA structures have been understudied.

Hence, it is necessary to elaborate on the various functions of assembly factors by studying more subtle perturbations, rather than resorting to merely assaying null phenotypes, to appreciate their functions at a deeper, mechanistic level. It might be the case that assembly factors have multiple roles in assembly, and such higher resolution studies would enable us to deconvolute these roles. Also, the only obvious function of many assembly factors that are essential for viability seems to be protein or RNA

binding. Thus, the study of such assembly factors provides an excellent framework for investigating the general principles governing the interaction networks among proteins (especially the non-enzymatic ones) and RNA, and how they function together as an ensemble inside the cell.

4.1.2. The A3 processing step and 'A3-factors'

Ribosomal RNA is transcribed as one long precursor that undergoes a series of processing steps before maturation (Fig. 4-1). The A3 processing step (boxed in Fig. 4-1) involves the exonucleolytic removal of ITS1 sequences from $27SA_3$ pre-rRNA to form the 27SBs pre-rRNA. This step is important as it generates the 5' end of the mature 5.8S RNA. Also, during the course of biogenesis, this step is thought to trigger a conformational switch from base pairing between ITS1 and the 5' end of 5.8S to base pairing between 25S rRNA and the 5' end of 5.8S RNA (the proximal stem) as observed in the mature ribosome. This switch further triggers the other related events of assembly like more stable association of a ribosomal protein, rpL17, which lines the polypeptide exit tunnel. Thus, the A3 step exemplifies the coordinated action of proteins and RNA to cause rRNA folding, processing and ribosomal protein binding. Salient points about this A3-processing step are highlighted below.

- Three exonucleases, Rat1/Rai1 heterodimer, Rrp17 and Xrn1, are involved in this processing.

- Apart from the exonucleases, a group of seven assembly factors were identified in pioneering studies in our lab and others that exhibit a characteristic phenotype where $27SA_3$ pre-rRNA processing is blocked leading to its accumulation and resulting in decreased production of 27SBs. These A3-factors include RNA binding proteins (Nop15, Cic1, and Rlp7), scaffolding proteins (Nop7, Erb1, Ytm1) and proteins with no predicted function (Rrp1). The pre-rRNA processing phenotype upon depleting Nop15 (Sahasranaman et al., 2011) is shown as an example in (Fig. 4-2).

Figure 4-1: Pre-rRNA processing pathway in *Saccharomyces cerevisiae*
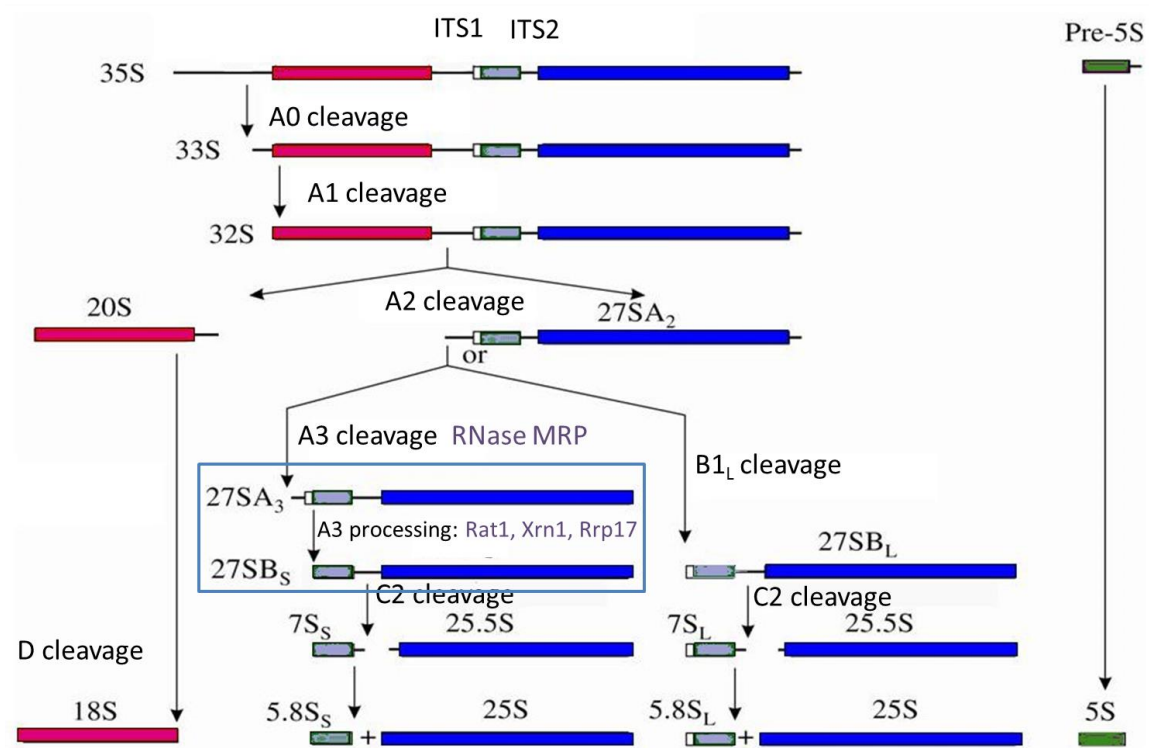
Fig. 4-1: Pre-rRNA processing pathway in *Saccharomyces cerevisiae.*

The small subunit-bound rRNA is shown in pink; the other rRNAs are destined to be part of the large subunit. The names of each pre-rRNA species are shown, and the steps used to process them are indicated.

Figure 4-2: Depletion of Nop15 results in accumulation of 27SA$_3$ pre-rRNA and a concomitant

decrease in 27SB$_S$ pre-rRNA
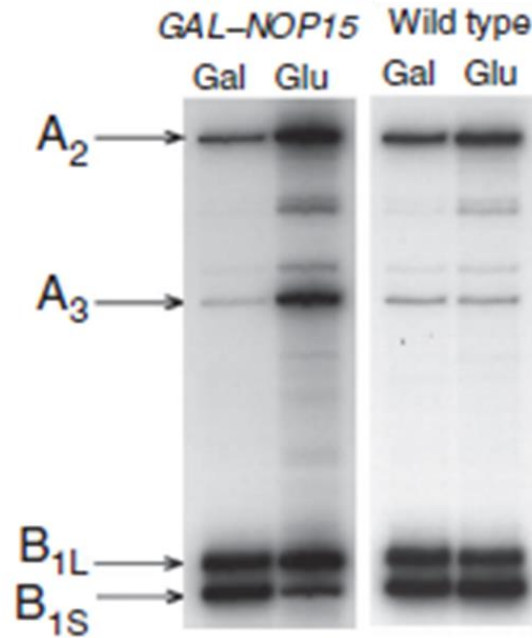
Fig. 4-2: Depletion of Nop15 results in accumulation of 27SA$_3$ pre-rRNA and a concomitant decrease in 27SB$_S$ pre-rRNA.

Steady state levels of pre-rRNA species are measured by reverse transcription using an oligonucleotide primer that binds to the ITS2 spacer. Corresponding strains used and the 5' ends of pre-rRNAs are indicated. Adapted from (Sahasranaman et al., 2011).

- Temporal studies on these proteins have demonstrated that they associate very early in assembly with 90S preribosomes. The last ones to enter, Nop15 and Rrp1, associate with 66S particles containing the $27SA_2$ pre-rRNA, much earlier than the step in which they participate (Sahasranaman et al., 2011).

- All of these A3-factors, except Rrp1, are interdependent for association with the preribosome (Sahasranaman et al., 2011).

- Also, the A3-factors do not seem to recruit the major exonuclease used for this step, Rat1. Rat1 is associated with preribosomes earlier than the step in which it functions, even before its substrate, the $27SA_3$ pre-rRNA, is formed.

- However, it seems that the A3-factors are necessary for the association of the DEAD-box helicase, Has1, to the large subunit (Dembowski et al., 2013b). It is thought that this enzymatic assembly factor Has1 couples the folding of Domain I of pre-rRNA and early pre-rRNA processing to subsequent pre-rRNA processing steps and stable assembly of ribosomal proteins.

- Apart from enabling $27SA_3$ processing, the A3-factors are also required for the association of four ribosomal proteins L17, L35, L26, L37 with the assembling ribosome, downstream of Has1 in the hierarchy of recruitment. Based on the crystal structure, these four proteins form a neighborhood adjacent to 5.8S rRNA in the mature ribosome, and line the polypeptide exit tunnel (Gamalinda et al., 2013). In summary, as alluded before, the A3-factors exemplify principles underlying ribosome biogenesis, participating in processing and folding of rRNA and also in the association of ribosomal proteins.

4.1.3. The ITS2 cluster - A3-factors of the ITS2 neighborhood

Among the A3-factors, my focus is on three A3-factors that bind the ITS2 rRNA spacer – Nop15, Cic1 and Rlp7. Though the ITS2 rRNA spacer is removed during the course of ribosome maturation, like the other spacers, it is indispensable for ribosome biogenesis. Complete omission of ITS2, even after replacement with counterparts from other species, fails to generate mature 25S and 5.8S rRNA (Cote and Peculis, 2001; Peculis and Greer, 1998; van Nues et al., 1995). Mutational analyses have been performed on ITS2 and key elements for processing were identified. These analyses agreed with evolutionary conservation data considerably (van Nues et al., 1995). Interestingly, in such analyses, some combinations of individually neutral deletions in ITS2 resulted in a processing defect, leading to the proposition that a higher-order structure of ITS2 might be important in ribosome biogenesis. Two different secondary structure conformations have been proposed for ITS2 – the so-called ring and hairpin structures (Joseph et al., 1999; Yeh and Lee, 1990). Peculis and colleagues proposed a dynamic conformational model for ITS2 function indicating that elements of both structural models were important for rRNA processing (Cote et al., 2002).

Studies aimed at identifying the binding sites of the A3-factors on the preribosome made use of a technique called Crosslinking and analysis of cDNA (CRAC). From these studies, it is evident that Nop15 and Cic1 cross link to ITS2 (Granneman et al., 2011). In addition, we have shown that a third A3-factor, Rlp7, also binds ITS2 (Babiano et al., 2013; Dembowski et al., 2013c). The ITS2 cluster proteins have been suggested to stabilize the ring conformation of ITS2 preferentially and preclude the formation of the hairpin conformation (Dembowski et al., 2013c; Granneman et al., 2011). Strikingly, these three factors that apparently regulate the formation of 5' end of 5.8S rRNA that is part of ITS1 are located near the 3' end of 5.8S rRNA in ITS2. A possible explanation of this conundrum is that these A3 factors may stabilize the proper RNA structure of domain I and make the preribosome amenable to further steps of

processing, as opposed to being directly involved in 27SA3 processing. A number of questions pertaining to the function of these ITS2 cluster A3-factor proteins remain unanswered, including:

- Do these A3-factors have roles other than their known role in A3 processing?

- How do these A3-factors affect a processing event that is diametrically on the opposite side of the preribosome?

- What is the significance of the binding of ITS2 cluster proteins to the ITS2 spacer?

We sought to answer these and other related questions through a systematic investigation of the network of interactions in the ITS2 neighborhood. We adopted a two-pronged approach to this investigation:

1) Studying **protein-protein interactions** formed by the ITS2 neighborhood proteins with the rest of the assembly factors, and

2) Studying the **protein-RNA interactions** in the ITS2 neighborhood.

These are explained in detail below in the Results section.

4.2. Results: Protein-protein interactions of the ITS2 cluster proteins

4.2.1. Targeted yeast-two-hybrid screen to identify potential interactions

We began by asking what protein-protein interactions are formed by the ITS2 cluster proteins, Rlp7, Nop15 and Cic1. Although we recognize the importance of identifying the complex matrix of protein-protein interactions by itself as an important step toward understanding the assembly of a complex RNP like the ribosome, our specific goals behind investigating the protein partners of the ITS2 cluster proteins can be summarized in three questions:

- Can we explain potential functions of the ITS2 cluster proteins by extrapolating from the functions of its protein partners?

- Considering these ITS2 cluster proteins participate in the A3 processing step, but localize to the site of the subsequent 27SB cleavage step in ITS2, do these proteins connect the A3 processing step to the subsequent 27SB cleavage step?

- Is the DEAD-box RNA helicase Has1 recruited by one of the ITS2 cluster proteins?

In order to address these questions, we designed a yeast-two-hybrid screen focused on Rlp7, Nop15 and Cic1. We tested pairwise interactions of these three proteins with 20 other proteins listed below, classified according to their function.

Other A3-factors: Pwp1, Has1, Rrp1

27SB-cleavage factors: Nop2, Nip7, Rrs1, Rpf2, Spb4, Dbp10, Tif6, Rlp24, Mak11, Nog1, Nsa2, Nog2

Ribosomal proteins: L17A, L26A, L35B, L37B, L11

Dr. Jill Dembowski generated most of these constructs in pACT and pAS vectors using the Gateway Cloning System. An exhaustive list of these constructs is available on the lab computer for reference

("Y2H strain list"). Any new constructs developed in this project (including those for a few ribosomal proteins not listed here) are indicated in the strain list in the Appendix. These pAS/pACT plasmid constructs were transformed into yeast-two-hybrid compatible PJ69a/α haploid strains of yeast. The haploid yeast bearing the pairwise test constructs were then mated to yield the diploids. Diploids that correspond to a positive interaction between two proteins are expected to grow on media lacking adenine and histidine. An initial screen was carried out to identify the putative positives by replica plating these diploids on Ade and His dropout media. The diploid containing only vectors (pAS x pACT) showed absolutely no growth in this preliminary screen, demonstrating that there are no systematic false positives.

4.2.2. Assaying the strength of the putative positive interactions

Diploids that showed any degree of growth (a total of 19 diploids) in this initial screen were then tested for growth on various concentrations of 3-aminotriazole (3AT)-containing media by spotting serial dilutions of log-phase cultures. For each diploid candidate chosen from the preliminary screen, we assayed their growth in the following 8 different types of media: C-Leu-Trp, C-Leu-Trp-Ade and C-Leu-Trp-His+3AT in 1, 2.5, 5, 10, 25 and 50 mM concentrations. The higher the strength of an interaction, the higher the concentration of 3AT that the corresponding diploid can tolerate. Further, the ability of a diploid to grow on Ade dropout media is an independent reporter of the interaction (Fig. 4-3).

Figure 4-3: Growth assay to test for strength of various interactions tested in the yeast two hybrid screen

A

1. pAS x pACT
2. Rlp7 x Rpf2
3. Rlp7 x Rrs1
4. Rlp7 x Nog2
5. Rlp7 x Rlp7
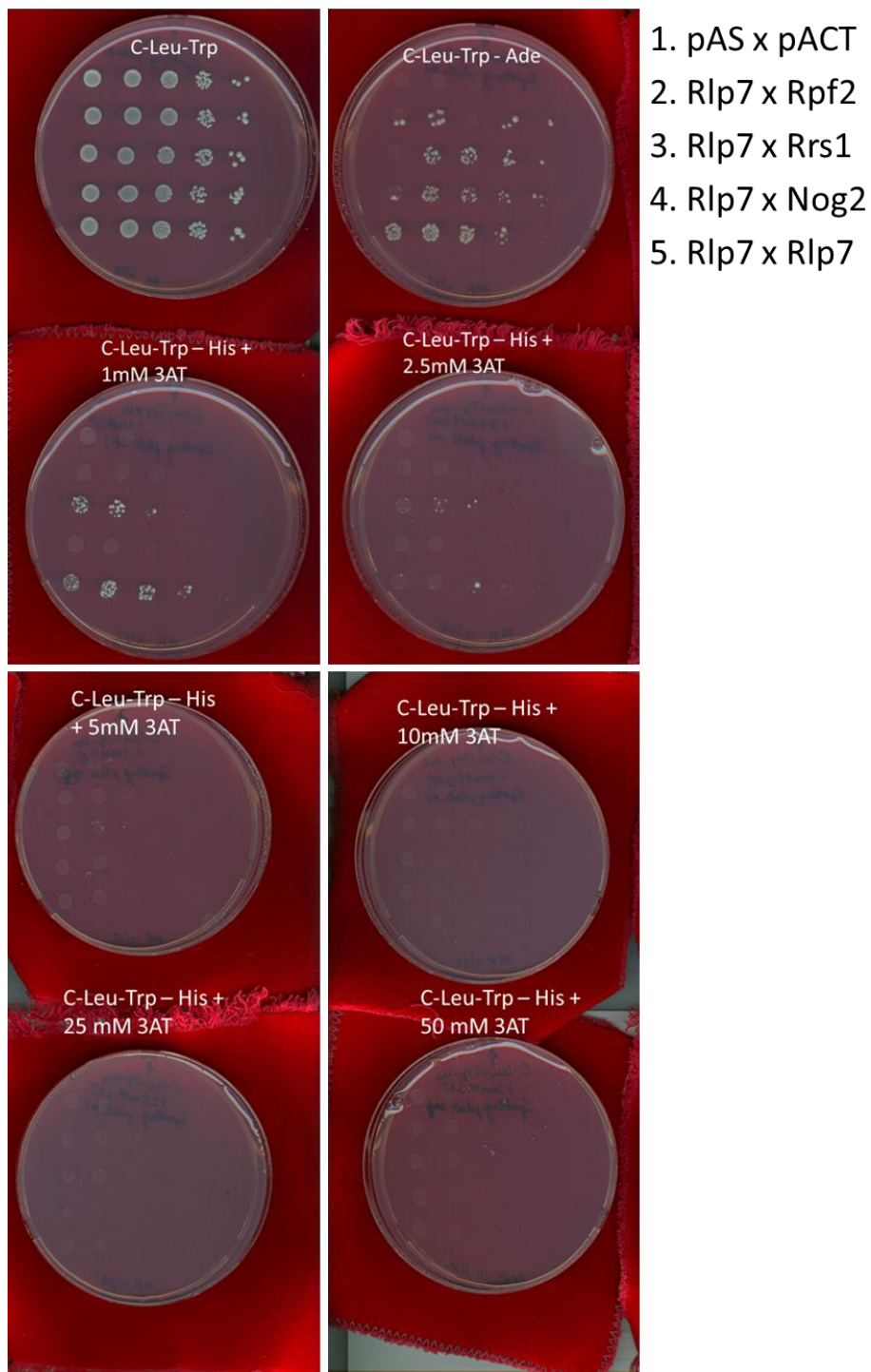
B
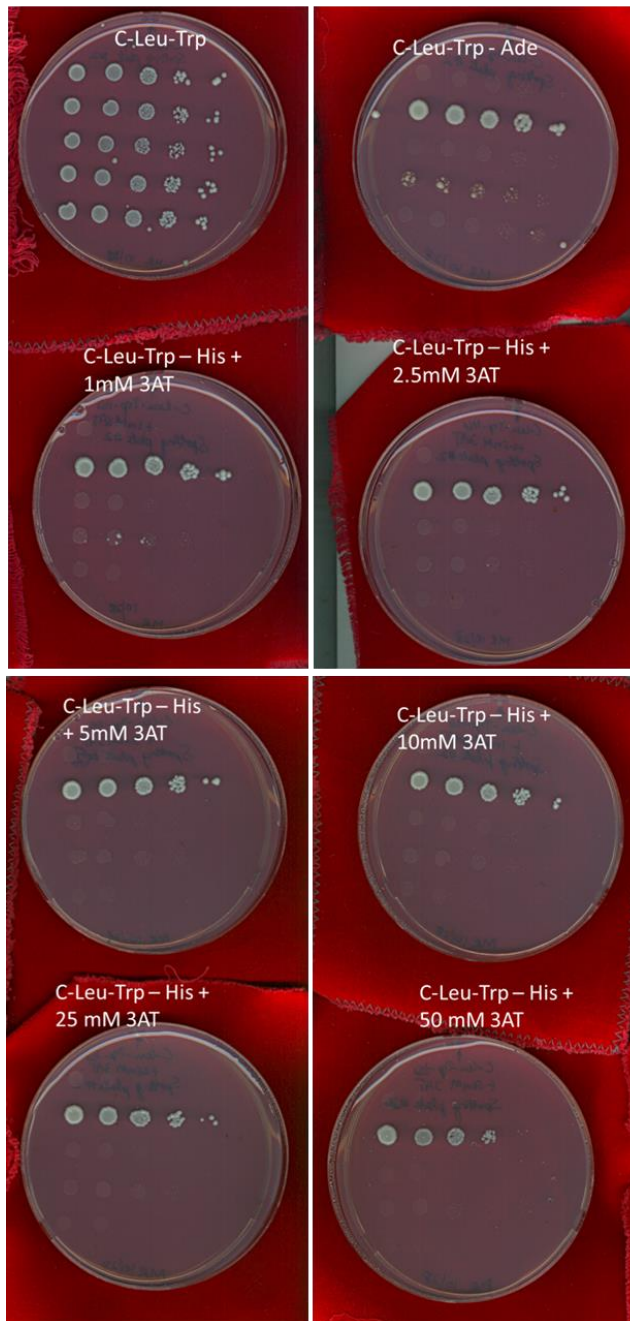
6. Cic1 x Rlp7
7. Nop15 x Nop15
8. Rlp7 x Nop15
9. Nsa2 x Nop15
10. Cic1 x Nop15

C

11. Nsa2 x Rlp7
12. Cic1 x Rlp7
13. Nop15 x Nop15
14. Has1 x Nop15
15. Rrp1 x Nop15

D

C-Leu-Trp

C-Leu-Trp - Ade

C-Leu-Trp – His + 1mM 3AT

C-Leu-Trp – His + 2.5mM 3AT

C-Leu-Trp – His + 5mM 3AT

C-Leu-Trp – His + 10mM 3AT

C-Leu-Trp – His + 25 mM 3AT

C-Leu-Trp – His + 50 mM 3AT
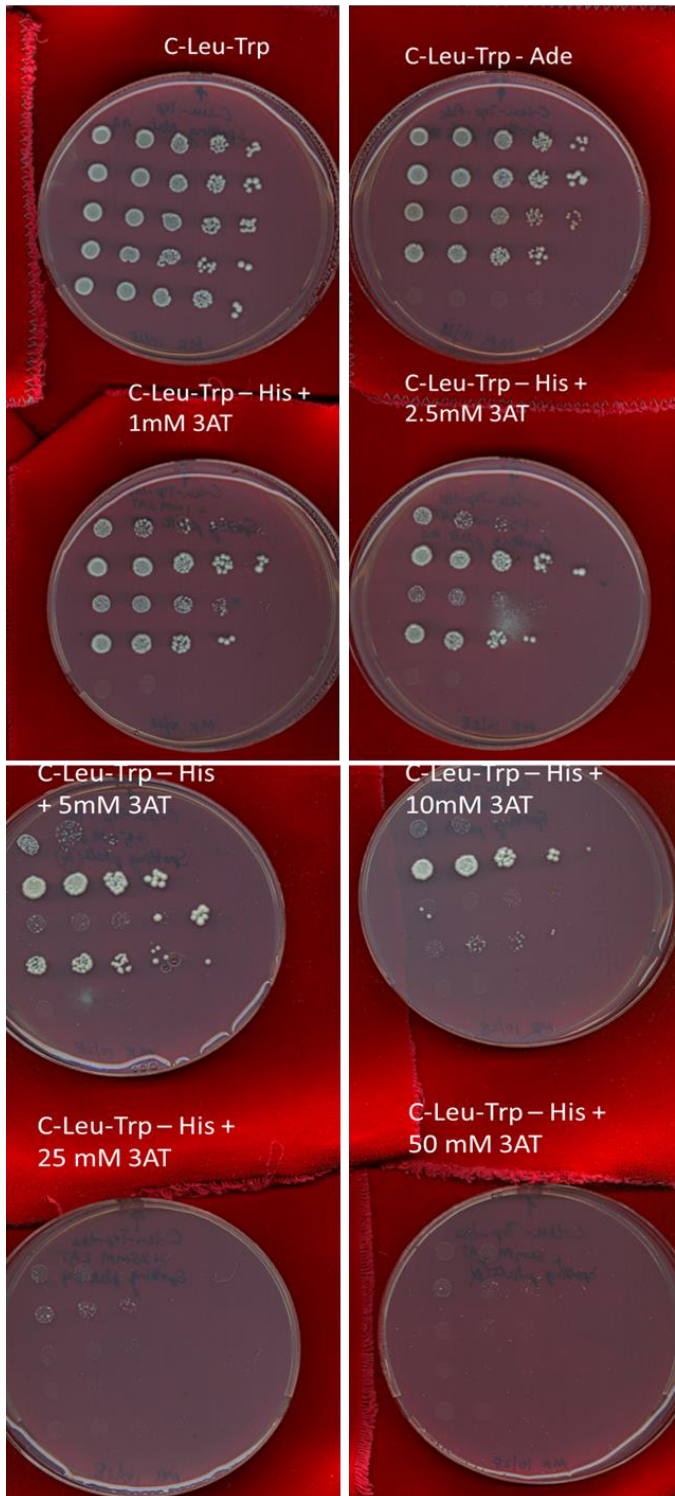
16. Nop15 x Cic1
17. Pwp1 x Cic1
18. Has1 x Cic1
19. Nop15 x Rlp7
20. Has1 x Rlp7

Fig. 4-3: Growth assay to test for strength of various interactions tested in the yeast two-hybrid screen.

Two-hybrid assays were carried out to test for interactions between the ITS2 neighborhood of proteins (Rlp7, Nop15, Cic1) and several other factors required for 27S pre-rRNA processing. 20 pairwise interactions were analyzed in total and hence there were 20 strains in all.

(A) Strains 1-5 are shown in this panel. The corresponding media and concentrations of 3AT (3-aminotrazol) used are indicated above each plate. Order of spotting on each plate, top to bottom, is mentioned on the side.

(B) Strains 6-10 are shown in this panel. The corresponding media and concentrations of 3AT used are indicated above each plate. Order of spotting on each plate, top to bottom, is mentioned on the side.

(C) Strains 11-15 are shown in this panel. The corresponding media and concentrations of 3AT used are indicated above each plate. Order of spotting on each plate, top to bottom, is mentioned on the side.

(D) Strains 16-20 are shown in this panel. The corresponding media and concentrations of 3AT used are indicated above each plate. Order of spotting on each plate, top to bottom, is mentioned on the side.

The identified interactions and the strength of each interaction are tabulated in Fig. 4-4A. In addition, we also represented the results schematically in Fig. 4-4B, where the thickness of each line roughly indicates the strength of the respective interactions. Despite the targeted nature of this screen where the proteins tested were tightly linked, functionally and physically (since they are part of the same preribosome), we found that only about 5% of the possible pairwise interactions tested positive for interactions, demonstrating the specificity of this yeast-two-hybrid screen (Dembowski et al., 2013c). We have discussed the implications of the identified interactions further in the Discussion section.

At this juncture, we decided to narrow our focus exclusively to protein-protein interactions formed by Rlp7, because of the two following findings:

(i)   Dr. Dembowski had identified the binding site for Rlp7 at and near ITS2 using CRAC. The protein-protein interaction data we found seemed to complement her data. Based on our protein-protein interaction assays, we asked if we can determine where Rlp7 is localized by identifying with which proteins it interacts.

(ii)   In addition to its role in $27SA_3$ processing, Rlp7 has also been implicated in 27SB processing. We asked if Rlp7 may be temporally linking A3 processing and the subsequent B-processing,

Figure 4-4: Summary of results from the yeast-two-hybrid screen

A

ITS2 cluster protein	Interacting partners	Strength of interaction
Nop15	Nop15	50mM
Nop15	Rlp7	5 mM
Nop15	Rrp1	5 mM
Nop15	Nsa2	Ade, mild
Nop15	Has1	Ade, 1 mM (JD)
Cic1	Nop15	5 mM
Cic1	Pwp1	10 mM
Cic1	Has1	2.5 mM
Rlp7	Rlp7	1 mM
Rlp7	Nsa2	1 mM, Ade
Rlp7	Rrs1	1mM , Ade
Rlp7	Nog2	Ade
Rlp7	Rpf2	Ade
Rlp7	Has1	10mM (JD)

B
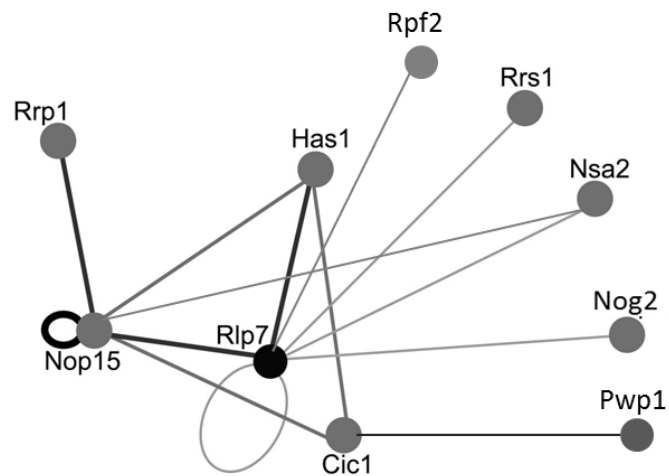
Fig. 4-4: Summary of results from the yeast-two-hybrid screen.

(A) Table summarizing results from the yeast-two-hybrid assay, shown in Fig. 4-3. JD indicates results found by Jill Dembowski independently.

(B) Two-hybrid interaction map. Roughly, relative strengths of interactions are shown with dark gray, thick lines representing strong interactions and light gray, thin lines representing weak interactions as determined by growth of two-hybrid strains on media containing increasing concentrations (1, 2.5, 5 and 50 mM) of 3-aminotriazol (3-AT).

4.2.3. Protein-protein interaction network of Rlp7

Having identified and verified protein partners of Rlp7 as described above, we wanted to use an orthogonal method to identify the protein partners of Rlp7, since the yeast-two-hybrid assay has a propensity for false positives and negatives. To this end, we performed high salt washes of bead-bound preribosomes that were affinity purified with Rlp7 as the bait protein. We initially optimized the concentration of salt in the buffer such that we would observe only the most relevant interactions. Following this, we affinity purified preribosomes; cut out bands corresponding to proteins that associated with Rlp7 under high salt conditions and sent them for mass spectrometry analysis.

Strikingly, the mass spectrometry results showed that Erb1 and Nop15 stably associated with Rlp7 (Fig. 4-5). This was again very consistent with the location of Rlp7, since previous work has shown that Nop15 and Erb1 crosslink near the ITS2/proximal stem, (Fig. 4-6), (Granneman et al., 2011).

To extend these experiments, we asked whether these observed interactions were mediated by RNA, by testing for the association of these protein partners with Rlp7 after RNase treatment. However, we did not succeed in optimizing the RNase concentration despite multiple efforts. In addition, we assayed the levels of a set of A3-factors and B-factors by western blotting, to confirm that they were indeed washed away under high salt conditions. The results we obtained from these westerns confirmed the mass-spectrometry data (Data not shown).

Figure 4-5: High salt wash of Rlp7-associated proteins
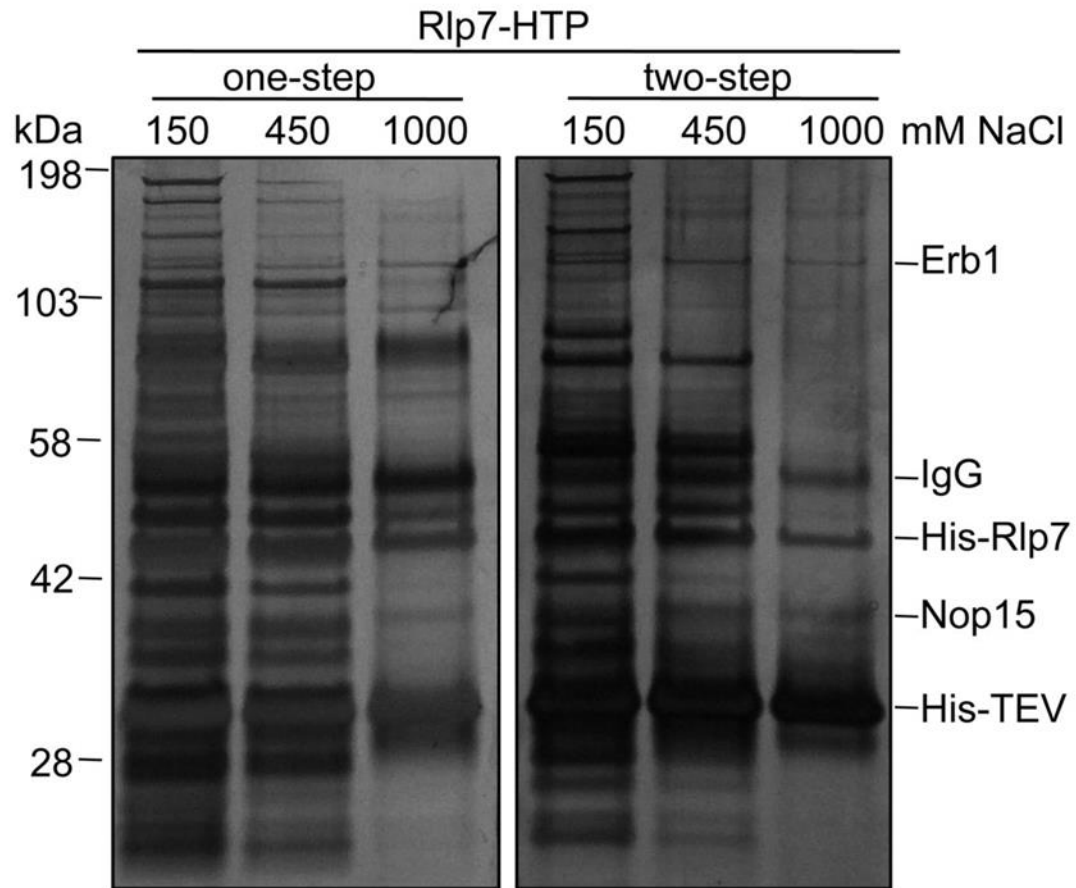
Fig. 4-5: High salt wash of Rlp7-associated proteins.

Rlp7-HTP was affinity purified from yeast cell lysates and complexes were washed with increasing concentrations of NaCl (150, 450, 1000 mM) to remove weakly associated proteins. One-step indicates that proteins were resolved after one-step purification on IgG-coated beads and two-step indicates that proteins were resolved after two-step purification on IgG- and Nickel-coated beads.

Figure 4-6: Cartoon showing the location of various ITS2 factors relative to 5.8S and 25S rRNA

A
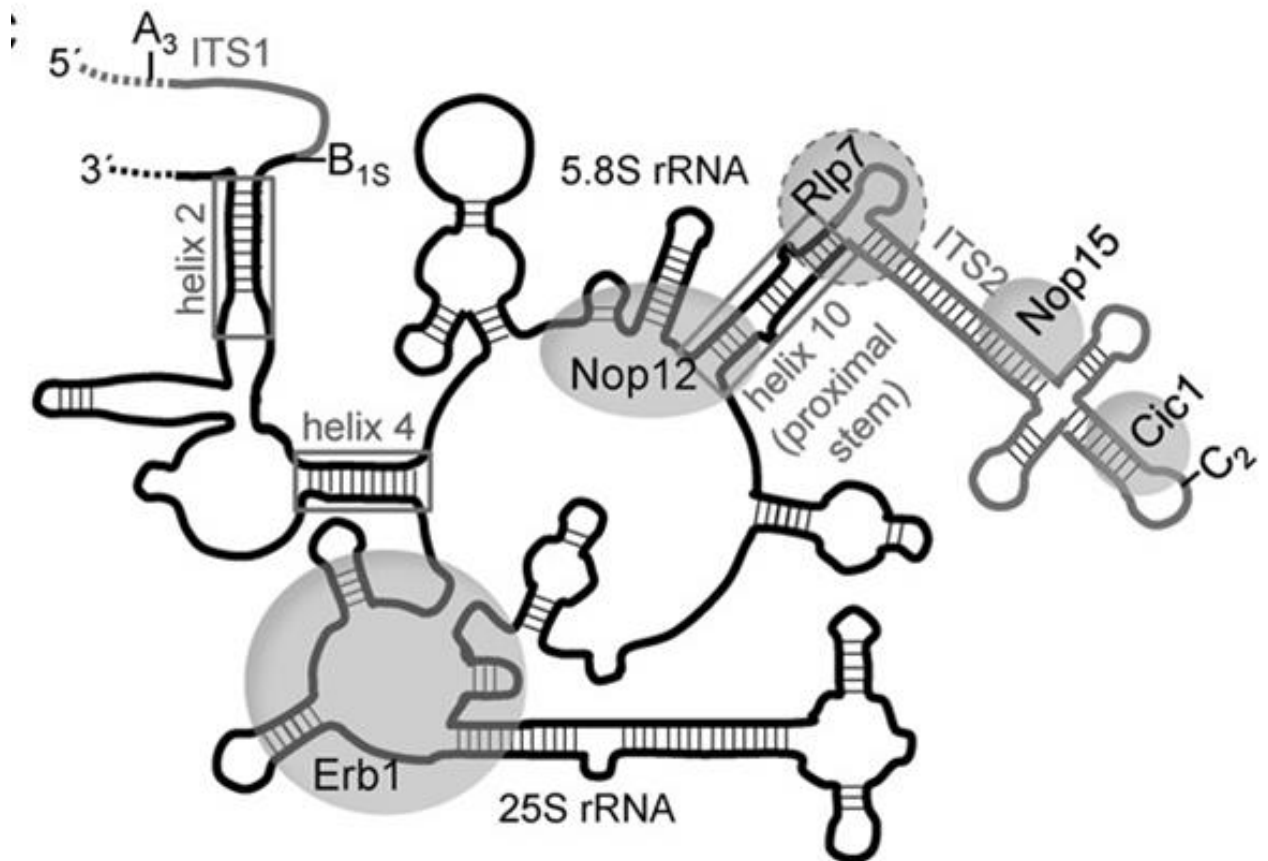
B
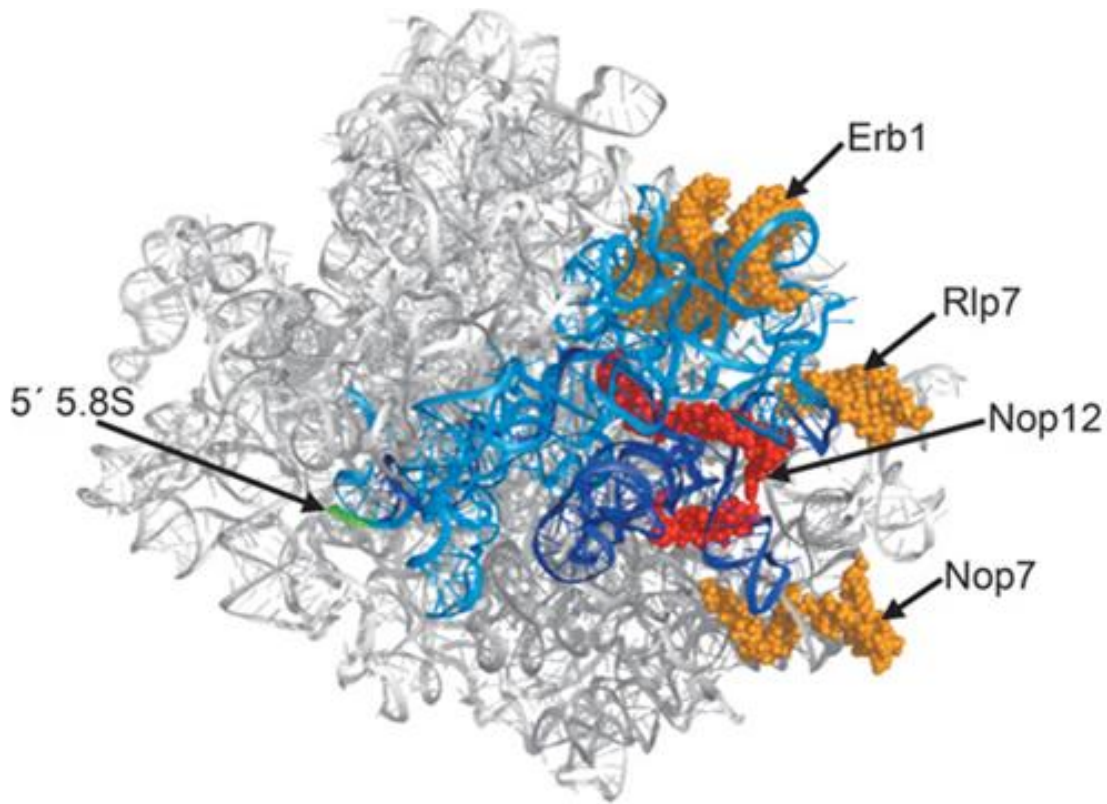
Fig. 4-6: Cartoon showing the location of various ITS2 factors relative to 5.8S and 25S rRNA.

(A) Cartoon representation of base pairing between 5.8S and 25S rRNAs in domain I. Sequences of mature rRNA are black and ITS1 and ITS2 are gray. Boxes indicate regions were 5.8S rRNA base pairs with 25S rRNA. Helix numbers are listed for 25S rRNA. Helix 10 is also known as the ITS2-proximal stem. Gray circles indicate the binding sites of Rlp7, Erb1, Nop12, Nop15 and Cic1 on pre-ribosomes. The A_3, B_{1S} and C_2 processing sites are indicated.

(B) PyMOL representation of the solvent accessible surface of the yeast 60S ribosomal RNA (PDB file 3U5H) (Ben-Shem et al. 2011). Domain I is blue (5.8 rRNA dark blue, 25S rRNA light blue), the 5´ end of 5.8S rRNA is green, and protein binding sites are shown in space-fill view. The binding site of Nop12 is red and the binding sites of Erb1, Rlp7 and Nop7 are orange.

### 4.3.	Results: Protein-RNA interactions of the ITS2 neighborhood

Since all three of the ITS2 cluster proteins Nop15, Cic1 and Rlp7 have predicted RNA-binding domains, we wanted to use this as a model to understand how RNA-binding assembly factors function in ribosome biogenesis. We started off by identifying the putative RNA binding domains in each of these proteins. Nop15 has a canonical RNA recognition motif (RRM), Rlp7 has an rpL7-like domain, and Cic1 has an rpL1-like domain (Fig. 4-7). Since no crystal structures were available for these proteins, we resorted to using homology-modeling based predictions of their structures using Phyre2 software (Fig. 4-8).

We decided to focus only on Nop15 as an example to understand the significance of RNA binding by the ITS2 cluster proteins, for the following reasons:

(A) Nop15 has a clear, canonical RNA Recognition Motif (RRM) which is a well-studied domain for RNA interactions.

B) The binding site of Nop15 in ITS2 is evolutionarily conserved, and has been shown to be important for processing by mutational studies.

(C) Nop15 binds to domain III of the ITS2 hairpin (stem IIIA of the ring), which has been implicated as a key player in the ring to hairpin conformational switch of ITS2.

We wanted to ask how the ability of Nop15 to bind ITS2 impacts various processes in ribosome biogenesis, such as association of ribosomal proteins and pre-rRNA processing. Hence, we mutated the RNA-binding site of Nop15 in order to potentially abrogate its ability to bind ITS2, and assessed the phenotypes of these mutants extensively. Owing to similarities in their binding site and function, we postulated that the principles that emerge for Nop15 could be extrapolated to Cic1 and Rlp7.

Figure 4-7: Domain architecture of ITS2-cluster proteins
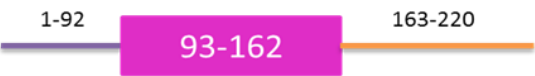
Name of protein	Domains and residues spanning them			Name of the domain
Nop15	1-92	93-162	163-220	RNA Recognition Motif
Rlp7	1-140	141-194	195-322	L7/L30 ribosomal protein domain
Cic1	1-42	42-287	287-376	L1 ribosomal protein domain

Fig. 4-7: Domain architecture of ITS2-cluster proteins.

Nop15, Rlp7 and Cic1 are shown schematically highlighting the major protein domains observed in each protein. The precise amino-acid resolution demarcations of the domains are indicated.

Figure 4-8: Predicted structures of ITS2 cluster proteins
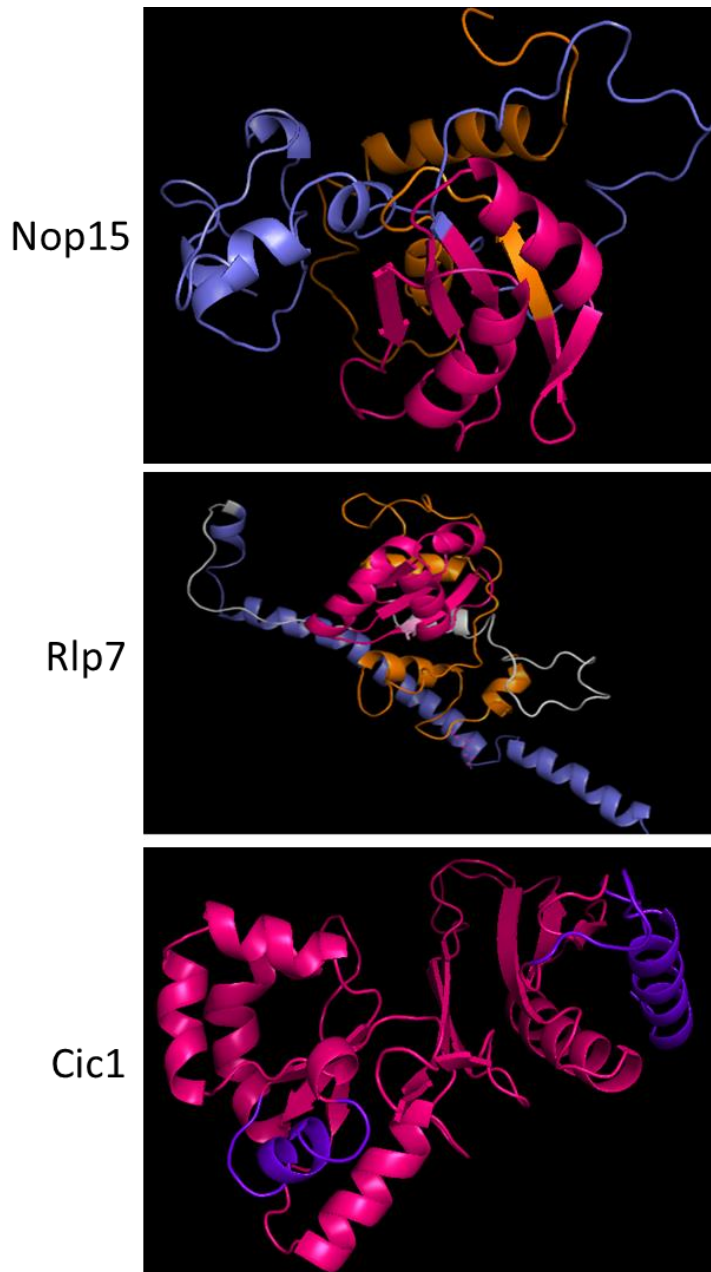
Fig. 4-8: Predicted structures of ITS2 cluster proteins.

Structures of Nop15, Rlp7 and Cic1 were predicted using homology modelling using Phyre2 software (http://www.sbg.bio.ic.ac.uk/phyre2/). Domains are colored as shown in Fig. 4-7. The canonical protein domain is shown in pink for each of the proteins.

4.3.1. *Cloning and setting up system for mutagenesis*

Although there were precedents for such mutational analysis in the lab before, the first step in performing an extensive mutational analysis of *NOP15* was to devise a robust system for mutating and assaying the phenotype of a protein using more modern resources. We sought to leverage the availability of highly efficient mutagenesis kits and newer strains for conditional expression of various proteins. First, we wanted to start off broadly and hence, we cloned both Nop15 and Cic1 in the following expression vectors: pRS315 (*LEU2*), pRS316 (*URA3*), KS⁺. Restriction enzymes *BamH1* and *HindIII* were used to clone the *NOP15* and *CIC1* ORFs, (along with sequences upstream and downstream of the ORF to include the *cis*-elements necessary for expression of these genes from their respective promoters) in these vectors. Successful cloning was confirmed by running restriction digested fragments on an agarose gel (Fig. 4-9) and subsequently by sequencing.

Figure 4-9: Cloning *NOP15* and *CIC1* in three different vectors
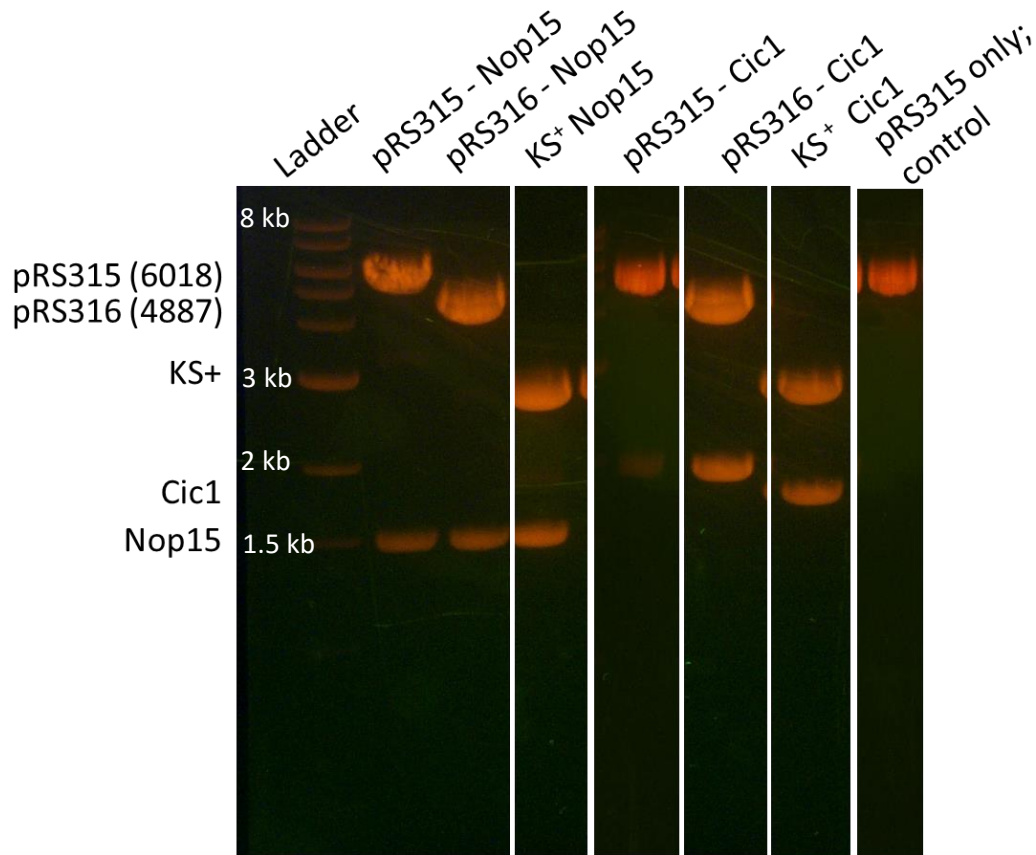
Fig. 4-9: Cloning *NOP15* and *CIC1* in three different vectors.

Plasmids were miniprepped from small cultures (2ml) cultures of DH5α cells transformed with the ligated products after cloning. These plasmids were digested with *BamH1* and *HindIII* in order to check for the presence of the insert and successful cloning and the digested sample was run on a 1% agarose gel and visualized by ethidium bromide staining. On the left side, expected sizes of each of the digested product are indicated. Only the positive candidates are shown here for clarity; and discontinuous lanes are shown with white space in between. The last lane (pRS315 only) is used as a representative negative control.

4.3.2. Plasmid-derived Nop15 and Cic1 rescue respective depletion phenotypes

We wanted to ensure that the ectopically expressed *NOP15* and *CIC1* would be expressed stably and would rescue the growth defect caused by shut-off of the endogenous genomic *NOP15* and *CIC1* respectively. Hence, we transformed these plasmids and tested for the ability of these plasmids to rescue the growth of a *GAL-HA-NOP15* or *GAL-CIC1* strain grown in glucose medium (Fig. 4-10). We found that the plasmids rescued the corresponding genomic depletions, as expected. For example, *NOP15* expressed from a plasmid, but not *CIC1*, rescued the growth defect of *GAL-HA-NOP15* (Fig. 4-10A, 4-10B) grown on glucose medium, and vice versa (Fig. 4-10C).

Figure 4-10: Plasmid-borne *NOP15*, but not *CIC1*, can rescue the growth defect that is observed

when transcription of genomic *NOP15* is shut off, and vice versa
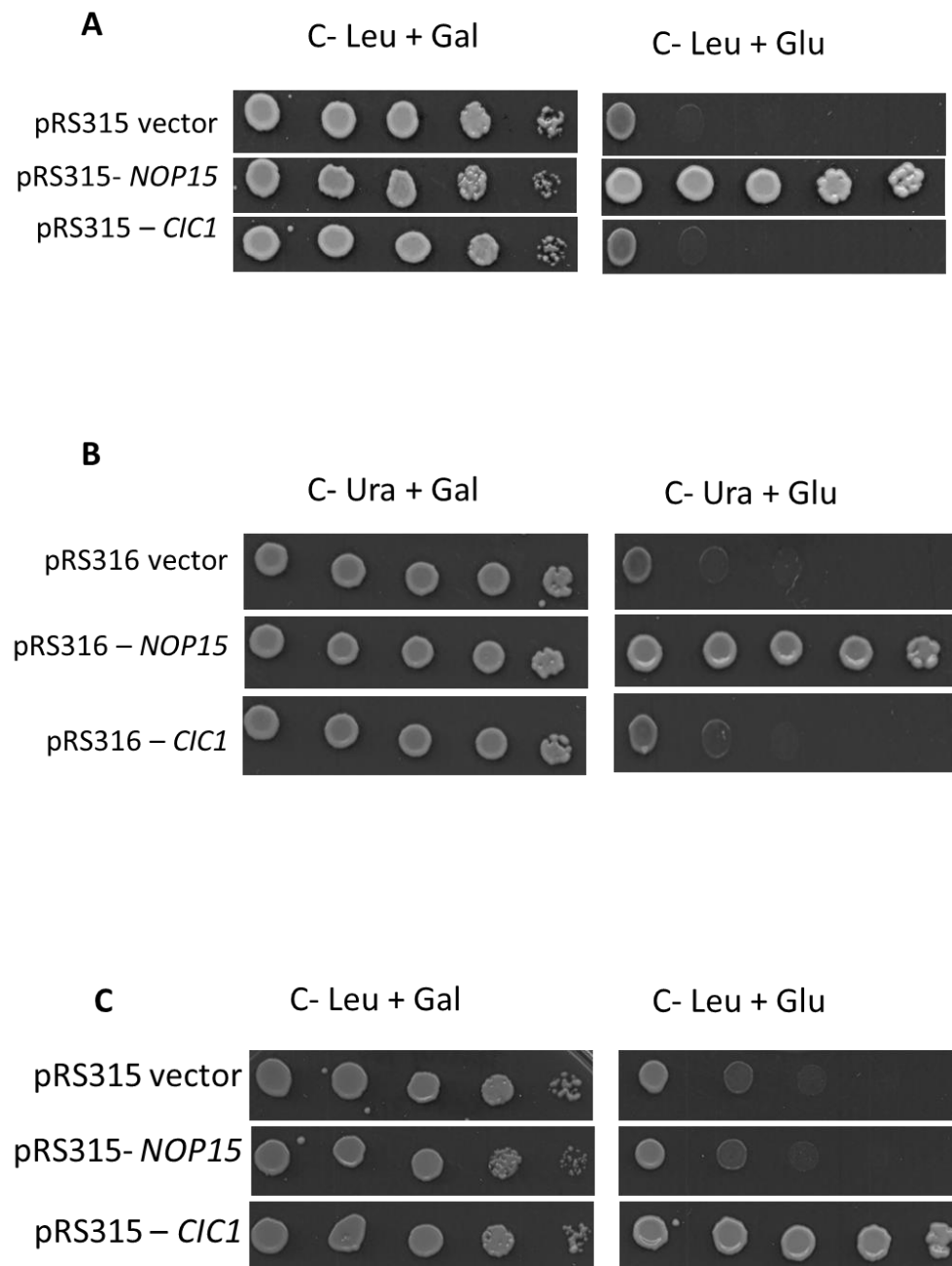
Fig. 4-10: Plasmid-borne *NOP15*, but not *CIC1*, can rescue the growth defect that is observed when transcription of genomic *NOP15* is shut off, and vice versa.

(A) Vector backbone (pRS315 vector, top panels), *NOP15* cloned in pRS315 (middle panels), or *CIC1* cloned in pRS315 (bottom panels) were transformed into the *GAL-HA-NOP15* strain. Upon shut off of the transcription of genomic *NOP15* (when grown on C-Leu+Glucose media, right panels), ectopically expressed *NOP15*, but not *CIC1* rescues growth.

(B) Vector backbone (pRS316 vector, top panels), *NOP15* cloned in pRS316 (middle panels), or *CIC1* cloned in pRS316 (bottom panels) were transformed into the *GAL-HA-NOP15* strain. Upon shut off of the transcription of genomic *NOP15* (when grown on C-Ura+Glucose media, right panels), ectopically expressed *NOP15*, but not *CIC1* rescues growth.

(C) Newly cloned *CIC1*, but not *NOP15*, can rescue the growth defect that is observed when transcription of genomic *CIC1* is shut off. Vector backbone (pRS315 vector, top panels), *NOP15* cloned in pRS315 (middle panels), or *CIC1* cloned in pRS315 (bottom panels) were transformed into the *GAL-CIC1* strain. Upon shut off of the transcription of genomic *CIC1* (when grown on C-Leu+Glucose media, right panels), ectopically expressed *CIC1*, but not *NOP15* rescues growth.

4.3.3. Mutagenesis of the RRM of Nop15

At this juncture, we decided to exclusively focus on Nop15, although the constructs for Cic1 were also generated. To begin with, we did a multiple sequence alignment of Nop15 from various organisms using the Clustal Omega software (Fig. 4-11). As mentioned before, Nop15 has a canonical RNA recognition motif (RRM). RRM-containing proteins are the largest group of eukaryotic single strand RNA binding proteins and have an eight amino acid consensus sequence. The typical RRM consists of four anti-parallel β-strands superimposed over two α-helices, with side chain aromatic residues that form stacking interactions with RNA (Clery et al., 2008; Kenan et al.; Maris et al., 2005). In Nop15, we identified F136, F139, Y134 and Y94 as the aromatic residues that could form base-stacking interactions (Fig. 4-12). Upon discussions with Dr. Gordon Rule, we decided to mutate these residues both to alanines and glycines, in order to minimize secondary effects that may arise due to either steric hindrance or overall instability of protein. In addition to these eight mutations, we also mutated the conserved Arg132 residue to glutamine, since there were precedents for this type of mutation to completely abrogate RNA binding (Lee and Nussbaum, 1989). We used the Quikchange mutagenesis kit from Agilent Technologies for the first time, mutated the *NOP15* gene clone in the pRS315 vector, and verified successful site-directed mutagenesis by sequencing. The mutations were carried out in two sets and the results of those are described below.

Figure 4-11: Multiple sequence alignment of Nop15 from various organisms
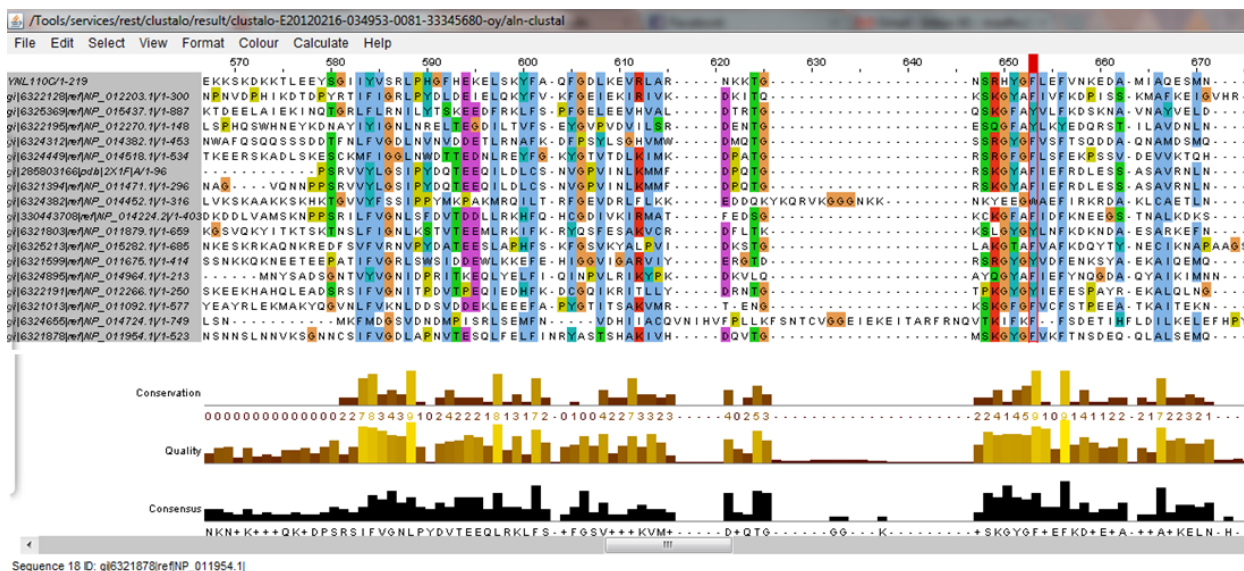
Fig. 4-11: Multiple sequence alignment of Nop15 from various organisms.

Only a section of the protein is shown for demonstration purposes. Clustal Omega was used to generate the alignment (http://www.ebi.ac.uk/Tools/msa/clustalo/). Residues are colored according to chemistry and histograms of conservation of each residue and quality of prediction are shown below the alignment. A consensus sequence generated from the alignment is shown at the bottom.

Figure 4-12: Nop15 has an RNA recognition motif (RRM)
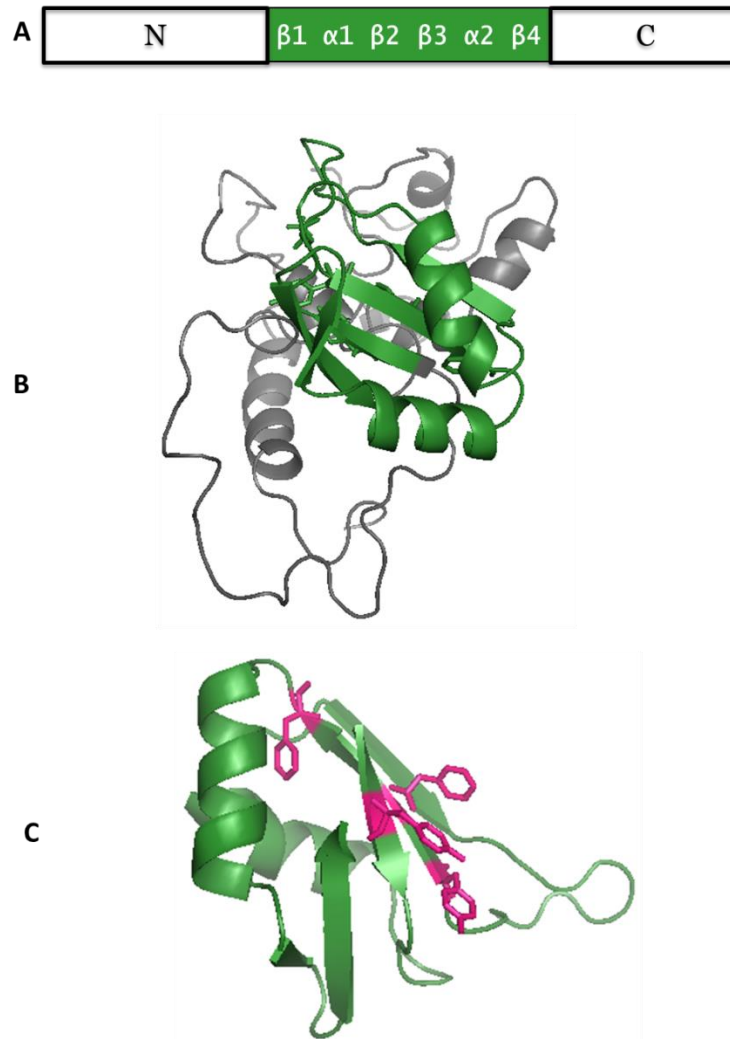
Fig. 4-12: Nop15 has an RNA recognition motif (RRM).

(A)   A schematic representation of a canonical RRM (green). N- and C-termini are indicated.

(B)   A secondary structure model of Nop15 predicted by homology modelling (Phyre2 software), with the RRM highlighted in green.

(C)   RRM of Nop15 is shown in green with the aromatic residues involved in RNA binding shown in pink.

4.3.4. Growth phenotypes of nop15 mutants

In order to assess the *in vivo* phenotype of the *nop15* mutants, we utilized the *GAL-HA-NOP15* strain that was already available in the lab (Fig. 4-13). We transformed the plasmids containing the *nop15* mutants into this strain. We assayed for the growth of these mutant strains by spotting serial dilutions on minimal media (C-Leu, in order to select for the plasmid) in the presence of galacatose (genomic *NOP15* expressed) or glucose (genomic *NOP15* repressed, plasmid-borne mutant expressed). WT plasmid and the vector backbone (pRS315) were used as positive and negative controls.

At 30°C (Fig. 4-14A), on galactose containing medium (left panels), all the strains showed a uniform level of growth. On glucose containing medium (right panels), *nop15* mutants F136G, F139G, Y134G showed a growth defect, while F139G and Y134G exhibited a nearly lethal growth phenotype. Similar results were observed at 18°C (Fig. 4-14B). At 37°C, the growth defect of the F136G mutant was exacerbated while F139G and Y134G showed lethality on glucose containing medium (Fig. 4-14C).

Figure 4-13: Schematic representation of the glucose repression in *GAL-HA-NOP15*
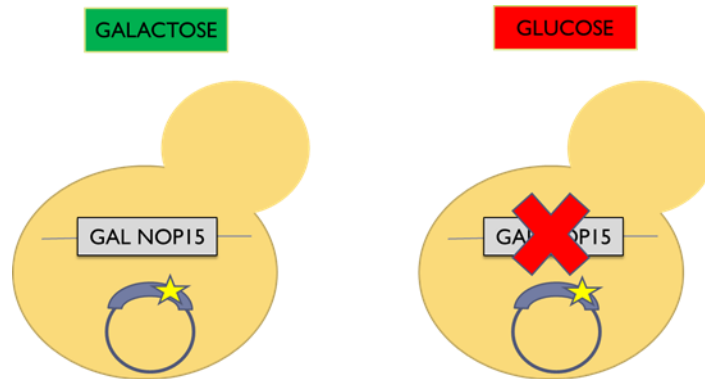
Fig. 4-13: Schematic representation of the glucose repression in *GAL-HA-NOP15.*

When grown in galactose, genomic *NOP15* is expressed. Upon shifting to glucose medium, genomic

expression of *NOP15* is shut off and the plasmid-derived Nop15 is the only source of Nop15 to the cell.

Mutations were carried out on this plasmid-borne copy of *NOP15* (indicated by a star).

Figure 4-14: Assaying growth phenotypes of various *nop15* mutants

A

B

C-Leu + Galactose   C-Leu + Glucose

18°C

WT Nop15
F136A
F136G
Y134A
Y94A

Null
WT Nop15
F139A
F139G
Y134G
Y94G
R132Q
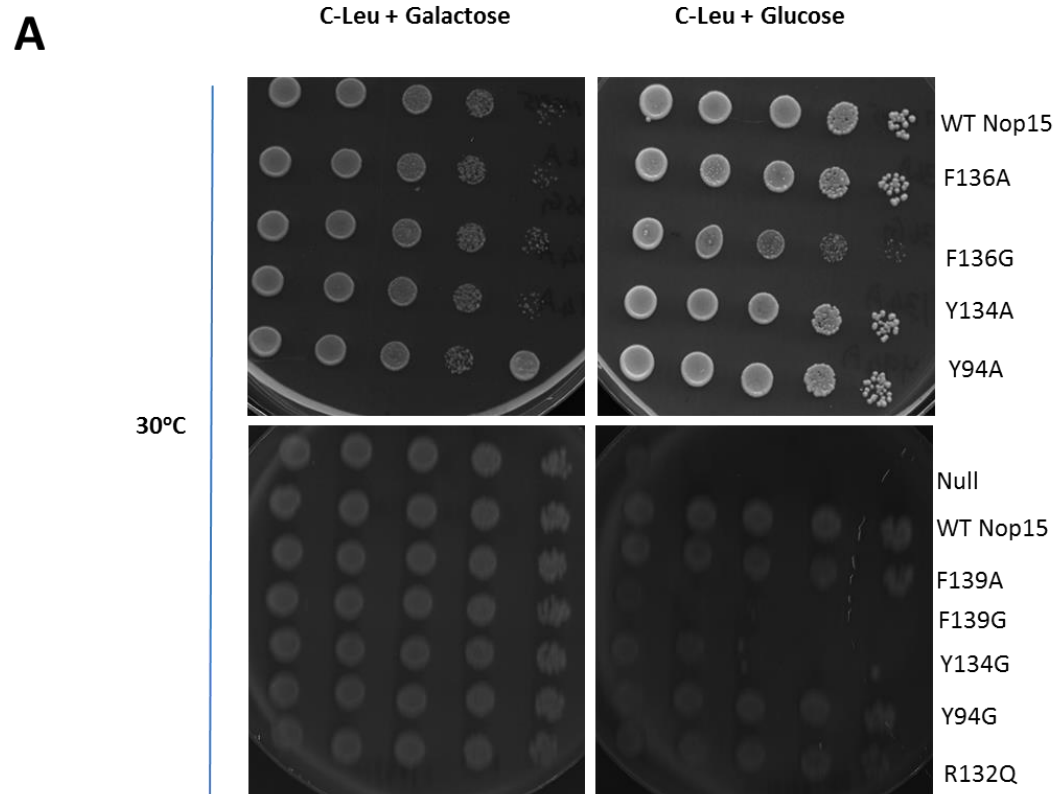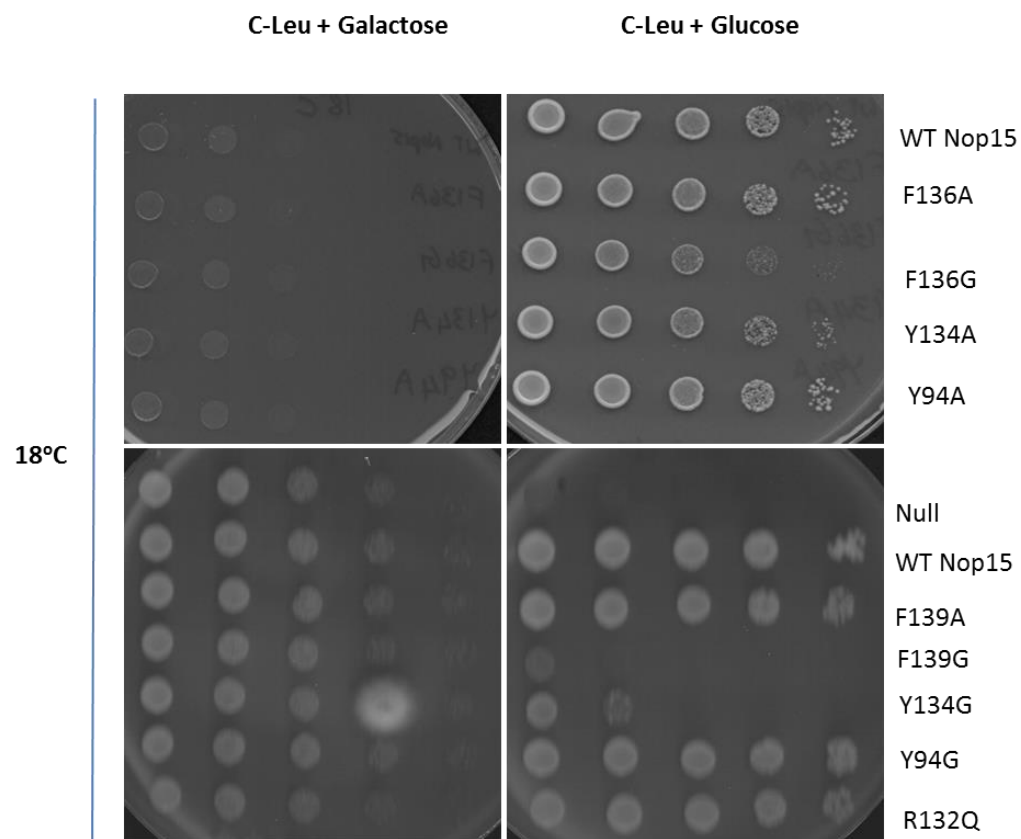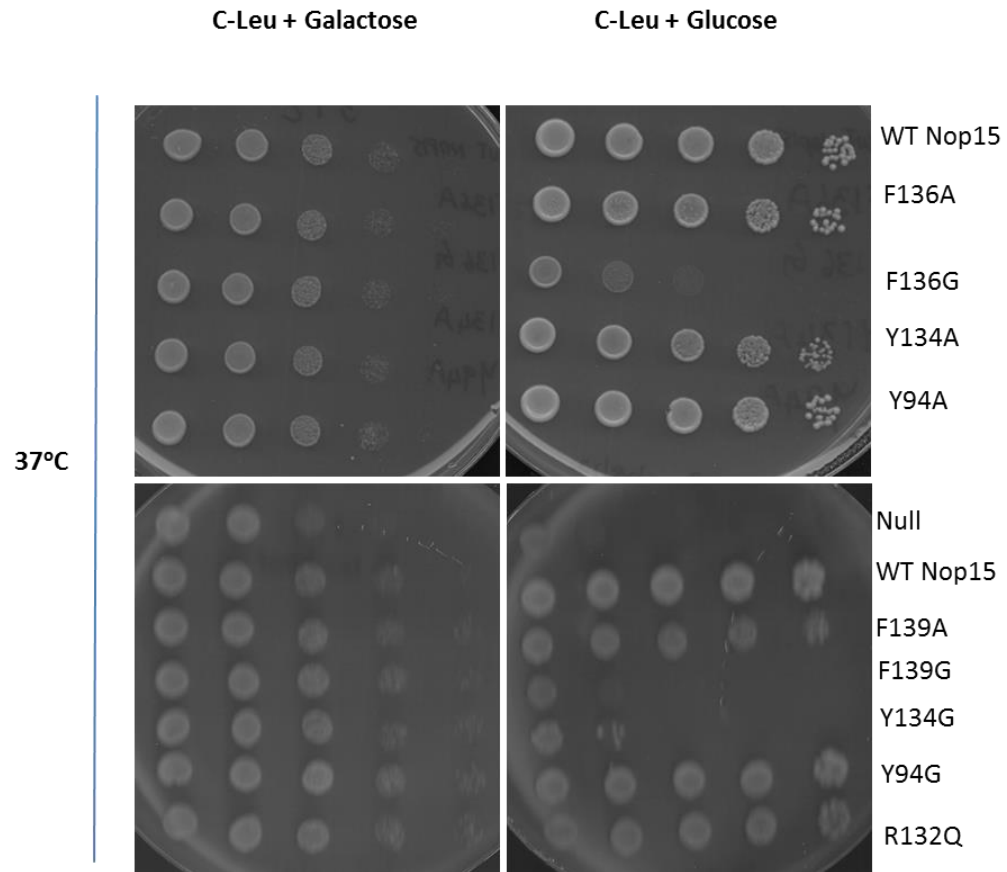
Fig. 4-14: Assaying growth phenotypes of various *nop15* mutants.

(A) Serial dilutions of strains with various *nop15* mutations (or controls), as indicated on the right, were spotted on to solid media. The strains were grown at 30°C in galactose medium (left panels), where genomic *NOP15* is expressed, or glucose medium (right panels), where it is repressed. Photographs were taken after three days of growth.

(B) Same as (A), except that the strains were grown at 18°C. Photographs were taken after five days of growth.

(C) Same as (A), except that the strains were grown at 37°C. Photographs were taken after four days of growth.

152

4.3.5. Some nop15 mutants show decreased levels of mature 25S rRNA

With this growth phenotype in mind, since Nop15 also has a moonlighting role in cytokinesis (Oeffinger and Tollervey, 2003), we assessed whether the growth defect in some *nop15* mutants was a consequence of an inability to synthesize stable 25S rRNA of the large ribosomal subunit. Hence, we extracted total RNA from the cell and measured the levels of 25S rRNA relative to 18S rRNA by running it on an agarose gel (Fig. 4-15). Since the synthesis of the large ribosomal subunit is mostly independent of that of the small ribosomal subunit carrying 18S rRNA, the expectation is that the ratio of 25S/18S rRNA would decrease in mutants that cannot synthesize 25S rRNA.

We found that, in line with their lethal growth phenotype, mutants F139G, Y134G and F136G (specifically at the higher temperature, shown in red) showed a decrease in the 25S/18S rRNA ratio when grown in glucose medium. Among the mutants that grew as well as the strain carrying the WT *NOP15* plasmid*,* we found that F136A and Y94A showed a slight decrease in the 25S/18S ratio. This effect was reproducible in at least two qualitative replicates (data for replicates not shown).

Figure 4-15: Some *nop15* mutants show decreased 25S/18S rRNA ratios
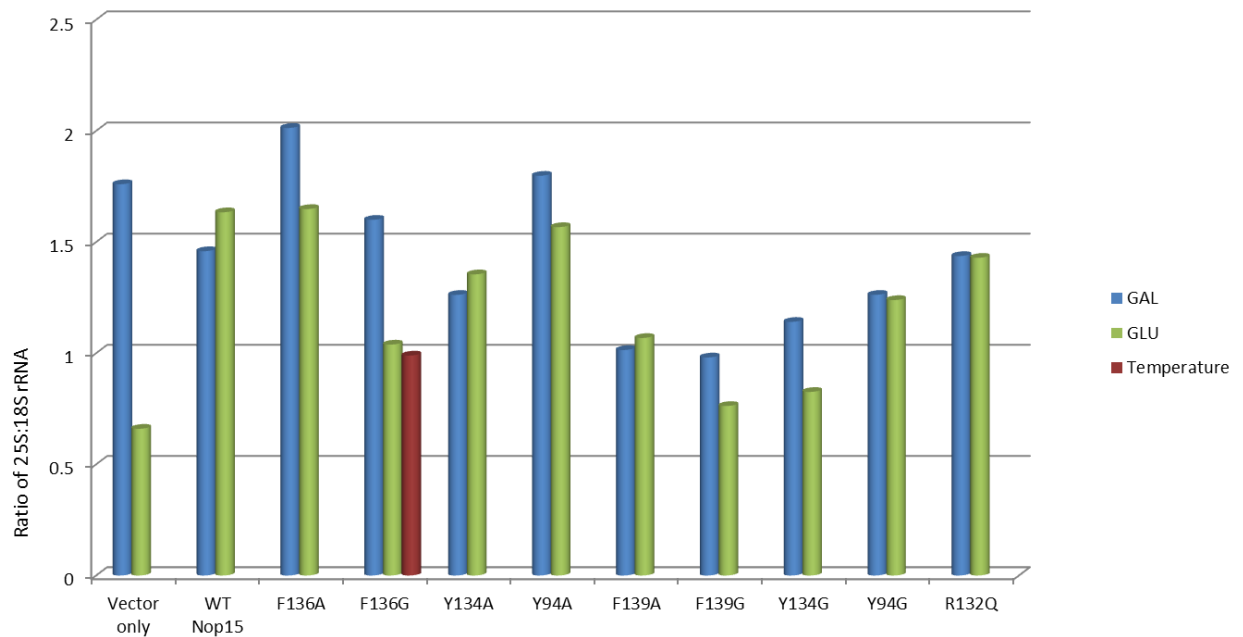
Fig. 4-15: Some *nop15* mutants show decreased 25S/18S rRNA ratios.

Ratio of steady-state mature 25S/18S rRNA is decreased in some, but not all, *nop15* mutants (indicated below the X-axis as evident by a decrease in the height of green bars compared to blue). The red bar represents the temperature-sensitive mutant that was subjected to an additional temperature shift to potentially accentuate the phenotype. Representative values are shown and this phenotype was reproduced at least twice qualitatively.

4.3.6. The lethal nop15 mutations cause a canonical A3-processing phenotype

As mentioned before, pre-rRNA maturation proceeds via a series of exonucleolytic and endonucleolytic processing steps (Fig. 4-1). Noting that the depletion of Nop15 causes an early A3-processing defect, we wanted to ask which, if any, pre-rRNA processing steps are affected in these *nop15* mutants. We extracted total RNA and performed a primer extension assay to detect various pre-rRNA species (Fig. 4-16). Two different gels were run with appropriate controls in order to reveal any potential pre-rRNA processing defects in these mutants.

It was evident that the mutants that showed a severe growth defect, such as F136G at 37°C, F139G and Y134G closely resembled the null phenotype of *NOP15* characterized by an accumulation of $27SA_3$ species and a concomitant decrease in $27SB_S$ species. Although F139A showed a slight increase in $27SA_3$ pre-rRNA levels, we did not detect a concomitant decrease in the levels of $27SB_S$ pre-rRNA. Also, the fact that this mutant did not show a decreased 25S/18S rRNA ratio suggested that, this effect may be unimportant or it may be an offshoot of loading. Errors in loading precluded us from making conclusions about F136A and Y94A, even though we had observed a slight decrease in 25S/18S rRNA in these mutants in the previous experiment (Fig. 4-15).

Figure 4-16: Primer extension assay to measure levels of various pre-rRNA species in various

***nop15* mutants**

A

1. Empty vector GAL
2. Empty vector Glu
3. WT Nop15 Gal
4. WT Nop15 Glu
5. F136A Gal
6. F136A Glu
7. F136G Gal
8. F136G Glu
9. F136G Glu (37°C shift)
10. Y134A Gal
11. Y134A Glu
12. Y94A Gal
13. Y94A Glu

B

1. Empty vector GAL
2. Empty vector Glu
3. WT Nop15 Gal
4. WT Nop15 Glu
5. F139A Gal
6. F139A Glu
7. F139G Glu
8. F139G Gal
9. Y134G Gal
10. Y134G Glu
11. Y94G Gal
12. Y94G Glu
13. R132Q Gal
14. R132Q Glu
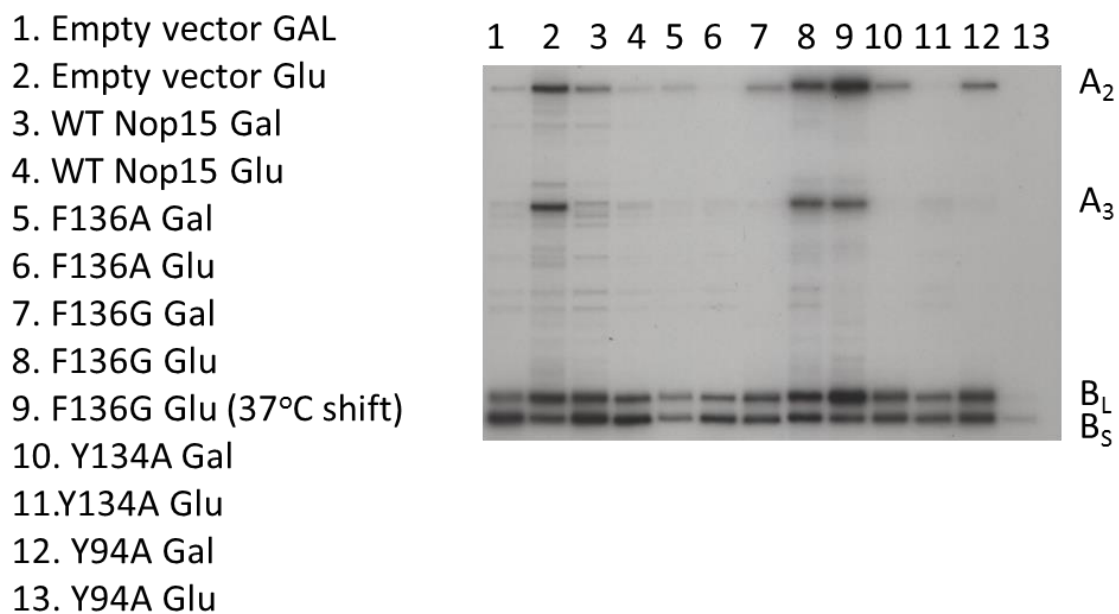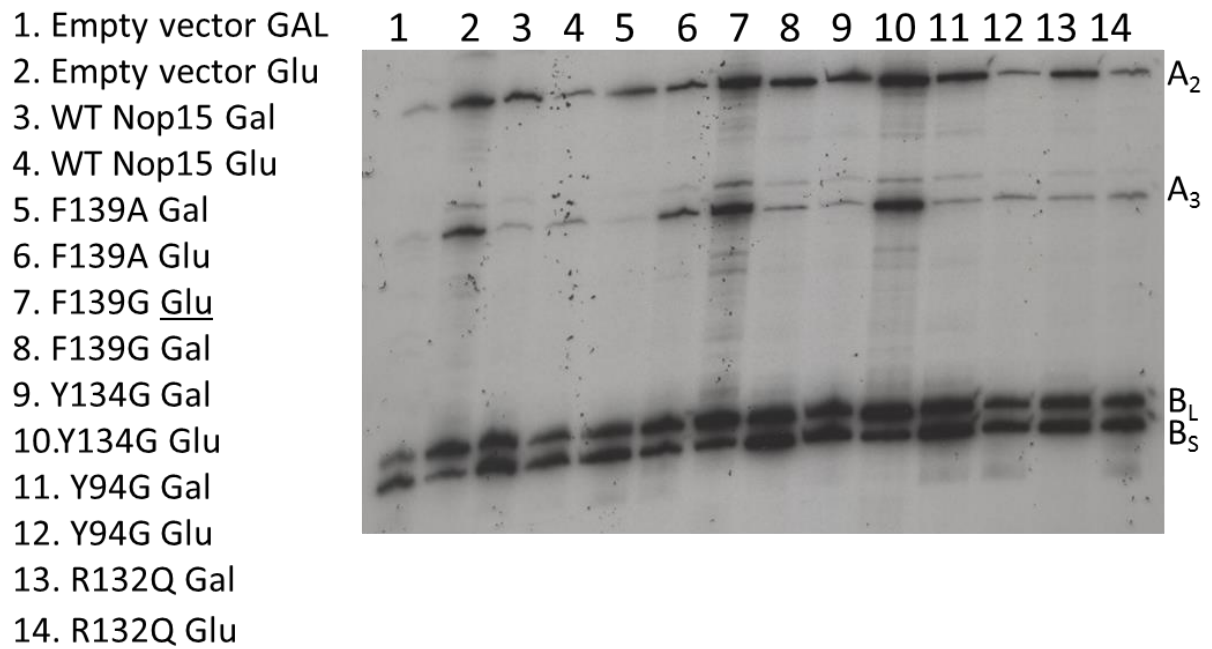
Fig. 4-16: Primer extension assay to measure levels of various pre-rRNA species.

Steady state levels of pre-rRNA species are measured by reverse transcription using an oligonucleotide primer that binds to the ITS2 spacer. Corresponding strains used (left) and the 5' ends of pre-rRNAs are indicated. The assay was done in two batches, shown (A) and (B) with their respective controls.

4.3.7. *Preribosome composition in nop15 mutants*

The depletion of Nop15 precludes the stable association of the interdependent A3-factors (Sahasranaman et al., 2011). We questioned if the lethal mutations might cause a similar effect on the interdependent A3-factors, possibly due to gross misfolding of the mutant protein. In order to determine the association of other A3-factors, we affinity-purified preribosomes using the assembly factor Rpf2 as the bait, ran an SDS gel to separate the proteins and visualized them by silver staining (Fig. 4-17). We observed that in each of the *nop15* mutants that exhibited a growth defect, as shown in (Fig. 4-14), the levels of the interdependent A3-factors Erb1, Nop7, Ytm1, and Rlp7 were decreased (lanes 5,7,9). This suggests that these mutants mimic the null phenotype of Nop15 (lane 3), where the interdependent A3-factors do not associate stably.

Figure 4-17: Assaying preribosome composition in *nop15* mutants by affinity purification

Fig. 4-17: Assaying preribosome composition in *nop15* mutants by affinity purification.

Preribosomes were affinity purified using TAP-tagged assembly factor Rpf2 as the bait. The proteins thus obtained were subjected to electrophoresis and visualized by silver staining. Lane 1 shows the protein markers. For all the other lanes, strains carrying various mutations and the media in which they were grown (GAL for galactose medium and GLU for glucose medium) are indicated. On the right, bands corresponding to various A3-factors are labeled, according to information from previous mass-spectrometric analyses.

4.3.8. Revisiting the F136A mutant

While the lethal mutations caused a phenotype akin to the null phenotype of Nop15, we were unable to test whether or not this effect is caused due to the gross unfolding of the mutant protein, irrespective of its ability to bind RNA, since we do not have an antibody against Nop15. An alternative to this scenario is that the mutations abolishing the binding of Nop15 to ITS2 do not interfere with the overall stability of the protein. Instead, they may be required for the association of Nop15 with the assembling ribosome.

Since we did not have the capability to distinguish between these possibilities, we decided to take a closer look at the F136A mutation that resulted in a mild decrease in the levels of 25S rRNA. We repeated the aforementioned assays for this mutant.

As mentioned before (Fig. 4-14), at all three temperatures tested, the F136A mutation did not affect the growth of the strains (Fig. 4-18). However, when we repeated the primer extension after adjusting for loading, we observed that this mutant caused a mild accumulation of $27SA_3$ pre-rRNA without a concomitant decrease in 27SB (Fig. 4-19). While we have since observed many mutants that cause a similar phenotype (Talkish et al., 2014a), this was one of the first times we had observed this effect and hence we proposed this was a weak 'A3 effect' that is not accompanied by turnover of preribosomes, as is the case with most strong A3-factor mutants.

Figure 4-18: Verifying the growth phenotype of *nop15-F136A* mutant
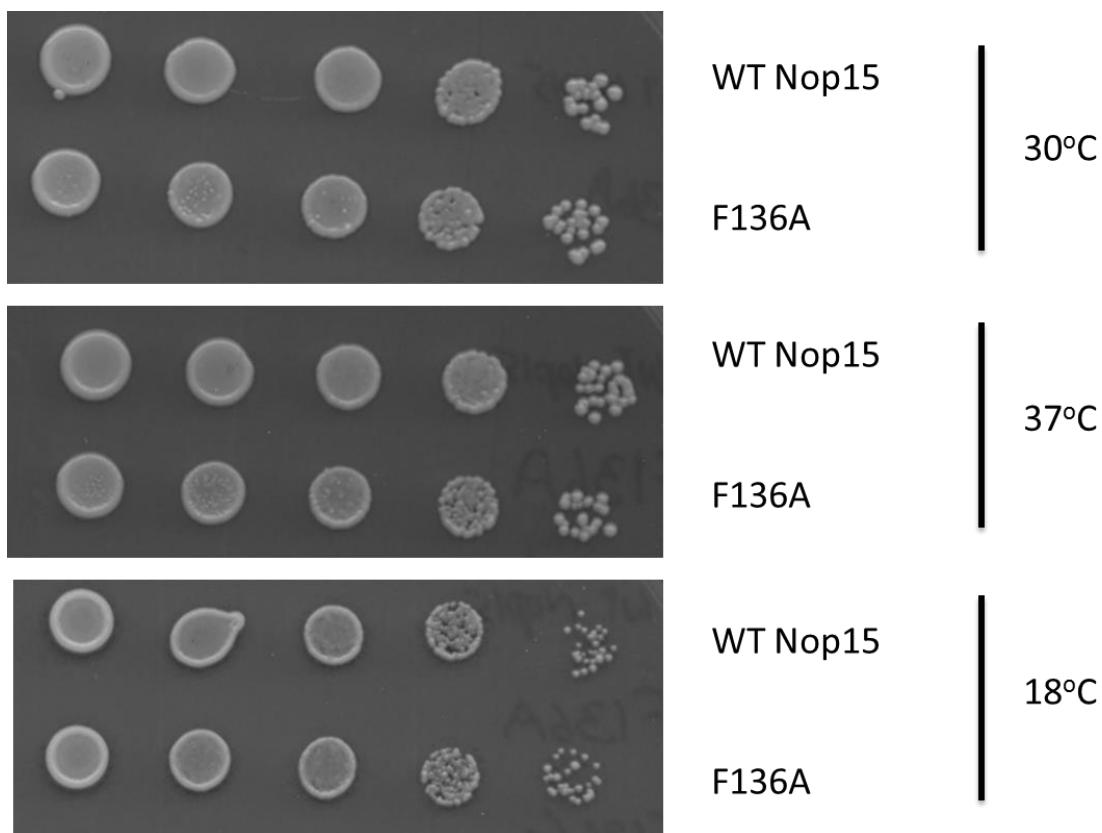
Fig. 4-18: Verifying the growth phenotype of *nop15*-F136A mutant.

Serial dilutions of strains with either wild-type or *nop15-F136A* mutant, as indicated on the right, were spotted on to solid media. The strains were grown at 30°C, 37°C or 18°C in galactose medium (left panels), where genomic *NOP15* is expressed, or glucose medium (right panels), where it is repressed.

Figure 4-19: Primer extension assay to measure levels of various pre-rRNA species in the
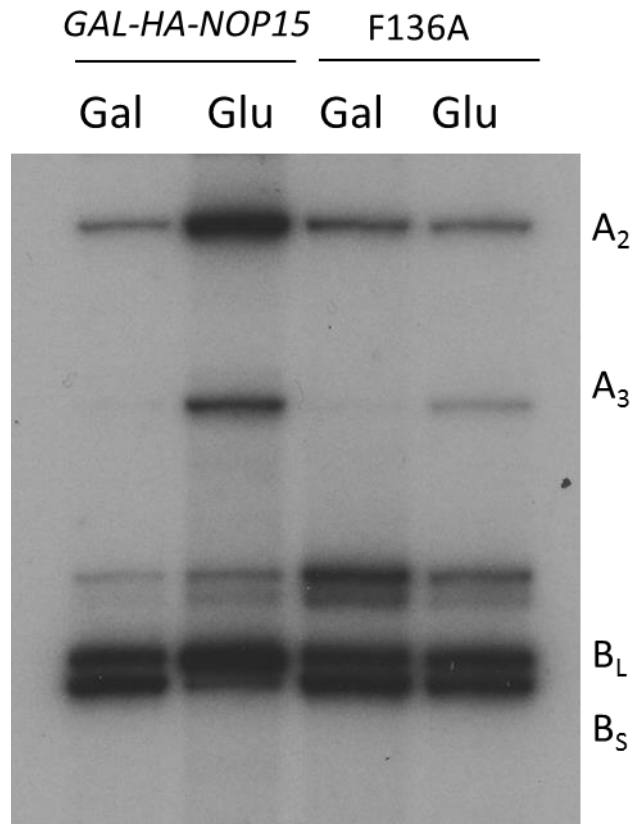
***nop15-F136A* mutant**

Fig. 4-19: Primer extension assay to assay levels of various pre-rRNA species in the *nop15*-F136A mutant.

 Steady state levels of pre-rRNA species are measured by reverse transcription of total RNA from various strains using an oligonucleotide primer that binds to the ITS2 spacer. Corresponding strains used and the 5' ends of pre-rRNAs are indicated.

We went ahead to assay changes in the protein composition of preribosomes in this mutant. Unlike other strong A3-factor mutations, this mutation did not affect the stable association of other interdependent A3-factors (Fig. 4-20), as observed by silver staining of proteins affinity-purified using TAP-tagged assembly factor Rpf2. In a canonical A3 mutant, it has been shown that there is a hierarchy of proteins that fail to stably associate: the interdependent A3-factors fail to associate, followed by the DEAD-box helicase Has1, and subsequently, the B-factors (such as Nog1, Rlp24, Nip7, Tif6) and the ribosomal proteins near the proximal stem (such as L17). Since the phenotype of the *nop15* F136A mutant was different from the Nop15 depletion phenotype, we assayed other proteins downstream of the A3-factors by western blotting (Fig. 4-21). With L5 as the loading control, we observed that the levels of neither the A3-factors (Nop7, Cic1, Has1) nor the B-factors (L17, Nog1, Rlp24, Nip7, Tif6) were affected by this mutation. However, the amount of B-factor Nog2, which is the last B-factor to associate before the subsequent 27SB processing occurs, was diminished. Although the magnitude of decrease in the level of Nog2 was small, this effect was reproducible.

Figure 4-20: Assaying preribosome composition in the *nop15 F136A* mutant by affinity purification
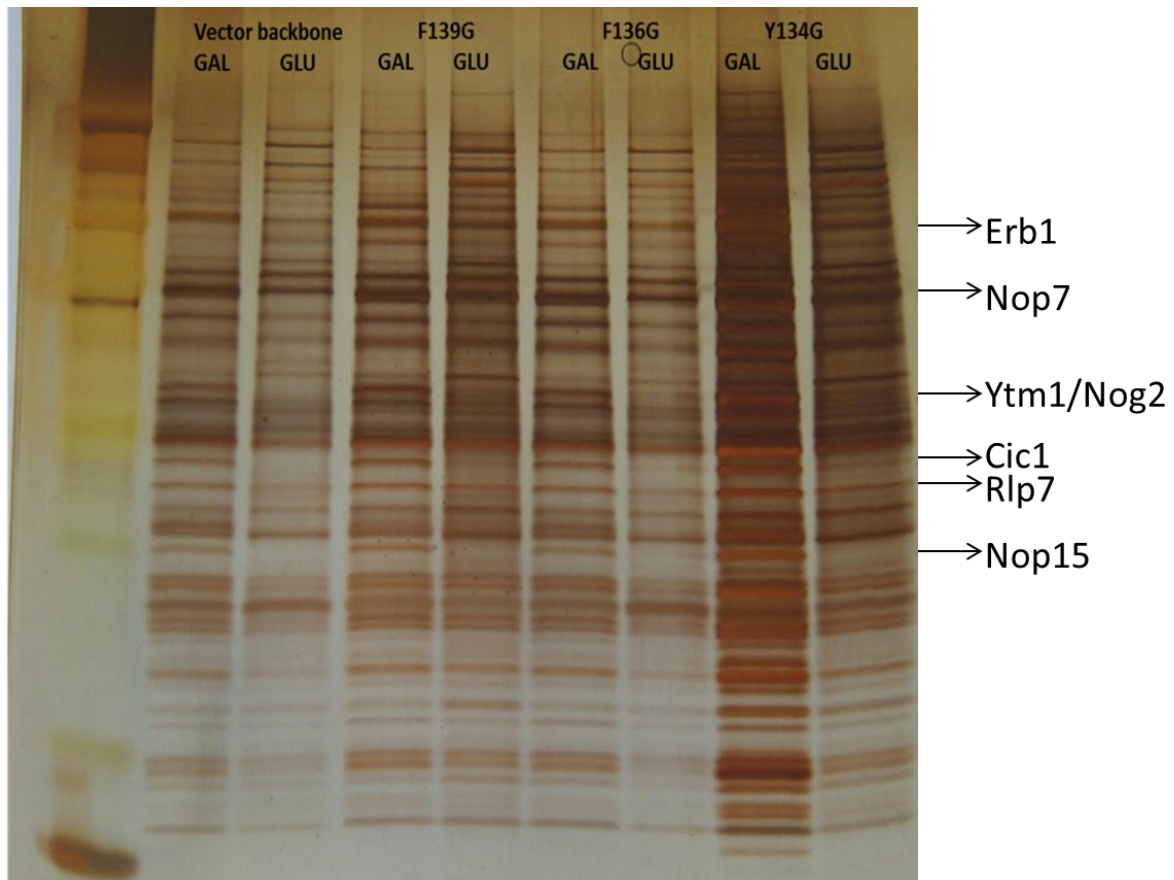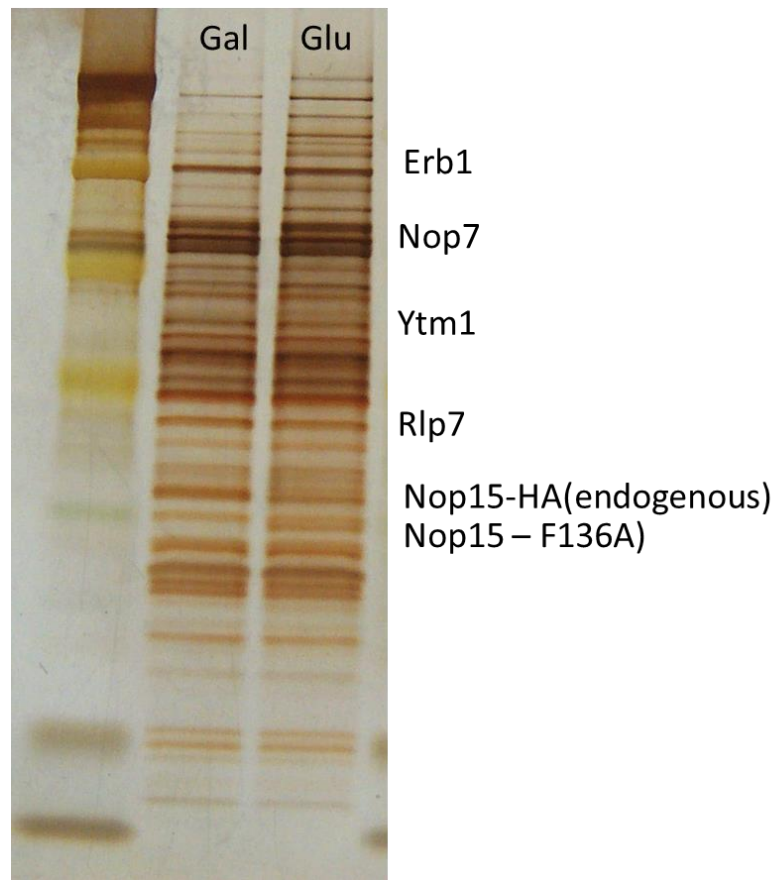

Fig. 4-20: Assaying preribosome composition in the *nop15* F136A mutant by affinity purification.

Preribosomes were affinity purified using TAP-tagged assembly factor Rpf2 as the bait. The proteins thus obtained were subjected to electrophoresis and visualized by silver staining. Lane 1 shows the protein markers. The lane marked as Gal indicates the wild-type like scenario where genomic *NOP15* is expressed. The lane marked as Glu indicates the scenario where *nop15*-F136A is the only source of Nop15 to the cell. On the right, bands corresponding to various A3-factors are labeled, according to information from previous mass-spectrometric analyses.

Figure 4-21: F136A mutation in Nop15 permits stable association of A3-factors, but causes

decreased association of the GTPase Nog2
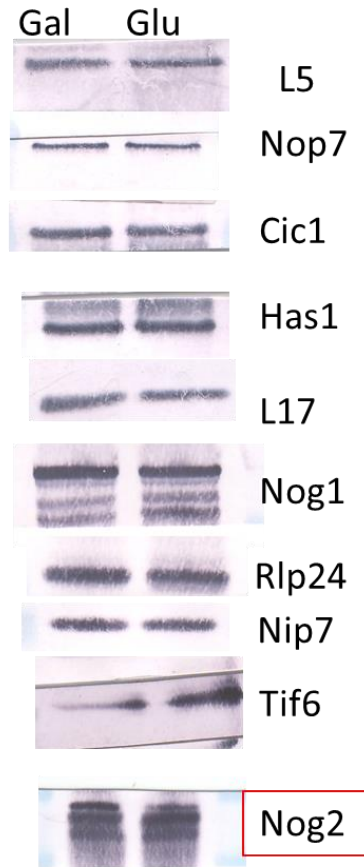
Fig. 4-21: F136A mutation in Nop15 permits stable association of A3-factors, but causes decreased association of the GTPase Nog2.

Western blotting of the proteins performed in a manner similar to that described in Fig. 4-19 and represented in a similar manner. The levels of A3-factors remain the same between WT (left, gal) and mutant (right, glu) strains. A mild decrease is reproducibly observed in the levels of the GTPase Nog2 (boxed).

Figure 4-22: Table summarizing the phenotypes of various *nop15* mutants

Mutation	Growth defect (Tested at 30ºC, 37ºC, 18ºC,	Cold RNA (25S/18S)	Pre-ribosome composition	Pre-rRNA processing phenotype
F136A	None	Very mild decrease, within error	None	None
F136G	Slightly slow at 30ºC and 18ºC. Very slow at 37ºC	Decreased	A3 like in general, Nop15 doesn't associate with preribosomes	27SA3 accumulates, along with slight 27SA2 accumulation, even more so after a temperature shift.
Y134A	None	Normal	None	None
Y94A	None	Normal	None	None
F139A	None	Normal	Nog2 does not associate.	Slight increase in 27SA3.
F139G	Very slow at all three temperatures	Decreased	A3 like, Nop15 doesn't associate with preribosomes.	Increase in 27SA3, concomitant decrease in 27SBs
Y134G	Slow at all three temperatures	Decreased	A3 like, Nop15 doesn't associate with preribosomes.	Increase in 27SA3, concomitant decrease in 27SBs
Y94G	None	Normal	-	None
R132Q	None	Normal	-	None

Fig. 4-22: Table summarizing the phenotypes of various *nop15* mutants.

4.3.9. *Recombinant expression of NOP15 for in vitro studies*

In parallel with the *in vivo* analysis, we wanted to assay the RNA binding ability of *nop15* mutant proteins. First, we wanted to show that WT Nop15 can bind RNA in a sequence-specific manner *in vitro*. We collaborated with the Rule lab for this experiment. For recombinant expression of *NOP15* in *E.coli*, we cloned *NOP15* in a suitable expression vector that incorporates a 6-His tag (pET22b+), using *BamHI* and *XhoI*. After verifying successful cloning by restriction digestion and sequencing, we transformed BL21 λDE3 cells with the pET22b+ borne *NOP15* and a pRARE plasmid in order to incorporate any rare codons. After growing the BL21 λDE3 cells to log phase, we induced expression by adding IPTG to a final concentration of 1mM. We did a time course of *NOP15* expression after induction (Fig. 4-23) by testing proteins from whole cell lysates separated on an SDS gel. Based on this, we chose 6 hours as the induction time, going forward. Then, we purified the protein using cobalt resin and saw that the protein was expressed with good yields (Fig. 4-24, top panel). However, we found that there were multiple other non-specific bands, which presumably result from other protein contaminants. In order to get a more pure sample of recombinant protein, we incorporated a cation-exchange chromatography step. We were able to eliminate nearly all but one extra non-specific band from our protein sample (Fig. 4-24, bottom panel). Thus, we were able to express and purify recombinant Nop15.

The next step in establishing the *in vitro* binding assay was to transcribe ITS2 *in vitro*. In order to do this, we tried to clone ITS2 into pRS315 using *SacI* and *HindIII* enzymes, and subsequently to use the T7 promoter for *in vitro* transcription. However, we did not succeed in building this construct even after numerous attempts, possibly because of the small size of the insert. Although we had multiple alternatives around this problem, including gene synthesis, since the mutations did not result in strong, distinctive phenotypes *in vivo*, we decided that these *in vitro* studies may not be informative.

Figure 4-23: Time course of expression, post IPTG-induction, to optimize recombinant expression
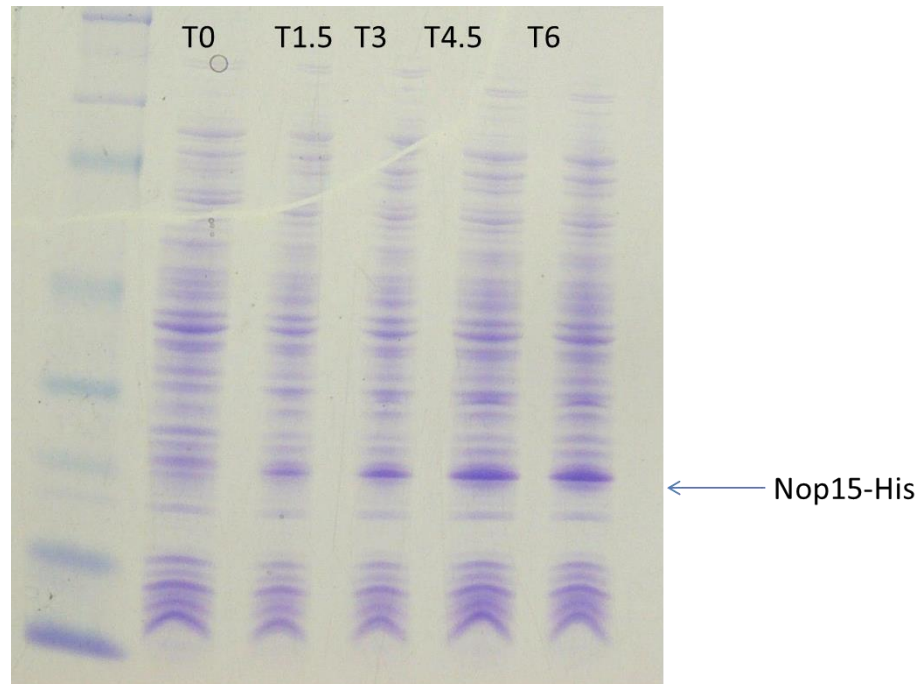
of *NOP15* in *E.coli*

Fig. 4-23: Time course of expression, post IPTG-induction, to optimize recombinant expression of *NOP15* in *E.coli*.

SDS-PAGE gel after cobalt affinity purification of the recombinant protein showing that the protein is stably expressed.

Figure 4-24: Recombinant expression and purification of *NOP15* in *E.coli*
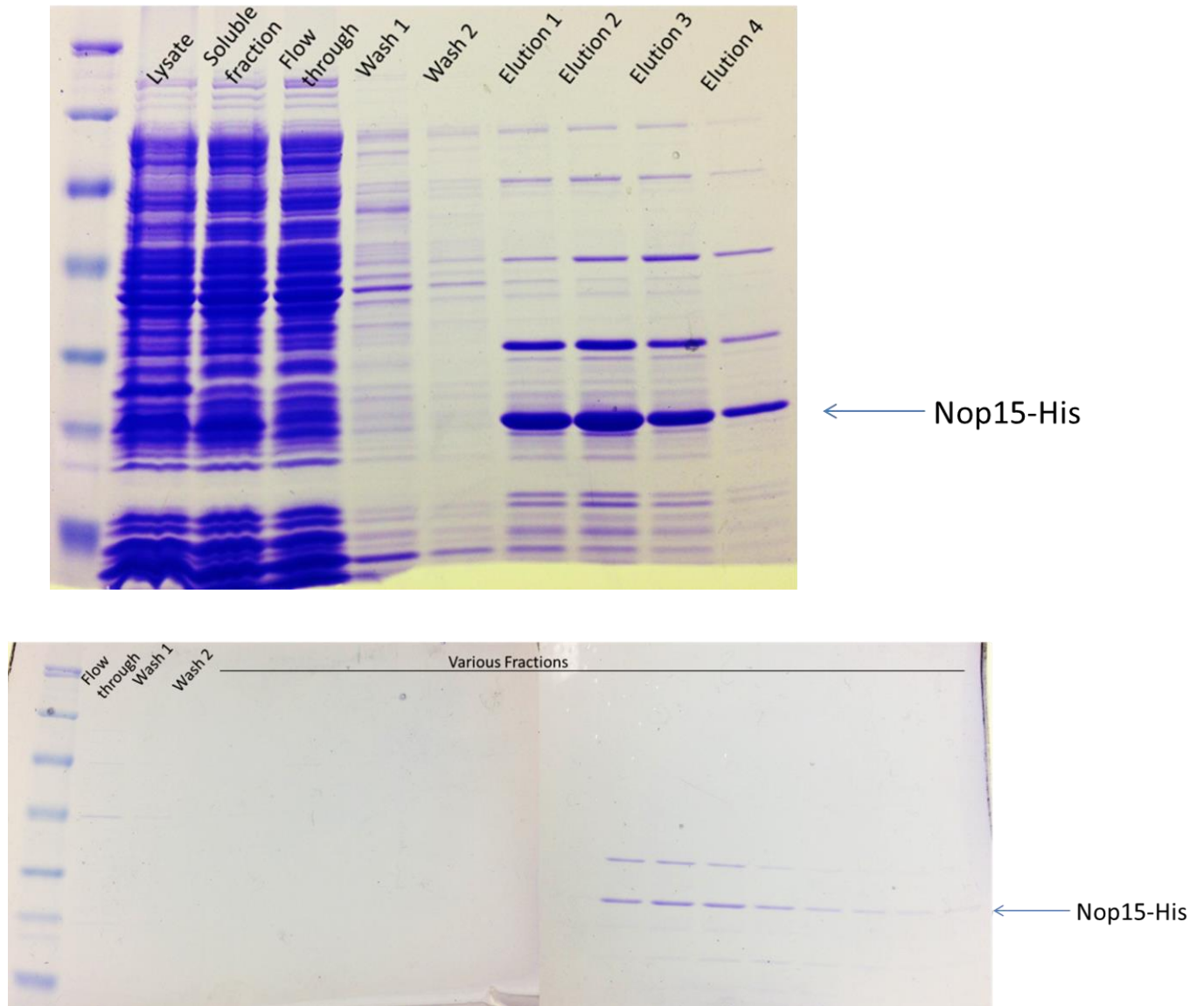
Fig. 4-24: Recombinant expression and purification of *NOP15* in *E.coli*.

Top: SDS-PAGE gel after cobalt affinity purification of the recombinant protein showing that the protein is stably expressed. Bottom: SDS-PAGE gel of different fractions from cation affinity chromatography showing purified Nop15.

4.4. Discussion: Protein-protein interactions of the ITS2 neighborhood proteins

Yeast two-hybrid assays were performed with Nop15, Cic1, Rlp7 against each other and an array of other proteins, including those that participate in the subsequent B-step where ITS2 is removed, with a goal to find potential interactions that provide valuable clues to understand the functions of these proteins. Taken together with yeast two-hybrid screens performed earlier in the lab by Dr. Dembowski, the picture that emerges (summarized in Fig. 4-4) reveals a complex network of interactions between these three proteins as well as with other key proteins involved in the A3-step and the subsequent B-step, which might connect them spatially with other neighborhoods on the pre-ribosome and temporally with subsequent steps in assembly. These data are supported by the facts that these three proteins (Nop15, Cic1 and Rlp7) have been cross-linked to ITS2 (Babiano et al., 2013; Dembowski et al., 2013c; Granneman et al., 2011). Further, most of our data is consistent with other protein-protein interaction screens, at least qualitatively (McCann and Baserga, 2014). In addition to revealing this wealth of information, we successfully established a yeast-two-hybrid bookshelf, which could potentially be used for any further analysis about interactions between proteins involved in the A3 and B steps.

4.4.1. The interaction network formed by Rlp7 confirms its localization

Consistent with the Rlp7 binding site we identified by CRAC, our two-hybrid results show that Rlp7 interacts with proteins that bind in the vicinity of ITS2. Rlp7 interacted with Nop15, which also interacted with Cic1, consistent with Rlp7, Nop15 and Cic1 all contacting ITS2 during ribosome assembly. Rlp7 and Nop15 were positive for interactions with themselves and therefore may have the potential to form dimers on or off pre-ribosomes. On the contrary, in the recently solved cryo-EM structures of preribosomes purified using the late nuclear assembly factor Nog2 as a bait, we do not see multiple copies of these proteins on the preribosome (Wu et al., manuscript under review).

We also observed interactions between Rlp7 and Ebp2. Ebp2 likely binds near the ITS2-proximal stem because it interacts with Brx1, Nop12, L8 and L15, which can be purified as a subcomplex (Zhang et al., 2004). R-proteins L8 and L15 contact the proximal stem (Ben-Shem et al., 2011) and Nop12 contacts the proximal stem and nearby sequences in 5.8S rRNA (Granneman et al., 2011). In support of two-hybrid data, interactions between Rlp7 and Ebp2 as well as Cic1 and Nop15 have previously been identified by protein-fragment complementation assays (Tarassov et al. 2008).

Relatively weak interactions were also observed between Rlp7, and Rpf2, Rrs1 and Nsa2. These factors were previously implicated in 27SB pre-rRNA processing. Even though these proteins are not located in in preribosomes in physical proximity to Rlp7 (Asano et al., 2015; Bassler et al., 2014; Kharde et al., 2015), the neighborhood around the central protuberance has been implicated in processing of ITS2 (7S pre-rRNA processing), which suggests that these proteins may be functionally linked, through indirect interactions mediated by a string of proteins.

As an orthogonal approach to identify factors that interact with Rlp7, we affinity purified Rlp7-associated pre-ribosomes from yeast cell lysates and identified proteins by mass spectrometry that remained associated with Rlp7 after washing with high salt (Fig. 4-5). We identified Nop15 and Erb1 by this assay. The observed interaction of Rlp7 with Nop15 supports two-hybrid data. Erb1 crosslinks to 25S rRNA of domain I (Granneman et al., 2011), which is less than 30 angstroms away from the Rlp7 CRAC site on the mature 60S ribosomal subunit (Fig. 4-6).

Taken together, these data support the identified binding site of Rlp7 at ITS2 and the ITS2-proximal stem of domain I near assembly factors Cic1, Nop15, Nop12 and Erb1 (Fig. 4-6). The recent cryo-EM structural model agrees with our finding about the localization of Rlp7 (Wu et al., manuscript under review)

It appears that the ITS2 cluster proteins are involved in maintaining the ring structure of ITS2 (Dembowski et al., 2013c; Granneman et al., 2011). Additionally, we propose that they either directly chaperone domain I folding or transmit conformational changes within ITS2 to the rest of the preribosome, by way of this extensive molecular network (Fig. 4-4).

4.4.2. Do the ITS2 cluster proteins recruit Has1?

The proteins Nop15, Cic1 and Rlp7 cluster near the 3′ end of 5.8S rRNA but trigger processing at the 5′ end of 5.8S rRNA. A remaining question is why do these proteins bind at a distance from the A3 processing site? Our data indicate that they may recruit the RNA helicase Has1 to pre-ribosomes, which may couple rRNA domain I folding to 27SA$_3$ pre-rRNA processing (Dembowski et al., 2013a). Rlp7, Nop15 and Cic1 all tested positive for interactions with the RNA helicase Has1. Although these interactions give the first clues about the location of Has1 on the preribosomes, the weak nature of the interactions also indicate that the interaction of Has1 with the ITS2 cluster proteins could be transient.

Additionally, it has been demonstrated that ITS2 proteins are required for Has1 to enter pre-60S ribosomes (Sahasranaman et al., 2011). Their close interactions observed in this study add further credence to the hypothesis that the ITS2 cluster proteins may recruit Has1. Has1 helps to stabilize the native conformation of domain I during assembly and is required for 27SA$_3$ and 27SB pre-rRNA processing (Dembowski et al., 2013a). Furthermore, Has1 is released from preribosomes just before ITS2 removal is initiated. Taken together, it appears that the ITS2 cluster proteins may function by recruiting Has1 and facilitating subsequent RNA rearrangements around the ITS2/proximal stem region of the preribosome, to trigger the cleavage and removal of ITS2.

4.5.   Discussion: rRNA interactions of Nop15

4.5.1. The RRM of Nop15 may contribute to its association with preribosomes

In the second part of this project to understand the protein-RNA interactions formed by the ITS2 cluster proteins, we systematically mutated all of the aromatic residues of Nop15 that could form base stacking interactions with pre-rRNA (summarized in Fig. 4-22). We substituted these aromatic residues with both Ala and Gly. We found that those mutations that resulted in a lethal growth phenotype also showed a strong $27SA_3$ pre-rRNA accumulation concomitant with a decrease in $27SB_S$ pre-rRNA levels (Fig. 4-16). These are single amino acid substitutions. If we assume that they do not cause the protein to grossly mis-fold, our results suggest that interfering with the RNA binding of Nop15 leads to its null phenotype, which corresponds to its near absence from preribosomes. This suggests that interaction with pre-rRNA may be necessary for the stable association of Nop15 to the preribosome. In other words, the function of Nop15 in $27SA_3$ pre-rRNA processing may be an exclusive consequence of its binding to ITS2.

Another potential model is that Nop15 can rearrange the pre-rRNA upon binding, which then enables the stable association of other A3-factors. In the absence of Nop15 binding, the pre-rRNA rearrangement does not happen and the interdependent A3-factors are not associated with the pre-ribosome. Although Nop15 has been shown to bind pre-rRNA *in vitro,* the sequence specificity of this interaction and the subsequent changes it can cause in RNA folding *in vivo,* have not been verified (Oeffinger and Tollervey, 2003). Thus, this model would be more complete and definitive with an *in vitro* RNA binding assay, such as an EMSA and a structure probing assay, to complement our phenotypic results obtained *in vivo*.

4.5.2. The nop15 F136A mutant provides new models for coupling 27SA3 pre-rRNA processing and subsequent steps in ribosome assembly

It is interesting that substituting an amino acid residue with alanine causes a different effect from that of substituting it with glycine, as observed in the case of F136 of Nop15. When mutated to Gly, this causes a $27SA_3$ pre-rRNA accumulation phenotype that is exacerbated at 37^oC. However, when this residue is mutated to Ala, it results in WT-like growth, accompanied by a mild accumulation of $27SA_3$ pre-rRNA and no decrease in $27SB_S$ pre-rRNA.

Further, the only downstream protein in the hierarchy that shows diminished levels of association with the preribosome is Nog2, a GTPase and the last B-factor to enter the preribosome before the 27SB processing step (Fig. 4-21). This makes the F136A mutant even more interesting. In general, when A3-factors are depleted, the accumulation of $27SA_3$ pre-rRNA is often accompanied by significant turnover of preribosomes (Jakovljevic et al., 2012). This may be the reason why we see a dramatic decrease in the levels of $27SB_S$ pre-rRNA in these mutants. In contrast, the F136A mutant might slow down processing of $27SA_3$, but not sufficiently enough to cause turnover of the assembling ribosome. This is evident from the fact that the level of $27SB_S$ pre-rRNA remains relatively stable in this mutant, although a pulse-chase assay would unequivocally establish this claim. In addition, most downstream protein factors, including ribosomal protein L17 remain stably associated. This suggests that the RNA rearrangements occurring at the proximal stem that permit the stable association of rpL17 may proceed unperturbed in this mutant.

The question that remains is how a slight delay in $27SA_3$ processing can be communicated to Nog2, a protein that binds near the peptidyl transferase center. This seems like a pertinent question to answer because the decreased association of Nog2 in this mutant suggests that even the presence of all of the protein factors upstream of Nog2 which are known to be necessary for the association of Nog2, is not sufficient to recruit Nog2. Somehow, there seems to be a communication channel between pre-rRNA processing occurring on the 5' end of 5.8S rRNA, proteins binding near the 3' end of 5.8S rRNA and the

association of GTPases to the active site of the assembling ribosome. Further experiments need to be

done to tease apart the exact mechanistic steps in this communication process.

4.6. Summary

In summary, we investigated the protein-protein and protein-RNA interactions formed by the ITS2 cluster proteins. Rlp7 was used as a case study for protein-protein interactions while Nop15 was used to study the protein-RNA interactions. We were able to identify a network of protein-protein interactions that highlighted how subsequent steps of ribosome assembly are spatially and temporally linked. In addition, we were able to localize Rlp7 to ITS2 and provide models for recruitment of the DEAD-box helicase Has1. Using our studies on Nop15-ITS2 interaction, we propose that binding of Nop15 to ITS2 may contribute to its functioning in A3-processing. Further, we speculate that the mere association of proteins that have been proposed to recruit the critical, PTC-binding GTPase Nog2 is not sufficient for its stable association. Instead, its association seems to be linked to successful completion of preceding steps, namely processing of $27SA_3$ pre-rRNA and stable association of ribosomal proteins.

Although further experiments are needed to unequivocally establish the models proposed here, this project marked a paradigm shift in our approach towards understanding ribosome assembly. Harnessing the power of missense mutants, this study started a wave of further studies that were designed to unmask and elaborate the specific roles of assembly factors that have until now been obscured by depletion phenotypes. The approach of studying proteins in the light of their protein interactions set a precedent for elucidating the roles of numerous proteins whose only predicted functions are RNA and protein-binding. Further, by placing the focus on the ITS2 neighborhood, our studies may eventually help in answering why the pre-rRNA spacers have evolved in the first place, considering how expensive it is for the cell to synthesize, fold and process these spacers.

In addition to these conceptual advancements, this project pioneered various technologies and tools in the lab that have pervaded almost every research project in the lab and have been adopted by everyone in the lab. Specifically, this was the first project that successfully optimized and utilized

QuikChange mutagenesis kits in the lab, and developed a general scheme of experimental design to assay site-directed mutants using newer kits and strains. Further, this project also served to develop robust systems for recombinant expression of proteins using more modern vectors and approaches.

Note: Special thanks to Dr. Jill Dembowski for the Rlp7 collaboration (Dembowski et al., 2013c) and sharing some of her yeast-two-hybrid data and strains. Thanks to the Rule lab and Sahil Sangani for sharing their expertise and reagents for recombinant purification of Nop15.

4.7. Materials and methods

- Strains expressing C-terminally His$_6$-TEV-protein A (HTP)-tagged proteins were generated according to the method described previously. Unless otherwise indicated, yeast were grown at 30°C in YEPD (2% dextrose, 2% peptone, 1% yeast extract) or YEPGal (2% galactose, 2% peptone,1% yeast extract) media and were harvested during mid-log phase growth. (Longtine et al., 1998; Rigaut et al., 1999)

- Movable open reading frames (Open Biosystems) were transferred into either the pACTGW-attR or pASGW-attR two-hybrid vector (Nakayama et al., 2002) using the Gateway recombination-based cloning system (Life Technologies). Plasmids were transformed into PJ69-4a (James et al., 1996) or PJ69-4α (Uetz et al., 2000) yeast, which were mated to test for potential protein–protein interactions. Pair-wise interactions were tested for activation of the **GAL-HIS3** reporter gene by initial screening for the ability to grow on media lacking histidine in the presence of 1 mM 3-AT according to the method described previously (James et al., 1996). Positive interactions were further tested for the strength of interaction by growth in the presence of increasing concentrations of 3-AT (1–50 mM).

- Whole-cell lysates were prepared from 350 mL cultures of the **RLP7-HTP** strain (JWY9262) according to the method previously described (Granneman et al., 2009) followed by affinity purification of Rlp7-HTP and associated proteins on 60 µL IgG-conjugated Dynal beads (Life Technologies) for 1 h at 4°C (Oeffinger et al., 2007). After binding, protein complexes were washed three times with TN buffer (50 mM Tris-HCl at pH7.8, 0.1% IGEPAL, 5 mM β-mercaptoethanol) containing 150, 450, or 1000 mM NaCl. Protein complexes were eluted from IgG beads by cleavage with 10U TEV Protease (Life Technologies) for 1 h at room temperature. Eluted proteins were either precipitated with 10% TCA or subjected to a second purification step on 100 µL Ni-NTA Agarose beads (Qiagen) for 2 h at 4°C followed by elution with 250 mM imidazole and precipitation with 10% TCA. All steps were carried out in TN150 buffer (containing 150 mM NaCl) unless otherwise indicated. Proteins were

separated on 4%–12% NuPAGE gels (Life Technologies) followed by silver staining according to standard procedures.

- For identification of proteins that associate with Rlp7 after high-salt wash, two-step purifications were carried out as described except that cell lysates were obtained from 2-liter cultures followed by purification on 400 μL IgG beads and 1 mL Ni-NTA Agarose beads. Proteins were separated on 4%–12% NuPAGE gels followed by silver staining with the SilverQuest Silver Staining Kit (Life Technologies). Gel slices were destained and dried and sent to Penn State Hershey Core Research Facilities for reduction, alkylation, trypsin digestion, and MALDI-TOF mass spectrometry. Peptides were analyzed by the ProteinPilot 4.0 program.

- Generation of *nop15* mutant alleles: The *S.cerevisiae NOP15* ORF including around 1000 bp upstream of the start codon and 200 bp downstream of the stop codon was cloned into pRS315 using *BamH1* and *HindIII*. Mutations were introduced using the Quickchange kit from Agilent Technologies. The mutations made are described in detail in the main text. Plasmids bearing mutant alleles were transformed into *GAL-HA-NOP15* (Sahasranaman et al., 2011), and maintained on media lacking leucine.

- RNA analysis: RNA from log-phase yeast cultures was extracted as described previously (Horsey et al., 2004). A Nano Drop spectrophotometer (Thermo Fisher) was used to quantify RNA. 5μg RNA was used for northern blotting. Primer extension was done as stated in (Talkish et al., 2014b)

- Protein extraction, Affinity purification, SDS-PAGE and Western blotting were performed as described in (Talkish et al., 2014b) and (Sahasranaman et al., 2011).

- For recombinant expression, a consensus protocol (Structural Genomics et al., 2008) was used with modifications suggested by the Rule lab using their protocols.

- Sequences of oligonucleotide probes are available upon request.

5. Technique Development: Yeast-three-hybrid assay

5.1.   Introduction

RNA binding proteins (RBPs) and ribonucleoprotein particles (RNPs) function in numerous cellular processes; in particular, they play vital roles in eukaryotic gene expression. The abundance of these interactions could arise from the fact that proteins can form many types of molecular interactions with RNA, such as electrostatic, hydrophobic, hydrogen-bonding and base-stacking interactions, similar to protein-DNA interactions. On the other hand, the specificity of RNA-protein interactions is largely dictated by the sequence or the secondary/tertiary structure of the RNA, along with specific motifs in the protein sequence. Owing to the ubiquity and importance RNA-protein interactions, identifying and studying RNA-protein interactions is at the center of many biological research problems.

5.1.1. Methods to assay RNA-protein interactions

Many different methods have been developed to assay RNA-protein binding. Some of the methods widely used *in vitro* include RNA electrophoretic mobility shift assay (EMSA), fluorescence in situ hybridization (FISH) and RNase protection based assays (Popova et al., 2015). These are widely followed up using studies *in vivo* that are based on crosslinking followed by pulldown approaches (CLIP, CRAC and RIP) and footprinting assays, in general (Cloonan et al., 2008; Granneman et al., 2011; Li et al., 2014; Murigneux et al., 2013). Other high-throughput approaches have also been developed to study this problem (Tome et al., 2014).

Two constraints dictated the choice of a method to assay RNA-protein interactions in our studies. First, we wanted to use an *in vivo* system so that the results from the RNA-protein interaction assay are directly meaningful in the context of the assembling ribosome inside the cell. Second, while many of the aforementioned approaches work well for large RNAs, smaller RNAs tend to behave promiscuously in these assays.

Hence, we decided to adapt a method called the 'three-hybrid' system roughly based on the yeast two-hybrid system (used in Chapter 4) that is widely used for assaying protein-protein interactions. This method is an *in vivo* method and can potentially work with small RNAs. In fact, reports from the Wickens and Fields labs that originally developed this method state that this method works best with RNAs that are <200nt long (Hook et al., 2005; Jaeger et al., 2004; Martin, 2012). Hence this method seemed suitable for our studies focused on expansion segments.

5.1.2. Assaying protein partners of rRNA expansion segments

The biological question that warranted the use of this three-hybrid system for RNA-protein interactions concerned binding of assembly factors to ribosomal RNA expansion segments. We proposed that expansion segments have evolved to offer bindings sites for additional eukaryote-specific protein components of the eukaryotic ribosome: the extensions of ribosomal proteins, eukaryotic ribosomal proteins and the wide range of eukaryote-specific assembly factors. Although methods like CRAC (Babiano et al., 2013; Bassler et al., 2014; Dembowski et al., 2013c; Granneman et al., 2011; Lebaron et al., 2013) had begun to identify the location of assembly factors on the preribosome, they are not scalable enough to ask pertinent protein binding questions from an RNA standpoint. From the perspective of rRNA expansion segments, since they are present on the surface of the ribosome and are seemingly exposed to the solvent, (Fig. 2-2), it is tempting to speculate that they participate in a variety of molecular interactions. In addition, data that emerged from the rRNA expansion segments project (Chapter 2) had shown us that the phenotypes of expansion segment deletions closely matched those of the depletion of ribosomal proteins that bound nearby (Fig. 2-14, Fig. 2-15).

We wanted to extend this observation to assembly factors and ask if the phenotypes of expansion segment deletions match the phenotypes of depletions of those assembly factors that bound nearby. While we can infer the interactions of r-proteins with ES from crystal structures of mature ribosomes

(Ben-Shem et al., 2011), such location information is available only for a very few assembly factors in preribosomes. Hence, we wanted to get a more robust picture of assembly factor contact points on the preribosome. Specifically, from the standpoint of expansion segments, we wanted to ask to which assembly factors a given expansion segment can bind. We began addressing this challenge using $ES5_L$ and $ES12_L$ as pilots. $ES5_L$ and $ES12_L$ are present in domains I and II of LSU rRNA (Fig. 2-1), and their deletion confers an early and a late-acting phenotype respectively (Fig. 2-12, Fig. 2-13). Also, they are small in size, which permits us to use them as a model for studying protein binding to small stretches of rRNA.

Below, we discuss the concept behind the three-hybrid system. In addition, as proof of principle, we describe the steps in utilizing this system to assay RNA-protein interactions using expansion segments $ES5_L$ and $ES12_L$ and a bookshelf of assembly factors that participate in the $27SA_3$ processing and B-processing steps. Further, we discuss potential shortcomings and address possible ways to troubleshoot and circumvent existing problems with this assay.

5.2. Results

5.2.1. Description of the yeast-three-hybrid assay

The three-hybrid assay consists of two hybrid proteins that bind to an MS2-tagged RNA. When all of these hybrid components come together, they have the potential to activate a reporter gene *in vivo,* (Fig. 5-1), (Sengupta et al., 1999; Zhang et al., 1999). This technique is based on the yeast-two-hybrid system that detects protein-protein interactions. Similar to the yeast-two-hybrid technique, the ability of yeast to grow or metabolize a chromogenic compound is an indicator of the strength of an RNA-protein interaction.

This system has two protein fusions and one RNA fusion. The only variables in the system are the RNA of interest and the protein of interest, the rest are fixed.

- Hybrid protein 1: LexA DNA binding domain + MS2-coat protein

- Tagged RNA: RNA of interest tagged with two MS2 RNA binding sites. Vectors are available to engineer the MS2 either to the 5' or 3' end of RNA, as desired.

- Hybrid protein 2: Protein of interest fused to a *GAL4* activation domain.

Fig. 5-1: Schematic diagram of the yeast-three-hybrid system.

LacZ represents any general reporter gene. Hybrid protein 1, tagged RNA and hybrid protein 2 are indicated. Illustration was adapted from the Wickens Lab website.

Hybrid protein 1 formed by the fusion of the LexA DNA binding domain to the MS2 coat protein, binds *cis*-elements upstream of a reporter gene using the DNA binding domain, e.g. the lexA operator. The MS2 coat protein can in turn bind the tagged RNA, through the two MS2 binding sites present on the tagged RNA of interest. If the RNA of interest interacts with the protein of interest, it recruits hybrid protein 2 that contains the transcription activation domain (AD or ACT).

Various vectors and strains for this assay are available from Marv Wickens' lab or Stan Fields' lab. See elsewhere for details on those (Zhang et al., 1999).

While we had an array of relevant strains and plasmids already available in the lab, (JWY6302: L40 strain, JWB4104: pIII-MS2-2, JWB4106-pIII-IRE-MS2, JWB4107: pAD-IRP), we decided to obtain a newer version of these vectors from the Wickens lab. We obtained the following vectors: pACT2, pAD-IRP, pIIIA/IRE-MS2, pIII/MS2-1, pIII/MS2-2. pIIIA/MS2-1, pIIIA/MS2-2, p3HR2, along with the yeast strains YBZ-1 and R40. See Appendix (strain list) for information on the entire gamut of strains, vectors related to yeast-three-hybrid.

Thus, in order to verify potential interactions, we transform both the RNA and protein fusion plasmids into one of the yeast strains mentioned above, or mate two strains containing an RNA plasmid and a protein plasmid, respectively. We will assay for growth of the resultant strain on media lacking histidine, in the presence of 3-aminotriazole (3AT), an inhibitor of the *HIS3* gene product, that minimizes background interactions. Only those strains containing a positive RNA-protein interaction will be able to grow on this medium lacking histidine in the presence of 3AT. One can use increasing concentrations of 3AT to semi-quantify the strength of interaction.

5.2.2. *Preliminary calibration of the system*

We wanted to calibrate the strengths of interactions of the positive and negative controls in the system and decide on a specific concentration of 3AT that would minimize false positives while permitting us to analyze the weak interactions. As a positive control, we used the iron response protein (IRP) binding to Iron response element (IRE) RNA. pAD and pACT are the protein plasmids, while pIIIA-IRE/MS2-2 and pIIIAMS2-2 are the RNA plasmids. Various yeast strains used here are YBZ-1, L40, and R40 (of the opposite mating type)

We wanted to test the effects of both mating and co-transformation, and hence we generated the following strains by transformation and further mated them to obtain all the four possibilities of positive and negative controls for RNA and protein.

- L40 strain bearing either one of the protein plasmids: pAD-IRP (+) or pACTII (-)
- R40 strain bearing either one of the RNA plasmids: pIIIA/IRE-MS2 (+) or pIIIA/MS2-2 (-)

We also co-transformed the following plasmids into the newer YBZ-1 strain:

- pAD-IRP (+) + pIIIA/IRE-MS2 (+)
- pAD-IRP (+) + pIIIA/MS2-2 (-)
- pACTII (-) + pIIIA/IRE-MS2 (+)
- pACTII (-) + pIIIA/MS2-2 (-)

To have a replicate from previous experiments, we also co transformed the following into the L40 strain:

- pACTII (-) + pIIIA/MS2-2 (-)
- pAD-IRP (+) + pIIIA/IRE-MS2 (+)

Once we generated the appropriate strains either by mating or co-transformation, we spotted serial dilutions of log-phase cultures of these strains on plates with increasing concentrations of 3AT (Fig. 5-2). Based on these results, we decided to use media with 2.5 mM 3AT as the cut off for positive interactions, as seen by the absence of growth of negative controls and the presence of readily discernable growth of the positive controls (rows D, H and J) . We observe that in the strains generated by mating, there seems to be some autoactivation by the presence of the RNA by itself (panel B).

Figure 5-2: Calibration of the appropriate concentration of 3AT for the yeast-three-hybrid screen

	IRE RNA	IRP	
A	-	-	Mating (L40 + R40)
B	+	-	
C	-	+	
D	**+**	**+**	
E	-	-	Co-transformation (YBZ-1)
F	+	-	
G	-	+	
H	**+**	**+**	
I	-	-	Co-transformation (L40)
J	**+**	**+**	
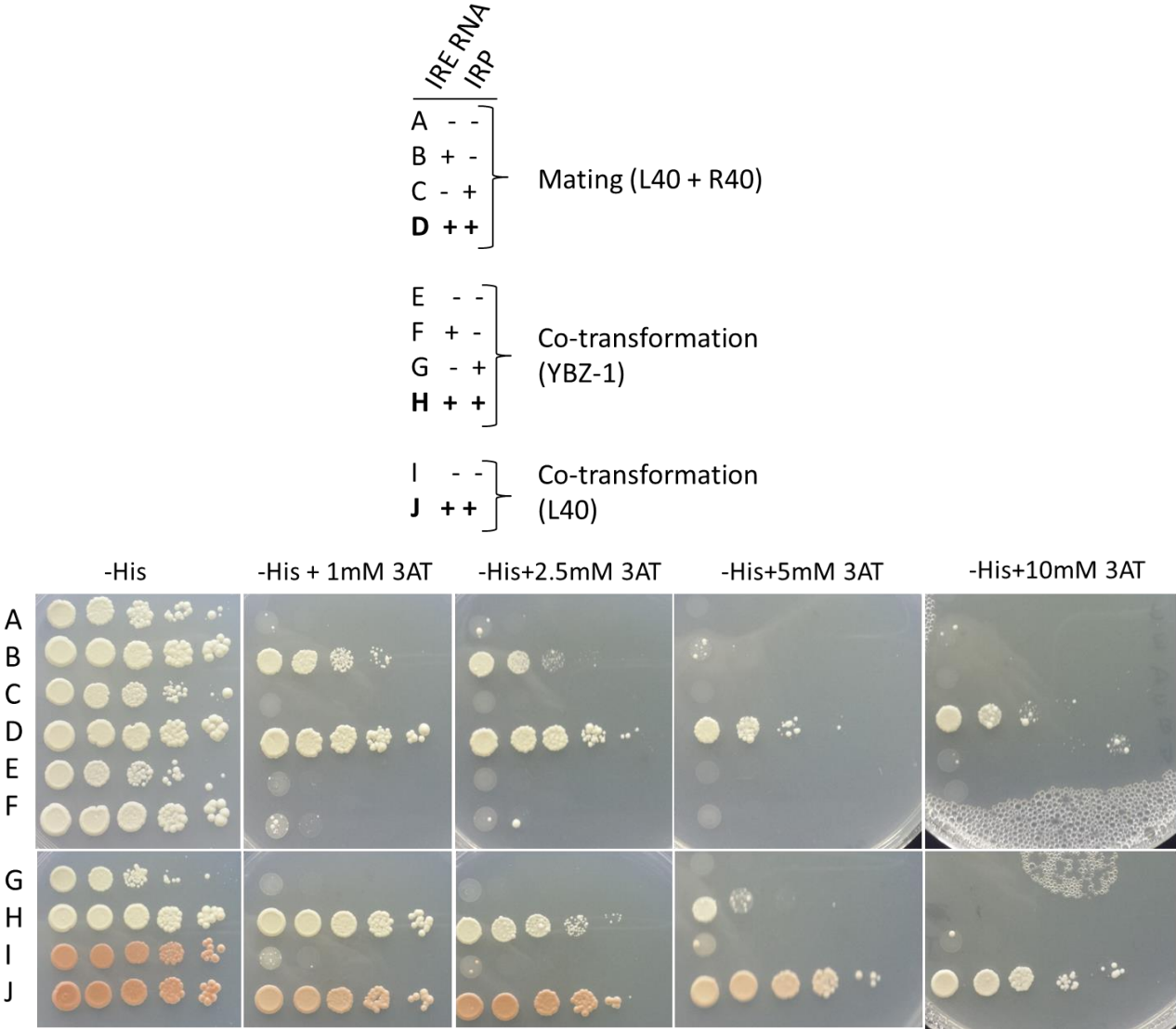
Fig. 5-2: Calibration of the appropriate concentration of 3AT for the yeast-three-hybrid screen.

Top: Legend showing various pairwise combinations of protein and RNA constructs either mated or co-transformed in the strains indicated on the right side.

Bottom: Serial dilutions of log-phase cultures of strains carrying pairwise combinations of various RNA-protein constructs. The composition of the media and 3AT concentrations used are indicated above each plate. Each row corresponds to strains (A-J) mentioned in the top panel.

5.2.3. Annealed duplex cloning to clone short DNA fragments into the vector to generate RNA-MS2 hybrids

Since our RNAs of interest (both ES5$_L$ and ES12$_L$) are short (<50 nucleotides), we were apprehensive about using conventional cloning by PCR amplification. Instead, we decided to synthesize (from IDT) and insert DNA containing the sequences for ES5$_L$ and ES12$_L$ individually, as an annealed duplex with appropriately modified *Sma1* and *Sph1* ends. See Fig. 5-3 for illustration. We digested pIIIA/MS2-2 with *Sma1* and *Sph1* and ligated the duplex insert by conventional protocols, such that the MS2 sites are 3' of the cloned ES5$_L$ and ES12$_L$. Appropriate ligation and correctness of the inserted sequence were verified by sequencing the resulting plasmid construct DNAs.

While this annealed duplex cloning technique is very useful for the yeast-three-hybrid assay, we believe this is an efficient way to clone any short fragment in a cost-efficient manner.

Figure 5-3: An example illustrating annealed duplex cloning
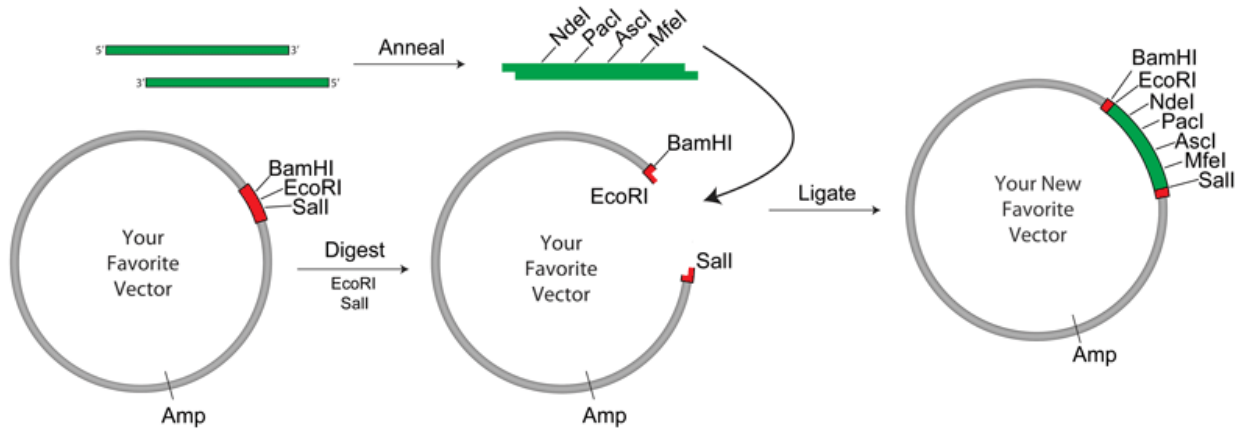
Fig. 5-3: An example illustrating annealed duplex cloning.

Illustration courtesy: https://www.addgene.org/plasmid-protocols/annealed-oligo-cloning/. In our experiment, the green fragment corresponds to the sequences coding for the RNA of interest with *Sma1* and *Sph1* sites on either end. pIIIA/MS2-2 was used as the vector, to introduce the MS2 tag at the 3' end of the RNA fragment.

5.2.4. Investigating proteins that interact with ES5$_L$ and ES12$_L$

Having cloned the ES sequences into the RNA-MS2 fusion plasmid, we then proceeded to explore our options for creating a library of various proteins that could be tested for potential interaction with these RNA fragments. We decided to use the bookshelf of protein-activation domain fusions that we had generated in the lab, although it was built on a vector backbone different from pACTII, since the vectors are advertised to be compatible with a wide variety of *GAL4* activation domain protein fusions.

We used the following assembly factor protein-activation domain fusions in pACT plasmid: Pwp1, Brix1, Ebp2, Nop12, Nop7, Ytm1, Erb1, Cic1, Nop15, Rrp1, Has1, Drs1, Rat1, Xrn1, Nsa2, Nop2, Nip7, Nog2, Rpf2, Rrs1, Tif6, Rlp24, Mak11, Nog1, Spb4, Dbp10. The vector backbone pACT was used as negative control and pAD-IRP construct was used as positive control as before. These were transformed into the L40 strain.

The RNA fusion plasmids pIIIA/MS2-2 (negative control, A), ES5-MS2 (B), ES12-MS2(C), pIII/IRE-MS2 (positive control, D) were transformed into the R40 strain.

Each L40 strain was mated with each of the four R40 strains described above to generate diploids carrying all possible pairwise combinations of protein and RNA plasmids. These are tabulated in Fig. 5-4. From this point, Luke Diorio-Toth, an undergraduate student in the lab, and I repeated these experiments independently. We then assayed for the ability of these diploid strains to grow on 3AT containing media, to screen for potential interactions (first four columns of spots in Fig. 5-4). To control for the number of inoculated cells on each plate, we replica plated using the same velvet onto media lacking 3AT and containing histidine, to demonstrate sufficient cells being present (last four columns of spots in Fig. 5-4). We assigned numerical scores to growth starting from 0.25 denoting one or two small petite colonies to >2 indicating full-blown growth in the spotted area.

Figure 5-4: Confounding results from the yeast-three-hybrid screen
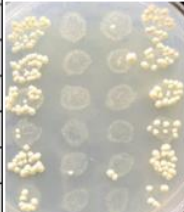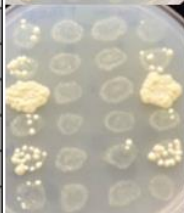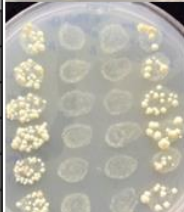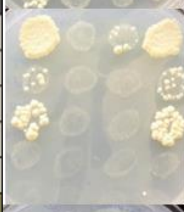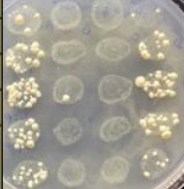
		pIIIA/MS2-2 (- control) [A]	ES5-MS2 [B]	ES12-MS2 [C]	pIII/IRE-MS2 (+ control) [D]	+2.5mM 3AT A B C D	No 3AT A B C D
1	pACT (-)	2		0.25	2		
2	Pwp1	2		0.5	2		
3	Brx1	2			2		
4	Ebp2	1			1		
5	Nop12	2		1	2		
6	Nop7	1	0.25		1		
7	Ytm1	0.5					
8	Erb1	1			1		
9	Cic1	3			3		
10	Nop15	0.5			0.25		
11	Rrp1	1		0.25	1		
12	Has1	0.25			0		
13	Drs1	2			1.5		
14	Rat1	2			1.5		
15	Xrn1	2			2		
16	Nsa2	2			2		
17	Nop2	2			1		
18	Nip7	2			2		
19	Nog2	4		0.5	4		
20	Rpf2	1			1		
21	Rrs1	2			3		
22	Tif6	0			0		
23	Rlp24						
24	Mak11	1			0.25		
25	Nog1	2			1		
26	Spb4	2	0.25		2		
27	Dbp10	2			2		
28	pAD-IRP (+)	2			1		

Fig. 5-4: Confounding results from the yeast-three-hybrid screen.

Rows corresponding to numbers (1-28) represent each of the protein-activation domain fusions tested. Columns (A-D) represent each of the tagged RNAs tested, as indicated in the table. Different plates are colored differently in the table. The images of plates (both with 2.5mM 3AT and without 3AT) are shown with the same scheme. Empirically, we assigned numbers to represent growth with 0.25 representing one or two petite colonies and >2 representing full-blown growth in the spotted area. The top row is the negative control to represent background activation and the bottom row is the positive control to represent expected growth on the other end of the spectrum. It is clear that the controls themselves do not behave as expected. Similar results were obtained in two experimental replicates.

The results were confounding, to say the least. Negative control (row 1) exhibited growth, when it did not do so in our previous assay (Fig. 5-3). Since the only difference between this and the previous round of optimization was the protein-activation domain fusion vector, this indicates that pACT and pACTII vectors do not behave identically in this assay. Somehow, none of the proteins exhibited a putative positive interaction with ES5-MS2 or ES12-MS2 fusions, but did so with the pIII/IRE-MS2-2 tagged RNA. Since the controls themselves do not work appropriately in two replicate experiments, we decided to not use this assay for any further interpretations.

We did not proceed with optimizing this further, since high resolution cryo-EM structures had become available, giving us information about contact points of ES with assembly factors. Since that evidence was more direct, we concluded that this assay was not necessary to understand ES-protein interactions in preribosomes.

5.3. Summary

We established the yeast-three-hybrid system as an assay to analyze protein interactions with rRNA expansion segments. I started by obtaining the relevant strains from the Wickens lab. We cloned ES5L and ES12L using the annealed duplex cloning in the appropriate RNA-MS2 hybrid vector. We tested different ways to perform the experiment, and optimized the suitable concentration of 3AT that can detect positive interactions. We decided to use a bookshelf/library of proteins cloned pACT for the actual screen, since we had it readily available, even though the optimization was done with pACTII. Unfortunately, although advertised as being similar, the results were not consistent.

Thus, we succeeded in generating a suitable workflow for assaying interactions of various proteins with small sections of RNA using yeast-two-hybrid, and determined 2.5 mM 3AT as a suitable concentration to use with such a screen. Other undergraduates have utilized this technique for a preliminary screen. Going further, we would like to highlight that this assay is limited by both the size of the RNA and the specific vector into which the protein is cloned, and the strengths of interactions are not generalizable. Hence, while this system may be used in specific-cases as a first-pass test of interaction, this system is not as robust as we had predicted it to be.

In vivo SHAPE for probing RNA structures

5.4. Introduction

RNA participates in numerous crucial cellular processes by forming extensive intermolecular and intramolecular structures driven by its base-pairing properties. Thus, investigating RNA structures underlies our understanding of the various functions of RNA in these cellular processes. Ribosomal RNA has been considered as a useful paradigm to understand RNA folding and structure-function relationships. On the other hand, rRNA has also posed a formidable challenge in such studies, especially in the context of the assembling ribosome, owing to its large size and heterogeneity. Over the past few decades, robust tools have been developed to assay RNA structure *in vitro*. These can be primarily classified as either those that form a chemical adduct or perform strand scission at specific places, such that the readout, often by a reverse transcription based assay, identifies the residues at the nucleotide level. Assaying RNA structure *in vivo* in yeast has been a challenge. Many techniques have been developed more recently to address this challenge (Loughrey et al., 2014; Talkish et al., 2014c), causing a resurgence in the use of RNA structure probing to broadly understand RNA structure and function in the cells (Kubota et al., 2015).

Here, we show how we adapted a recent SHAPE (Selective 2' hydroxyl acylation analyzed by primer extension) technique (Spitale et al., 2013) to study rRNA structure *in vivo*. We briefly describe the optimization steps, and demonstrate how we have been able to utilize SHAPE to faithfully detect the footprint of ribosomal proteins on ribosomal RNA, as a proof of principle. We start by discussing a few methods in vogue to assay RNA structures; see (Kubota et al., 2015; Weeks, 2010) for more details.

5.4.1. Methods to probe RNA structure

While the use of cryo-EM and X-ray crystallographic approaches to investigate RNA structures have yielded breakthrough discoveries and still are useful in understanding ribosome biogenesis (Ben-Shem et al., 2011; Bradatsch et al., 2012; Leidig et al., 2014) (Wu et al., manuscript under review), these approaches are proportionally more challenging and time-consuming as the size and complexity of the RNA increases. As we begin to ask mechanistic questions about the state of rRNA folding and other longer RNAs in various experimental conditions, it becomes intractable to exclusively utilize these three-dimensional approaches to investigate RNA structure.

In vitro methods: While cryo-EM has revolutionized our field in the past few years, researchers have conventionally used chemical probing as an alternative to these three-dimensional approaches in their studies of RNA folding pathways, rRNA secondary structure transitions and protein-RNA interactions. Chemical probing approaches that probe the structure of RNA *in vitro* have been used for decades now and fall broadly into two categories: (1) those that assay structure using small molecules that form a chemical adduct at specific places in RNA, and (2) those that induce strand scission that can be detected either by end labeling or by primer extension.

Small molecules such as DMS, kethoxal, and CMCT form base-specific adducts, which are then detected as primer extension stops, since the adduct blocks the reverse transcriptase. A more general, base non-specific approach has been to study the 2' acylation of RNA (SHAPE) by a class of reagents (such as 1M7 and NMIA). Unlike previous adduct-based techniques that correlate primarily with solvent accessibility, SHAPE measures nucleotide flexibility (McGinnis et al., 2012; Merino et al., 2005).

With respect to the class of techniques that induce strand scission at specific nucleotides, various RNases have been used, primarily in studies of protein-RNA binding. Hydroxyl radicals, often generated by Fenton chemistry, have also been utilized to induce RNA strand breaks in a base-non-specific manner,

depending on the degree of solvent exposure of the nucleotide. Since this method is quick, owing to the short half-life of hydroxyl radicals, these have primarily driven many studies that investigated RNA folding (Costa and Monachello, 2014; Ingle et al., 2014). A related method that assays the position of 2'-OH is in-line probing, which has been used in studies of various riboswitches (Regulski and Breaker, 2008).

Since we have always been interested in RNA structures on the assembling ribosome, we tried to utilize Fenton chemistry to assay RNA structure in lysates, then purify pre-ribosomes and assay the structure of rRNA by primer extension. Even after multiple rounds of optimization, we were not able to successfully develop this method to reproducibly report RNA structure (data not shown). Further, we decided that trying to establish *in vivo* methods was a better alternative, especially in light of the questions we wanted to ask.

In vivo methods: While one cannot deny the valuable contributions made by the aforementioned *in vitro* methods to advance our knowledge of RNA structure, *in vivo* RNA structures may be quite different because of the influences on RNA folding of molecular crowding, protein binding, and the co-transcriptional nature of cellular processes such as splicing and pre-rRNA processing. *In vivo* DMS probing has been the workhorse for *in vivo* methods, especially in the case of the study of the assembling ribosome (Swiatkowska et al., 2012; Talkish et al., 2014c). Hydroxyl radical footprinting of RNA using hydroxyl radicals generated in cells by X-ray beams from synchrotron radiation enabled studies of fast RNA folding (Adilakshmi et al., 2009). Much of our understanding of RNA folding in the small subunit rRNA comes from these studies (Adilakshmi et al., 2008; Clatterbuck Soper et al., 2013).

In addition, landmark studies using SHAPE, which reports RNA nucleotide flexibility in a base-non-specific manner, was performed on ribosomal RNA using the 1M7 reagent *in vivo* (McGinnis et al., 2015; McGinnis and Weeks, 2014). The rationale behind this method is that local nucleotide flexibility makes a

particular nucleotide a better nucleophile in certain conformations. Thus, when probed with an electrophilic acylating agent, these nucleotides are more heavily modified. The advantages of SHAPE over other small molecule-based methods like DMS are that it is base-non-specific, and that it reports RNA backbone flexibility as opposed to the state of the base. Recently, the Chang lab developed two SHAPE reagents NAI and FAI, which have enhanced solubility and half-life times (Spitale et al., 2013). They also demonstrated that NAI can be used to study RNA structure in yeast *in vivo*. This chapter is based on adapting their reagent in our lab, optimizing the conditions for the SHAPE experiment and using it to study the footprint of two non-essential ribosomal proteins.

High-throughput methods: Perhaps the biggest breakthrough in recent times in our study of RNA structures is a result of incorporating high-throughput approaches to conventional modes of probing RNA structure *in vivo*. Our lab, in collaboration with the McManus lab, has been a pioneer in this field, adopting a high-throughput approach to study RNA structures using DMS modification of ribosomes *in vivo* (Talkish et al., 2014c). Other approaches such as SHAPE-MaP, SHAPE-Seq and icSHAPE have turned out to be powerful to inform us of structure changes on a more global scale (Loughrey et al., 2014; Smola et al., 2015; Spitale et al., 2015). Before the advent of these technologies, assays of RNA structure were heavily limited by the number of nucleotides that could be assayed on a sequencing gel. By incorporating high-throughput approaches and concomitant developments in computational methods to analyze these *in vivo* results, researchers have now increased the usefulness of these experiments to understand RNA structure-function relationships in large RNPs such as the ribosome.

As mentioned before, below, we describe how we adapted the SHAPE protocol published by the Chang lab using NAI as the electrophile, and our attempts in rendering this approach high-throughput in collaboration with the McManus lab.

5.5.   Results and Discussion

5.5.1. Synthesis of NAI and optimizing RNA extraction after NAI treatment

In order to synthesize a 1M stock of 2-methyl nicotinic acid (NAI), we followed the steps described previously (Spitale et al., 2013). Briefly, 137 mg of 2-methylpyridine-3-carboxylic acid was added to 0.5 ml of DMSO. Separately, 162 mg of 1-1'-carbonyldiimidazole was dissolved in 0.5 ml DMSO. This 1-1' carbonyldiimadazole solution was then added drop by drop to the 2-methylpyridine-3-carboxylic acid solution. As a special note, the protocol calls for 2-methyl nicotinic acid, which is sold as 2-methylpyridine-3-carboxylic acid commercially. Also, the solubility of this chemical in DMSO is very low, but addition of 1-1' carbonyldiimadazole dissolves it completely after gas evolution. It is important to mix the reactants drop-by-drop to prevent splattering due to the effervescence. NAI that was used in our experiments was always made in small batches and frozen at -80°C in aliquots. NAI was thawed to room temperature before opening the aliquots. As much as possible, we avoided using freeze-thawed NAI for experiments, although we did not have any particular reason to doubt the stability of NAI after a freeze-thaw cycle.

The original protocol had called for RNA extraction using the hot phenol method; one of the authors had emphasized that the hot phenol method worked better than bead beating (personal communication). Following NAI treatment, we tried to optimize RNA extraction by the hot phenol method multiple times in vain. Hence, we decided to use our protocol for RNA extraction using the commercially available phenol-chloroform-isoamyl alcohol reagent and bead beating. We have not encountered any significant additional background stops in primer extension that could be attributed to using the bead beating method, over and above those in published data (data not shown).

5.5.2. Steps in optimizing the protocol and replicating published results

Having established the synthesis of NAI, we worked closely with the McManus lab for the initial optimization of this technique. As shown in Fig. 5-5, we optimized the protocol and replicated published results using NAI to assay for changes in 5S rRNA both *in vivo* and *in vitro.* After treating cells with 100mM or 500mM NAI for an hour *in vivo,* (DMSO was used as the negative control), we extracted RNA by bead beating and assayed for reverse transcription stops in 5S rRNA by primer extension using a radiolabeled oligonucleotide primer (lanes 2,3 and 4, Fig. 5-5). Gemma May from the McManus lab used the same batch of 100 mM NAI to probe her RNAs *in vitro* for 0, 10, 30 or 60 mins and we included those samples as well (lanes 5-8). As evident in lane 1 of Fig. 5-5, where total RNA from the wild-type W303 yeast strain was used for primer extension with the newly-designed 5S oligonucleotide primer, there seems to be an unusually high level of background. The background stops detected using other oligonucleotide primers on the same samples were much lower (data not shown). A dose-time dependent increase in modifications was roughly evident. Making inferences from the modifications and comparing them to the published data, we observe that our data were consistent with published data (indicated by an asterisk below). In fact, we were able to detect more modifications. Noting that the nucleotide numbers corresponding to published data, the sequence of 5S rDNA in *Saccharomyces Genome Database (SGD)* and the comparative RNA database website are different, the modifications we observed are listed below in SGD nomenclature:

In vivo SHAPE: C94*, C93*, T86*, C74*, G65, A64, G57, A56, T50

In vitro SHAPE: C93, C92, G91*, U90, G87*, T86**, G85, A84 (G), C74, A64*, G65*, C58*, A56, A55, G52*, C37, C38, C32*

We note that there are more modifications observed *in vitro* than *in vivo*, which is not surprising taking into account variations caused by binding of proteins, cell permeability of the reagent, etc.,

Figure 5-5: Assaying the flexibility of nucleotides in 5S rRNA by SHAPE *in vivo* and *in vitro*

1 – W303 total RNA
2 – No NAI, *In vivo*
3 – NAI *In vivo* 100mM
4- NAI *In vivo*, 500 mM

5- NAI *In vitro,* 0 mins
6- NAI *In vitro*, 10 mins
7- NAI *In vitro*, 30 mins
8- NAI *In vitro,* 60 mins

9- A
10- U
11- G
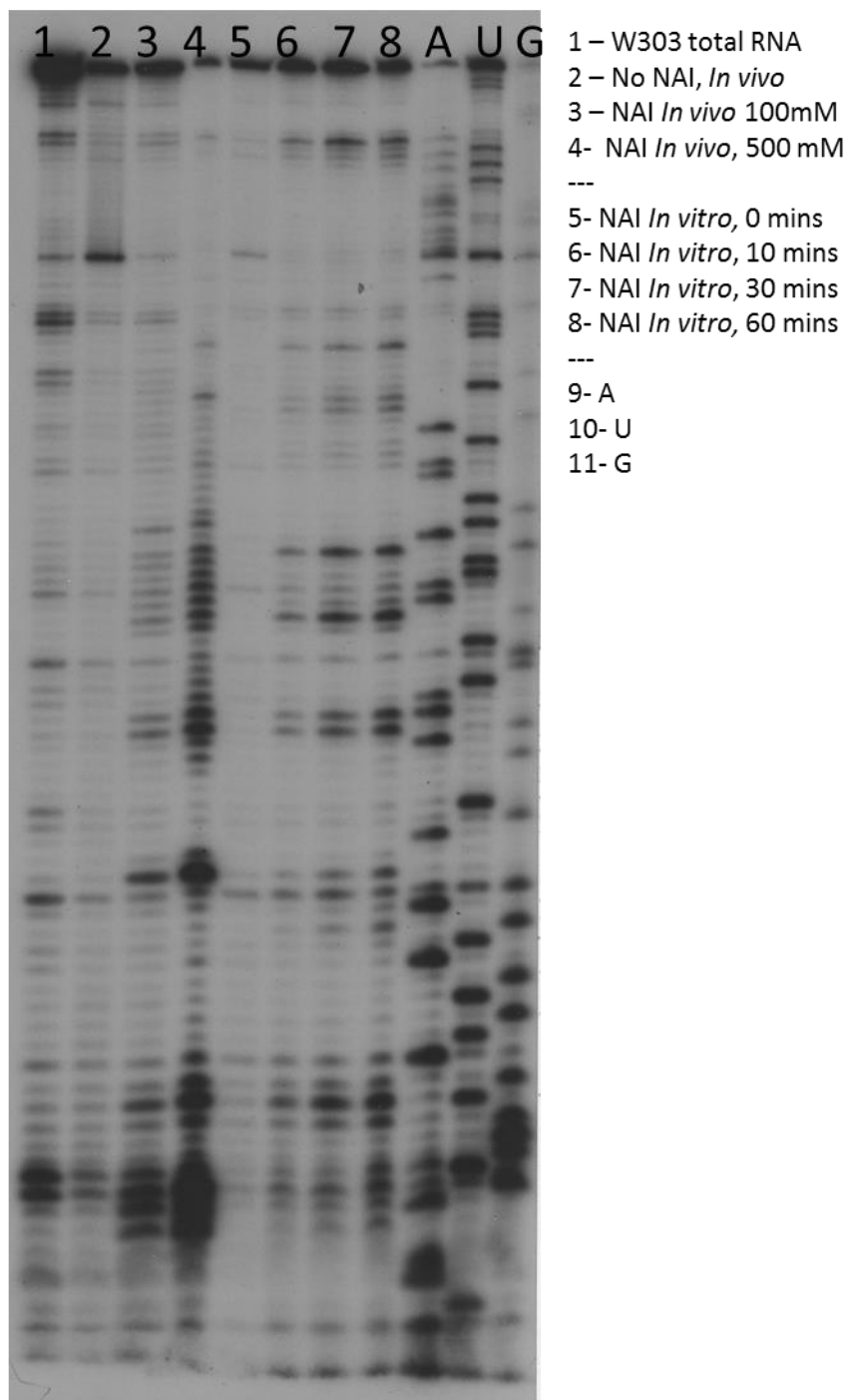
Fig. 5-5: Assaying the flexibility of nucleotides in 5S rRNA by SHAPE *in vivo* and *in vitro.*

Lanes 1 - 4: *In vivo* SHAPE, with increasing concentrations of NAI. Lane 1: Total RNA from W303 strain; lane 2, 3, 4: DMSO (negative control), 100mM NAI and 500mM NAI treated RNA, respectively. Lanes 5-8: Time course of *in vitro* SHAPE with RNA extracted after 0, 10, 30 and 60 min of 100 mM NAI treatment, respectively. The sequencing lanes are also shown. Primer extension was done after RNA extraction using an oligonucleotide primer that binds 5S rRNA.

5.5.3. SHAPE analysis on the L26ΔΔ mutant

Having shown that we were able to replicate originally published results, we then went ahead with establishing that the changes using our newly developed technique are consistent with data published from our lab using DMS probing on the ribosomal protein knockout strain L26ΔΔ (Talkish et al., 2014c).

First, we began by doing a concentration course (data not shown) and a time course experiment to narrow down the optimal NAI treatment conditions (Fig. 5-6). Using these, we decided to go ahead with 100 mM NAI treatment for one hour as the appropriate treatment for further studies. The exact modifications are discussed at the end of the next section. Fig. 5-10 and Fig. 5-11 show a region of 5.8S rRNA that ribosomal protein L26 binds, where we observe specific changes corresponding to contact sites of ribosomal protein L26. We also observed no modifications in DMSO treated cells, as expected.

Figure 5-6: Time course of treatment with NAI
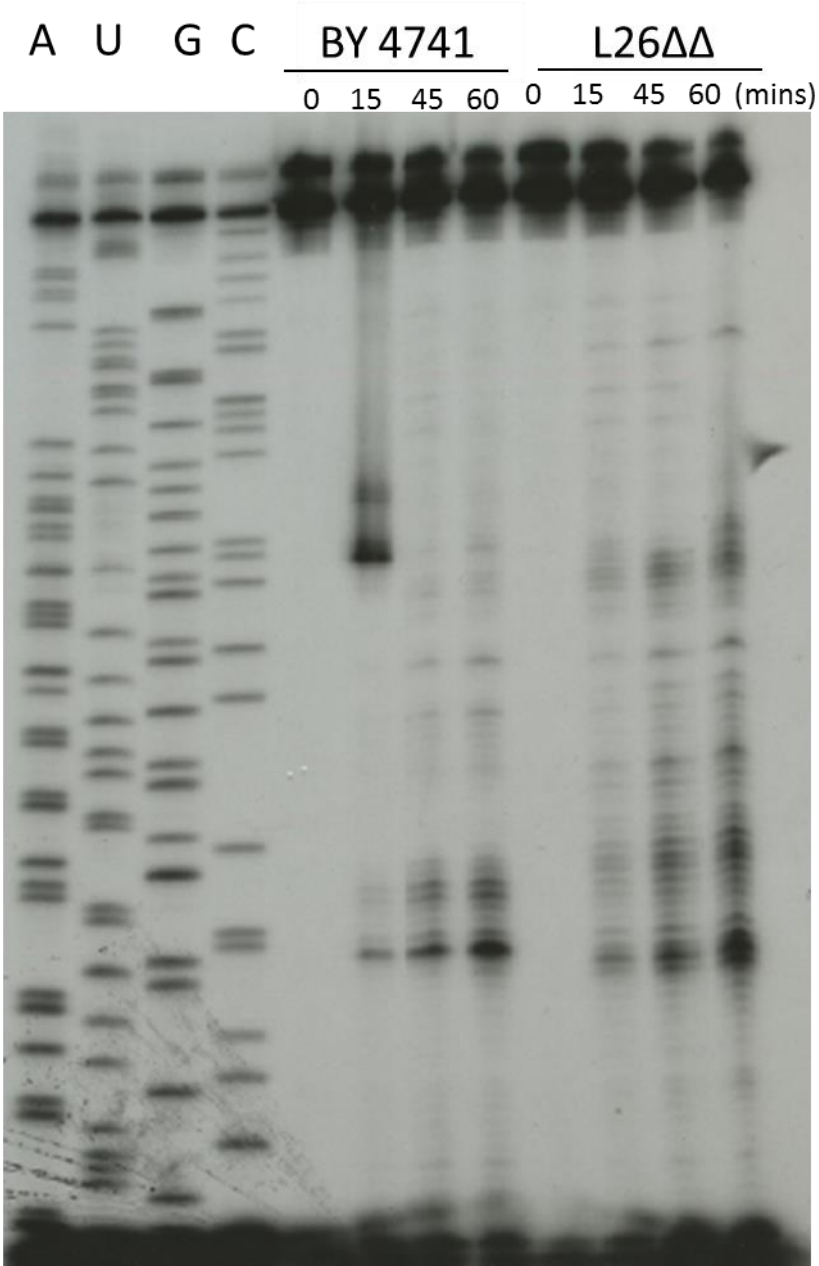
Fig. 5-6: Time course of treatment with NAI.

Sequencing lanes are shown first. The modifications in WT (BY4741) and in a ribosomal protein knockout mutant (L26ΔΔ) were assayed. The time course of 100 mM NAI treatment is indicated in the corresponding lanes. An oligonucleotide primer capable of detecting 5.8S was used (2996-5.8S).

5.5.4. SHAPE analysis on the L39Δ mutant

Ribosomal protein L39 functions in late nuclear steps of ribosome assembly; some of its contact points with 5.8S rRNA roughly overlap with those of ribosomal protein L26. rpL39 is a non-essential ribosomal protein whose absence causes a severe growth defect at lower temperature (Fig. 5-7). We chose this protein over others since we suspected that it might assist in proper structuring of rRNA near the peptidyl transferase center, owing to its proximity. The cold-sensitive nature of this mutant, further added our hypothesis that the absence of this protein may result in abnormal RNA folding events within rRNA.

Figure 5-7: Knockout of r-protein L39, but not L26, results in a cold-sensitive phenotype
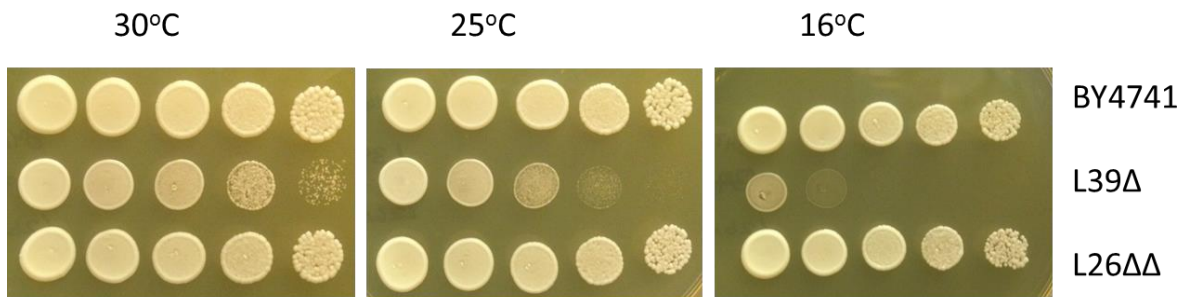
Fig. 5-7: Knockout of r-protein L39, but not L26, results in a cold-sensitive phenotype.

Serial dilutions of log phase yeast cultures of strains indicated on the right (BY4741 is wild-type) were spotted onto YEPD solid media and grown for 3 days at 30°C, 4 days at 25°C and 5 days at 16°C.

First, we asked if we can detect changes and identify the absence of the footprint of ribosomal protein L39 on 5.8S rRNA, in a L39Δ mutant strain. Next, if there were any observed changes, above and beyond those corresponding to the footprint of the protein, we asked if these would be exacerbated at colder temperatures. In parallel, this would also enable us to test if our SHAPE experiment could potentially be used at different temperatures.

Hence, we performed SHAPE experiment on wild-type, L26ΔΔ and L39Δ strains, first comparing the footprint of ribosomal protein L39 to the footprint of ribosomal protein L26. The results obtained were consistent between two experimental replicates.

Further, in a subsequent experiment, we also performed SHAPE experiments on the L39Δ samples at three different temperatures ($30^{o}C$, $25^{o}C$ and $16^{o}C$), assaying for modifications in 5.8S rRNA. First of all, these results were consistent with the previously shown biological replicate (Fig. 5-6). Second, the footprint of rpL26 was different from that of rpL39, demonstrating specificity (Fig. 5-8, Fig. 5-9). All of the changes observed were in single-stranded regions devoid of protein (even in the wild-type sample), demonstrating that the electrophilic reaction is specific and representative of nucleotide flexibility. Using these data, we mapped the modified nucleotides specific to the knockout strains onto the secondary structure of 5.8S rRNA and the crystal structure (Fig. 5-10 and Fig. 5-11). Strikingly, the modifications threaded the nucleotides that form protein contacts extremely well, suggesting that SHAPE using NAI can be utilized as an accurate predictor of the presence/absence of protein binding and nucleotide flexibility.

Figure 5-8: Assaying the flexibility of nucleotides in 5.8S rRNA by SHAPE
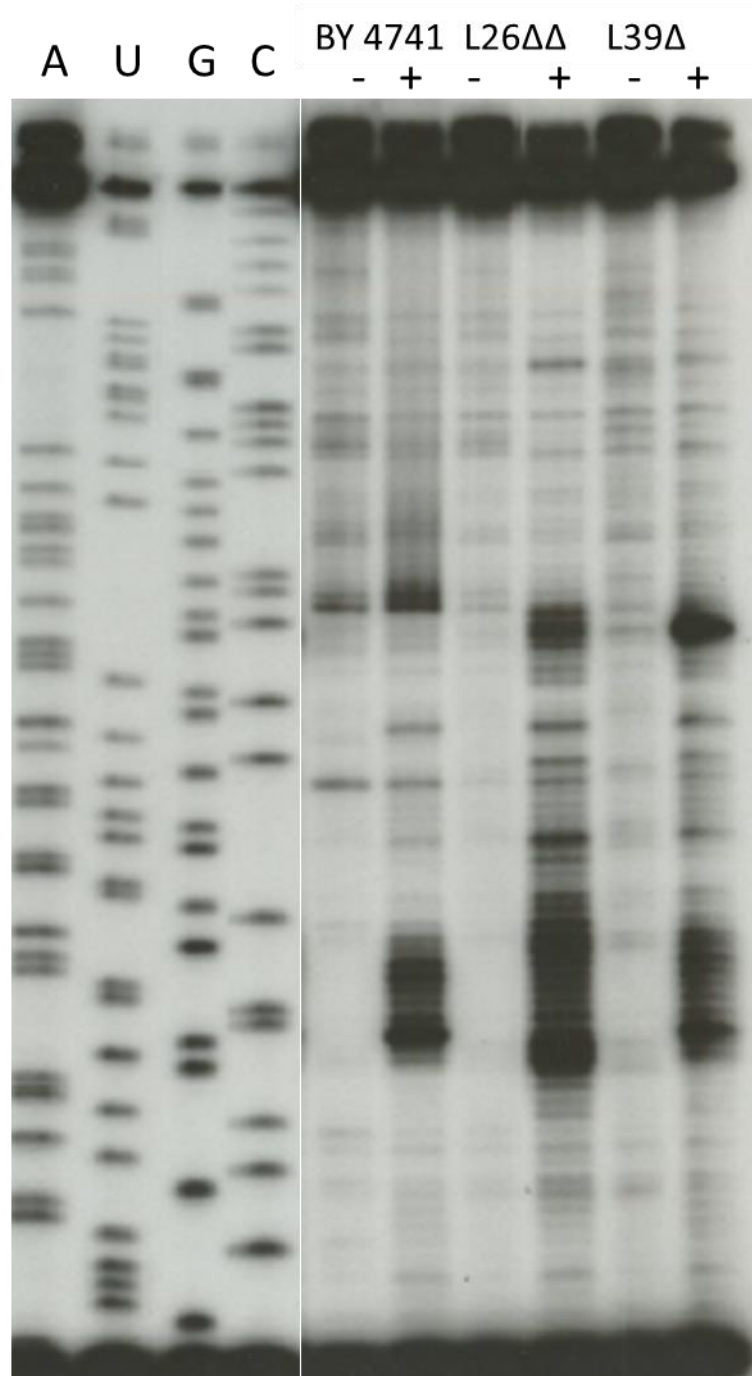
Fig. 5-8: Assaying the flexibility of nucleotides in 5.8S rRNA by SHAPE.

In vivo SHAPE on BY4741, L26ΔΔ and L39Δ is shown. '-' denotes treatment with DMSO for 60 min as the negative control, '+' denotes treatment with 100mM NAI for 60 min. An oligonucleotide primer that can detect 5.8S rRNA was used for reverse transcription (2996-5.8S).

Figure 5-9: Assaying the flexibility of nucleotides in 5.8S rRNA by SHAPE in r-protein knockout strains at different temperatures
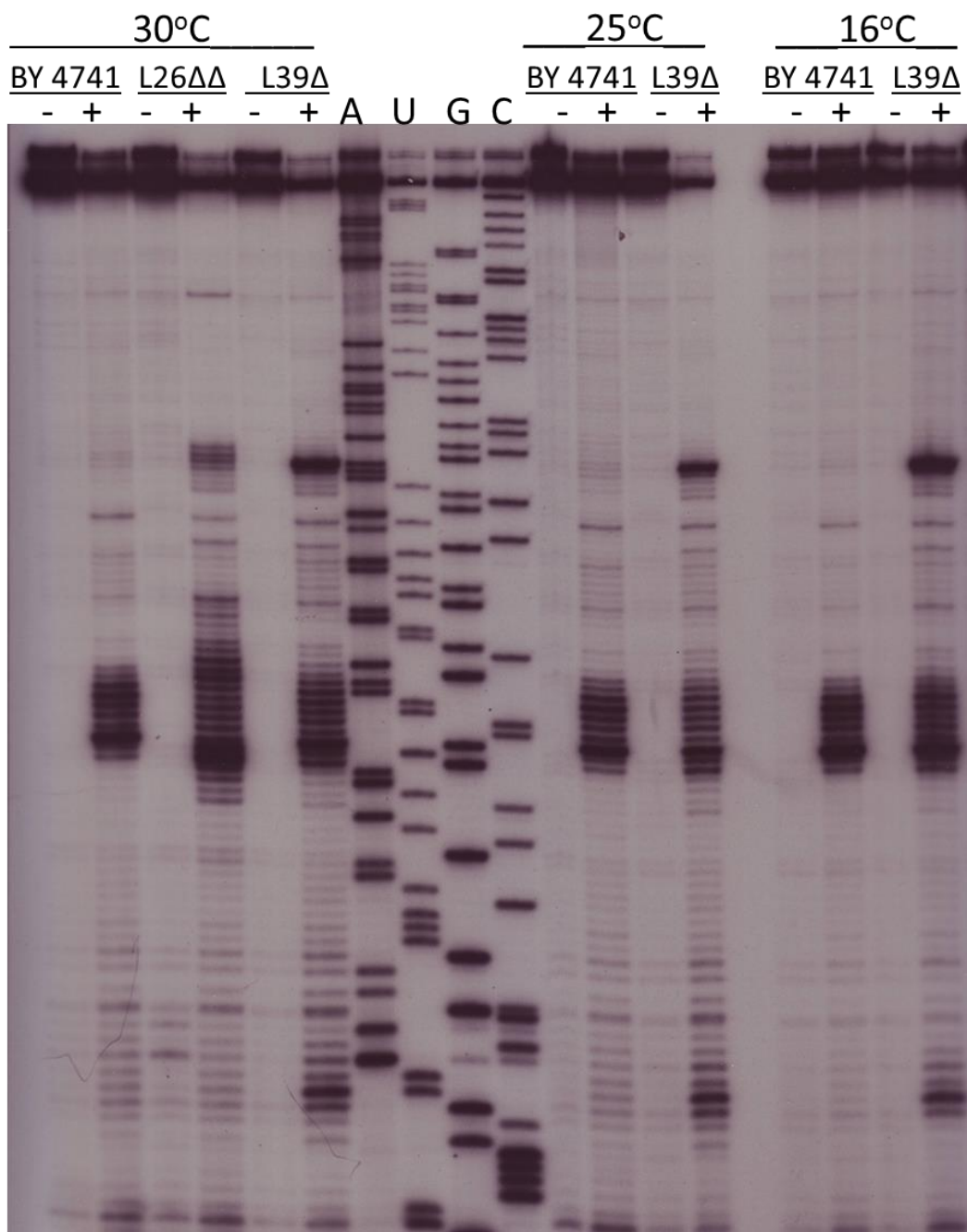
Fig. 5-9: Assaying the flexibility of nucleotides in 5.8S rRNA by SHAPE in r-protein knockout strains at different temperatures.

In vivo SHAPE on BY4741, L26ΔΔ and L39Δ is shown. '-' denotes treatment with DMSO for 60 min as the negative control, '+' denotes treatment with 100mM NAI for 60 min. An oligonucleotide primer that can detect 5.8S rRNA was used for reverse transcription (2996-5.8S). The temperatures at which the experiments were done, the sequencing ladder and the strain names are indicated.

Figure 5-10: Nucleotide modifications in various strains mapped onto the secondary structure of 5.8S rRNA
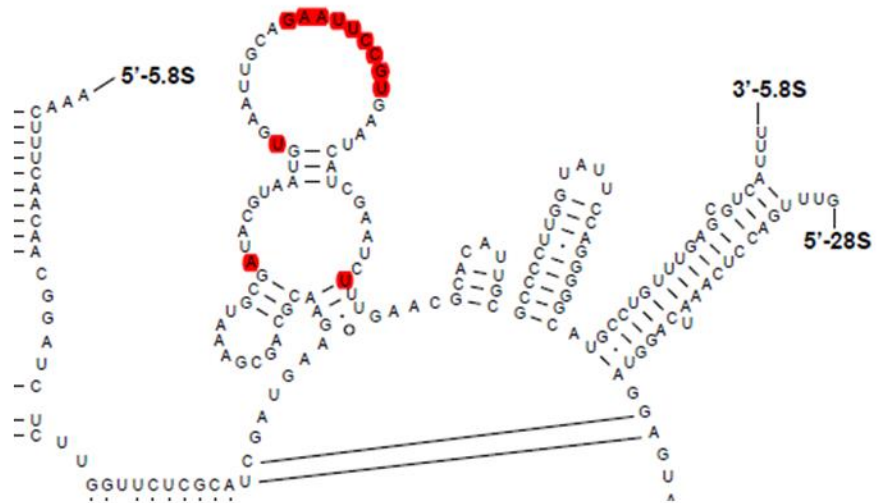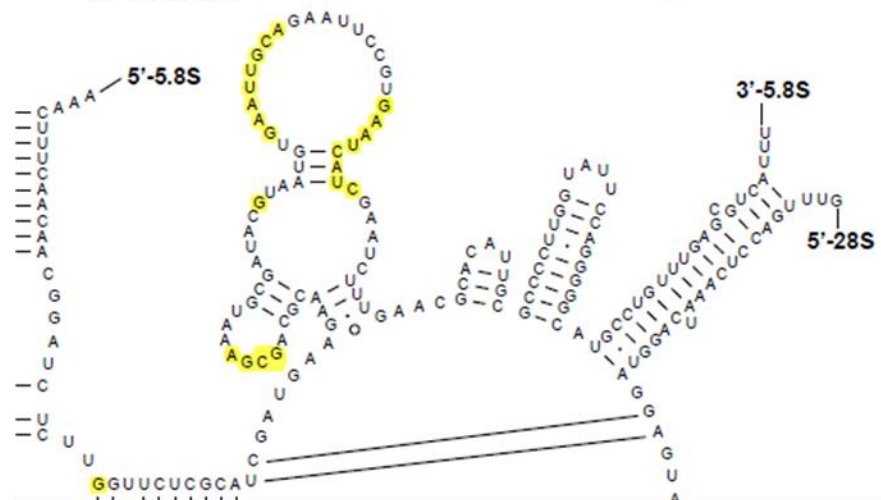
Fig. 5-10: Nucleotide modifications in various strains mapped onto the secondary structure of 5.8S rRNA.

The secondary structure of 5.8S RNA showing SHAPE modified nucleotides in WT BY4741 (top, red highlights), and nucleotides modified (after subtraction of background and WT modifications) in L26ΔΔ (middle, yellow highlights) and L39Δ (bottom, orange highlights).

Figure 5-11: Nucleotides modified by SHAPE correspond precisely with the footprints of respective proteins
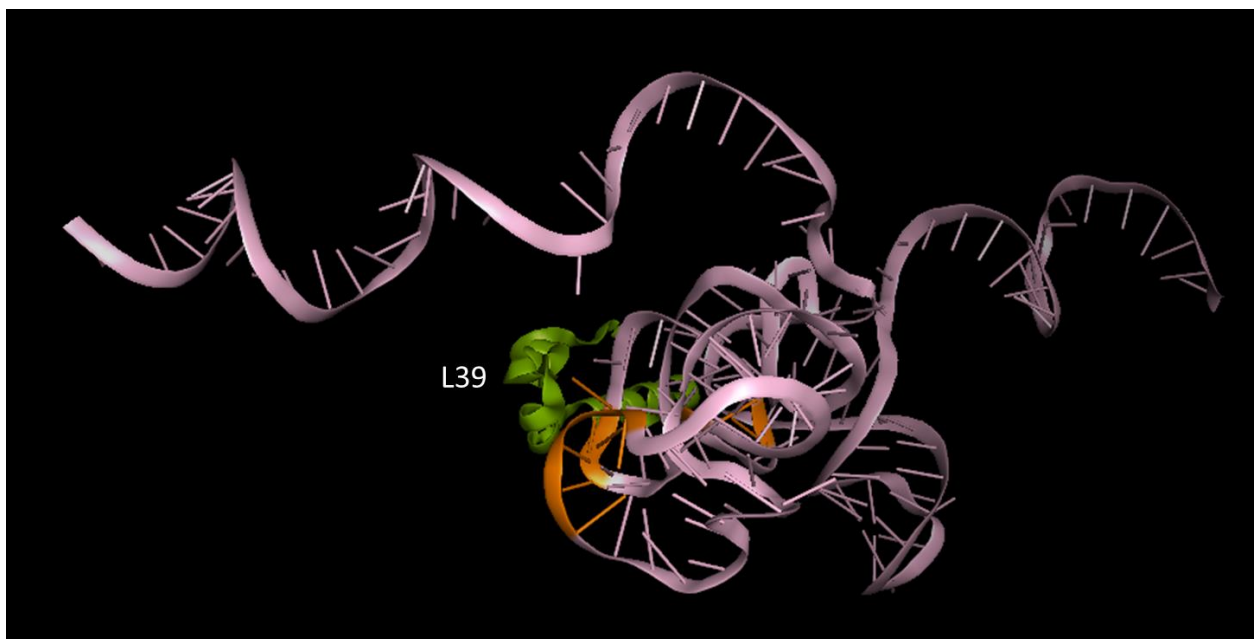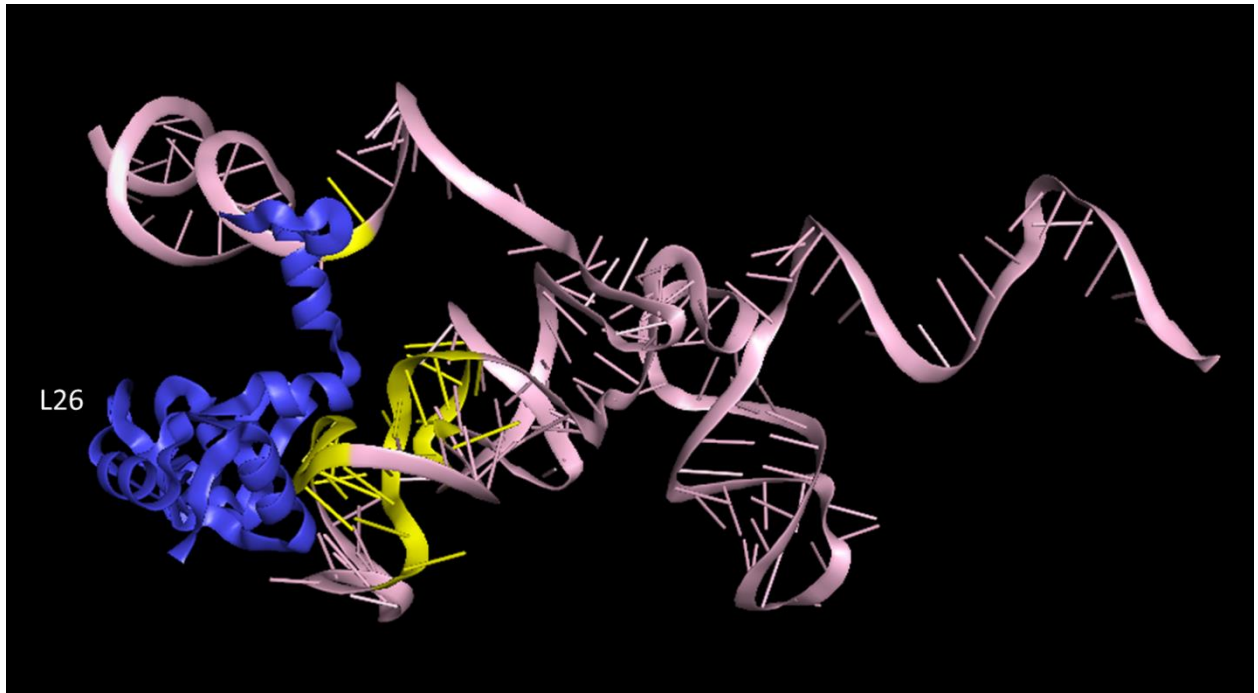
Fig. 5-11: Nucleotides modified by SHAPE correspond precisely with the footprints of respective proteins.

Top: Pymol image of 5.8S rRNA (pink) with L26 (blue). SHAPE modified nucleotides are marked in yellow.

Bottom: Pymol image of 5.8S rRNA (pink) with L39 (green). SHAPE modified nucleotides are marked in orange.

5.5.5. Attempts at making SHAPE high-throughput

We did not observe any more nucleotide modifications than the footprint of these proteins, even at different temperatures (Fig. 5-9) possibly because our analysis was restricted only to 5.8S rRNA. In order to assay changes more globally, we wanted to create libraries from NAI treated RNA and use deep sequencing to identify modifications. Although we already had an ongoing workflow for such an approach using ModSeq, we wanted to utilize the Weissman lab's newer approach for building libraries (Rouskin et al., 2014), in collaboration with the McManus lab. We performed further optimization steps towards this goal, but we decided that the earlier ModSeq work flow to make libraries was more efficient.

5.6. *Summary*

In conclusion, we have shown how we adapted SHAPE using NAI as a method to assay *in vivo* RNA structure and demonstrated the efficacy of this technique by predictably and reproducibly verifying the footprint of two ribosomal proteins. Practically everyone in our lab has routinely begun to use this technique, demonstrating its robustness. Further, we also shared our NAI and the protocol with other members of our department and CNAST (Chakrabarti lab). As a next step based on this method, Dr. Jason Talkish has made attempts to purify preribosomes after NAI treatment. Once optimized, it promises to be a powerful tool to determine RNA structural changes in assembling ribosomes.

Note: We thank Gemma May from the McManus lab for her help with building libraries for high-throughput sequencing from NAI-treated RNA.

6. Conclusions and Future Directions

Here, I have described how I analyzed ribosome biogenesis from the standpoints of ribosomal RNA, ribosomal protein and assembly factors. Apart from discerning the specific roles of rRNA expansion segments, ribosomal protein L5 and assembly factors that form the ITS2 cluster in ribosome biogenesis, this broad approach also permitted me to provide examples for how, in general, rRNA, r-protein and assembly factors function in ribosome biogenesis, with a special spotlight on eukaryote-specific features. In addition, I have developed valuable tools that have since been widely-adopted in the lab. Below, I have highlighted various future research directions resulting from the findings of this thesis work.

rRNA expansion segments:
- I have adapted a system to analyze rRNA mutations. This system can be used to assay any mutations in rRNA to complement protein mutations, especially ones that disrupt r-protein-rRNA contacts.
- I would like to better understand the evolution of expansion segments by substituting yeast expansion segments with those of other eukaryotes. If it turns out that these substitutions are deleterious, I suggest substituting the corresponding protein counterparts.
- Within expansion segments of yeast, I would like to analyze the effects of finer mutations as opposed to complete deletions. It is important to note that, sequence level changes are less likely to be informative since the sequences of expansion segments are highly variable. Hence, I suggest resorting to secondary structure-level changes. This will permit deeper understanding of the mechanistic roles of expansion segments, particularly when combined with the wealth of protein-interaction data available from high-resolution structural studies.

- I would like to replace expansion segments of *S.cerevisiae* with expansion segments from other yeasts to understand how they differ between closely related evolutionary species.

- While the ultimate evidence of functional co-evolution of rRNA-r-protein elements will result from tandem mutagenesis of rRNA and corresponding proteins that bind to it, the limited availability of relevant yeast strains poses a challenge to this approach. I recommend developing or adapting other means of studying rDNA mutations including but not limited to, systems that more rapidly shut off endogenous rRNA, CRISPR-based methods, and systems that make use of Pol I to transcribe the mutants (to minimize rRNA folding effects in mutants due to differences in transcription rates between Pol I and Pol II).

Ribosomal protein L5:

- In order to analyze the mutations that have already been described, one would need to complement these results with analysis of protein composition of the preribosomes by mass-spectrometry.

- I want to complement our pre-rRNA processing and protein composition assays with studies of rRNA structure, specifically focusing on changes in 5S rRNA structure.

- If it is found that there are reproducible changes in certain mutants that indicate defects in rotation of the 5S rRNP, I recommend performing cryo-EM studies in this mutant in order to discern structural changes at a global scale.

- I also recommend studying translation defects in the *rpl5*-C-terminal truncation mutant, by assaying growth on media containing translation-inhibiting drugs.

- I would like to follow-up on the non-essential disease mutations by assaying them under conditions of stress.

ITS2 cluster proteins:

- I recommend using our yeast-two-hybrid bookshelf as a starting point for assays of protein interactions and particularly for projects about mutants that lack specific interactions.

- Our collaboration with Penn State Hershey Center for mass spectrometry has continued. I recommend high-salt wash as a potential complementary assay for analyzing protein-protein interactions.

RNA structure probing:

- SHAPE has advanced the way we assay RNA structures significantly. I would like to extend the scope of this assay by making the analysis high-throughput (similar to ModSeq) since we are limited by the number of nucleotides that one can assay on a sequencing gel.

- In addition, adapting protocols that combine SHAPE and affinity purification will permit us to analyze changes in RNA structures in specific steps of ribosome biogenesis.

Bibliography

Adilakshmi, T., Bellur, D.L., and Woodson, S.A. (2008). Concurrent nucleation of 16S folding and induced fit in 30S ribosome assembly. Nature *455*, 1268-1272.

Adilakshmi, T., Soper, S.F., and Woodson, S.A. (2009). Structural analysis of RNA in living cells by in vivo synchrotron X-ray footprinting. Methods Enzymol *468*, 239-258.

Anger, A.M., Armache, J.P., Berninghausen, O., Habeck, M., Subklewe, M., Wilson, D.N., and Beckmann, R. (2013). Structures of the human and Drosophila 80S ribosome. Nature *497*, 80-85.

Armache, J.P., Jarasch, A., Anger, A.M., Villa, E., Becker, T., Bhushan, S., Jossinet, F., Habeck, M., Dindar, G., Franckenberg, S*., et al.* (2010a). Cryo-EM structure and rRNA model of a translating eukaryotic 80S ribosome at 5.5-A resolution. Proceedings of the National Academy of Sciences of the United States of America *107*, 19748-19753.

Armache, J.P., Jarasch, A., Anger, A.M., Villa, E., Becker, T., Bhushan, S., Jossinet, F., Habeck, M., Dindar, G., Franckenberg, S*., et al.* (2010b). Localization of eukaryote-specific ribosomal proteins in a 5.5-A cryo-EM map of the 80S eukaryotic ribosome. Proceedings of the National Academy of Sciences of the United States of America *107*, 19754-19759.

Asano, N., Kato, K., Nakamura, A., Komoda, K., Tanaka, I., and Yao, M. (2015). Structural and functional analysis of the Rpf2-Rrs1 complex in ribosome biogenesis. Nucleic Acids Res *43*, 4746-4757.

Babiano, R., Badis, G., Saveanu, C., Namane, A., Doyen, A., Diaz-Quintana, A., Jacquier, A., Fromont-Racine, M., and de la Cruz, J. (2013). Yeast ribosomal protein L7 and its homologue Rlp7 are simultaneously present at distinct sites on pre-60S ribosomal particles. Nucleic Acids Res *41*, 9461-9470.

Bassler, J., Paternoga, H., Holdermann, I., Thoms, M., Granneman, S., Barrio-Garcia, C., Nyarko, A., Lee, W., Stier, G., Clark, S.A*., et al.* (2014). A network of assembly factors is involved in remodeling rRNA elements during preribosome maturation. J Cell Biol *207*, 481-498.

Ben-Shem, A., Garreau de Loubresse, N., Melnikov, S., Jenner, L., Yusupova, G., and Yusupov, M. (2011). The structure of the eukaryotic ribosome at 3.0 A resolution. Science *334*, 1524-1529.

Ben-Shem, A., Jenner, L., Yusupova, G., and Yusupov, M. (2010). Crystal structure of the eukaryotic ribosome. Science *330*, 1203-1209.

Bernier, C.R., Petrov, A.S., Waterbury, C.C., Jett, J., Li, F., Freil, L.E., Xiong, X., Wang, L., Migliozzi, B.L., Hershkovits, E*., et al.* (2014). RiboVision suite for visualization and analysis of ribosomes. Faraday Discuss *169*, 195-207.

Bradatsch, B., Leidig, C., Granneman, S., Gnadig, M., Tollervey, D., Bottcher, B., Beckmann, R., and Hurt, E. (2012). Structure of the pre-60S ribosomal subunit with nuclear export factor Arx1 bound at the exit tunnel. Nat Struct Mol Biol *19*, 1234-1241.

Calvino, F.R., Kharde, S., Ori, A., Hendricks, A., Wild, K., Kressler, D., Bange, G., Hurt, E., Beck, M., and Sinning, I. (2015). Symportin 1 chaperones 5S RNP assembly during ribosome biogenesis by occupying an essential rRNA-binding site. Nature communications *6*, 6510.

Chan, J.C., Hannan, K.M., Riddell, K., Ng, P.Y., Peck, A., Lee, R.S., Hung, S., Astle, M.V., Bywater, M., Wall, M*., et al.* (2011). AKT promotes rRNA synthesis and cooperates with c-MYC to stimulate ribosome biogenesis in cancer. Sci Signal *4*, ra56.

Clark, C.G., Tague, B.W., Ware, V.C., and Gerbi, S.A. (1984). Xenopus laevis 28S ribosomal RNA: a secondary structure model and its evolutionary and functional implications. Nucleic Acids Res *12*, 6197-6220.

Clatterbuck Soper, S.F., Dator, R.P., Limbach, P.A., and Woodson, S.A. (2013). In vivo X-ray footprinting of pre-30S ribosomes reveals chaperone-dependent remodeling of late assembly intermediates. Mol Cell *52*, 506-516.

Clery, A., Blatter, M., and Allain, F.H. (2008). RNA recognition motifs: boring? Not quite. Current opinion in structural biology *18*, 290-298.

Cloonan, N., Forrest, A.R.R., Kolle, G., Gardiner, B.B.A., Faulkner, G.J., Brown, M.K., Taylor, D.F., Steptoe, A.L., Wani, S., Bethel, G.*, et al.* (2008). Stem cell transcriptome profiling via massive-scale mRNA sequencing. Nat Meth *5*, 613-619.

Cmejla, R., Cmejlova, J., Handrkova, H., Petrak, J., Petrtylova, K., Mihal, V., Stary, J., Cerna, Z., Jabali, Y., and Pospisilova, D. (2009). Identification of mutations in the ribosomal protein L5 (RPL5) and ribosomal protein L11 (RPL11) genes in Czech patients with Diamond-Blackfan anemia. Hum Mutat *30*, 321-327.

Cole, S.E., and LaRiviere, F.J. (2008). Chapter 12. Analysis of nonfunctional ribosomal RNA decay in Saccharomyces cerevisiae. Methods Enzymol *449*, 239-259.

Costa, M., and Monachello, D. (2014). Probing RNA folding by hydroxyl radical footprinting. Methods in molecular biology (Clifton, N.J.) *1086*, 119-142.

Cote, C.A., Greer, C.L., and Peculis, B.A. (2002). Dynamic conformational model for the role of ITS2 in pre-rRNA processing in yeast. RNA *8*, 786-797.

Cote, C.A., and Peculis, B.A. (2001). Role of the ITS2-proximal stem and evidence for indirect recognition of processing sites in pre-rRNA processing in yeast. Nucleic Acids Res *29*, 2106-2116.

Dahlberg, A.E. (1989). The functional role of ribosomal RNA in protein synthesis. Cell *57*, 525-529.

Danilova, N., and Gazda, H.T. (2015). Ribosomopathies: how a common root can cause a tree of pathologies. Disease models & mechanisms *8*, 1013-1026.

De Keersmaecker, K., Atak, Z.K., Li, N., Vicente, C., Patchett, S., Girardi, T., Gianfelici, V., Geerdens, E., Clappier, E., Porcu, M.*, et al.* (2013). Exome sequencing identifies mutation in CNOT3 and ribosomal genes RPL5 and RPL10 in T-cell acute lymphoblastic leukemia. Nature genetics *45*, 186-190.

de la Cruz, J., Karbstein, K., and Woolford, J.L., Jr. (2015). Functions of ribosomal proteins in assembly of eukaryotic ribosomes in vivo. Annu Rev Biochem *84*, 93-129.

Dembowski, J.A., Kuo, B., and Woolford, J.L., Jr. (2013a). Has1 regulates consecutive maturation and processing steps for assembly of 60S ribosomal subunits. Nucleic Acids Res.

Dembowski, J.A., Kuo, B., and Woolford, J.L., Jr. (2013b). Has1 regulates consecutive maturation and processing steps for assembly of 60S ribosomal subunits. Nucleic Acids Res *41*, 7889-7904.

Dembowski, J.A., Ramesh, M., McManus, C.J., and Woolford, J.L., Jr. (2013c). Identification of the binding site of Rlp7 on assembling 60S ribosomal subunits in Saccharomyces cerevisiae. RNA *19*, 1639-1647.

Deshmukh, M., Stark, J., Yeh, L.C., Lee, J.C., and Woolford, J.L., Jr. (1995). Multiple regions of yeast ribosomal protein L1 are important for its interaction with 5 S rRNA and assembly into ribosomes. J Biol Chem *270*, 30148-30156.

Freed, E.F., Bleichert, F., Dutca, L.M., and Baserga, S.J. (2010). When ribosomes go bad: diseases of ribosome biogenesis. Molecular bioSystems *6*, 481-493.

Fromont-Racine, M., Senger, B., Saveanu, C., and Fasiolo, F. (2003). Ribosome assembly in eukaryotes. Gene *313*, 17-42.

Gamalinda, M., Jakovljevic, J., Babiano, R., Talkish, J., de la Cruz, J., and Woolford, J.L., Jr. (2013). Yeast polypeptide exit tunnel ribosomal proteins L17, L35 and L37 are necessary to recruit late-assembling factors required for 27SB pre-rRNA processing. Nucleic Acids Res *41*, 1965-1983.

Gamalinda, M., Ohmayer, U., Jakovljevic, J., Kumcuoglu, B., Woolford, J., Mbom, B., Lin, L., and Woolford, J.L., Jr. (2014). A hierarchical model for assembly of eukaryotic 60S ribosomal subunit domains. Genes Dev *28*, 198-210.

Gamalinda, M., and Woolford, J.L., Jr. (2014). Deletion of L4 domains reveals insights into the importance of ribosomal protein extensions in eukaryotic ribosome assembly. RNA *20*, 1725-1731.

Gamalinda, M., and Woolford, J.L., Jr. (2015). Paradigms of ribosome synthesis: Lessons learned from ribosomal proteins. Translation (Austin) *3*, e975018.

Gazda, H.T., Sheen, M.R., Vlachos, A., Choesmel, V., O'Donohue, M.F., Schneider, H., Darras, N., Hasman, C., Sieff, C.A., Newburger, P.E., *et al.* (2008). Ribosomal protein L5 and L11 mutations are associated with cleft palate and abnormal thumbs in Diamond-Blackfan anemia patients. Am J Hum Genet *83*, 769-780.

Gerbi, S. (1996). Expansion segments: regions of variable size that interrupt the universal core secondary structure of ribosomal RNA. Ribosomal RNA structure, evolution, processing, and function in protein biosynthesis, 71-87.

Goll, J., and Uetz, P. (2006). The elusive yeast interactome. Genome Biol *7*, 223.

Gonzalez, I.L., Gorski, J.L., Campen, T.J., Dorney, D.J., Erickson, J.M., Sylvester, J.E., and Schmickel, R.D. (1985). Variation among human 28S ribosomal RNA genes. Proc Natl Acad Sci U S A *82*, 7666-7670.

Granneman, S., Kudla, G., Petfalski, E., and Tollervey, D. (2009). Identification of protein binding sites on U3 snoRNA and pre-rRNA by UV cross-linking and high-throughput analysis of cDNAs. Proc Natl Acad Sci U S A *106*, 9613-9618.

Granneman, S., Petfalski, E., and Tollervey, D. (2011). A cluster of ribosome synthesis factors regulate pre-rRNA folding and 5.8S rRNA maturation by the Rat1 exonuclease. EMBO J *30*, 4006-4019.

Green, R., and Noller, H.F. (1997). Ribosomes and translation. Annu Rev Biochem *66*, 679-716.

Gutell, R.R., Gray, M.W., and Schnare, M.N. (1993). A compilation of large subunit (23S and 23S-like) ribosomal RNA structures: 1993. Nucleic Acids Res *21*, 3055-3074.

Halic, M., Becker, T., Pool, M.R., Spahn, C.M., Grassucci, R.A., Frank, J., and Beckmann, R. (2004). Structure of the signal recognition particle interacting with the elongation-arrested ribosome. Nature *427*, 808-814.

Hancock, J.M., and Dover, G.A. (1988). Molecular coevolution among cryptically simple expansion segments of eukaryotic 26S/28S rRNAs. Mol Biol Evol *5*, 377-391.

Hannan, K.M., Sanij, E., Hein, N., Hannan, R.D., and Pearson, R.B. (2011). Signaling to the ribosome in cancer--It is more than just mTORC1. IUBMB life *63*, 79-85.

Harnpicharnchai, P., Jakovljevic, J., Horsey, E., Miles, T., Roman, J., Rout, M., Meagher, D., Imai, B., Guo, Y., Brame, C.J., *et al.* (2001). Composition and functional characterization of yeast 66S ribosome assembly intermediates. Mol Cell *8*, 505-515.

Henras, A.K., Soudet, J., Gerus, M., Lebaron, S., Caizergues-Ferrer, M., Mougin, A., and Henry, Y. (2008). The post-transcriptional steps of eukaryotic ribosome biogenesis. Cell Mol Life Sci *65*, 2334-2359.

Henry, Y., Wood, H., Morrissey, J.P., Petfalski, E., Kearsey, S., and Tollervey, D. (1994). The 5' end of yeast 5.8S rRNA is generated by exonucleases from an upstream cleavage site. EMBO J *13*, 2452-2463.

Hofer, A., Bussiere, C., and Johnson, A.W. (2007). Mutational analysis of the ribosomal protein Rpl10 from yeast. J Biol Chem *282*, 32630-32639.

Hook, B., Bernstein, D., Zhang, B., and Wickens, M. (2005). RNA–protein interactions in the yeast three-hybrid system: Affinity, sensitivity, and enhanced library screening. RNA *11*, 227-233.

Horsey, E.W., Jakovljevic, J., Miles, T.D., Harnpicharnchai, P., and Woolford, J.L., Jr. (2004). Role of the yeast Rrp1 protein in the dynamics of pre-ribosome maturation. RNA *10*, 813-827.

Ingle, S., Azad, R.N., Jain, S.S., and Tullius, T.D. (2014). Chemical probing of RNA with the hydroxyl radical at single-atom resolution. Nucleic Acids Res *42*, 12758-12767.

Jaeger, S., Eriani, G., and Martin, F. (2004). Results and prospects of the yeast three-hybrid system. FEBS Letters *556*, 7-12.

Jakovljevic, J., Ohmayer, U., Gamalinda, M., Talkish, J., Alexander, L., Linnemann, J., Milkereit, P., and Woolford, J.L., Jr. (2012). Ribosomal proteins L7 and L8 function in concert with six A(3) assembly factors to propagate assembly of domains I and II of 25S rRNA in yeast 60S ribosomal subunits. RNA *18*, 1805-1822.

James, P., Halladay, J., and Craig, E.A. (1996). Genomic libraries and a host strain designed for highly efficient two-hybrid selection in yeast. Genetics *144*, 1425-1436.

Jeeninga, R.E., Van Delft, Y., de Graaff-Vincent, M., Dirks-Mulder, A., Venema, J., and Raue, H.A. (1997). Variable regions V13 and V3 of Saccharomyces cerevisiae contain structural features essential for normal biogenesis and stability of 5.8S and 25S rRNA. RNA *3*, 476-488.

Jenner, L., Melnikov, S., Garreau de Loubresse, N., Ben-Shem, A., Iskakova, M., Urzhumtsev, A., Meskauskas, A., Dinman, J., Yusupova, G., and Yusupov, M. (2012). Crystal structure of the 80S yeast ribosome. Current opinion in structural biology *22*, 759-767.

Joseph, N., Krauskopf, E., Vera, M.I., and Michot, B. (1999). Ribosomal internal transcribed spacer 2 (ITS2) exhibits a common core of secondary structure in vertebrates and yeast. Nucleic Acids Res *27*, 4533-4540.

Kenan, D.J., Query, C.C., and Keene, J.D. RNA recognition: towards identifying determinants of specificity. Trends in Biochemical Sciences *16*, 214-220.

Kharde, S., Calvino, F.R., Gumiero, A., Wild, K., and Sinning, I. (2015). The structure of Rpf2-Rrs1 explains its role in ribosome biogenesis. Nucleic Acids Res *43*, 7083-7095.

Klinge, S., Voigts-Hoffmann, F., Leibundgut, M., Arpagaus, S., and Ban, N. (2011). Crystal structure of the eukaryotic 60S ribosomal subunit in complex with initiation factor 6. Science *334*, 941-948.

Klinge, S., Voigts-Hoffmann, F., Leibundgut, M., and Ban, N. (2012). Atomic structures of the eukaryotic ribosome. Trends Biochem Sci *37*, 189-198.

Kos, M., and Tollervey, D. (2010). Yeast pre-rRNA processing and modification occur cotranscriptionally. Mol Cell *37*, 809-820.

Kressler, D., Bange, G., Ogawa, Y., Stjepanovic, G., Bradatsch, B., Pratte, D., Amlacher, S., Strauss, D., Yoneda, Y., Katahira, J.*, et al.* (2012). Synchronizing nuclear import of ribosomal proteins with ribosome assembly. Science *338*, 666-671.

Kressler, D., Hurt, E., and Bassler, J. (2010). Driving ribosome assembly. Biochim Biophys Acta *1803*, 673-683.

Kubota, M., Tran, C., and Spitale, R.C. (2015). Progress and challenges for chemical probing of RNA structure inside living cells. Nat Chem Biol *11*, 933-941.

Lebaron, S., Segerstolpe, A., French, S.L., Dudnakova, T., de Lima Alves, F., Granneman, S., Rappsilber, J., Beyer, A.L., Wieslander, L., and Tollervey, D. (2013). Rrp5 binding at multiple sites coordinates pre-rRNA processing and assembly. Mol Cell *52*, 707-719.

Lee, J.T., and Nussbaum, R.L. (1989). An arginine to glutamine mutation in residue 109 of human ornithine transcarbamylase completely abolishes enzymatic activity in Cos1 cells. The Journal of clinical investigation *84*, 1762-1766.

Leidig, C., Bange, G., Kopp, J., Amlacher, S., Aravind, A., Wickles, S., Witte, G., Hurt, E., Beckmann, R., and Sinning, I. (2013). Structural characterization of a eukaryotic chaperone—the ribosome-associated complex. Nat Struct Mol Biol *20*, 23-28.

Leidig, C., Thoms, M., Holdermann, I., Bradatsch, B., Berninghausen, O., Bange, G., Sinning, I., Hurt, E., and Beckmann, R. (2014). 60S ribosome biogenesis requires rotation of the 5S ribonucleoprotein particle. Nature communications *5*, 3491.

Li, X., Song, J., and Yi, C. (2014). Genome-wide mapping of cellular protein-RNA interactions enabled by chemical crosslinking. Genomics, proteomics & bioinformatics *12*, 72-78.

Liang, W.Q., and Fournier, M.J. (1997). Synthesis of functional eukaryotic ribosomal RNAs in trans: development of a novel in vivo rDNA system for dissecting ribosome biogenesis. Proc Natl Acad Sci U S A *94*, 2864-2868.

Lo, K.-Y., Li, Z., Bussiere, C., Bresson, S., Marcotte, E.M., and Johnson, A.W. (2010). Defining the pathway of cytoplasmic maturation of the 60S ribosomal subunit. Molecular cell *39*, 196-208.

Longtine, M.S., McKenzie, A., 3rd, Demarini, D.J., Shah, N.G., Wach, A., Brachat, A., Philippsen, P., and Pringle, J.R. (1998). Additional modules for versatile and economical PCR-based gene deletion and modification in Saccharomyces cerevisiae. Yeast *14*, 953-961.

Loughrey, D., Watters, K.E., Settle, A.H., and Lucks, J.B. (2014). SHAPE-Seq 2.0: systematic optimization and extension of high-throughput chemical probing of RNA secondary structure with next generation sequencing. Nucleic Acids Res *42*.

Maris, C., Dominguez, C., and Allain, F.H. (2005). The RNA recognition motif, a plastic RNA-binding platform to regulate post-transcriptional gene expression. The FEBS journal *272*, 2118-2131.

Martin, F. (2012). Fifteen years of the yeast three-hybrid system: RNA–protein interactions under investigation. Methods *58*, 367-375.

Martin, R., Straub, A.U., Doebele, C., and Bohnsack, M.T. (2013). DExD/H-box RNA helicases in ribosome biogenesis. RNA biology *10*, 4-18.

McCann, K.L., and Baserga, S.J. (2014). Driving nucleolar assembly. Genes Dev *28*, 211-213.

McCann, K.L., Charette, J.M., Vincent, N.G., and Baserga, S.J. (2015). A protein interaction map of the LSU processome. Genes Dev *29*, 862-875.

McGinnis, J.L., Dunkle, J.A., Cate, J.H.D., and Weeks, K.M. (2012). The Mechanisms of RNA SHAPE Chemistry. Journal of the American Chemical Society *134*, 6617-6624.

McGinnis, J.L., Liu, Q., Lavender, C.A., Devaraj, A., McClory, S.P., Fredrick, K., and Weeks, K.M. (2015). In-cell SHAPE reveals that free 30S ribosome subunits are in the inactive state. Proceedings of the National Academy of Sciences *112*, 2425-2430.

McGinnis, J.L., and Weeks, K.M. (2014). Ribosome RNA Assembly Intermediates Visualized in Living Cells. Biochemistry *53*, 3237-3247.

Melnikov, S., Ben-Shem, A., Garreau de Loubresse, N., Jenner, L., Yusupova, G., and Yusupov, M. (2012). One core, two shells: bacterial and eukaryotic ribosomes. Nat Struct Mol Biol *19*, 560-567.

Merino, E.J., Wilkinson, K.A., Coughlan, J.L., and Weeks, K.M. (2005). RNA Structure Analysis at Single Nucleotide Resolution by Selective 2'-Hydroxyl Acylation and Primer Extension (SHAPE). Journal of the American Chemical Society *127*, 4223-4231.

Mizushima, S., and Nomura, M. (1970). Assembly mapping of 30S ribosomal proteins from E. coli. Nature *226*, 1214.

Montanaro, L., Trere, D., and Derenzini, M. (2008). Nucleolus, ribosomes, and cancer. The American journal of pathology *173*, 301-310.

Moore, P.B., and Steitz, T.A. (2011). The roles of RNA in the synthesis of protein. Cold Spring Harbor perspectives in biology *3*, a003780.

Murigneux, V., Saulière, J., Roest Crollius, H., and Le Hir, H. (2013). Transcriptome-wide identification of RNA binding sites by CLIP-seq. Methods *63*, 32-40.

Musters, W., Boon, K., van der Sande, C.A., van Heerikhuizen, H., and Planta, R.J. (1990). Functional analysis of transcribed spacers of yeast ribosomal DNA. EMBO J *9*, 3989-3996.

Musters, W., Concalves, P.M., Boon, K., Raue, H.A., van Heerikhuizen, H., and Planta, R.J. (1991). The conserved GTPase center and variable region V9 from Saccharomyces cerevisiae 26S rRNA can be replaced by their equivalents from other prokaryotes or eukaryotes without detectable loss of ribosomal function. Proc Natl Acad Sci U S A *88*, 1469-1473.

Musters, W., Venema, J., van der Linden, G., van Heerikhuizen, H., Klootwijk, J., and Planta, R.J. (1989). A system for the analysis of yeast ribosomal DNA mutations. Mol Cell Biol *9*, 551-559.

Nakayama, M., Kikuno, R., and Ohara, O. (2002). Protein-protein interactions between large proteins: two-hybrid screening using a functionally classified library composed of long cDNAs. Genome research *12*, 1773-1784.

Nazar, R.N., Yaguchi, M., Willick, G.E., Rollin, C.F., and Roy, C. (1979). The 5-S RNA binding protein from yeast (Saccharomyces cerevisiae) ribosomes. Evolution of the eukaryotic 5-S RNA binding protein. Eur J Biochem *102*, 573-582.

Nierhaus, K.H., and Dohme, F. (1974). Total Reconstitution of Functionally Active 50S Ribosomal Subunits from Escherichia coli. Proceedings of the National Academy of Sciences of the United States of America *71*, 4713-4717.

Nishimura, K., Kumazawa, T., Kuroda, T., Katagiri, N., Tsuchiya, M., Goto, N., Furumai, R., Murayama, A., Yanagisawa, J., and Kimura, K. (2015). Perturbation of ribosome biogenesis drives cells into senescence through 5S RNP-mediated p53 activation. Cell reports *10*, 1310-1323.

Nogi, Y., Yano, R., Dodd, J., Carles, C., and Nomura, M. (1993). Gene RRN4 in Saccharomyces cerevisiae encodes the A12.2 subunit of RNA polymerase I and is essential only at high temperatures. Molecular and Cellular Biology *13*, 114-122.

Noller, H.F. (2012). Evolution of protein synthesis from an RNA world. Cold Spring Harbor perspectives in biology *4*, a003681.

Nomura, M. (1973). Assembly of bacterial ribosomes. Science *179*, 864-873.

Oeffinger, M., and Tollervey, D. (2003). Yeast Nop15p is an RNA-binding protein required for pre-rRNA processing and cytokinesis. The EMBO Journal *22*, 6573-6583.

Oeffinger, M., Wei, K.E., Rogers, R., DeGrasse, J.A., Chait, B.T., Aitchison, J.D., and Rout, M.P. (2007). Comprehensive analysis of diverse ribonucleoprotein complexes. Nature methods *4*, 951-956.

Ohmayer, U., Gamalinda, M., Sauert, M., Ossowski, J., Poll, G., Linnemann, J., Hierlmeier, T., Perez-Fernandez, J., Kumcuoglu, B., Leger-Silvestre, I.*, et al.* (2013). Studies on the assembly characteristics of large subunit ribosomal proteins in S. cerevisae. PLoS One *8*, e68412.

Panse, V.G., and Johnson, A.W. (2010). Maturation of eukaryotic ribosomes: acquisition of functionality. Trends Biochem Sci *35*, 260-266.

Peculis, B.A., and Greer, C.L. (1998). The structure of the ITS2-proximal stem is required for pre-rRNA processing in yeast. RNA *4*, 1610-1622.

Poll, G., Braun, T., Jakovljevic, J., Neueder, A., Jakob, S., Woolford, J.L., Jr., Tschochner, H., and Milkereit, P. (2009). rRNA maturation in yeast cells depleted of large ribosomal subunit proteins. PLoS One *4*, e8249.

Popova, V.V., Kurshakova, M.M., and Kopytova, D.V. (2015). [Methods to study the RNA-protein interactions]. Molekuliarnaia biologiia *49*, 472-481.

Rappsilber, J. (2011). The beginning of a beautiful friendship: cross-linking/mass spectrometry and modelling of proteins and multi-protein complexes. J Struct Biol *173*, 530-540.

Rawling, D.C., and Baserga, S.J. (2012). In vivo approaches to dissecting the function of RNA helicases in eukaryotic ribosome assembly. Methods Enzymol *511*, 289-321.

Regulski, E.E., and Breaker, R.R. (2008). In-line probing analysis of riboswitches. Methods in molecular biology (Clifton, N.J.) *419*, 53-67.

Rigaut, G., Shevchenko, A., Rutz, B., Wilm, M., Mann, M., and Seraphin, B. (1999). A generic protein purification method for protein complex characterization and proteome exploration. Nature biotechnology *17*, 1030-1032.

Ripmaster, T.L., Vaughn, G.P., and Woolford, J.L., Jr. (1992). A putative ATP-dependent RNA helicase involved in Saccharomyces cerevisiae ribosome assembly. Proc Natl Acad Sci U S A *89*, 11131-11135.

Rodriguez-Galan, O., Garcia-Gomez, J.J., and de la Cruz, J. (2013). Yeast and human RNA helicases involved in ribosome biogenesis: current status and perspectives. Biochim Biophys Acta *1829*, 775-790.

Rodriguez-Galan, O., Garcia-Gomez, J.J., Kressler, D., and de la Cruz, J. (2015). Immature large ribosomal subunits containing the 7S pre-rRNA can engage in translation in Saccharomyces cerevisiae. RNA Biol *12*, 838-846.

Röhl, R., and Nierhaus, K.H. (1982). Assembly map of the large subunit (50S) of Escherichia coli ribosomes. Proceedings of the National Academy of Sciences of the United States of America *79*, 729-733.

Rouskin, S., Zubradt, M., Washietl, S., Kellis, M., and Weissman, J.S. (2014). Genome-wide probing of RNA structure reveals active unfolding of mRNA structures in vivo. Nature *505*, 701-705.

Ruggero, D., and Pandolfi, P.P. (2003). Does the ribosome translate cancer? Nature reviews. Cancer *3*, 179-192.

Ruiz Linares, A., Hancock, J.M., and Dover, G.A. (1991). Secondary structure constraints on the evolution of Drosophila 28 S ribosomal RNA expansion segments. J Mol Biol *219*, 381-390.

Sahasranaman, A., Dembowski, J., Strahler, J., Andrews, P., Maddock, J., and Woolford, J.L., Jr. (2011). Assembly of Saccharomyces cerevisiae 60S ribosomal subunits: role of factors required for 27S pre-rRNA processing. EMBO J *30*, 4020-4032.

Scheper, G.C., van der Knaap, M.S., and Proud, C.G. (2007). Translation matters: protein synthesis defects in inherited disease. Nat Rev Genet *8*, 711-723.

Schmeing, T.M., and Ramakrishnan, V. (2009). What recent ribosome structures have revealed about the mechanism of translation. Nature *461*, 1234-1242.

Schmitt, M.E., and Clayton, D.A. (1993). Nuclear RNase MRP is required for correct processing of pre-5.8S rRNA in Saccharomyces cerevisiae. Mol Cell Biol *13*, 7935-7941.

Schrodinger, LLC (2015). The PyMOL Molecular Graphics System, Version 1.8.

Sengupta, D.J., Wickens, M., and Fields, S. (1999). Identification of RNAs that bind to a specific protein using the yeast three-hybrid system. Rna *5*, 596-601.

Shajani, Z., Sykes, M.T., and Williamson, J.R. (2011). Assembly of bacterial ribosomes. Annu Rev Biochem *80*, 501-526.

Smola, M.J., Rice, G.M., Busan, S., Siegfried, N.A., and Weeks, K.M. (2015). Selective 2[prime]-hydroxyl acylation analyzed by primer extension and mutational profiling (SHAPE-MaP) for direct, versatile and accurate RNA structure analysis. Nat. Protocols *10*, 1643-1669.

Spahn, C.M., Beckmann, R., Eswar, N., Penczek, P.A., Sali, A., Blobel, G., and Frank, J. (2001). Structure of the 80S ribosome from Saccharomyces cerevisiae--tRNA-ribosome and subunit-subunit interactions. Cell *107*, 373-386.

Spitale, R.C., Crisalli, P., Flynn, R.A., Torre, E.A., Kool, E.T., and Chang, H.Y. (2013). RNA SHAPE analysis in living cells. Nat Chem Biol *9*, 18-20.

Spitale, R.C., Flynn, R.A., Zhang, Q.C., Crisalli, P., Lee, B., Jung, J.-W., Kuchelmeister, H.Y., Batista, P.J., Torre, E.A., Kool, E.T.*, et al.* (2015). Structural imprints in vivo decode RNA regulatory mechanisms. Nature *519*, 486-490.

Steitz, T.A. (2008). A structural understanding of the dynamic ribosome machine. Nat Rev Mol Cell Biol *9*, 242-253.

Steitz, T.A., and Moore, P.B. (2003). RNA, the first macromolecular catalyst: the ribosome is a ribozyme. Trends Biochem Sci *28*, 411-418.

Stelter, P., Huber, F.M., Kunze, R., Flemming, D., Hoelz, A., and Hurt, E. (2015). Coordinated Ribosomal L4 Protein Assembly into the Pre-Ribosome Is Regulated by Its Eukaryote-Specific Extension. Mol Cell *58*, 854-862.

Structural Genomics, C., China Structural Genomics, C., Northeast Structural Genomics, C., Graslund, S., Nordlund, P., Weigelt, J., Hallberg, B.M., Bray, J., Gileadi, O., Knapp, S.*, et al.* (2008). Protein production and purification. Nature methods *5*, 135-146.

Sulima, S.O., Gulay, S.P., Anjos, M., Patchett, S., Meskauskas, A., Johnson, A.W., and Dinman, J.D. (2014a). Eukaryotic rpL10 drives ribosomal rotation. Nucleic Acids Res *42*, 2049-2063.

Sulima, S.O., Patchett, S., Advani, V.M., De Keersmaecker, K., Johnson, A.W., and Dinman, J.D. (2014b). Bypass of the pre-60S ribosomal quality control as a pathway to oncogenesis. Proceedings of the National Academy of Sciences of the United States of America *111*, 5640-5645.

Sweeney, R., Chen, L., and Yao, M.C. (1994). An rRNA variable region has an evolutionarily conserved essential role despite sequence divergence. Molecular and Cellular Biology *14*, 4203-4215.

Swiatkowska, A., Wlotzka, W., Tuck, A., Barrass, J.D., Beggs, J.D., and Tollervey, D. (2012). Kinetic analysis of pre-ribosome structure in vivo. Rna *18*, 2187-2200.

Talkish, J., Campbell, I.W., Sahasranaman, A., Jakovljevic, J., and Woolford, J.L. (2014a). Ribosome Assembly Factors Pwp1 and Nop12 Are Important for Folding of 5.8S rRNA during Ribosome Biogenesis in Saccharomyces cerevisiae. Molecular and Cellular Biology *34*, 1863-1877.

Talkish, J., Campbell, I.W., Sahasranaman, A., Jakovljevic, J., and Woolford, J.L., Jr. (2014b). Ribosome assembly factors Pwp1 and Nop12 are important for folding of 5.8S rRNA during ribosome biogenesis in Saccharomyces cerevisiae. Mol Cell Biol *34*, 1863-1877.

Talkish, J., May, G., Lin, Y., Woolford, J.L., Jr., and McManus, C.J. (2014c). Mod-seq: high-throughput sequencing for chemical probing of RNA structure. Rna *20*, 713-720.

Talkish, J., Zhang, J., Jakovljevic, J., Horsey, E.W., and Woolford, J.L., Jr. (2012). Hierarchical recruitment into nascent ribosomes of assembly factors required for 27SB pre-rRNA processing in Saccharomyces cerevisiae. Nucleic Acids Res *40*, 8646-8661.

Tarassov, K., Messier, V., Landry, C.R., Radinovic, S., Serna Molina, M.M., Shames, I., Malitskaya, Y., Vogel, J., Bussey, H., and Michnick, S.W. (2008). An in vivo map of the yeast protein interactome. Science *320*, 1465-1470.

Taylor, D.J., Devkota, B., Huang, A.D., Topf, M., Narayanan, E., Sali, A., Harvey, S.C., and Frank, J. (2009). Comprehensive molecular structure of the eukaryotic ribosome. Structure *17*, 1591-1604.

Teng, T., Mercer, C.A., Hexley, P., Thomas, G., and Fumagalli, S. (2013). Loss of tumor suppressor RPL5/RPL11 does not induce cell cycle arrest but impedes proliferation due to reduced ribosome content and translation capacity. Mol Cell Biol *33*, 4660-4671.

Tenson, T., and Mankin, A. (2006). Antibiotics and the ribosome. Mol Microbiol *59*, 1664-1677.

Thomson, E., Ferreira-Cerca, S., and Hurt, E. (2013). Eukaryotic ribosome biogenesis at a glance. J Cell Sci *126*, 4815-4821.

Tome, J.M., Ozer, A., Pagano, J.M., Gheba, D., Schroth, G.P., and Lis, J.T. (2014). Comprehensive analysis of RNA-protein interactions by high-throughput sequencing-RNA affinity profiling. Nat Meth *11*, 683-688.

Trakselis, M.A., Alley, S.C., and Ishmael, F.T. (2005). Identification and mapping of protein-protein interactions by a combination of cross-linking, cleavage, and proteomics. Bioconjug Chem *16*, 741-750.

Uetz, P., Giot, L., Cagney, G., Mansfield, T.A., Judson, R.S., Knight, J.R., Lockshon, D., Narayan, V., Srinivasan, M., Pochart, P.*, et al.* (2000). A comprehensive analysis of protein-protein interactions in Saccharomyces cerevisiae. Nature *403*, 623-627.

van Beekvelt, C.A., Kooi, E.A., de Graaff-Vincent, M., Riet, J., Venema, J., and Raue, H.A. (2000). Domain III of Saccharomyces cerevisiae 25 S ribosomal RNA: its role in binding of ribosomal protein L25 and 60 S subunit formation. J Mol Biol *296*, 7-17.

van Nues, R.W., Rientjes, J.M., Morre, S.A., Mollee, E., Planta, R.J., Venema, J., and Raue, H.A. (1995). Evolutionarily conserved structural elements are critical for processing of Internal Transcribed Spacer 2 from Saccharomyces cerevisiae precursor ribosomal RNA. J Mol Biol *250*, 24-36.

Veldman, G.M., Klootwijk, J., de Regt, V.C., Planta, R.J., Branlant, C., Krol, A., and Ebel, J.P. (1981). The primary and secondary structure of yeast 26S rRNA. Nucleic Acids Res *9*, 6935-6952.

Wakeman, J.A., and Maden, B.E. (1989). 28 S ribosomal RNA in vertebrates. Locations of large-scale features revealed by electron microscopy in relation to other features of the sequences. Biochem J *258*, 49-56.

Ware, V.C., Tague, B.W., Clark, C.G., Gourse, R.L., Brand, R.C., and Gerbi, S.A. (1983). Sequence analysis of 28S ribosomal DNA from the amphibian Xenopus laevis. Nucleic Acids Res *11*, 7795-7817.

Warner, J.R. (1999). The economics of ribosome biosynthesis in yeast. Trends Biochem Sci *24*, 437-440.

Warner, J.R. (2001). Nascent ribosomes. Cell *107*, 133-136.

Waters, A.P., White, W., and McCutchan, T.F. (1995). The structure of the large subunit rRNA expressed in blood stages of Plasmodium falciparum. Mol Biochem Parasitol *72*, 227-237.

Weeks, K.M. (2010). Advances in RNA structure analysis by chemical probing. Current opinion in structural biology *20*, 295-304.

Woodson, S.A. (2008). RNA folding and ribosome assembly. Curr Opin Chem Biol *12*, 667-673.

Woodson, S.A. (2015). RNA folding retrospective: lessons from ribozymes big and small. Rna *21*, 502-503.

Woolford, J. (2015). Assembly of ribosomes in eukaryotes. RNA *21*, 766-768.

Woolford, J.L., Jr., and Baserga, S.J. (2013). Ribosome biogenesis in the yeast Saccharomyces cerevisiae. Genetics *195*, 643-681.

Yaguchi, M., Rollin, C.F., Roy, C., and Nazar, R.N. (1984). The 5S RNA binding protein from yeast (Saccharomyces cerevisiae) ribosomes. An RNA binding sequence in the carboxyl-terminal region. Eur J Biochem *139*, 451-457.

Yeh, L.C., Deshmukh, M., Woolford, J.L., and Lee, J.C. (1996). Involvement of lysine 270 and lysine 271 of yeast 5S rRNA binding protein in RNA binding and ribosome assembly. Biochim Biophys Acta *1308*, 133-141.

Yeh, L.C., and Lee, J.C. (1990). Structural analysis of the internal transcribed spacer 2 of the precursor ribosomal RNA from Saccharomyces cerevisiae. J Mol Biol *211*, 699-712.

Yokoyama, T., and Suzuki, T. (2008). Ribosomal RNAs are tolerant toward genetic insertions: evolutionary origin of the expansion segments. Nucleic Acids Res *36*, 3539-3551.

Yu, H., Braun, P., Yildirim, M.A., Lemmens, I., Venkatesan, K., Sahalie, J., Hirozane-Kishikawa, T., Gebreab, F., Li, N., Simonis, N.*, et al.* (2008). High-quality binary protein interaction map of the yeast interactome network. Science *322*, 104-110.

Zhang, B., Kraemer, B., SenGupta, D., Fields, S., and Wickens, M. (1999). Yeast three-hybrid system to detect and analyze interactions between RNA and protein. Methods Enzymol *306*, 93-113.

Zhang, J., Harnpicharnchai, P., Jakovljevic, J., Tang, L., Guo, Y., Oeffinger, M., Rout, M.P., Hiley, S.L., Hughes, T., and Woolford, J.L., Jr. (2007). Assembly factors Rpf2 and Rrs1 recruit 5S rRNA and ribosomal proteins rpL5 and rpL11 into nascent ribosomes. Genes Dev *21*, 2580-2592.

Zhang, W., Morris, Q.D., Chang, R., Shai, O., Bakowski, M.A., Mitsakakis, N., Mohammad, N., Robinson, M.D., Zirngibl, R., Somogyi, E.*, et al.* (2004). The functional landscape of mouse gene expression. J Biol *3*, 21.

Zhang, Y., Ma, C., Yuan, Y., Zhu, J., Li, N., Chen, C., Wu, S., Yu, L., Lei, J., and Gao, N. (2014). Structural basis for interaction of a cotranslational chaperone with the eukaryotic ribosome. Nat Struct Mol Biol *21*, 1042-1046.

Zhou, X., Hao, Q., Zhang, Q., Liao, J.M., Ke, J.W., Liao, P., Cao, B., and Lu, H. (2015). Ribosomal proteins L11 and L5 activate TAp73 by overcoming MDM2 inhibition. Cell death and differentiation *22*, 755-766.

Manuscript in review:

Wu, S., Tutuncuoglu, B., Yan, K., Tan, D., Gamalinda, M., Li, Z., Zhang, Y., Yuan, Y., Jakovljevic, J., Lei, J., Dong, M., Woolford, J.L., Gao, N. Structures of the nucleoplasmic pre-60S ribosomes in yeast (2016)

Appendices

A.1. Characterization of Nop16

Initial interest in the yet uncharacterized non-essential assembly factor, Nop16, was triggered by the fact that its association with preribosomes is affected upon depletion of other proteins that our lab has studied (Has1, Rlp7 and L8). Based on the result of this mass spectrometry analysis, we suspect that Nop16 might be involved in either the $27SA_3$ processing, or the subsequent C2 cleavage step. Nop16 deletion was shown to have a temperature-sensitive defect in large subunit biogenesis, as evident by a sucrose gradient experiment, (Fig. A-1), (Harnpicharnchai et al., 2001). Hence, a current graduate student Salini Konikkat and I decided to collaborate on characterizing the role of this protein in ribosome assembly. My contribution to the project has been as follows:

- I performed the initial assays on the commercially available Nop16 deletion strain (JWY7002 and JWY7003), but soon realized that it was not behaving as advertised (Fig. A-2)

- I TAP-tagged the assembly factor Rpf2 in the W303 background. The tagging was verified by Western and the candidate marked with a star in (Fig. A-3) was chosen.

- I knocked out the *NOP16* ORF in the *RPF2-TAP* W303 strain background successfully. The deletion was verified by amplification of the locus by PCR, as shown in (Fig. A-4).

- I did spotting assays at three different temperatures to investigate if there were any growth defects, but did not find any. Hence, *NOP16* is indeed non-essential (Fig. A-5).

- In order to identify whether this mutant exhibits a pre-rRNA processing defect, I did a primer extension assay with an oligonucleotide primer that hybridizes to ITS2 (ITS2-B) to assess different pre-rRNA intermediates. Although the results are not very conclusive, it appears that it has a slight

accumulation of 27SA$_2$ and 27SA$_3$. Also, this result reiterated the fact that there was no exacerbation of the knockout phenotype at 37°C (Fig. A-6).

- I did RPF2-TAP pull-downs to see if any changes were observed in the pre-ribosome composition. Consistent with a weak, confusing RNA phenotype, I did not observe any striking changes in the pre-ribosome composition among the proteins tested – Nop7, Cic1, Has1, L17, Rlp7, Tif6, Nog1, Nog2, Nsa2, Rlp24. This probably shows that Nop16 doesn't have an observable ribosome assembly phenotype within the scope of the sub-processes that we are interested in (Fig. A-7).

- We tried to knock it out in diploid W303 in order to sporulate and proceed further, but didn't quite succeed (Fig. A-8).

- We propose that Nop16 seems to be playing a very mild, if any, role in ribosome biogenesis. Perhaps, further combination mutants with other non-essential assembly factor mutants might yield more conspicuous phenotypes.

Fig. A-1
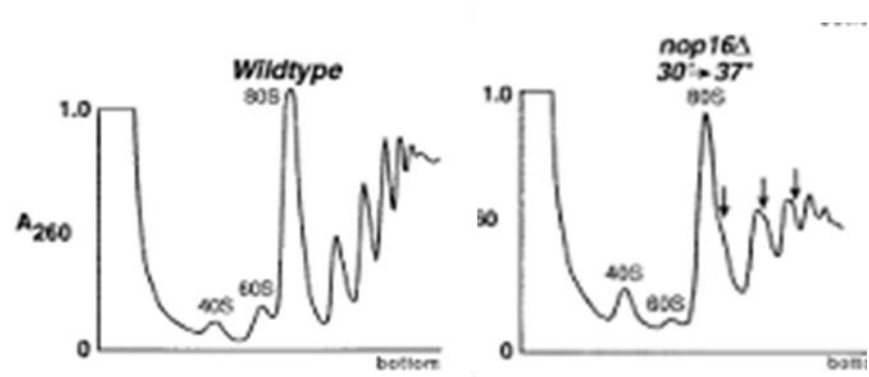
Fig. A-2
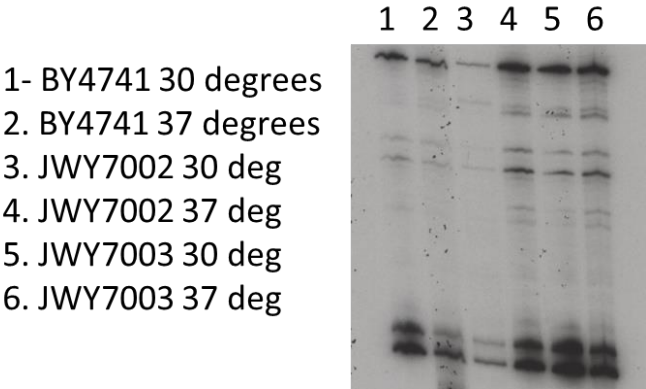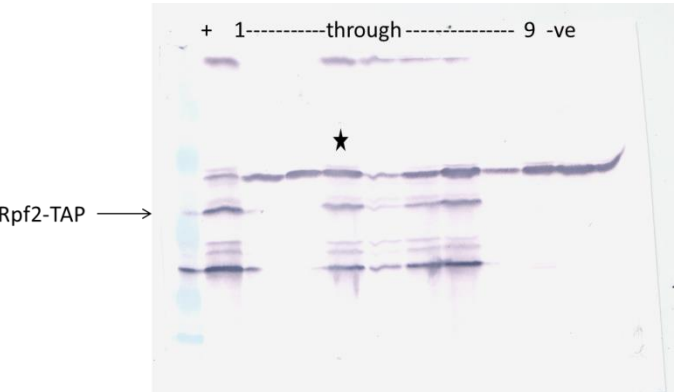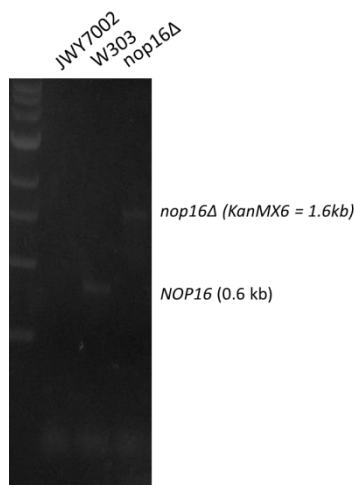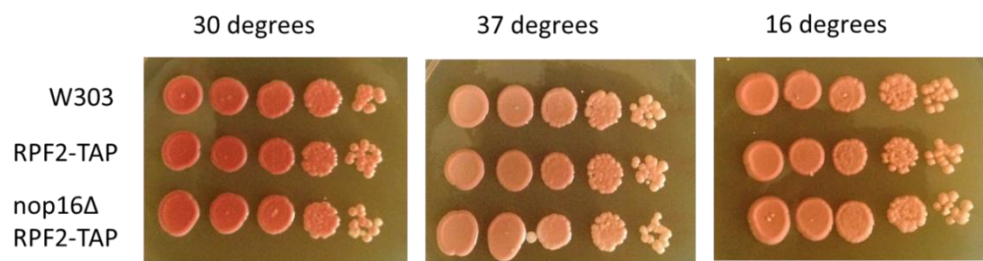
1- BY4741 30 degrees
2. BY4741 37 degrees
3. JWY7002 30 deg
4. JWY7002 37 deg
5. JWY7003 30 deg
6. JWY7003 37 deg

Fig. A-3

Fig. A-4

JWY7002 W303 nop16Δ

nop16Δ (KanMX6 = 1.6kb)

NOP16 (0.6 kb)

Fig. A-5

	30 degrees	37 degrees	16 degrees
W303			
RPF2-TAP			
nop16Δ RPF2-TAP			

Fig. A-6

30 °C   37° C

W303 RPF2 TAP nop16 Δ RPF2 TAP JWY7002   W303 RPF2 TAP nop16 Δ RPF2 TAP JWY7002

A_2

A_3

B_L
B_S

Fig. A-7

Erb1

Nop7

Ytm1

Rlp7

Nop15

L5
Nop7
Cic1

Has1
L17
Nog1
Tif6
Rlp24

Nip7
Nog2
Nsa2

Fig. A-8

HIS

M KK|-|Kan|1 2 3 4 5 6

HIS (~1.6kb)

NOP16
(0.6kb)

Harnpicharnchai, P., Jakovljevic, J., Horsey, E., Miles, T., Roman, J., Rout, M., Meagher, D., Imai, B., Guo, Y., Brame, C.J., *et al.* (2001). Composition and functional characterization of yeast 66S ribosome assembly intermediates. Molecular cell *8*, 505-515.

A.2. Strain List - Bacteria

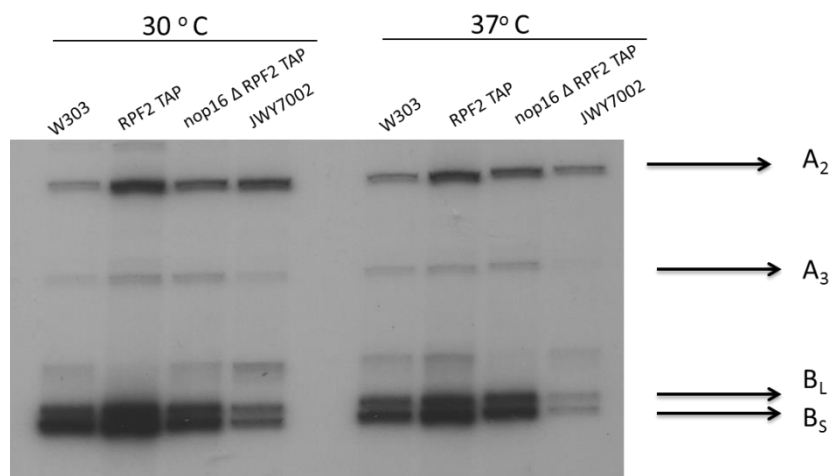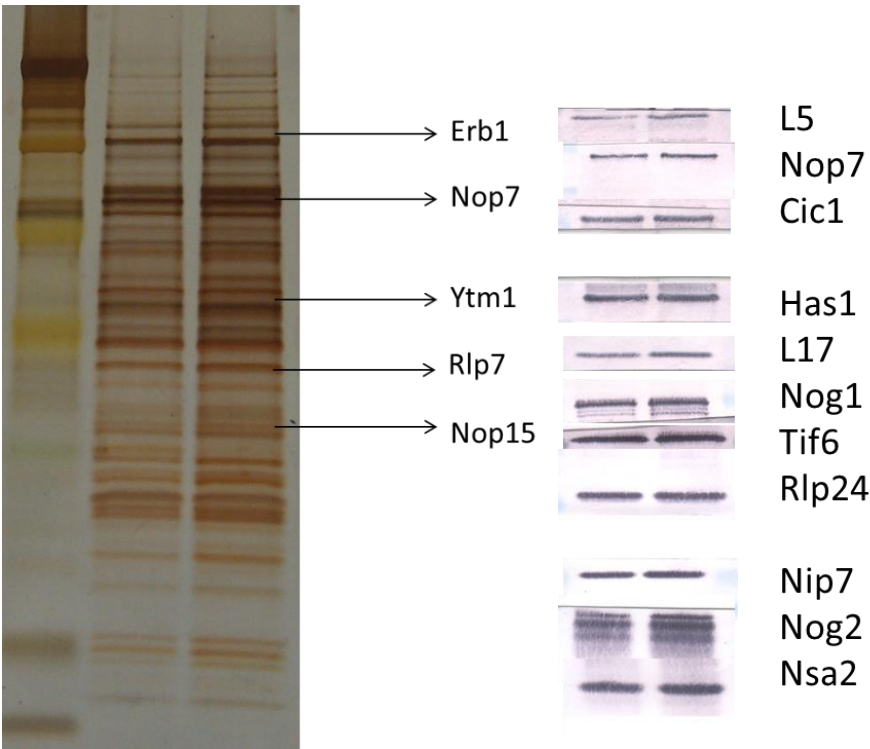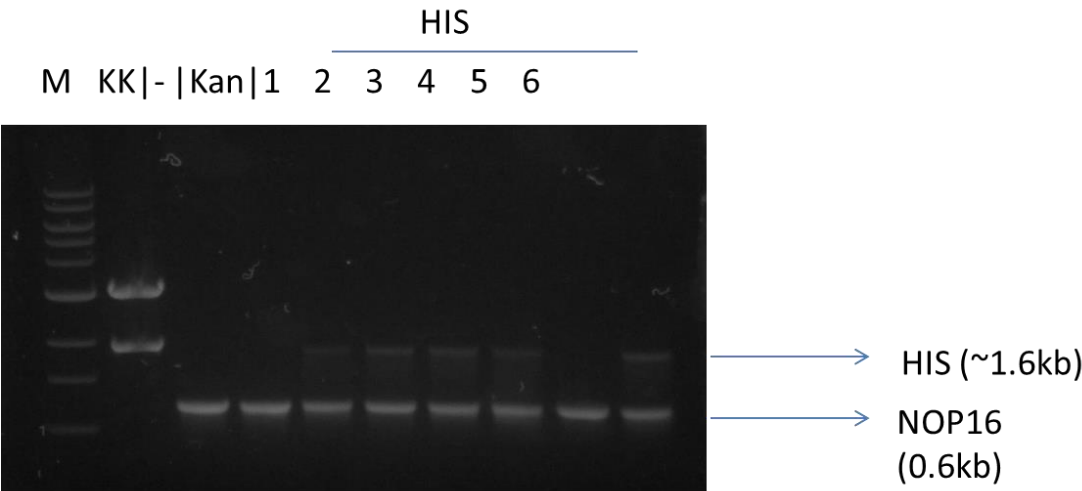|			
JWB8301	pAS vector	JWB7602	LB + AMP
JWB8302	pACT vector	JWB7601	LB + AMP
JWB8303	pDONR221 vector	JWB7618	LB + AMP
JWB8304	L4B (YDR012W) mORF		LB + AMP
JWB8305	L9A(YGL147C) mORF		LB + AMP
JWB8306	L16B(YNL069C) mORF		LB + AMP
JWB8307	L18B(YNL301C) mORF		LB + AMP
JWB8308	L32(YBL092W) mORF		LB + AMP
JWB8309	L4B pACT		LB + AMP
JWB8310	L4B pAS		LB + AMP
JWB8311	L9A pACT		LB + AMP
JWB8312	L9A pAS		LB + AMP
JWB8313	L16B pACT		LB + AMP
JWB8314	L16B pAS		LB + AMP
JWB8315	L18B pACT		LB + AMP
JWB8316	L18B pAS		LB + AMP
JWB8317	L32 pACT		LB + AMP
JWB8318	L32 pAS		LB + AMP
JWB8319	DH5α harboring cloned *NOP15* in pRS315		LB + AMP
JWB8320	DH5α harboring cloned *NOP15* in pRS316		LB + AMP
JWB8321	DH5α harboring cloned *CIC1* in pRS315		LB + AMP
JWB8322	DH5α harboring cloned *CIC1* in pRS316		LB + AMP
JWB8323	DH5α harboring cloned *NOP15* in pRS315 with F136A Clone #1		LB + AMP
JWB8324	DH5α harboring cloned *NOP15* in pRS315 with F136A Clone #2		LB + AMP
JWB8325	DH5α harboring cloned *NOP15* in pRS315 with F136G Clone #1		LB + AMP
JWB8326	DH5α harboring cloned *NOP15* in pRS315 with F136G Clone #2		LB + AMP
JWB8327	DH5α harboring cloned *NOP15* in KS+		LB + AMP
JWB8328	DH5α harboring cloned *CIC1* in KS+		LB + AMP
JWB8329	DH5α harboring pET22b+ vector backbone		LB + AMP
JWB8330	DH5α with cloned *NOP15* ORF in pET22b+		LB + AMP
JWB8331	DH5α with cloned *NOP15* in pRS315 with Y134A mutation		LB + AMP
JWB8332	DH5α with cloned *NOP15* in pRS315 with Y94A mutation		LB + AMP
JWB8333	DH5α with cloned *NOP15* in pRS315 with F139A mutation		LB + AMP
JWB8334	DH5α with cloned *NOP15* in pRS315 with F139G mutation		LB + AMP
JWB8335	DH5α with cloned *NOP15* in pRS315 with Y134G mutation		LB + AMP
JWB8336	DH5α with cloned *NOP15* in pRS315 with		LB + AMP

	Y94A mutation		
JWB8337	DH5α with cloned *NOP15* in pRS315 with R132Q mutation		LB + AMP
JWB8338	BL21 with pRARE and *NOP15* cloned in pET22b+		LB + AMP + CAM
JWB8339	BL21 with pRARE expression host from the Rule lab	Rule lab	LB + CAM
JWB8340	pWL160 from Fournier (Also from MG)	JWB7859	LB + AMP
JWB8341	pWL160 with ES3Δ (XL10 gold cells)		LB+AMP
JWB8342	pWL160 with ES5Δ (XL10 gold cells)		LB+AMP
JWB8343	pWL160 with ES7Δ (XL10 gold cells)		LB+AMP
JWB8344	pWL160 with ES9Δ (XL10 gold cells)		LB+AMP
JWB8345	pWL160 with ES12Δ (XL10 gold cells)		LB+AMP
JWB8346	pWL160 with ES10Δ (XL10 gold cells)		LB+AMP
JWB8347	pWL160 with ES15Δ (XL10 gold cells)		LB+AMP
JWB8348	pWL160 with ES15tetraΔ (XL10 gold cells) (this was the one used)		LB+AMP
JWB8349	pWL160 with ES19Δ (XL10 gold cells)		LB+AMP
JWB8350	pWL160 with ES20Δ (XL10 gold cells)		LB+AMP
JWB8351	pWL160 with ES26Δ (XL10 gold cells)		LB+AMP
JWB8352	pWL160 with ES31Δ (XL10 gold cells)		LB+AMP
JWB8353	pWL160 with ES39Δ (XL10 gold cells)		LB+AMP
JWB8354	pWL160 with ES41Δ (XL10 gold cells)		LB+AMP
JWB8355	pWL160 with ES27hΔ (XL10 gold cells)		LB+AMP
JWB8356	None		
JWB8357	None		
JWB8358	None		
JWB8359	None		
JWB8360	None		
JWB8361	pACTII	Wickens Lab (yeast three hybrid)	LB+AMP
JWB8362	pAD-Iron response protein (pAD-IRP)	Wickens Lab (yeast three hybrid)	LB+AMP
JWB8363	pIII/MS2-1	Wickens Lab (yeast three hybrid)	LB+AMP
JWB8364	pIII/MS2-2	Wickens Lab (yeast three hybrid)	LB+AMP
JWB8365	pIIIA/MS2-1	Wickens Lab (yeast three hybrid)	LB+AMP
JWB8366	pIIIA/MS2-2	Wickens Lab (yeast three hybrid)	LB+AMP
JWB8367	pIIIA/Iron response element-MS2 (pIIIA/IRE-MS2)	Wickens Lab (yeast three hybrid)	LB+AMP
JWB8368	p3HR2	Wickens Lab (yeast three hybrid)	LB+AMP

JWB8369	ES5 cloned in pIIIA/MS2-2 (Candidate #5)		LB+AMP
JWB8370	ES12 cloned in pIIIA/MS2-2 (Candidate #2)		LB+AMP
JWB8371	*RPL5* ORF in pRS315 (DH5α cells)		LB+AMP
JWB8372	*rpl5* 31-37 Ala SDM in JWB8371 (XL10 Gold cells)		LB+AMP
JWB8373	*rpl5* K41A SDM in JWB8371 (XL10 Gold cells)		LB+AMP
JWB8374	*rpl5* K41E SDM in JWB8371 (XL10 Gold cells)		LB+AMP
JWB8375	*rpl5* A291V SDM in JWB8371 (XL10 Gold cells)		LB+AMP
JWB8376	*rpl5* G138S SDM in JWB8371 (XL10 Gold cells)		LB+AMP
JWB8377	*rpl5* Y129G SDM in JWB8371 (XL10 Gold cells)		LB+AMP
JWB8378	*rpl5* ΔC starting at aa. 273 SDM in JWB8371 (XL10 Gold cells)		LB+AMP
JWB8379	*rpl5 173-179*Ala SDM in JWB8371 (XL10 Gold cells)		LB+AMP

A.3. Strain List – Yeast

JWY10401	*GAL-HA-NOP15 MATα ura3-52 trp1-Δ101 lys2-801 his3-Δ200 leu2-Δ1 nop15::GAL-3HA-NOP15 TRP1*	JWY8292	YEPGal
JWY10402	*GAL-HA-NOP15* carrying WT *NOP15* on pRS315		C-Leu+Gal
JWY10403	*GAL-HA-NOP15* carrying *NOP15* with F136A mutation on pRS315		C-Leu+Gal
JWY10404	*GAL-HA-NOP15* carrying *NOP15* with F136G mutation on pRS315		C-Leu+Gal
JWY10405	*GAL-HA-NOP15* carrying *NOP15* with Y134A mutation on pRS315		C-Leu+Gal
JWY10406	*GAL-HA-NOP15* carrying *NOP15* with Y94A mutation on pRS315		C-Leu+Gal
JWY10407	*GAL-HA-NOP15 RPF2-TAP MATα ura3-52 trp1-Δ101 lys2-801 his3-Δ200 leu2-Δ1 nop15::GAL-3HA-NOP15 TRP1 rpf2::RPF2-TAP URA3*	JWY8294	YEPGal
JWY10408	GAL-HA-NOP15 RPF2-TAP carrying WT *NOP15* on pRS315		C-Leu+Gal
JWY10409	*GAL-HA-NOP15 RPF2-TAP* carrying *NOP15* with F136A mutation on pRS315		C-Leu+Gal
JWY10410	*GAL-HA-NOP15 RPF2-TAP* carrying *NOP15* with F136G mutation on pRS315		C-Leu+Gal
JWY10411	*GAL-HA-NOP15 RPF2-TAP* carrying *NOP15* with Y134A mutation on pRS315		C-Leu+Gal
JWY10412	*GAL-HA-NOP15 RPF2-TAP* carrying *NOP15* with Y94A mutation on pRS315		C-Leu+Gal
JWY10413	*GAL-HA-NOP15* carrying pRS315 vector backbone		C-Leu+Gal
JWY10414	*GAL-HA-NOP15 RPF2-TAP* carrying pRS315 vector backbone		C-Leu+Gal
JWY10415	*GAL-HA-NOP15 RPF2 TAP* carrying *NOP15* in pRS315 with F139A mutation		C-Leu+Gal
JWY10416	*GAL-HA-NOP15 RPF2 TAP* carrying *NOP15* in pRS315 with F139G mutation		C-Leu+Gal
JWY10417	*GAL-HA-NOP15 RPF2 TAP* carrying *NOP15* in pRS315 with Y134G mutation		C-Leu+Gal
JWY10418	*GAL-HA-NOP15 RPF2 TAP* carrying *NOP15* in pRS315 with Y94G mutation		C-Leu+Gal
JWY10419	*GAL-HA-NOP15 RPF2 TAP* carrying *NOP15* in pRS315 with R132Q mutation		C-Leu+Gal
JWY10420	W303A parent *MATα leu2-3,112 trp1-1 can1-100 ura3-1 ade2-1 his3-11,15*	JWY8904	YEPD
JWY10421	*RPF2-TAP (URA3)* W303A background clone #1 *MATα leu2-3,112 trp1-1 can1-100 ura3-1 ade2-1 his3-11,15 rpf2:: RPF2-TAP URA3*		YEPD
JWY10422	Same as above Clone #2		YEPD
JWY10423	NOY504 PolI ts- strain *MATα rrn4::LEU2 ade2-101 ura3-1 trpl-lleu2-3,112 his3-11 canl-100*	JWY9051	YEPD
JWY10424	*RPF2 TAP (URA3)* NOY504 PolI ts strain *MATα*	SK	YEPD

	rrn4::LEU2 ade2-101 ura3-1 trpl-lleu2-3,112 his3-11 canl-100 rpf2::RPF2-TAP URA3		
JWY10425	*NOP7 TAP(URA3)* NOY504 PolI ts strain *MATa rrn4::LEU2 ade2-101 ura3-1 trpl-lleu2-3,112 his3-11 canl-100 nop7::NOP7-TAP URA3*		YEPD
JWY10426	YBZ-1 *MATα, ura3-52, leu2-3, -112, his3-200, trp1-1, ade2, LYS2::(LexAop)-HIS3, URA3::(lexA-op)-lacZ, and LexA-MS2 MS2 coat*	Wickens Lab yeast three hybrid	YEPD
JWY10427	R40 coat strain (Same as L40, but MATα)	Wickens Lab yeast three hybrid	YEPD
JWY10428	L40 coat strain *MATa, ura3-52, leu2-3,-112, his3-200, trp1-1, ade2, LYS2:: (lexAop)-HIS3, URA3::(lexA op)-lacZ and LexA MS2 coat (TRP1)*	Wickens Lab yeast three hybrid	YEPD
JWY10429	NOY504 with pRS314		C-Trp+Gal
JWY10430	NOY504 with pWL160		C-Trp+Gal
JWY10431	NOY504 with pWL160 with ES3Δ		C-Trp+Gal
JWY10432	NOY504 with pWL160 with ES5Δ		C-Trp+Gal
JWY10433	NOY504 with pWL160 with ES7Δ		C-Trp+Gal
JWY10434	NOY504 with pWL160 with ES9Δ		C-Trp+Gal
JWY10435	NOY504 with pWL160 with ES10Δ		C-Trp+Gal
JWY10436	NOY504 with pWL160 with ES12Δ		C-Trp+Gal
JWY10437	NOY504 with pWL160 with ES15Δ		C-Trp+Gal
JWY10438	NOY504 with pWL160 with ES19Δ		C-Trp+Gal
JWY10439	NOY504 with pWL160 with ES20Δ		C-Trp+Gal
JWY10440	NOY504 with pWL160 with ES26Δ		C-Trp+Gal
JWY10441	NOY504 with pWL160 with ES27hΔ		C-Trp+Gal
JWY10442	NOY504 with pWL160 with ES31Δ		C-Trp+Gal
JWY10443	NOY504 with pWL160 with ES39Δ		C-Trp+Gal
JWY10444	NOY504 with pWL160 with ES41Δ		C-Trp+Gal
JWY10445	*RPF2 TAP* (URA3) NOY504 PolI ts strain		YEPD
JWY10446	*GAL-HA-L5* in W303 *MATa leu2-3,112 trp1-1 can1-100 ura3-1 ade2-1 his3-11,15 rpl5::GAL-3HA-RPL5 TRP1*		YEPGal
JWY10447	*GAL-HA-L5* in W303 clone #2		YEPGal
JWY10448	*GAL-HA-L5* in W303 clone #3		YEPGal
JWY10449	*GAL-HA-L5 NOP7-TAP*, derived from JWY10446 (clone #1) *MATa leu2-3,112 trp1-1 can1-100 ura3-1 ade2-1 his3-11,15 rpl5::GAL-3HA-RPL5 TRP1 nop7::NOP7-TAP URA3*		YEPGal
JWY10450	Same as above Clone #2		